Numéro d'ordre: 41531

THESE

presentée à

ECOLE DOCTORALE SCIENCES POUR L'INGENIEUR
UNIVERSITE DE LILLE 1

pour obtenir le titre de

DOCTEUR DE L'UNIVERSITE

Spécialité: ELECTRONIQUE

par

Vincent BRIDIER

Contribution au développement d'une nouvelle plateforme de caractérisation non linéaire pour amplificateurs de puissance hyperfréquences pour les applications radar

Soutenance devant la commission d'examen le 20 Novembre 2014

Membres du Jury:

Prof.	Dominique SCHREURS	KU Leuven	Rapporteur
Prof.	Denis BARATAUD	Xlim	Rapporteur
Dr. HDR	Jean-Louis CAZAUX	Thales Alenia Space	Membre
Dr.	Philippe EUDELINE	Thales Air Systems	Membre
Prof.	Daniel PASQUET	LaMIPS et ENSEA	Membre
Dr.	Damien DUCATTEAU	IEMN	Membre
Prof.	Gilles DAMBRINE	IEMN	Directeur
Dr.	Hans-Joachim SIMON	Rohde&Schwarz Munich	Invité
Dr.	François GRAUX	Rohde&Schwarz France	Invité

"Solutions nearly always come from the direction you least expect, which means there's no point trying to look in that direction because it won't be coming from there"

Douglas Adams, *The Salmon of Doubt*

To my beloved, family and friends

Acknowledgements

I am indebted to so many people that it seems impossible to me to thank all the way they deserve. Please forgive me if my words do not express my gratitude as well as each of you would expect and rightfully claim or if I fail to explicitly mention you. I know that without each and any of you, this project would have most certainly failed regardless of the amount of energy I would have provided.

I would like to express my gratitude to Mister **Jean-Cristophe PRUNET**, President of Rodhe&Schwarz France, Mister **Jacques JOURDA** presently Sales Manager in Rohde&Schwarz Canada and Mister **Yann AUFFRET**, Sales Manager in Rodhe&Schwarz France for having me as a member of their team during the three years of this work. Many acknowledgments go to Mister **Christian EVERS**, formerly manager of the Network Analysis Department for the interest and the support he gave to this work from the first day by hosting me in Rohde&Schwarz Munich, and for understanding the advances induced by nonlinear characterization. My gratitude goes as well to Mister **Josef WOLF**, Director of the Spectrum and Network analysis division in Munich for hosting me for more than a year and a half in his department.

I would also like to thank Doctor **Philippe EUDELINE**, Technical Director at Thales Air Systems, for his interest in this project and for hosting me many times in the Innovation Department, as an intern and during this work and for accepting to be a member of the Jury.

Many thanks naturally go to Professor **Gilles DAMBRINE**, Professor at Université de Lille 1 and Deputy Director of IEMN, for accepting to be my advisor and to Doctor **Damien DUCATTEAU** for regularly hosting me in the Characterization Department of IEMN he was managing until recently and being my advisor de facto in the domain of RF characterization. I am extremely thankful for the time, the supervision and the support they could provide throughout this work.

My gratitude also goes to Doctor **François GRAUX** from Rodhe&Schwarz France for spending an incredible amount of time and energy for the success of this project, all the piece of advice he shared with me during this years and the always positive and constructive attitude independently on how dire the situation seemed at times. Of course I cannot forget to thank all the rest of the Test and

Measurement team, and in particular Misters **Philippe SEURRE** and **Frederic MOLINA-COVA** for their availability, unconditionally sharing their expertise and helping me with carrying some measurements as well as for the nice times we spent during their visits to Munich.

I could not talk about Munich without thanking all the Network Analysis Department as well as the RF Module Design Department and the Q-pass department for all the help and letting me borrow so much of their equipment and for the friends I found there. In particular, I would like to thank Doctor **Hans-Joachim SIMON** for his constant help and support during the years and mentoring me despite his extremely dense schedule. I would also like to thank the best Team Assistant ever, Misses **Carola STROISCH** for all the help she provided to me over time, notably an extremely complete and useful dictionary of technical words including translation of words in German, English and French that she wrote. This Rosetta Stone of RF engineering has been literally life saving when deciphering technical documentation in German and while writing this thesis.

I would like to address my sincere gratitude to Doctor **Michel STANISLAWIAK**, formerly in Thales Air Systems, whose passion for amplifier designing and teaching is highly communicative, for the guidance and for all the direct talks we could have during this work and while he was mentoring me as an intern. Many thanks also to Mister **Maxime OLIVIER**, engineer at Thales Air Systems, for introducing me to the world of RF and load pull characterization when I was still an intern and for being so friendly and helpful during the entire duration of this work.

Many many thanks to Mister **Etienne OKADA**, engineer at IEMN, for restlessly helping with the validation of the nonlinear system and many thanks to all the Characterization Team, which good mood allied to extreme competence made the time spent among them extremely pleasant and fruitful.

I would like to express my appreciation and gratitude to Doctor **Marc VANDEN BOSSCHE**, Doctor **Frans VERBEYST** and Doctor **Guillaume PALLIONCY** for introducing me to the nonlinear world by hosting me at NMDG for a short period and for providing to the project enough material to start rebuilding a nonlinear system of our own when the relationship between Rohde&Schwarz and NMDG was deteriorating, as they were in no way obliged to do so.

I want also to thank Doctor **Matthieu CAILLET** and Mister **Mike LEFFEL** respectively from Rohde&Schwarz Canada and America for expressing their interest for the nonlinear characterization through many questions that helped me clarifying the concepts and the extremely pleasant times we had during our meetings.

I express my extreme gratitude towards Professor **Denis BARATAUD**, from Université de Limoges, for reviewing this work despite his numerous responsibilities and to Professor **Dominique SCHREURS**, from Katholieke Universiteit Leuven, for accepting to review this work and for hosting the INMMIC2014 conference in Leuven, which was the first conference I ever had the chance to participate to, making it a pleasant (even if partially stressful) memory.

I sincerely thank Professor **Daniel PASQUET**, from LaMIPS and ENSEA, for accepting to be a member of the Jury and for communicating to me and to many of my former classmates at ENSEA the passion for RF engineering. Many thanks to Doctor HDR **Jean-Louis CAZAUX**, from Thales Alenia Space, for being a member of the Jury.

I would like to thank all my friends for the good moments shared, even if we saw each other a lot less in the past years. A big big thank to all the friends that allowed me in countless occasions and with no time limitation to use their sofa during the numerous work related trips between France and Germany.

Finally I would like to thank my loved ones, whose support has always been limitless and unconditional. In particular I would like to thank my mother **Hélène GERMANI** and my grandmother **Margherita ARNAUDO**, may they be as proud of me as I am proud to have been raised by them.

Contents

List of Figures

List of Tables

Acronyms

D	Directivity.
RT	Reflection Tracking.
SM	Source Match.
ADC	Analog to Digital Converter.
AGC	Auto Gain Control.
BJT	Bipolar Junction Transistor.
CMOS	Complementary Metal Oxide Semiconductor.
CW	Continuous Wave.
CZT	Chirp-Z Transform.
DAC	Digital to Analog Converter.
DDS	Direct Digital Synthesis.
DFT	Discrete Fourier Transform.
DSP	Digital Signal Processing.
DUT	Device Under Test.
ENOB	Effective Number of Bits.
EVM	Error Vector Magnitude.
FFT	Fast Fourier Transform.

FMCW	Frequency Modulation Continuous Wave.
FPGA	Field-Programmable Gate Array.
FT	Fourier Transform.
HBT	Heterojunction Bipolar Transistors.
HEMT	High Electron Mobility Transistor.
HPR	Harmonic Phase Reference.
IF	Intermediary Frequency.
InP MMIC	Indium Phosphide Monolithic Microwave Integrated Circuit.
LDMOS	Laterally Diffused Metal Oxide Semiconductor.
LSB	Least Significant Bit.
LSNA	Large Signal Network Analyzer.
LTI	Linear and Time Invariant.
MTA	Microwave Transition Analyzer.
MTI	Moving Target Indication.
MTTF	Main Time To Failure.
NCO	Numerically Controlled Oscillator.
NLTL	NonLinear Transmission Line.
NRZ	Non Return to Zero.
NVNA	Nonlinear Vector Network Analyzer.
OCXO	Oven Controlled Temperature (X)crystal Oscillators.
OSM	Open Short Match.

PA	Power Amplifier.
PAE	Power Added Efficiency.
PLL	Phase-Locked Loop.
PRBS	Pseudo-Random Bits Sequence.
PRF	Pulse Repetition Frequency.
RBW	Resolution BandWidth.
RF	Radio Frequency.
RMS	Root Mean Square.
SFDR	Spurious Free Dynamic Range.
SINAD	SIgnal to Noise And Distortion.
SNR	Signal to Noise Ratio.
SRD	Step Recovery Diode.
SSPA	Solid State Power Amplifier.
SSPG	Split Signal Pulse Generator.
TCXO	Temperature Compensated (X)crystal Oscillator.
THD	Total Harmonic Distortion.
TOSM	Thru Open Short Match.
VCO	Voltage Control Oscillator.
VNA	Vector Network Analyzer.
XO	(X)crystal Oscillator.

Physical Constants

Speed of Light	c	$=$	$2.997\ 924\ 58 \times 10^{8}\ m.s^{-1}$
Boltzmann constant	K	$=$	$1.380\ 648\ 8 \times 10^{-23}\ m^{2}.kg.s^{-2}.K^{-1}$

General introduction

Since the second world war, ground radar systems have acquired an increased importance from their beginning as strategic technology for air control to nowadays key element of the fast delivery of goods and people through the air or for weather forecasting. Their indispensable role in the present technological era makes them, despite the passing decades since their invention, the subject of many researches for improvement.

In particular, the power amplifier is probably the key component of the emission system, as its performance will define the radar performance for example in terms of range, reliability, efficiency and electrical consumption. Every step towards the understanding of power amplifier technologies and how to improve their functioning triggers extended requirements in terms of radio frequency measurement capabilities and precision.

In the last decades, measurement of radar power amplifier went from the measurement of powers in continuous waves, to the measurement of complex signals in pulsed conditions in both time and frequency domain. Every time a measurement gained in capabilities, it allowed power amplifier designers to take into account new phenomena, improving their design accordingly.

The state of the art in terms of measurement is the nonlinear characterization, that allows to quantify the nonlinear behavior of radar power amplifier accurately at compression in magnitude and phase, allowing the use of high efficiency functioning classes of amplifier. If this measurement can be performed in continuous wave and periodic pulsed condition, it is yet not available to measure real non periodic radar pulse train which would bring new insight to designers.

The objective of this industrial research is, by the collaboration of radar designers, instrument designers and nonlinear characterization experts, to provide an extension of nonlinear characterization to realistic radar trains.

The first chapter will present the basics of the radar functioning and the reasons triggering the need of complex radar pulse train. Then the main axis of power amplifier improvement will be presented followed by a description of linear and nonlinear measurements that are required by the radar designers. This chapter will conclude on the description of this industrial project, its actors, and event that shaped its content.

The second chapter will focus on the conception of an instrument for nonlinear measurement characterization. First a description and then a comparison of the available receiver technologies will be presented to evaluate each of them in terms of nonlinear characterization capabilities. After choosing the receiver technology more suited to the context of this work, a description of the instrument that will be upgraded for nonlinear characterization will be presented. Then the required upgrades for nonlinear measurement will be described and implemented, to finally conclude this chapter on the validation of the instrument in continuous wave and show how it compares to state of the art equivalent solutions.

The third and final chapter will deal with the upgrade of the designed instrument to periodic pulsed measurement and how it can be extended to non periodic pulse measurement to some extent. Finally, a new implementation of the instrument is proposed, enabling actual measurement in radar pulse trains according to the requirements of the partner radar designers. This chapter concludes on examples of nonlinear measurements in radar pulse train that were so far inaccessible.

Chapter 1

Context of the study

1.1 Introduction

Advances in solid state components have opened the way for higher performance systems. In particular wide band gap semiconductors have allowed a leap forward for system requiring high power and high efficiency such as radar system. However the extreme operating conditions of the radar transmitter generate effects in those new semiconductor technologies that were not previously accounted for, triggering new specialized measurement needs. In particular the understanding of the non linear behavior of the radar Power Amplifier (PA) is a key to even more performing systems.

In this chapter, we will describe the basic functioning of a commonly used type of radar and how it can be affected by the application the system is designed for and the engineering choices.

Later, we will show the importance of the power amplifier in a radar system and how wide band gap semiconductors are of prime importance to improve the system.

Then an overview of different usual measurement techniques for radar power amplifier characterization and design will be presented.

Finally, a description of the research project is given, including the definition of the requirements and study boundaries, a presentation of the members of the

project composed of three different groups with distinct interest as well as the series of events that shaped the content of this work.

1.2 Radar system description

1.2.1 Brief radar history [1]

The second half of XIX$^{\text{th}}$ century has seen major progresses in the understanding of one of the fundamental fields of physics, electromagnetism. The formulation by J. C. Maxwell of a set of equations describing how electric and magnetic fields are altered by each other and by static and flowing charges has triggered numerous new experiments and practical and theoretical discoveries. One of the emblematic inventions directly induced by Maxwells laws is the radar (acronym for RAdio Detection And Ranging but the invention is so well spread that the term radar is often used as an appellative).

While the attribution of radars invention to a single person is made impossible by the multiplicity of works and discoveries in the western part of the world during the XXth century, C. Hülsmeyer's "'Telemobiloskop"' is considered as radar's ancestor. Relying on the experiment conducted by H. R. Hertz demonstrating in 1888 that an electromagnetic wave is reflected by a metallic wall, C. Hülsmeyer designed in 1904 a system emitting a radio signal which reflected part is detected by two bipolar antennas.

The constantly improving radio detection systems finally came in vital during World War Two. After the war the respective rises of civil aviation and meteorology have spread radar systems outside of the military sphere where it still keeps an essential role. Even if the most popularly know application nowadays is speed evaluation for road safety, radar system is one of the inventions on which relies today's globalized world.

1.2.2 Operating principle [2] [3]

Radar is a system for detection and location of objects (or targets). It operates by transmitting electromagnetic signals and receiving the signals reflected (called

echoes) by remote targets, extracting information about the detected objects [4]. Generic radar block diagram is presented in Figure 1.1.

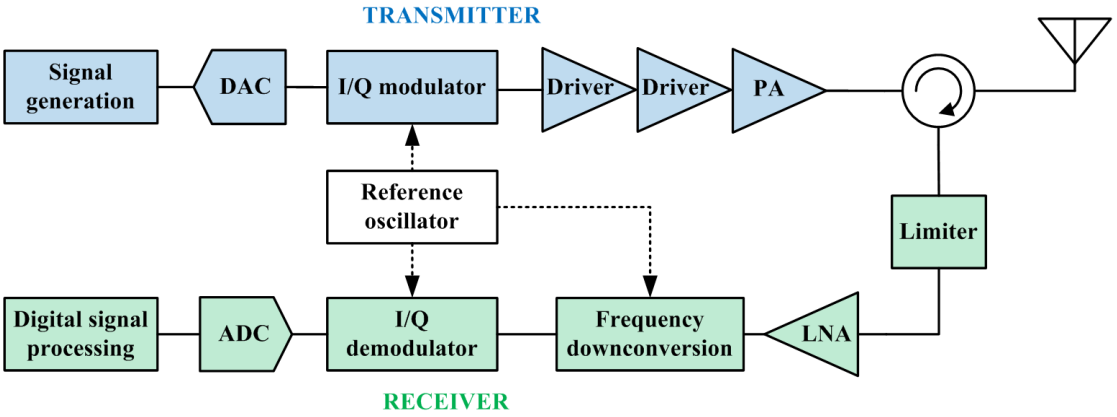

FIGURE 1.1: Basic Radar block diagram composed of the transmitter, the receiver and the antenna blocks

The transmitter has for role to condition the signal to be emitted by the antenna block. The RF signal is first modulated and then amplified. The amplification part is often composed of many high frequency amplifiers whose number depends on the desired output power that may range from some Watts for short range radar to several KiloWatts for longer ranges.

The receiver is here to condition the echo to make it suitable for the data treatment that will give the wanted information. The receiver is designed to measure extremely low power signal. In fact the echos power is supposed to be only a small portion of the transmitted signal due to scattering and absorption of the original wave. Therefore a limiter is present in order to prevent destruction of the receiver in case of echoes with power higher than the maximum rating of the receiver. In order to use the receiver at best Signal to Noise Ratio (SNR) possible, the signal is amplified by a low noise amplifier and then down converted at intermediary frequency (as it is easier to work with low frequencies) to finally be demodulated and digitized for data treatment. Data treatment will not be described but it is important to sort out useful echoes from clutter (unwanted echo from the ground, sea, rain, insects, birds, aurora etc).

The antenna block is composed of a circulator and an antenna. The circulator is directing emitted and received signal to the rightful path and must therefore have an excellent isolation while the antenna is in charge of the emission and reception of electromagnetic signal. If part of the transmitted signal was to leak to the receiver

path, it would degrade the minimum detectable signal if emission and reception are made at the same time (most of the system are alternating these modes). In the other direction, signal coming from the antenna going to the transmitter may disturb the power amplifier decreasing its performance. For the same reason, a good matching of the antenna is required.

Radar signals are generally time dependent, therefore synchronization is necessary and insured by the local oscillator.

Different types of radar exist depending on the application they are designed for, influencing the performance required. Figure 1.2 shows a non exhaustive classification of radar system according to their functioning principle. The generic block diagram of Figure 1.1 is related to primary pulse radar.

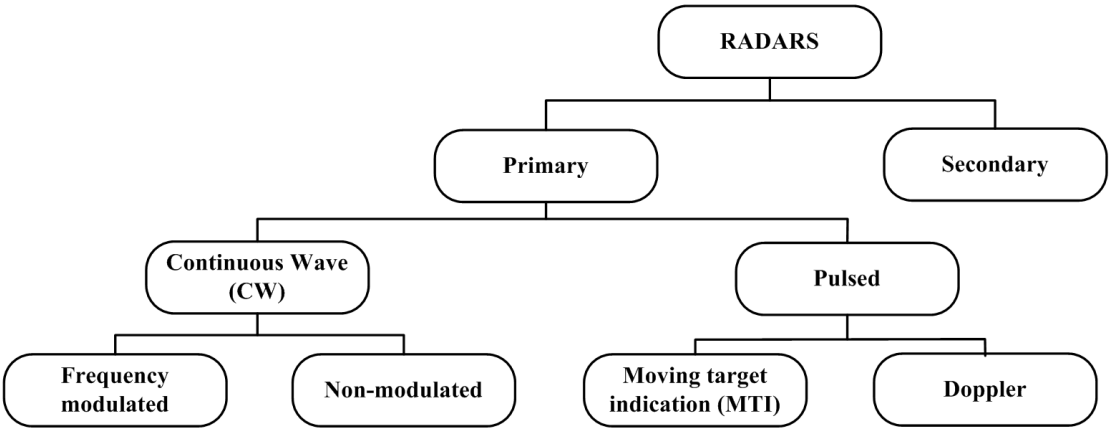

FIGURE 1.2: Classification of Radar type according to their function and principle

Primary radars are designed to collect information from passive echoes, having to adapt their frequencies and waveforms accordingly to the target distance and physical characteristics thus the variety of primary radar compared to standardized secondary radar. Because of the proximity of the hardware configuration between radar types, it is often possible to use a same radar system in different functioning mode. For example Frequency Modulation Continuous Wave (FMCW) radar can easily be used as Continuous Wave (CW) radar by turning off the modulator.

On the opposite, secondary radars are used on objects that can actively send back complex information about themselves (such as identification, speed and altitude) thanks to a transponder. It is used for both civil air traffic and military operations (with allied aircrafts). For civil applications, the information exchange

IEEE band name	Frequency (GHz)	Applications	Scope of the study
UHF	0.3-1	Communication, broadcasting, early detection for air defense, wind profiling	Yes
L	1-2	Air traffic management and surveillance	Yes
S	2-4	Short range detection and weather radar, used in landing site for aircraft approach	Yes
C	4-8	Weather radar, mobile military surveillance and missile guiding	Partially
X	8-12.5	Civil and military maritime navigation	No
Ku	12.5-18	Civil and military maritime navigation	No
K	18-26.5	Airport surface detection equipment	No
Ka	26.5-40	Airport surface detection equipment	No
mm	40-100	Park assistance for automotive, short range targeting, body scanning gate for security check	No

TABLE 1.1: The frequency bands and their usage defined according to IEEE band segmentation

protocol as well as the signals frequencies and waveforms characteristics are standard and defined by the International Civil Aviation Organization. Minimal radar performance is also defined to be eligible to equip aircraft.

Every type of radar implies specialized hardware and data treatment; the frequency used by the radar depends on its application like shown in Table 1.1. This study will be focusing on the particular case of primary pulse radars in S-band (2-4GHz).

Pulse radars transmit as their name suggests pulsed RF signal such has the one in Figure 1.3 in order to extract information from the target. The information most commonly required is location and radial speed of a target. The main characteristics of the pulsed signal are the pulse width τ, the period T or its reciprocal the Pulse Repetition Frequency (PRF) and the carrier frequency f_c (or the equivalent wavelength λ). The role of the carrier frequency has already been explained and as for the other characteristics their importance will be explained in the following parts. For the following explanations it would be useful to keep in mind the frequency domain representation of a pulsed RF signal shown in Figure 1.4.

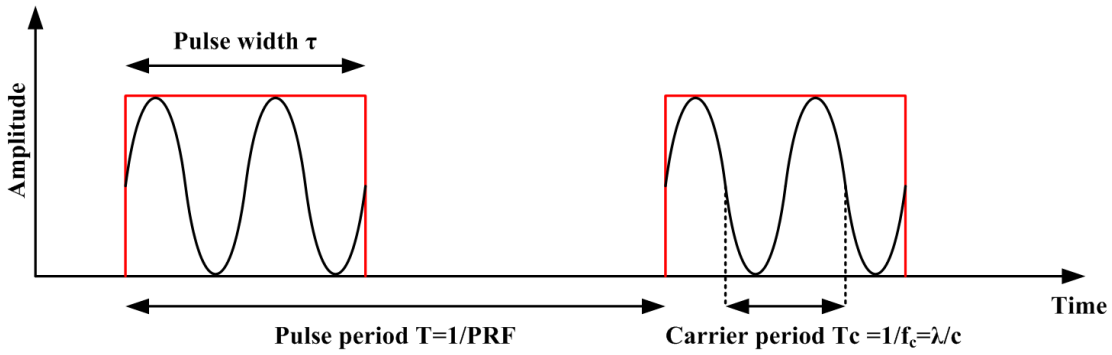

FIGURE 1.3: Simple time domain representation of an RF pulse used in pulsed Radar

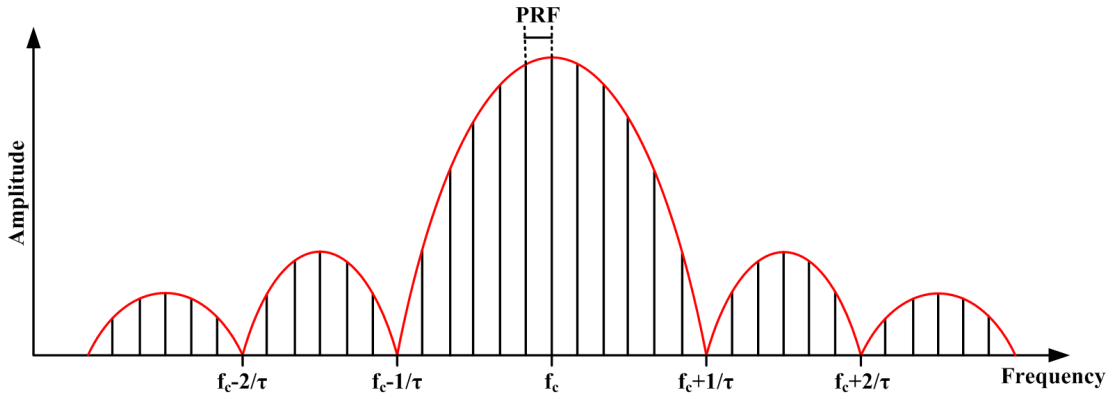

FIGURE 1.4: Frequency domain representation of the pulse defined in Figure 1.3

1.2.3 Location determination principle with primary pulse radar [2] [5]

Location is defined using spherical like coordinate system centered on the radar by the distance to a target (range), the elevation angle between the line of sight and an horizontal plane measured upward and the azimuth defined relatively to a horizontal direction (usually north) measured clockwise [4] as shown in Figure 1.6. The range R is determined from the time delay between an emitted pulse and its echo as in Figure 1.5 by:

$$R = \frac{c.\Delta t}{2} \tag{1.1}$$

The range determination of one target is limited by the maximum possible range. The relationship between the range, the target and the system characteristics is

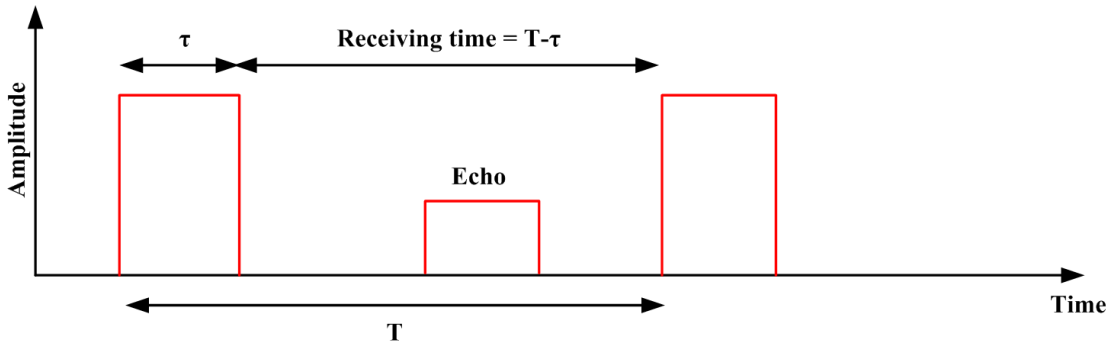

FIGURE 1.5: Schematic definition of a radar echo. An echo must arrive before the emission of next pulse to be usable by the radar

expressed by the simplified radar equation:

$$R = \sqrt[4]{\frac{P_T.G_T^2.\lambda^2.\sigma}{(4\pi)^3.P_R.L}} \tag{1.2}$$

Where,

P_T is the transmitted power in $Watt$

G_T is the antenna gain

σ is the radar cross section in m^2

λ is the signal wavelength in m

R is the range in m

L is the aggregated loss

P_R is the received power in Watt

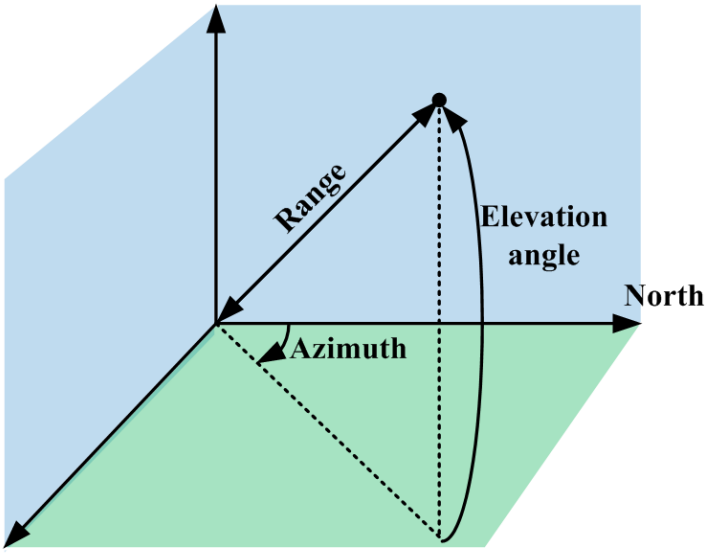

FIGURE 1.6: Radar system coordinates, not to be confused with spherical coordinates

It is possible for given radar and target to evaluate the maximum and minimum range knowing the minimum detectable signal and the maximum power before receiver saturation using Equation 1.2. The range depends equally on the receiver dynamic and the transmitter output power.

In the case of pulse radar however the pulsed signal characteristics has a strong influence on the range. Pulse radars cannot receive an echo during the emission of a pulse. This is the cause of two limitations of the range, the blind range and the maximum unambiguous range.

The blind range is the minimum range that radar can detect. When a target is close enough from the radar it can happen that its echo is received while the radar is still emitting the pulse. The blind range R_B is expressed as a function of the pulse width τ and the speed of light as:

$$R_B = \frac{\tau.c}{2} \tag{1.3}$$

In order to be detected or not be misinterpreted an echo must come back during the silence following the transmitted pulse it is the echo of. The maximum unambiguous range R_U is the maximum detectable range before the next pulse is emitted and defined as:

$$R_U < \frac{c}{2.PRF} \tag{1.4}$$

The angular coordinates of a target can be determined using the knowledge of the directivity of the antenna. In fact the power of the echo depends on the location of the target in the main lobe. The better the directivity of the antenna the better the evaluation of the location is.

Sequential measurements are also used to determine the angular coordinate. The tracking radar illuminates the target at different angles until the evaluation of the azimuth and the elevation angle is possible. This concept includes technique such as conical scanning and sequential lobing measurement and is sensible to pulse to pulse stability of the emitter and to scintillation.

A quicker and more accurate method uses monopulse receiver antenna. Having more than one beam simultaneously, it is possible to compute the angular coordinates comparing the received signal from each lobe using a single pulse. This technique implies the use of one receiver per beam but offers immunity against

the transmitter pulse to pulse instability. Phased array antenna is suitable for monopulse technique as the antenna is composed of multiple independent cells.

The elevation angle determination depends on the refraction in the air. A model of the refraction is usually used to correct the angle and can be found in [4].

In the common case of multiple target detection and location, figures of merit of radar system are the range and the angular resolution.

Range resolution is defined as the ability to distinguish between two targets solely by the measurement of their range [4]. It depends on the performance of the receiver, the nature of the targets and for pulse radar on the pulse width. For pulse radar the theoretical lower limit of the range resolution R_{res} corresponds to half of the pulse width as shown in Equation 1.5. Range resolution can be increased thanks to pulse compression technique that implies frequency modulation inside the pulses.

$$R_{res} \geq \frac{\tau.c}{2} \tag{1.5}$$

Angular resolution is the ability to distinguish between two targets solely by the measurement of their angle, usually expressed in terms of the minimum angle separation by which two targets at a given range can be distinguished [4]. The angular resolution depends on the vertical and horizontal width of radars main lobe (there is in fact angular resolution for azimuth and for elevation angle). The required distance between two targets or cross-range separation d_{CR} is calculated from the radar beam width in angular coordinates θ_{beam} and the range R by:

$$d_{CR} = R.\theta_{beam} \tag{1.6}$$

Two targets can be differentiated if they are discernible in at least one of the coordinates.

1.2.4 Radial speed determination principle for pulse radar [5]

The radial speed of the target can be determined by multiple range measurements or by taking advantage of Doppler Effect.

Multiple range method uses the range measurement described in Section 1.2.3 at two different times in order to deduce the radial speed V_r using:

$$V_r = \frac{\Delta R}{\Delta t} \tag{1.7}$$

Doppler Effect is the change of frequency of a periodic event for an observer moving relatively to the emitter. The principle was proposed by C. Doppler in 1842. For the particular case of electromagnetic waves one also talks about Doppler-Fizeau Effect from H. Fizeau that proposed the principle for electromagnetic waves in 1848. A simple example for radar system would be a ground stationary system that is illuminating a target moving towards the radar. The phase change $phi(t)$ of the transmitted signal at a given time is defined by its range change $R(t)$ using Equation 1.8 provided that the targets speed is negligible compared to speed of light (hence avoiding relativistic effects).

$$\phi(t) = \frac{4\pi.R(t)}{\lambda} \tag{1.8}$$

Between two different times the relative phase change relates to the radial velocity V_r of the target as:

$$\frac{d\phi(t)}{dt} = \frac{4\pi}{\lambda}.\frac{dR(t)}{dt} = \frac{4\pi}{\lambda}.V_r \tag{1.9}$$

As phase derivative is equal to the angular frequency we define the Doppler frequency f_D:

$$f_D = \frac{2.V_r}{\lambda} \tag{1.10}$$

A radar system can quantify speed by evaluation of the Doppler frequency or the relative phase shift caused by Doppler Effect on coherent pulses. The speed evaluation based on Doppler Effect is generally more accurate than the multiple range measurements technique and is therefore preferred. Table 1.2 shows the Doppler frequency according to the radial speed and the frequency used by the radar. We can see that stability of the transmitter and receiver is extremely important as the Doppler frequency variation is extremely small compared to the radar frequency.

Typically the Doppler frequency is bigger than the PRF of the pulse train therefore it is difficult to find it with a few pulses. Measuring the phase shift between

Radial velocity \ Carrier frequency	S-band 3GHz	C-band 5.6GHz	X-band 9.35GHz
1m/s	20Hz	≈37.5Hz	≈62.5Hz
10m/s	200Hz	≈375Hz	≈625Hz
50m/s	1000Hz	≈1876Hz	≈3125Hz

TABLE 1.2: Doppler frequency versus radial speed of the target and carrier frequency of the radar pulse

several pulses instead is a more performing approach that is preferred but also implies a good phase stability of the radar system.

Sadly Moving Target Indication (MTI) radar and pulse Doppler radar suffer from speed ambiguities. As with pulse radar we are sampling the wavelength, aliasing can happen. Nyquist-Shannon theorem tells us that we need a sampling frequency strictly superior to twice the Doppler frequency which in terms of velocity translates to:

$$V_{max} = \frac{\lambda.PRF}{2} \tag{1.11}$$

Every radial velocity with absolute value superior to the unambiguous maximum velocity V_{max} cannot be unambiguously known. In the particular case of a target with a velocity equal to or entire multiple of the unambiguous maximum velocity, the target would appear as fixed. This phenomenon is called blind speed in the particular case of MTI radar.

There is also a lower limit to the detectable velocity. If the Doppler frequency shift has a value that is included into the main lobe of the pulse bandwidth it will not be detectable. Therefore the Doppler frequency must be superior to half of the bandwidth of the pulsed signal which translates to a minimal measurable velocity:

$$V_{min} = \frac{\lambda}{2\tau} \tag{1.12}$$

In the case of multiple target detection one must care about the velocity resolution. It is defined as the minimum radial velocity difference between two targets at the same range to make them distinguishable. For the multiple range measurements method it depends on the range resolution. Pulse Doppler radars have a velocity resolution that improves with increase of the PRF.

1.2.5 Choice and evaluation of radar pulse train characteristics

A pulse train is defined as a sequence of pulses at PRF used to accomplish a given task. A pulse train of duration inferior to the time before receiving an echo is referred to as pulse burst.

We have seen previously that the PRF of a pulse train has an influence on the performance of the radar system for pulse Doppler radar:

- A low PRF gives good range but a bad velocity determination and decreases the maximum range
- A high PRF gives a good velocity but a bad range determination

The radar designer must always compromise between conflicting performance when designing the pulse train that will be used. An often used solution to circumvent the dilemma between range and velocity it is possible to alternate pulse trains with high and low PRF. An equivalent compromise must be applied to the pulse width as we have seen that a short pulse decrease the blind range and the minimum detectable velocity while reducing the maximum range at constant PRF and requesting a larger operating bandwidth.

A pulse train must be chosen accordingly to the application range and velocity requirements. Examples of requirements versus application are shown in Table 1.3 in the case of pulse Doppler radar.

To evaluate the suitability of a radar waveform $s(t)$ in terms of accuracy, resolution, freedom from ambiguities and reduction of clutter, the ambiguity function 1.13 is used. It is the squared magnitude $\mid \chi(t_d, f_D) \mid^2$ of the function that describes the response of a radar receiver to targets displaced in range delay t_d and Doppler frequency f_D from a reference position where $\chi(0,0)$ is normalized to unity [4] [6].

$$\chi(\tau_d, f_d) = \int_{-\infty}^{\infty} s(t)s^*(t+t_d)e^{j2\pi f_d t}dt \tag{1.13}$$

Examples of ambiguity function calculation can be found in [5]. The pulse train allowing the best results and versatility are almost never periodic. They are varying over time to overcome theoretical limitations of pulse radar as well as practical

Radar application	Requirement
Airborne or spaceborne surveillance	Long detection range; accurate range data
Airborne interceptor or fire control	Medium detection range; accurate range, velocity data
Ground-based surveillance	Medium detection range; accurate range data
Slow-moving target detection	Medium detection range; accurate range, velocity data
Missile seeker	May not need true range information
Meteorological	High velocity and range data resolution

TABLE 1.3: Pulse Doppler applications and induced requirements [2]

deteriorating effect of the hardware such as transient effects. The radar system and particularly the emitter must be designed in order to handle these constantly varying waveforms.

1.3 Power amplification for radar application

1.3.1 Influence of power amplifier on the radar system

The power amplifier is the key element of the transmission path. Its performance and characteristics are directly defining the performance of the entire system.

The power, that an amplifier can provide, has a direct influence on the number of amplifier in parallel needed to reach the power the desired range requires. In fact to achieve the pursued power, amplification is often ensured by many amplifier blocks in parallel. A small number of power amplifiers allow to reduce the size of the system which is an advantage, especially for mobile radars.

The transition frequency of the power amplifier is also important as it defines the maximum frequency the amplifier can be used at while providing the power requested. As explained in Section 1.2.2 the working frequency is chosen accordingly to the application required from the radar.

The bandwidth of the amplifier is also important. The use of pulse compression technique to increase the radar resolution using in-pulse frequency modulation

(chirp) implies that the radar works on a large frequency bandwidth. For example in S-band the objective is superior to one fifth of the S-band coverage. A large bandwidth is also an advantage against jamming that can be caused by natural obstacles, other radar system in the vicinity. In fact a simple counter measure against jamming is to change frequency which is a lot more efficient when the bandwidth is large enough. The bandwidth of a radar system is limited by the power amplification of the emitter as it is narrowband.

As seen previously, radar systems often use the comparison of the echoes of coherent pulses in order to get accurate velocity or location change. The emitted pulses must be as identical as possible as a small error can make a fixed target appear as a moving one and trigger false alarm. The pulse to pulse stability [7] of the power amplification is determinant as it quantifies the ability of the emitter to produce identical pulses, especially when the pulse train is composed of non periodic signal as explained in Section 1.2.4.

Radars are used to detect unpredictable events that require constant functioning and then must be resistant against failure. Reliability of the system is so important that a radar system often includes twice the hardware it actually needs in order to have a quick back up. The reliability of the radar directly depends on the reliability of the parts that are used in stress conditions such as the power amplifier. The Main Time To Failure (MTTF) of a power amplifier depends on its working temperature. A lot of effort is put in order to control this temperature using efficient amplifiers and high performance cooling systems.

The best way to reduce the need of cooling system while obtaining the same output power is to increase the efficiency of the power amplifier. Increasing the efficiency of the amplifier also allows reducing the size of power supplies. High efficiency power amplifier tends to simplify the radar and reduce the functioning energy cost which is not negligible for a system that is almost never turned off.

The performance of a power amplifier are influenced by the technology used, its functioning class and its environment.

1.3.2 Power amplification for radar application [8]

Historically the power amplification of the transmitter stage was ensured by vacuum tubes that could output around megawatts in pulse mode [1]. Nowadays Solid

State Power Amplifier (SSPA) have replaced them in most applications thanks to better characteristics. In fact SSPA are more reliable and better suited for large pulses; they have a higher transition frequency, a better efficiency which implies smaller power supplies and it is easier to design amplifier with large bandwidth while being extremely less bulky than vacuum tubes allowing increased system integration. An advantage of SSPA is also the quasi nonexistent warming time compared to vacuum tube (guitar players for instance know well that vacuum tube amplifier need to warm up while solid state transistor amplifier can be used right after turning them on).

Semiconductors and their characteristics for power amplification

Among the transistors used for solid state power amplifier, some semiconductor materials are particularly fitted for high frequency power amplification needed for radar. The semiconductors are defined by intrinsic properties that influence their potential performance [9].

The main characteristic of interest of semiconductors for high power amplifier is the band gap width. It is defined as the energy needed for an electron to jump from the valence band to the conductance band when excited. The larger the band gap is, the better the transistor can handle high current/voltage which is suited for power application.

The breakdown field depends directly on the band gap, it corresponds to the maximum field that the transistor can handle before breaking. It quantifies the capacity to support high biasing voltage, the bigger the value of the field the better for power application. The high frequency capability is favored by the electron mobility. The more mobile the electrons are the quicker they can react to a perturbation hence the higher working frequency.

The saturated peak electron mobility is defined accordingly to a field applied to the semiconductor. In a semiconductor the electrons can only reach a determined maximum velocity as a function of the apply field because of collisions between each other when they are too numerous in the pinched section of the semiconductor. The bigger this characteristic is the better a transistor made with this material can work at high frequency and power.

Material	Bandgap [eV]	Electron mobility [C.m^2/V.s]	Saturated peak electron velocity [$10e^7$ cm/s]	Critical breakdown field [$10e^6$ V/cm]	Thermal conductivity [W/cm.K]
Si	1.1	1500	1	0.3	1.5
GaAs	1.42	8500	1.2	0.4	0.5
InP	1.35	5400	1.4	0.5	0.7
SiC	3.26	700	2	2	4.5
GaN	3.49	900	1.5	3.3	1.7
Diamond	5.6	4500	2	20	25

TABLE 1.4: Semiconductors principal characteristics for power amplification [10] [11] [12] [13]

Finally the thermal conductivity of the material will tell us how well the heat generated by the transistor during functioning will be dissipated. A high thermal conductivity ensures a better reliability of the transistor as the component is less affected by hot points that can break it.

As shown in Table 1.4 wide band gap material and in particular the material from III-V group have intrinsic properties that are extremely interesting for high power transistor. For extremely high frequencies InP or GaAs are often used because of there high electron mobility. The most promising material for power application would be the diamond but the high cost of production as limited the spread of this technology but it is still investigated [14]. GaN transistor on the other hand have received a lot of attention showing interesting properties and reached market. This material brings high power densities capabilities as well as a good transition frequency. It is replacing the Si material in power application despite the low production cost and maturity of the silicon technology. Nevertheless because of the low thermal conductivity of GaN, the high efficiency applications are often favored. Despite generally inferior intrinsic capabilities compared to GaN, SiC is also used for high power application at low frequencies. At higher frequencies however it is mostly used as a substrate for GaN transistor in order to take advantage of its good thermal conductance.

Functioning classes for radar power amplification

The capabilities of each material can be favored or limited by the functioning class of the power amplifier. The variety of functioning classes and their utility is

explained by N.O. Sokal in this presentation [15].

The sinusoidal classes A, AB, B and C are extensively explained in [16]. Their name come from the fact that they can be explained using a single sinusoidal signal. For radar power amplification, the main requirements are on the output power and the efficiency so AB and B classes are used. The main source of dissipated power in the power amplifier (and therefore lost for amplification) comes from the product of the amplifier's output voltage with the output current. Efficiency is therefore increased when minimizing the coexistence of the output voltage and current.

This idea is the base of the switching classes also called high efficiency classes. E, F and F^{-1} classes are described in [17] and [18]. They are called switching classes because their common concept is to minimize the dissipated power by the amplifier by having the maximum output voltage when the output current is at its minimum (ideally 0A) like for an open switch and vice versa. This is done by using the harmonics of the signal, theoretically an infinity of harmonics for E class as for a switch, and only a subset of even (F^{-1} class) or odd (F class) harmonics. The best efficiency is obtained at compression of the transistor when harmonic content is rich. The commutation classes are therefore not suited in this form for application requiring linearity but they are intensively investigated for radar power amplification.

Transistor architecture for power amplification

Finally different transistor architecture take more or less advantage of intrinsic properties of the semiconductors and of the functioning classes to favor high power amplification. Three architecture are mostly used for radar application in S-band
.

The Bipolar Junction Transistor (BJT) in Si is often used for S-band radar applications. Despite its limited power gain and transition frequency, the SiGe HBT profits from a well known and stabilized technology showing good enough performance in S-band. It is possible to find commercially transistor from Microsemi® that can output 100W at $100\mu s$ pulse width and 10% duty cycle pulsed conditions for 8dB power gain in AB class. High efficiency is not the strength point of this power transistor as it often shows less than 35% Power Added Efficiency (PAE).

The different Heterojunction Bipolar Transistors (HBT), while having better efficiency than Si BJT, did not know a great success for radar application because of lower power gain for the SiGe or the difficulty to control the base emitter voltage for GaAs. Despite those inconveniences, GaAs or SiGe HBT is often used at lower output power for telecommunications.

The Laterally Diffused Metal Oxide Semiconductor (LDMOS) in Si is the most commonly used power transistor for S-band radar application. As for the BJT Si it takes advantage of the stabilized Si Complementary Metal Oxide Semiconductor (CMOS) process while presenting an average of 5dB more power gain and 10 points more PAE than the BJT at equivalent output power and functioning class. The main drawback of this technology is the frequency with a maximum frequency around 3.8GHz for commercially available component.

Since the year 2000, High Electron Mobility Transistor (HEMT) in GaN has been the topic of many researches and publications. One of the reference work published in 2004 by Wu [19] showed that a single transistor (power transistor are often composed of many elementary transistors) can reach 8W output power with a power gain of 14dB and a PAE of almost 55% at 4GHz in AB-class. One advantage compared to the two other technologies presented is the higher transition frequency. This transistor is foreseen as the replacement of silicon transistors for radar applications as well as for mm-wave approach radar for automotive and aircraft landing assistance.

A non exhaustive selection of cased transistor can be found in Table 1.5 for technology comparison.

As promising as HEMT GaN is, it is not yet fully understood and non negligible memory effects are still negating the best theoretical performance to the designers. Memory effects are defined as effects affecting the response of the transistor that depends on the transistor history. One often split those effects between thermal and electrical effects depending on their origin.

For example an often encountered electrical effect is trapping effect. The trapping effect is a phenomenon that blocks the electrons (hence trapping) in a layer of the transistor where they are not supposed to accumulate affecting the performance of the transistor [20].

Part Number	Frequency [GHz]	P_{out} [W]	Gain [dB]	η [%] drain / collector	V_{DS} / V_{CC}	Impulsion
Transistor HEMT GaN						
UMS CHK080A-SRA	up to 3.5	100	13	65	50	???
CREE CGH35240	3.1 - 3.5	240	11.6	57	28	???
Integra IGN2735M250	2.7 - 3.5	250	10	55	32	300μs / 10%
Transistor LDMOS Si						
Freescale MRF7S35120HSR3	3.1 - 3.5	120	12	40	32	100μs / 20%
Integra ILD3135M120	3.1 - 3.5	154	10.4	41	32	300μs / 10%
NXP BLS7G2933S-150	2.9 - 3.3	150	13.5	47	32	300μs / 10%
Transistor Bipolar Si						
Integra IB2934M100	2.9 - 3.4	100	9 - 10	50	36	100μs / 10%
Microsemi 3134-180P	3.1 - 3.4	180	8.6	45	36	100μs / 10%
NXP BLS2731-110	2.7 - 3.1	110	7-8	35-42	40	100μs / 10%

TABLE 1.5: Commercialized cased transistor technologies comparison

In HEMT GaN technology, the increase of temperature of the transistor tends to decrease the performance of the transistor [21]. The performance of the transistor therefore depends on its previous thermal state that can be due to self heating or previous power injection as when used in radar systems.

For radar application, the power amplifier is used in varying pulsed condition as seen in Section 1.2.5 and therefore memory effects will have a constantly evolving influence. To design high performance amplifiers, one may want to use as realistic signals as possible in order to be sure to take those effects into account in the real functioning conditions. Furthermore the performances objectives and high efficiency functioning classes require deeper insight into the transistor behavior at the fundamental and the harmonics and therefore new measurement concepts.

1.4 Microwave measurements for design and characterization of radar power amplifiers

1.4.1 Load and source pull technique [22]

Source and load pull technique is not strictly speaking a measurement technique. It is a measurement environment control technique meaning that it helps to control one of the parameters of the measurement. As an oven helps controlling the temperature of the experiment, source and load pull allows to control the impedance presented to a DUT at its accesses. It is one of the main tools of radar power amplifier designer and as such will be shortly described as any type of measurement undertaken during this work regarding radar amplification may be coupled to this technique. Source and load pull is often in radar power amplifier design for:

- Impedance matching during design of the radar power amplifier
- Characterize the evolution of the transistor performance (mostly gain, output power and PAE) as function of the impedance presented at the source and the load
- Characterize the sensibility to mismatch of the power amplifier (which is important in the case of phased array antenna)

In order to control the impedance, three main techniques are used; passive load synthesis, active load synthesis and hybrid synthesis.

Passive load synthesis

Passive load synthesis is based on an electro-mechanic device called "tuner" in microwave engineering. A tuner is usually composed in Radio Frequency (RF) domain of a slotted coaxial line which characteristic impedance is locally modified by one or more stubs as shown in Figure 1.7 changing the reflection coefficient presented by the tuner. A vertical displacement of the stub changes the magnitude of the reflection coefficient according to Equation 1.14 and a horizontal one changes its phase.

$$Z_c = \frac{1}{2\pi}\sqrt{\frac{\mu_0\mu_r}{\epsilon_0\epsilon_r}}\ln(\frac{b}{a}) \tag{1.14}$$

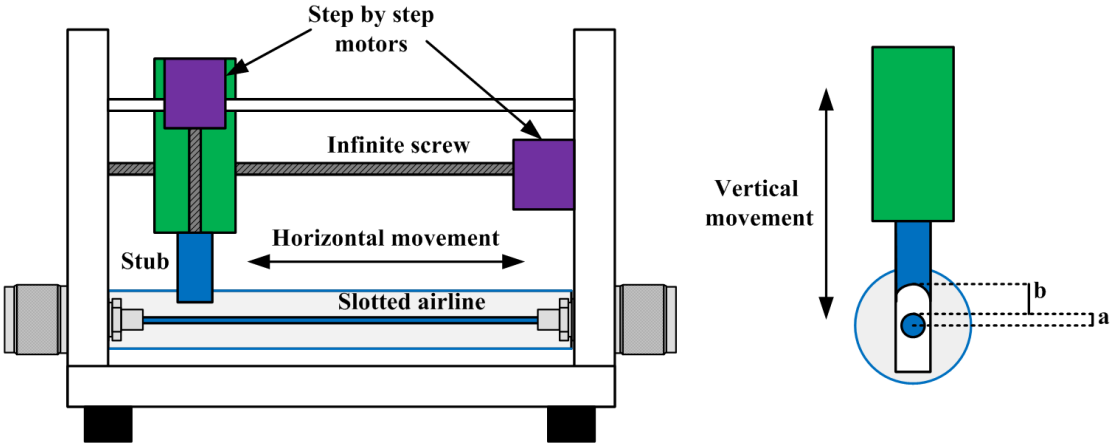

FIGURE 1.7: Microwave tuner description for passive load synthesis

The displacements are insured by extremely precise step by step motors as the precision and repeatability of movement characterize the precision of the synthesis, the magnitude of the reflection coefficient is particularly concerned as it follows a logarithmic law.

Many types of tuner have been designed over the years including resonator for harmonic rejection or a given number of stubs for control of impedance at several harmonics or high reflection coefficient synthesis.

In order to synthesize wished impedance at the output of a Device Under Test (DUT), the tuner must be characterized using a VNA at several vertical and horizontal positions of its stubs at every frequency of interest, also known as tuner calibration. The drawbacks of the technique are that this characterization is time consuming depending on the requirements and that the accuracy of the synthesis highly depends on the repeatability of the tuner and on the accuracy of the VNA.

At RF up to 50GHz, despite the fact that it is not possible to synthesize total reflection (usually limited to 0.8/0.9 magnitude up to 18GHz, lower at higher frequencies), the high bandwidth, the good power handling (often superior to 100W in S-band) and the ease of use of present systems makes it the most commonly used impedance synthesis in the industry. The two main tuner constructors are MAURY® and FOCUS MICROWAVE®. A typical bench used for radar power amplifier characterization and design using passive impedance synthesis is shown in Figure 1.8.

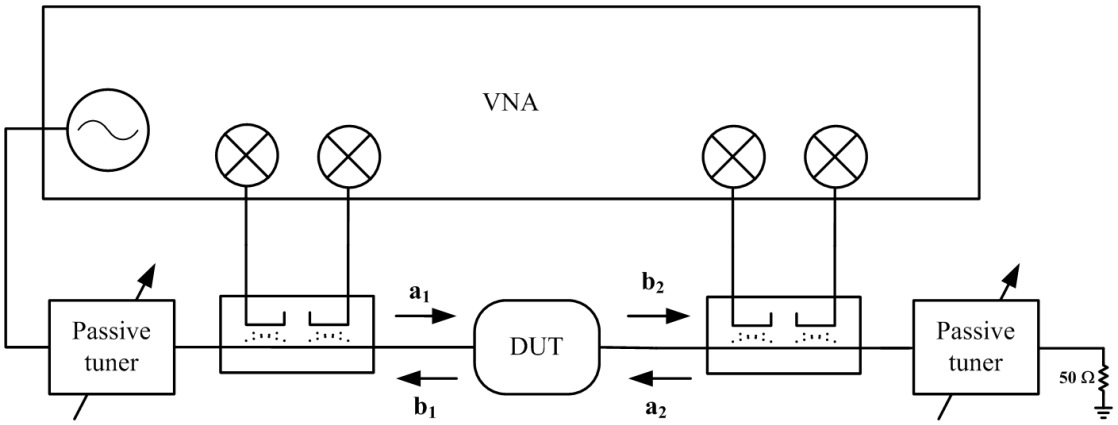

FIGURE 1.8: Typical bench combining measurement and loadpull techniique for radar power amplifier characterization

Active load synthesis

Instead of changing the characteristics of the propagation media, **active impedance synthesis** relies on the generation of the wave that would have reflected a passive load of given wanted reflection coefficient as expressed by Equation 1.15. Both relative magnitude and phase have to be controlled constantly.

$$\Gamma(f) = \frac{a_2(f)}{b_2(f)} \tag{1.15}$$

The first published system using active was proposed by Y. Takayama [23] in 1976 and is presented in Figure 1.9. This system is limited to the impedance control of the fundamental frequency and is not well suited to power sweeping as the impedance is strongly dependent on the excitation signal.

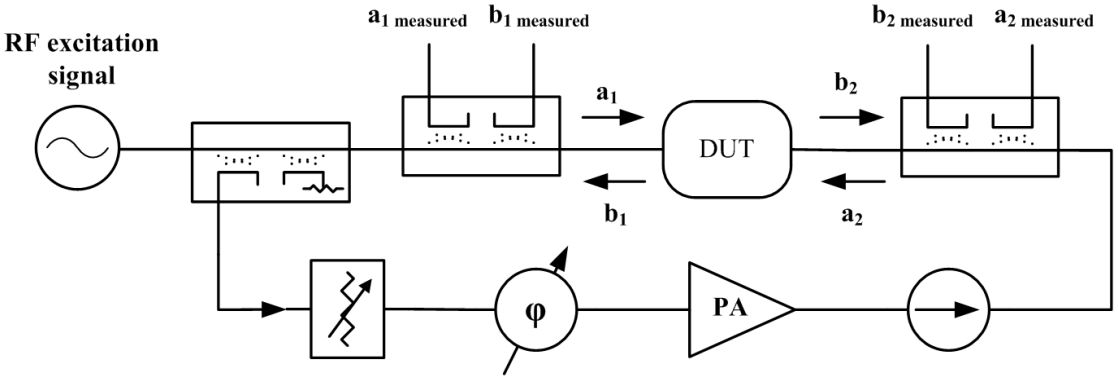

FIGURE 1.9: Active impedance using a loop extracting part of the excitation signal for signal synchronization by Takayama

Later the concept of active loop in Figure 1.10 was proposed. Compared to Takayama's setup the synthesized impedance does not directly depends on the excitation signal therefore it is easier to use such a technique for power sweeping. It is also possible to use all the tones at the output of the DUT and so perform multi harmonics impedance synthesis by multiplying the loops. One drawback of this method is the non negligible risk of oscillation, especially when synthesizing a high reflection coefficient.

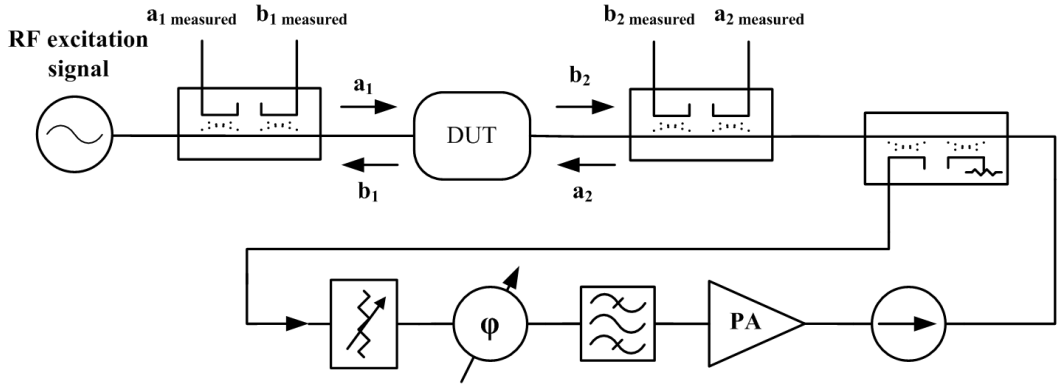

FIGURE 1.10: Active loop example extracting the signal from the output of the device under test

Taking advantage of a new generation of RF synthesizer that can be controlled in amplitude and phase, the open loop configuration in Figure 1.11 was proposed. It allows synthesizing impedances without diverting part of the incident wave which solves the problem of oscillation caused by the active loop concept. However it is possible that the convergence algorithm fails to synthesize the wanted impedance because of changes in the incident wave quicker than the algorithm iteration time. Since some year the open loop concept can be performed directly by a VNA.

Every active synthesis system presented needs measurement of the waves to dynamically follow the eventual changes in the incident wave. Active systems have for advantage to be able to synthesize total reflection and tend to be quicker than passive load pull techniques. In the particular case of power characterization they are difficult to implement because of the extremely high power needed to synthesize a high reflection coefficient and the difficulty to keep it steady. Since the improvement of the sources in terms of stability in frequency, phase and power, the possibility to have synchronized sources and the reduced size of the synthesizer that allows the technique to be embedded on VNAs, it is possible to find it in the

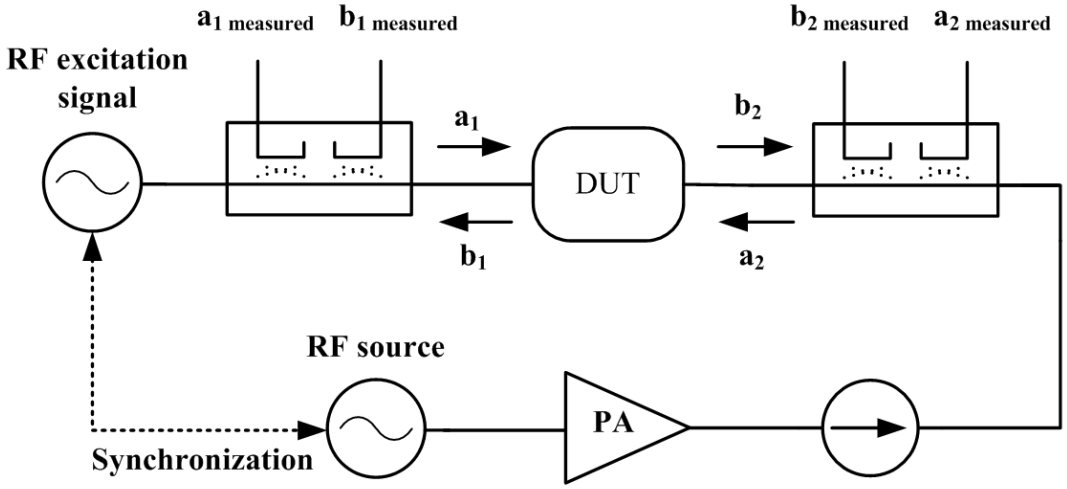

FIGURE 1.11: Active synthesis using open loop, providing more stability

industry at low powers. High power active synthesis can be only found in research laboratory.

Hybrid load synthesis

In order to profit from advantages of both passive and active synthesis concept and minimize their drawbacks, **hybrid setups** are proposed. All of them rely on the relative position of the passive tuner compared to the active loop.

For example in the system in Figure 1.12 the active synthesis is performed going through the passive tuner. This may find limitations in the fact that the tuner can have important losses especially at high frequencies which finally prevents from decreasing drastically the power needed to synthesize a load.

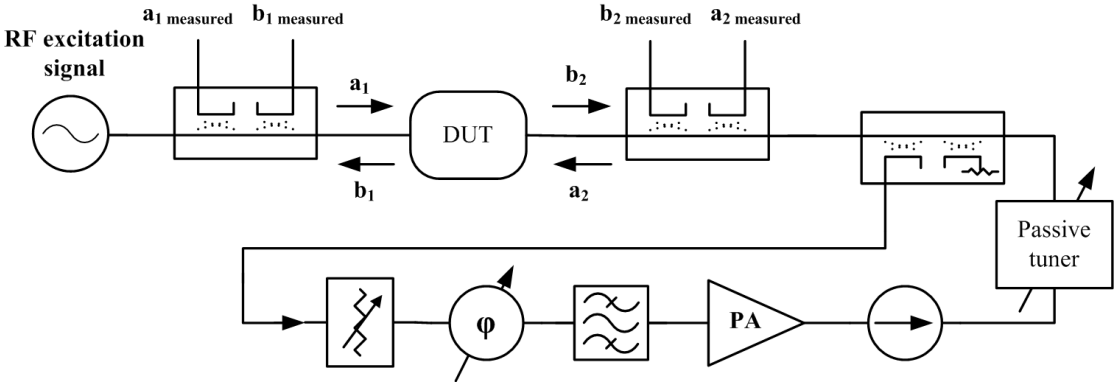

FIGURE 1.12: Load synthesis using both active and passive load pull. The signal for active synthesis flows through the Tuner

Another example in Figure 1.13 proposed for high power does not send the wave for active synthesis through the tuner. However the use of a coupler with a relatively high coupling factor (around 6dB) degrades both the passive and active synthesis at the same time by creating losses.

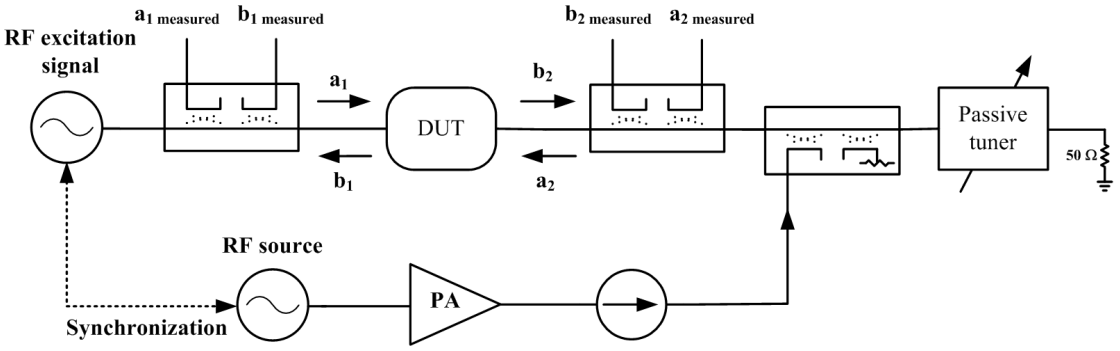

FIGURE 1.13: Load synthesis using both active and passive load pull. The signal for active synthesis does not flows through the tuner avoiding the tuner losses

In this study we will not deal with load pull techniques any longer but it is important to keep in mind that any measurement system destined to radar power amplifier will probably integrate one of these common test benches as load pull is a widely used experiment environment control technique in the radar community.

1.4.2 Linear measurement

For a long time the Linear and Time Invariant (LTI) system was considered an acceptable approximation for radar power amplifier.A system is said to be linear when a linear combination of signals at the input of the system is giving the same combination of output signals. This definition is an emanation of the superposition principle used in physics. This property should remain true whatever the power of the input signal. Nevertheless it is not physically possible to increase the power indefinitely without encountering saturation or destruction of the object. Therefore LTI system theory is only valid in so called small signal.

The time invariance is the fact that the system response is the same whenever the input signal is applied.

In frequency domain, as the Fourier Transform (FT) or the Fast Fourier Transform (FFT) are linear operators, the properties of LTI system imply that the input

and output spectra are composed of exactly the same tones. For low frequencies, LTI system are characterized using voltage and current measured at any point of the input and the output of the system as the system dimension is negligible compared to the signal wavelength. At high frequencies ($\gg$ 100MHz), the dimension of the system are comparable or bigger to the wavelength making the measurement of voltage and current position dependent as scattering effects cannot be neglected anymore.

Even if for high frequencies the concept of equivalent voltage and current taking into account the position dependency is well established and physically relevant, the concepts introduced by K. Kurokawa of power wave and scattering parameters (S-parameters) [24] have been widely used because of their simplicity and ease of use in common given conditions.

Power waves are complex numbers defined in Equation 1.16 and Equation 1.17 used to help the designer visualize power flow, they have no physical existence.

$$a = \frac{V + I.\hat{Z}}{2\sqrt{\Re(\hat{Z})}} \tag{1.16}$$

$$b = \frac{V - I.\hat{Z}^*}{2\sqrt{\Re(\hat{Z})}} \tag{1.17}$$

They are designed to solve matching problem by simplifying the research of maximum power transfer and are therefore particularly used by power amplifier designers. Power waves can be indifferently time or frequency dependent (in addition to the obvious source or load impedance dependence) but the later is usually preferred because of the ease of representing scattering phenomenon as a function of the frequency f.

S-Parameters matrix fully characterizes a LTI system. For example a two port LTI system is characterized by:

$$\begin{pmatrix} b_1(f) \\ b_2(f) \end{pmatrix} = \begin{pmatrix} S_{11}(f) & S_{12}(f) \\ S_{21}(f) & S_{22}(f) \end{pmatrix} \begin{pmatrix} a_1(f) \\ a_2(f) \end{pmatrix} \tag{1.18}$$

The frequency and reference impedance dependent S-parameters are defined by the following ratio of power waves:

$$S_{11}(f) = \frac{b_1(f)}{a_1(f)}|_{a_2=0} \tag{1.19}$$

$$S_{12}(f) = \frac{b_1(f)}{a_2(f)}|_{a_1=0} \tag{1.20}$$

$$S_{21}(f) = \frac{b_2(f)}{a_1(f)}|_{a_2=0} \tag{1.21}$$

$$S_{22}(f) = \frac{b_2(f)}{a_2(f)}|_{a_1=0} \tag{1.22}$$

One drawback of power wave concept is that if the source or load "'complex port number"' $\hat{Z}$ is not real and positive, it cannot be used to cascade linear circuits [25] and is limited to the only impedance matching use. The simple example of a perfect transition shows that power waves are discontinuous if the "'complex port number"' has an imaginary part different than zero. However if the port impedance is real and positive the power waves reduce to impedance normalized traveling wave which are continuous. From now on we will always define both the reference impedance and the port complex number as being equal to 50 Ohm treating indifferently power waves as impedance normalized traveling waves or traveling waves.

Having characterized an LTI system with S-parameters, it is now possible to know the answer of the system to a linear combination of tones as long as the small signal condition is respected.

The strength of S-parameters and power wave representation when used properly is that many useful characteristics of a power amplifier can be directly derived from them. For example for a two port amplifier:

$|S_{11}|$ = Reflection coefficient of the power amplifier's input when output is matched (1.23)

$|S_{22}|$ = Reflection coefficient of the power amplifier's output when input is matched (1.24)

$|S_{21}|^2$ = Transducer power gain with Z_0 load and source (1.25)

$|S_{12}|^2$ = Reverse transducer power gain with Z_0 load and source or power isolation (1.26)

An instrument that can measure all the waves at the ports of an LTI system to calculate the S-parameters and doing it at each frequency of interest would completely characterize the system. A VNA is specially suited for this purpose. A typical LTI system that needs to be characterized is the passive attenuator. It is often used to protect a measurement instrument when dealing with high power; the knowledge of its S-parameters allows shifting the measurement plane of the instrument thanks to de-embedding technique.

On the opposite, the radar power amplifier used at compression cannot be considered as a LTI system because the linearity condition is broken due the power dependency and the production of harmonics. Nevertheless in S-band the non linearity is often simply ignored and only the behavior at the fundamental frequency is observed as a power dependent value.

In the past for the particular case of radar power amplifier design, only the powers at input and output were required. The typical radar characterization bench consisted of measuring the input power, the reflected input power by the amplifier and the output power with power meters as shown in Figure 1.14. This scalar approach has the advantage of simplicity. The contribution of the harmonics on the measured power was neglected. Nevertheless a VNA was used to characterize the different path to have the power value at the power amplifier port. It was also used to characterize the passive matching circuit of the amplifier to be able to use de-embedding to have the power values at the transistor accesses.

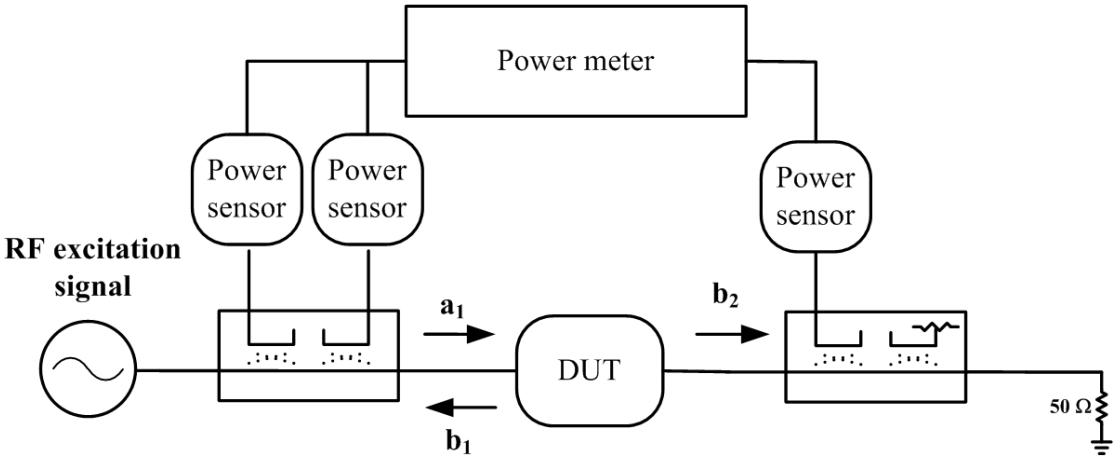

FIGURE 1.14: Example of scalar system, no phase information is measured limiting the use to power acquisition

A newer approach directly includes the VNA on the test bench as shown in Figure 1.15 providing the magnitude and phase behavior of the DUT. Calibration of the VNA is performed in the measurement plane so the different paths do not need to be characterized anymore. This approach, slightly more complex to implement, gives better insight about the amplifier behavior than scalar measurement. In that case S-parameters are used as a power dependent value (which may or not be precisely determined) despite the obvious non linearity.

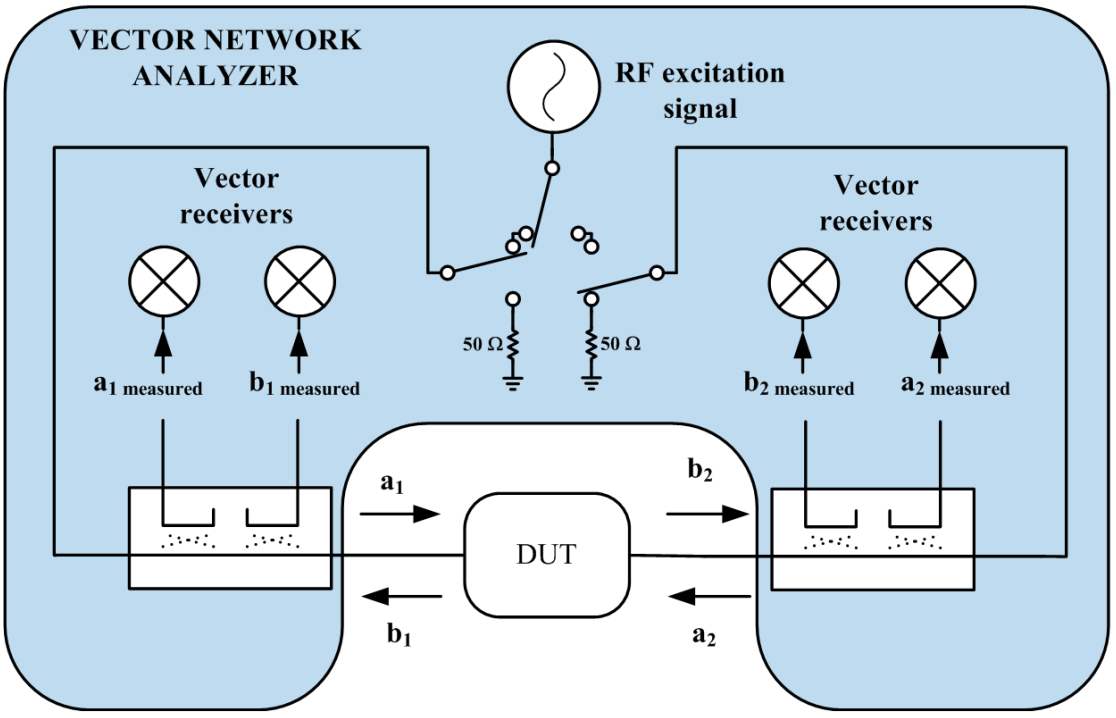

FIGURE 1.15: Example of a vector system. Both magnitude and phase of a signal are measured, fully characterizing linear networks

Since the last two decades the need of understanding effects taking place in different transistor technologies and the general research for higher efficiency has triggered the development of non linear measurement as the previously presented simplifications and approximation were not allowing access to enough knowledge.

1.4.3 Nonlinear Measurement

Generally a system that is not linear is qualified as non linear. However not every non linear systems are equivalent. Considering a system that deviates from

linearity trough a second order term we have:

$$b_2 = S_{21}.a_1 + S_{nl2}.a_1^2 \tag{1.27}$$

When applying an excitation signal of $A\cos(\omega t)$ the system response is:

$$b_2 = \frac{A^2.S_{nl2}}{2} + A.S_{21}.\cos(\omega t) + \frac{A^2}{2}.S_{nl2}.\cos(2\omega t) \tag{1.28}$$

One can see that the system generates a second frequency but that the fundamental signal is unaffected. Using the LTI approximation in that case could be acceptable if we use the system with a single tone. Now if we consider a third order deviation instead:

$$b_2 = S_{21}.a_1 + S_{nl3}.a_1^3 \tag{1.29}$$

When applying the same signal as previously we obtain:

$$b_2 = (A.S_{21} + \frac{3.A^3}{4}.S_{nl3})\cos(\omega t) + \frac{A^3}{4}.S_{nl3}.cos(3\omega t) \tag{1.30}$$

In this case not only there is generation of a new frequency but we also have a modification of the response at the excitation frequency that depends on the input power, affecting the linearity at the fundamental. It would be a rough approximation that may not be good enough.

These two simple theoretical examples show that every non linear system, as they may present a different kind or degree of non linearity, may require different measurement method or performance to be characterized.

In this study, we will mainly focus on the measurement of non linear system that when excited by a periodic signal outputs a signal of the same period. This description fits particularly well a power amplifier working at compression as it outputs the fundamental frequency it was excited by and an undetermined set of harmonic frequencies. We will not deal with chaotic system.

As the behavior of an amplifier is highly dependent on the power of the driving signal, the use of power waves ratios is not indicated as we lose the incident power information which is important as we have seen in the theoretical case of a third order non linearity. Instead we will use the knowledge of the measured incident and reflected waves at each port. The measurement and manipulation of time domain voltage and current waveform is particularly important for the high

efficiency classes. Measurement of those waveforms can be completed indifferently in time domain measuring all the spectral components at the same time or in frequency domain measuring one spectral component at a time minding for the phase coherence. The second chapter will be entirely dedicated to the description of non linear measurement in both domains.

Efforts have been put in order to extract a model out of the collected data. The first attempt was an extension of S-parameters called hot S-parameters [26]. This model was not fitting so well to the behavior of the components in deep compression and has been abandoned for the Poly Harmonic Distortion (PHD) model [27] or the Cardiff model of P. Tasker [28]. The general problem encountered by those models is that the number of parameters that influence them is so important that they have almost no predictive capability when S-parameter for linear system had a lower degree of freedom. We will not deal with the issue of modeling in this work.

Brief history of instrumentation for nonlinear measurement

Non linear measurement as it was just described answers to the need of pushing the knowledge about devices such as transistor further than their linear behavior. As VNA where developed starting from the sixties to answer to the need of practical measurement of S-Parameters, new setups and specialized instruments for nonlinear characterization had to be developed.

The first published work about a nonlinear measurement setup we could find is the one from M. Sipilä et al. [29] in 1988. The setup shown in Figure 1.16 relied on a time domain approach using a 14GHz sampling oscilloscope and a coupler allowing measurement of time domain voltage and current waveforms at the input and output of a DUT in a 50 Ohm environment. To shift the measurement plane to the DUT ports, Sipilä used a calibration of the traveling waves in the frequency domain that consists of two steps:

- Measurement of scattered parameters of the chain at each needed frequency with a VNA
- Measurement of the incident wave power using a standard such as an open or a short to deduce the incident wave power by measuring the reflected

wave. This measurement as to be reproduced for every power used during the characterization of the amplifier.

Despite some limitations due to the sampling oscilloscope triggering and speed of measurement, a calibration requiring many unpractical steps and the rough assumption of perfect sampling head which neglige amplitude and phase distortions, this work present most of the characteristics of modern NVNA.

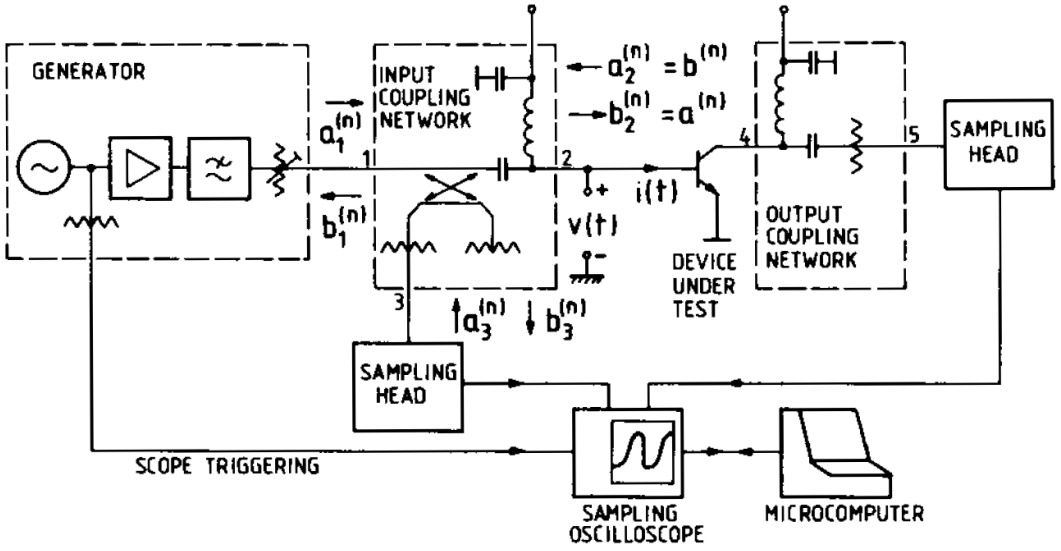

FIGURE 1.16: First setup comparable to modern nonlinear instruments by Sipilä [29]

One year later U. Lott proposed the frequency domain setup of Figure 1.17 based on a VNA and power meter measurement also in a 50Ohm environment [30]. This setup relies greatly on the RF source HP8350 that has two RF outputs, one that can output a signal between 2.3 and 7GHz and another where that base signal can be multiplied up to 26.5GHz. The first output is used as excitation signal for the DUT while the multiplied signal is used as reference for the VNA working only in forward measurement. The S_{21} is therefore measured for every harmonic with preserved phase coherence. Thanks to an absolute calibration procedure in phase using a "golden" diode and in amplitude with a power meter extremely similar to the one used in present NVNA, U. Lott was able to extract the b_2 wave from the S_{21} measurement at each frequency. This setup profits from the better dynamic and speed of the VNA compared to Sipilä's sampling oscilloscope but only the b_2 traveling wave is measured and the calibration procedures suffers from the fact that the "golden" diode is not characterized but considered as ideal.

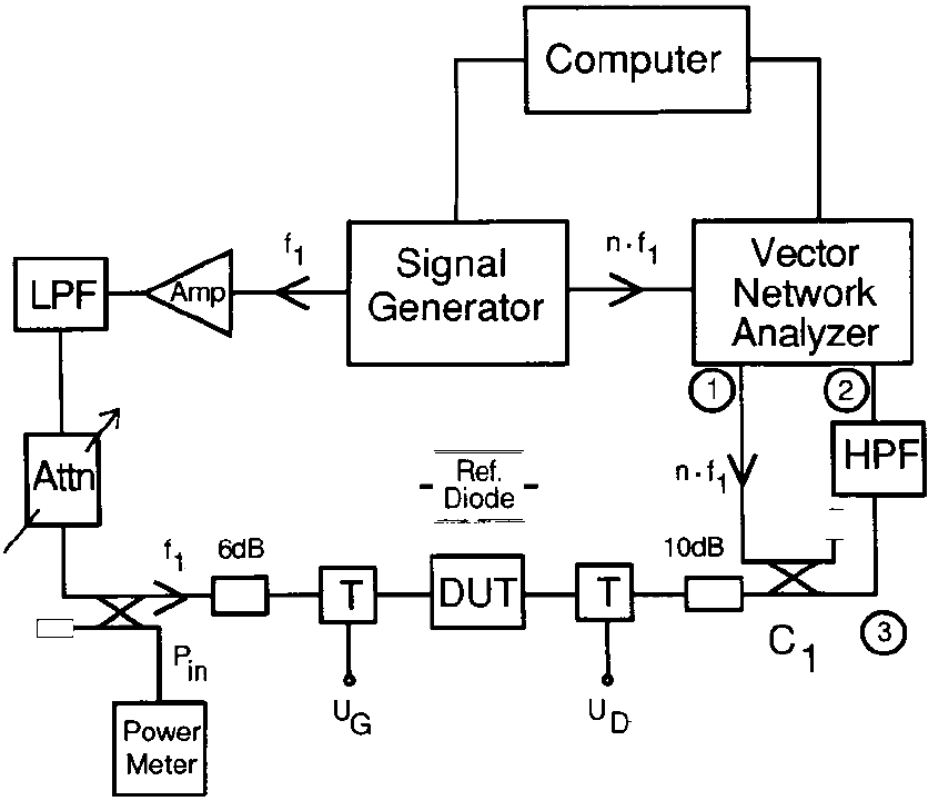

FIGURE 1.17: Setup of U.Lott making use for the first time of a golden device for calibration purpose [30]

In 1990, G. Kompa and F. Van Raay [31] developed a test bench with a time domain approach improved compared to Sipilä's setup. As shown in Figure 1.18 the setup is composed of both VNA and sampling oscilloscopes. The VNA is used for calibration and to measure the S-Parameters of the DUT at the fundamental while the oscilloscope is used to measure the harmonic. The test set is close to the one of a VNA except the reflected wave from the output load is not available. This setup allowed for the first time as far as we know to measure the nonlinear behavior of the DUT using the measurement of incident, reflected and transmitted waves. Compared to Silipä's method, the calibration is not dependent on the input incident wave and the incident wave is used as time reference for all the signals and not to trigger the oscilloscope avoiding triggering imprecision at high frequencies. Nevertheless the use of switches reduce even more the measurement speed compared to the use of single sampling oscilloscope and the calibration relies on the fact that the sampling heads induce no phase distortion.

The year 1992 has been an important year for nonlinear characterization with the commercialization of the Microwave Transition Analyzer (MTA) by Hewlett

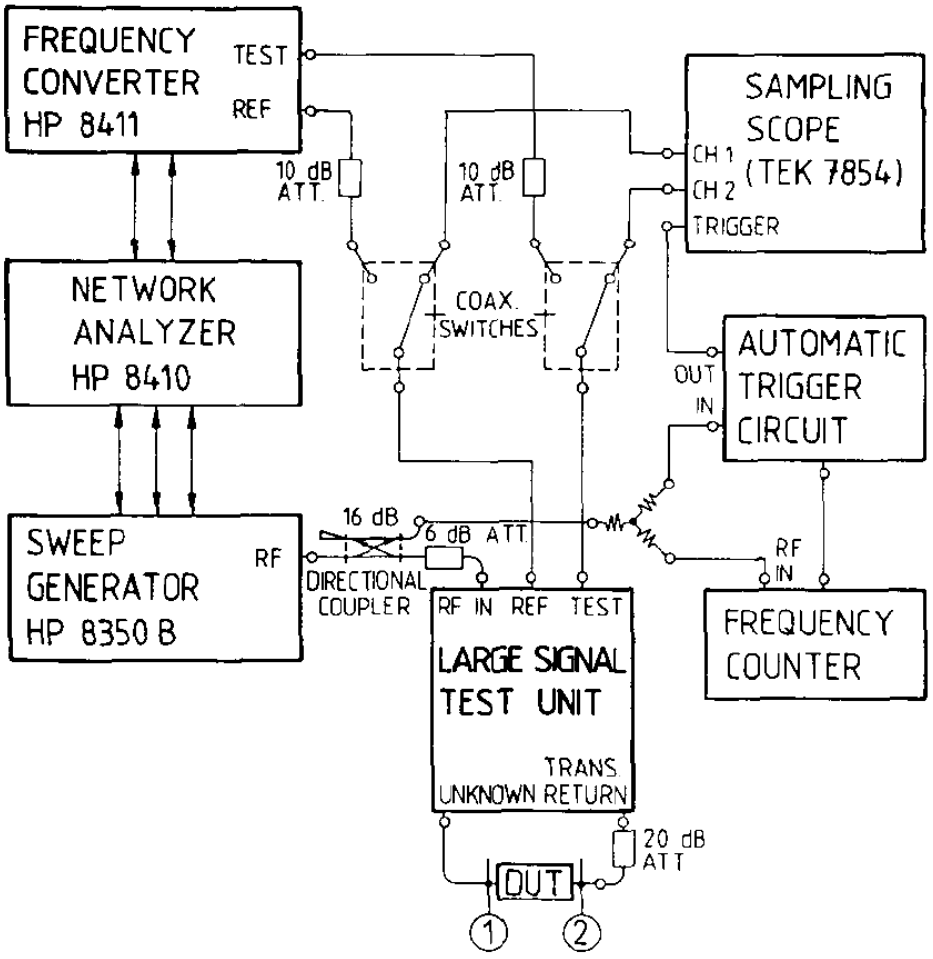

FIGURE 1.18: Time domain setup of Kompa and Van Raay [31]

Packard® [32]. This sampler based time domain instrument presently discontinued could directly measure the amplitude and phase of fundamental and harmonics up to 40GHz. F. Van Raay and G. Kompa replaced in the VNA and sampling oscilloscope of the setup of their previous work by a MTA as shown in Figure 1.19 increasing the measurement speed. The MTA had no calibration procedure implemented in its firmware therefore they had to implement one of their own. They took advantage of the VNA capability of the MTA to vector calibrate their setup using a Thru Open Short Match (TOSM) method. The MTA has been used in several different setup for nonlinear characterization since its release [33] [34] [35].

In 1995 J. Verspecht and his colleagues used two synchronized MTA [36] in order to have a four channels measurement system allowing complete characterization of a two port DUT. This setup is the first prototype of Large Signal Network Analyzer (LSNA) which still presently is a reference for nonlinear characterization. The

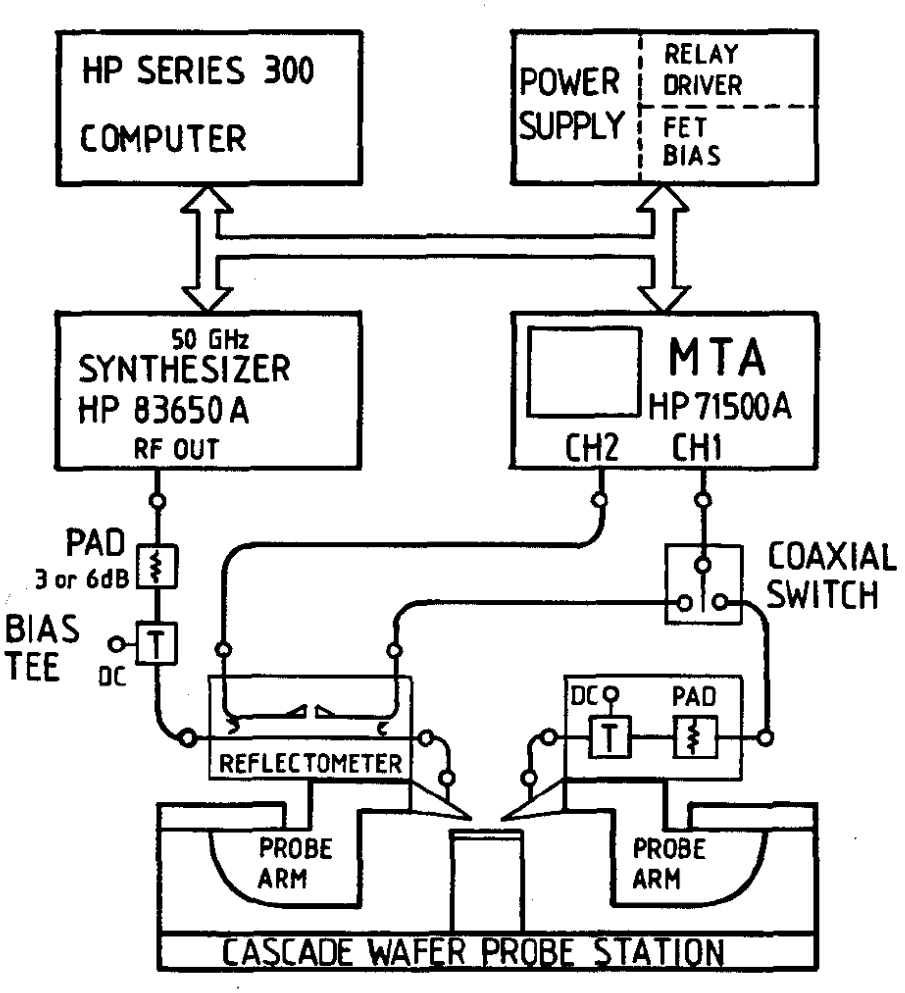

FIGURE 1.19: Setup of Kompa using a MTA with a custom calibration procedure [32]

calibration of this prototype is composed of a VNA calibration and of the absolute calibration as it was proposed by U. Lott. We will be seeing this calibration method in detail in Section 2.4.3 as it is still the calibration method in use today. The LSNA has received a lot of developments allowing it to measure pulsed signal and envelope measurement, it is now discontinued but still in use in many laboratories such as XLIM with J-P. Teyssier [37] and IEMN with D.Ducatteau [38] in France.

In the 1998, mixer based frequency domain approaches using VNA was proposed and applied on amplifiers and frequency multipliers by D.Barataud [39] at XLIM as an alternative to the LSNA. This system had all the characteristics of the presently commercialized solutions; for example by NMDG®, Mesuro® and Agilent Technologies®.

In the last years oscilloscopes, in particular real time oscilloscopes, are being used again for nonlinear measurement due to improvements of their digitizers.

In this work we will be studying the modern NVNA, focusing particularly on the mixer based instruments, but considering the LSNA as the reference instrument as it was specially designed for the purpose of nonlinear characterization.

1.5 Project description

1.5.1 Characterization requirements of the project

The previous description of the study context underlines that improvement of radar systems and in particular the radar power amplifier goes through advanced characterization of the amplifiers within the actual functioning conditions the amplifier is designed for. Thales Air Systems, facing this fact required from a measurement system to be able to:

- Capture the nonlinear behavior of the tested connectorized high power amplifier up to the the third harmonic with a fundamental frequency located in the S-band, implying an effective bandwidth of the measurement system going at least up to 12GHz.
- Visualize frequency and time domain signal indifferently as time domain is well suited for observing load cycles or the overlap between output current and voltage determinant for efficiency while frequency domain allows better visualization of frequency dependent effects as scattering.
- Measure signal in pulsed condition, moreover within non periodic radar pulse train defined by the user corresponding to the actual radar functioning.

Of all the requirements, the measurement of pulsed signal in non periodic radar pulse conditions is the one that triggered this project in order to fulfill it. All the other requirements could be answered with a commercially available nonlinear system.

1.5.2 Building of the project

It appears from the requirements description that the problematic of improving radar systems goes through acquiring expertise in different but complementary fields of the RF engineering, the radar power amplifier design and the instrumentation design. Different, as the set of knowledge required to build radar power amplifiers and a measurement instrument are not the same. Complementary, as each field feed the other toward scientific and engineering progress as there is no power amplification without characterization and characterization is useless without an artifact to measure.

This is the reason why this industrial project, built under the French state CIFRE PhD convention [40] meaning that the student is paid by the company triggering the research project, gather more than a single company or laboratory but instead a collaboration between a set of them. The core group of the project is composed of the following set of entities that signed a collaboration contract:

- **Thales Air Systems®** in Rouen, France, is a radar design and manufacturing group. Its success relies in particular on the expertise in radar power amplification and therefore the knowledge on innovative transistor technologies, their behavior and the capability to quantify these behaviors in realistic conditions for radar application. Thales Air systems defined the requirements of the measurement system that they failed to fulfill with commercially available systems.

- **Rohde&Schwarz France®** is the interface of Rohde&Schwarz® in France and has a double purpose. The first objective is to propose characterization solutions to groups in France relying on the characterization capabilities of Rhode&Schwarz®. The second objective is to provide to Rohde&Schwarz knowledge on customers requirements and innovative characterization needs so new adapted solutions can be proposed in the future. Rohde&Schwarz France® was the employer of the author during this project.

- **Institut d'Electronique de Microélectronique et de Nanotechnologie (IEMN)** in Lille, France, is a research institute of the Université Lille Nord de France (UMR CNRS 8520). Among many fields one of its domain of expertise is both linear and nonlinear characterization of RF components.

The IEMN also provides the scientific guidance of the project and mentored the author all along the project.

To answer to the nonlinear characterization aspect, the project was relying on the help and expertise of NMDG®, as they are providing a mixer based NVNA solution that can work on Rohde&Schwarz® VNA. When the project started, NMDG® and Rohde&Schwarz® had a commercial partnership so it was possible to rely on NMDG® for the nonlinear acquisition aspect. The companies taking part more or less directly to this study are shown in Figure 1.20.

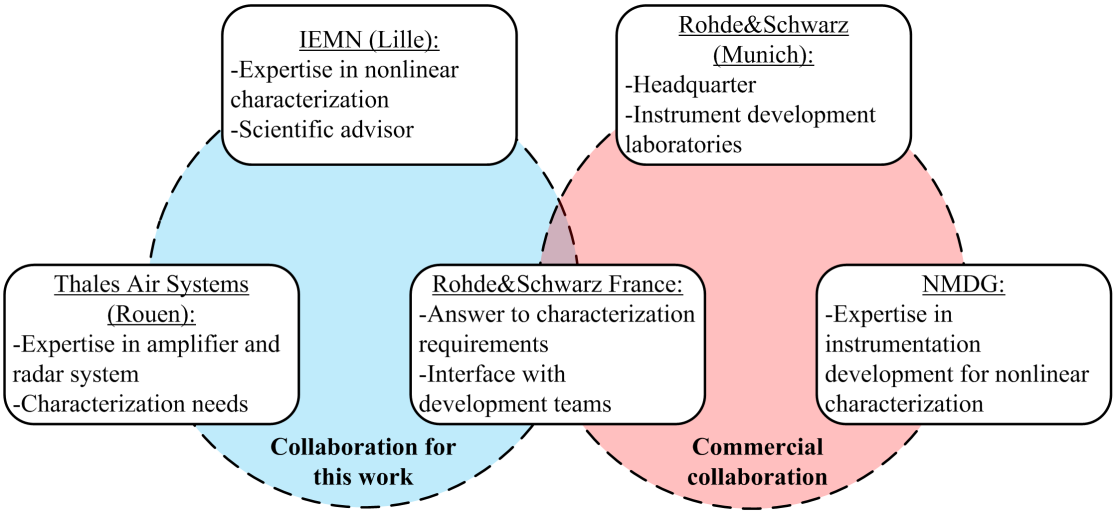

FIGURE 1.20: Project organization between the core group of three entities and related entities

Sadly, within a year in the project, the commercial agreement between NMDG® and Rohde&Schwarz® was broken for unrelated reasons, leaving the project without nonlinear solution nor expertise on building a nonlinear system as shown on Figure 1.21. This unexpected event triggered the need of designing a nonlinear solution of our own almost from scratch as some hardware could be acquired from NMDG®.

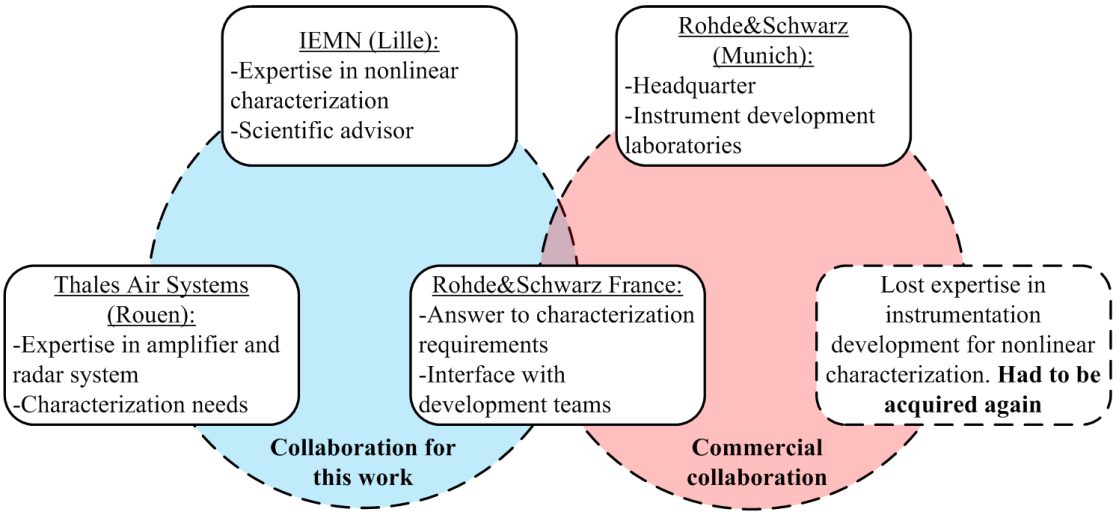

FIGURE 1.21: Project organization between the core group of three entities and related entities after loss of NMDG

1.6 Conclusion

We have seen in this chapter how a deep knowledge of high power amplifier can help improve the radar system. The importance of radar system is such that it deserves dedicated tools and measurements in order to gain in performance. One of the most pressing requirements is to propose a measurement system that can characterize the power amplifier in the actual functioning conditions it will be used once integrated in the radar, which is not yet commercially available. We will propose such a measurement in this work, in particular for the case of S-band primary pulse radar.

As it was explained in the project description of Section 1.5, unexpected events forced us to rebuild nonlinear measurement system from scratch. The designing of such a system will be the topic of the next chapter.

Chapter 2

Conception of nonlinear measurement instrument

2.1 Introduction

The answer to the needs of Thales Air Systems® in terms of radar power amplification nonlinear characterization from Rohde&Schwarz® was to provide the instruments required for nonlinear characterization without providing the entire nonlinear solution as Rohde&Schwarz® had no direct knowledge on nonlinear measurement conception. This part was relying on NMDG® that could not participate to this project after a year due to unrelated commercial disagreement, leaving the project without other viable alternatives than design a new solution of our own from the available instruments in Rohde&Schwarz®.

The first part of this chapter aims at describing and comparing the different measurement acquisition methods available for nonlinear method that were encountered in Section 1.4.3. The acquisition method will not be described and compared from instrument to instrument but instead from the more general point of view of class of receivers. Then a method and an instrument fitting the requirements will be chosen among the possibilities offered by Rohde&Schwarz®.

Once the solutions evaluated, a description of the instrument and its component will be proposed underlining the key features that will influence the nonlinear characterization.

Finally, a nonlinear solution will be implemented and, thanks to the expertise and measurement capabilities of the IEMN, validated in CW as a first step to achieve measurement in non periodic radar waveforms as needed by Thales Air Systems.

2.2 Instrument architecture suitable for nonlinear measurement

2.2.1 Analog to digital conversion

Since 1980 period, Digital Signal Processing (DSP) appeared in instrumentation and later became prevalent as it as many advantages compared to analog signal processing such as increased flexibility, a relatively lower cost for equivalent or superior processing complexity and the ease to store the digital signals compared to analog signal. These advantages are gain at the cost of a poorer resolution. However most of the signal measured by the instruments are analog therefore before benefiting from the digital signal processing we must transform the analog signal into a digital one. This operation is performed by the ADC that is the base block of all modern instruments using DSP. The counter part of the ADC, the Digital to Analog Converter (DAC) is also often used for signal synthesis making them also a base component of trans-receiver. Many architectures of ADC can be found in [41] but they are all reducible to two main steps as shown in Figure 2.1, the sampling and the quantization.

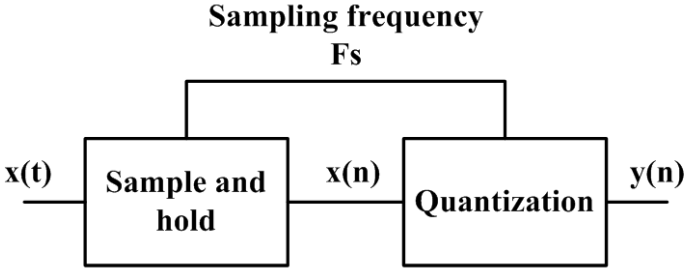

FIGURE 2.1: Common block diagram of an ADC

The sampling operation comes directly from the fact that the digital components work in discrete time up to a maximum frequency (at the time of this work around 500MHz). The analog signal is sampled for quantization at the frequency

f_s therefore the bandwidth of the analog signal to be converted is theoretically limited for a single ADC to the Nyquist's frequency $f_s/2$.

The quantization is the conversion of the analog signal sample into a corresponding digital value. Theoretically, the precision of the quantization depends on the number of bits used to represent the analog signal and therefore on the number of quantization steps (that some constructor call quantization resolution). The speed of this operation has a direct influence on the maximum sampling frequency of the ADC.

For high sampling frequencies applications, the most widely used for single tone analog signal are the Spurious Free Dynamic Range (SFDR), the SNR and the Total Harmonic Distortion (THD) as represented in Figure 2.2. These figures of merit are usually extracted from the spectral analysis of the converted signal. The following description of the figure of merits is following the recommendations of the appropriate IEEE standard for ADC [42].

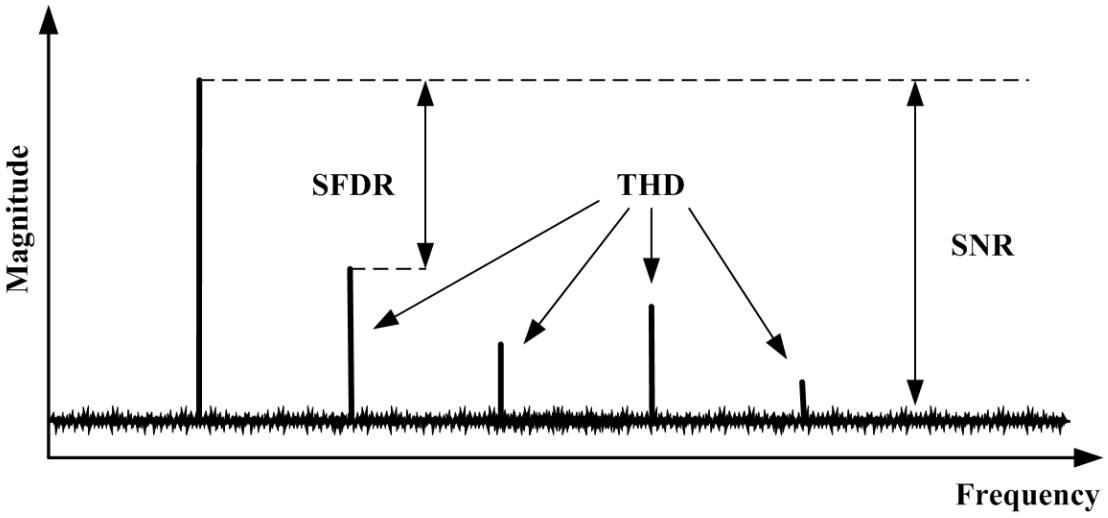

FIGURE 2.2: Main figure of merit for ADC performance evaluation

The SFDR is defined as the difference in dBc between the Root Mean Square (RMS) amplitude of the output signal $A(fundamental)$ and the RMS amplitude of the worst spurious $A(HighestSpurious)$ over the specified Nyquist bandwidth. Some constructor do not consider harmonic frequencies as worst spurious. Both definition are slightly different than the dynamic range definition which is the difference between the amplitude of the highest signal before compression of the

ADC and the amplitude of the lowest detectable signal.

$$SFDR = 20\log_{10}(\frac{A(fundamental)}{A(HighestSpurious)}) \tag{2.1}$$

SFDR determines the smallest detectable amplitude in presence of a large blocking signal.

The SNR of an ADC is the ratio between the RMS amplitude of the signal to the square root of the noise power spectrum over the Nyquist frequency range.

$$SNR = 20\log_{10}(\frac{A(fundamental)}{\sqrt{\sum Noise(Band)^2}}) \tag{2.2}$$

The THD is the ratio of the sum of the harmonics to the fundamental frequency. Generally only the first six harmonics are used.

$$THD = 20\log_{10}(\frac{\sqrt{\sum Harmonics^2}}{A(fundamental)}) \tag{2.3}$$

Often the THD is considered as noise and gather with the SNR into the SIgnal to Noise And Distortion (SINAD). The theoretical model of a ADC states that the maximum quantization error is equal to $\frac{3}{2}$, but a real circuit will be influenced by all sources of noise and distortion quantified by the SINAD, reducing the effective quantization resolution. A figure of merit that characterizes how far an ADC is from theoretical model is the Effective Number of Bits (ENOB) which is the logarithmic difference between ideal and effective quantization noise converted in bits.

$$ENOB = \frac{SINAD - 20\log_{10}(\frac{3}{2})}{20\log_{10}(2)} = \frac{SINAD - 1.76}{6.02} \tag{2.4}$$

The equation 2.5 is only valid for full scale analog signal, in case of input with a lower amplitude the ENOB value must be corrected as following:

$$ENOB = \frac{SINAD - 1.76 + 20\log_{10}(\frac{FullScaleAmplitude}{InputAmplitude})}{6.02}) \tag{2.5}$$

Generally the ENOB quantifies the quality of an ADC, but is also influenced by the jitter of the sampling clock. In fact the measurement time uncertainty will increase the noise of the ADC and therefore reduce the ENOB if the jitter effect is

superior to the quantization error. Jitter tends to increase with the clock frequency making it highly influential in high speed ADC.

All the suitable instruments for nonlinear characterization integrate analog to digital conversion to use the possibilities of digital signal processing. Independently of their specific architecture, all the instruments, we will see in following parts, can be reduced to three parts: the RF front end, the analog to digital conversion and the digital signal processing.

In theory a 16 bits ADC should have a dynamic range of 96dB but the noise and distortion effects may make it drop of more than 10dB. As the noise increases linearly with the bandwidth B in Hz according to Equation 2.6, where T is the temperature in Kelvin and K the Boltzmann constant, a large bandwidth ADC will have a lower dynamic range and quantization resolution. This is a fundamental physical limitation that was also shown in [43] using Heisenberg's uncertainty principle.

$$N = KBT \tag{2.6}$$

A tradeoff between bandwidth and dynamic range has to be considered, explaining why it is uncommon to find high resolution ADC with a large bandwidth. To limit the effects of this tradeoff, different techniques can be used such as dithering or oversampling or when possible both at the same time.

Dithering

Dithering is a particular case of stochastic resonance concept [44] that use additional controlled noise to improve the detection of a low power signals [45]. The additional noise allows the Least Significant Bit (LSB) of the ADC to oscillate between 0 and 1 in presence of a small signal allowing its detection over time through averaging. This method increases the dynamic of the ADC at the cost of increased noise as shown in Figure 2.3. As an increase of the noise also result in a loss of dynamic, one must chose wisely the level of added noise to not lose the benefit of dithering or use noise shaping to limit the increase of noise into a useless band as in Figure 2.4. Dithering can be considered as a modification of the discretization in amplitude. Many dithering techniques and their practical implications can be found in [46].

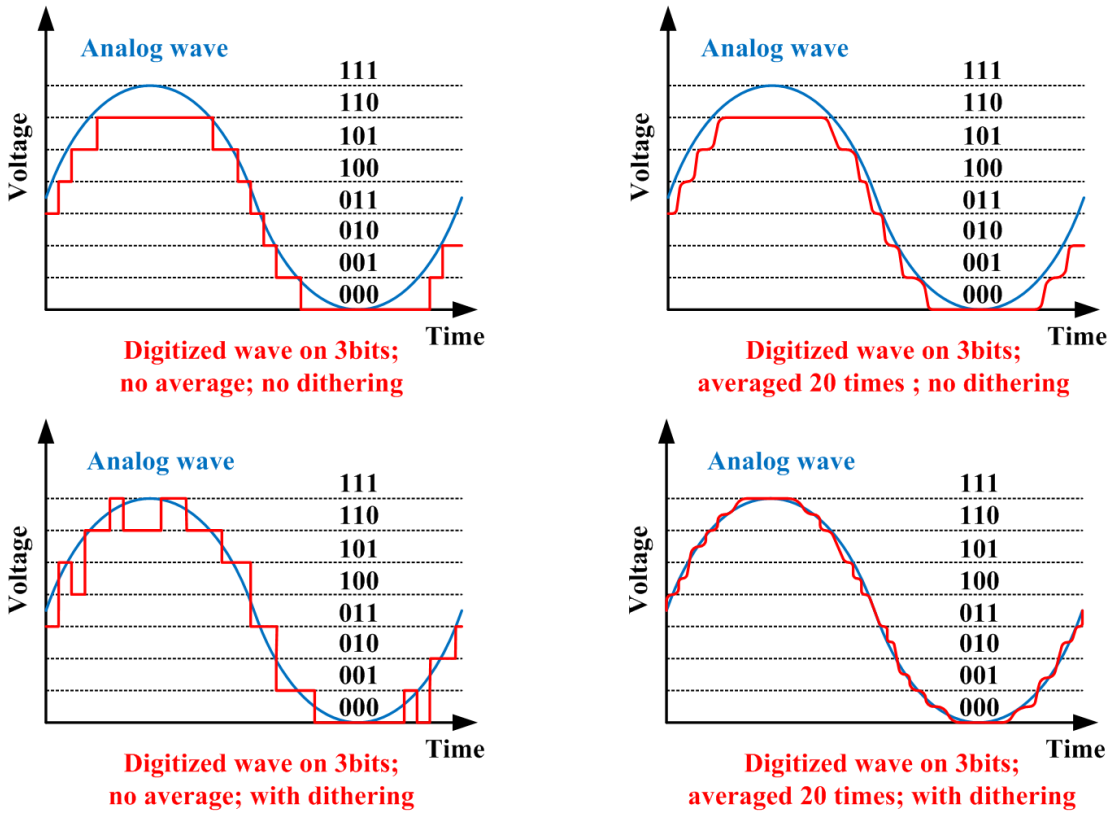

FIGURE 2.3: Effect of signal dithering on the sampled signal in time domain, with and without averaging

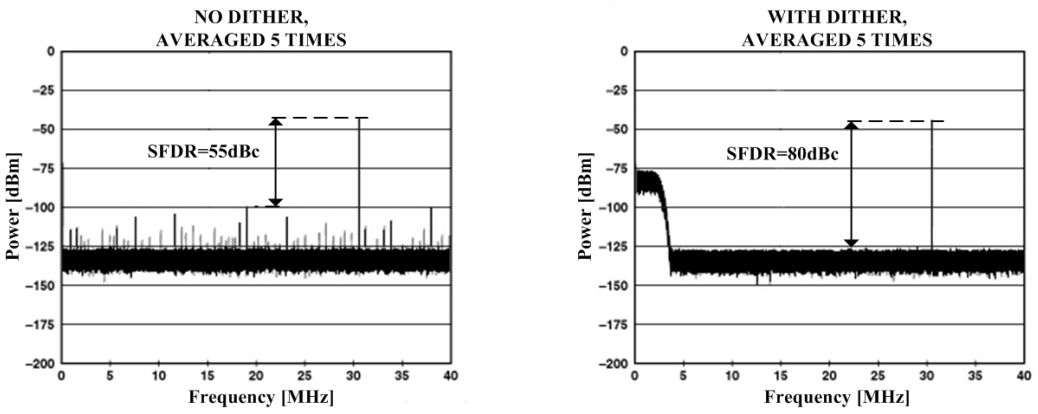

FIGURE 2.4: Noise shaping for dithering in frequency domain, the noise is added on a part of the bandwidth that will not be used

Oversampling

Sampling an analog signal above its Nyquist's frequency is called oversampling. Oversampling a signal by N means that the signal is sampled at N times its Nyquist rate. Having N times more sample than required it is then possible to decimate them until reaching a number of samples corresponding to the Nyquist

rate. Such decimation can be done for example by averaging the sampling result on N samples. Oversampling improves the SNR and therefore improves the ENOB of 1 bit every time the sampling frequency is multiplied by 4 compared to the Nyquist rate. Oversampling can be considered as a modification of the discretization in time. Dithering and oversampling are often used together as dithering requires decimation to be effective.

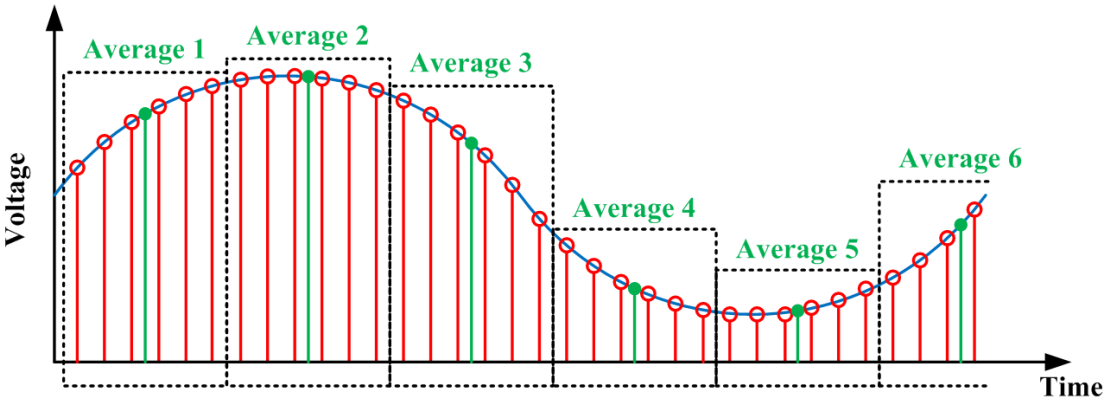

FIGURE 2.5: Signal sampled above Nyquist's frequency or oversampled. Sampling frequency can be reduced in this example by averaging

2.2.2 Digitizer based architecture

A digitizer is the most straightforward application of the ADC. The role of the digitizer is to take care of signals that fits the Nyquist theorem. The low pass filter before the ADC in Figure 2.6 is called anti-aliasing filter as it is used to cut every frequency above the Nyquist's frequency. The digital version of the signal is then memorized until processing.

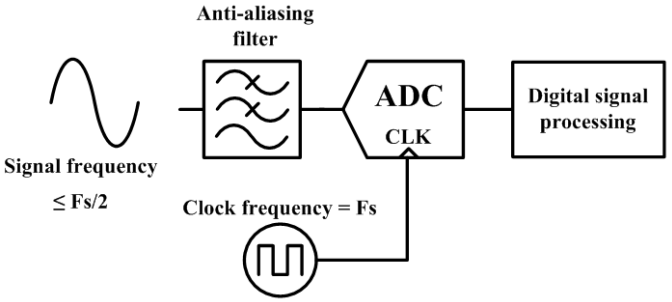

FIGURE 2.6: Common digitizer block diagram

Using the oversampling method it is possible to lower the constraint on the anti-aliasing filter as in that case the first aliasing frequency is not happening in the

frequency band of the analog signal. The filter does not need to be as steep as if we where sampling at the minimum sampling rate. The use of dithering may not be possible because of the increase of noise.

The performance of a digitizer is mostly the performance of the ADC so the same figure of merits we have seen in the previous part apply. To increase the bandwidth of a digitizer, ADC interleaving technique is often used.

ADC interleaving

ADC interleaving is a technique that uses a number N of ADCs sampling simultaneously the same signal with a defined clocking relationship between them, producing digital signals that once combined result in a sampling bandwidth N times superior the the one of a single ADC. Figure 2.7 shows an example with two ADCs.

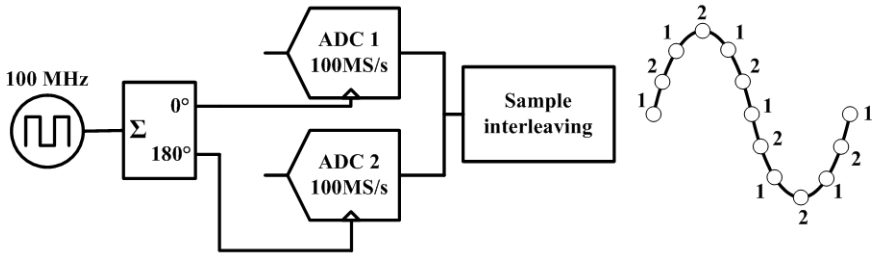

FIGURE 2.7: Principle of interleaving. In this example the sampling frequency is doubled

For interleaving to work, both ADCs must have the same sampling rate. The clock signal of each ADC must be phase shifted according to Equation 2.7 in order to have a uniform repartition of the samples in time. Then the digital signal is reassembled using a multiplexer thus doubling the bandwidth compared to a single ADC.

$$\Delta\phi = \frac{n-1}{m}.2\pi \tag{2.7}$$

with n the ADC index and m the total number of ADCs

This technique however generates spurs in the output spectrum caused by the imperfections in associating ADCs with slightly different characteristics. There are four basic mismatches that cause imperfection in interleaving ADCs, the offset mismatch, the gain mismatch, timing mismatch and bandwidth mismatch.

The offset mismatch is a difference of DC offset between the ADCs. The interleaved digital signal will be alternating between those different DC values at the frequency $f_s/2$ creating a spur at the same frequency in the output spectrum as shown in Figure 2.8. As the spur is always located at the same frequency independently of the analog signal frequency or even in absence of analog signal it is easy to recognize the phenomena. It is solvable by modifying the DC offset of one of the ADCs to fit the offset of the other.

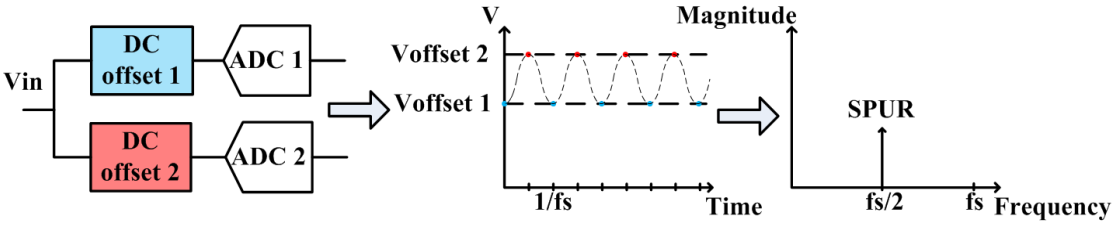

FIGURE 2.8: Offset mismatch using interleaving creating a spur at frequency $f_s/2$

Contrary to offset mismatch, gain mismatch appears only in presence of an analog signal. Two ADCs having different gain will create an interleaved response with spur signals at $f_s/2 \pm f_{analog}$ as shown in Figure 2.9. Improving the gain matching of the ADCs is again the solution.

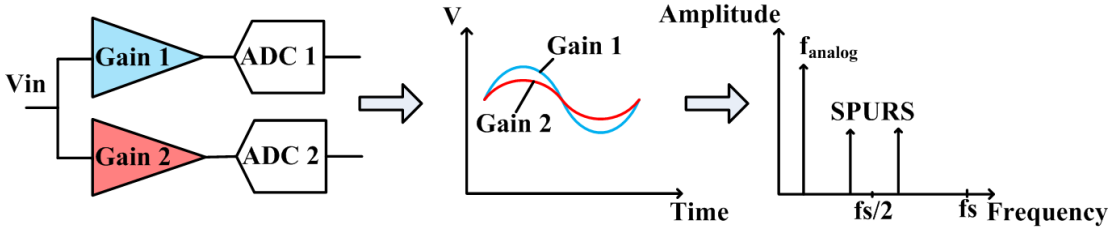

FIGURE 2.9: Gain mismatch using interleaving creating a spurs at frequencies $f_s/2 \pm f_{analog}$

Another source of spurs at $f_s/2 \pm f_{analog}$ is timing mismatch shown in Figure 2.10. Timing mismatch is actually a sum of multiple timing phenomena such as phase mismatch on both the analog or clocking path of the ADCs or clock skew. This effect can be limited with appropriate circuit design.

Bandwidth mismatch can also be limited with appropriate circuit design. Bandwidth mismatch happens when the dispersion parameters in both ADCs analog path are not identical, therefore we see frequency dependent gain and phase mismatch that also produce a spur at $f_s/2 \pm f_{analog}$.

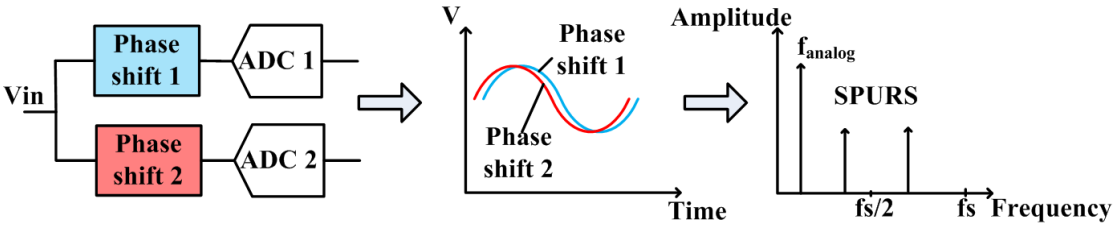

FIGURE 2.10: Interleaving timing mismatch interleaving creating a spurs at frequencies $f_s/2 \pm f_{analog}$

These phenomenon are practically limiting interleaving to 8 to 12 bits ADCs preventing instruments using this method to combine large bandwidth with high resolution and dynamic range. Nevertheless new digital signal processing and design could allow to interleave 15bits ADCs [47] enabling 125MHz sampling frequency.

Instruments based on digitizer architecture

This type of architecture is used by a category of spectrum analyzer called FFT analyzer. The FFT analyzer is a low frequency spectrum analyzer that is not so common anymore [48].

Digitizer are used also in the more common digital oscilloscopes.There are many types of digital oscilloscopes having all their own capabilities but one can roughly separate them in two categories, real time and equivalent time digital oscilloscopes.

A real time oscilloscope or single shot oscilloscope is digitizing an analog signal at a rate equal or above the Nyquist frequency. Interleaving is usually used to be able to operate at bandwidths up to several dozens of GHz [49] relying only on digitizer. Such an oscilloscope can be used to measure transient or glitches in the signal.

Equivalent time oscilloscopes is able to acquire signals that have a bandwidth above the Nyquist frequency at the condition that the signal is periodic. The oscilloscope in that case store samples acquired at different period of the signal until it has enough of them to reconstruct the signal. Using this technique it is possible to measure high bandwidth signals at the cost of measurement speed.

2.2.3 Sampler based architecture

Contrary to a digitizer, a sampler also measure signal that may be superior to half the sampling frequency. Sampling under the Nyquist frequency is usually referred as under-sampling, bandpass sampling, Intermediary Frequency (IF) sampling or harmonic sampling.

Under-sampling leads to the aliasing phenomena that prevents correct signal analysis. Nevertheless if during digital signal processing we know what are the frequencies that we are detecting it is possible to identify all the tones despite aliasing.

As we can see in Figure 2.11, samplers have no aliasing filter but instead a sampling head or a track hold device. The role of the sampling head or the track hold device is to down-convert the analog signal into a new signal that has a bandwidth suitable for the ADC to digitize it. The bandwidth of the ADC depends on the expected bandwidth of the IF signal, setting limitations on the dynamic.

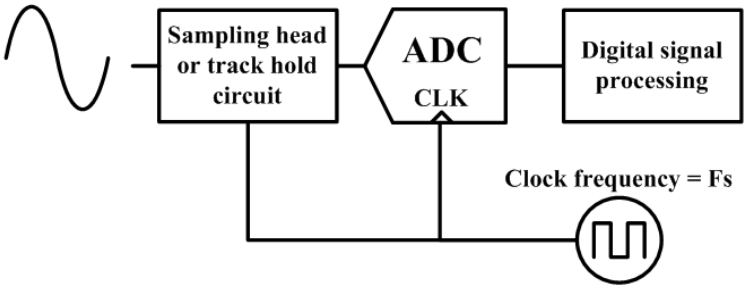

FIGURE 2.11: Common sampler block diagram

With this type of architecture it is possible to use oversampling and to some extent dithering. Dithering however is dangerous to use in that case because it may degrade too much the dynamic while it is already degraded by the use of large bandwidth ADCs. ADC interleaving should be usable but also at the cost of a resolution limitation.

The history of samplers is extensively described in [50], we will see in particular the subharmonically pumped mixer.

Subharmonically pumped mixer

Subharmonically pumped mixers are mixers that use the harmonics of a local oscillator in order to down-convert a signal. This type of mixer was developed to be used at high frequencies where the synthesis of a high-power low noise LO source was difficult to obtain.

To be used as a sampler, the mixer's local oscillator continuous wave is replaced by a pulsed signal. The pulsed signal is generated by feeding an continuous signal to a pulse generator that will generate a pulsed signal with the same period as the continuous signal.

In the frequency domain this means that the mixer has for LO signal a comb with a tone spacing equal to the frequency of the signal feeding the pulse generator and a bandwidth depending on the rising time of the pulse. This comb also limits the tone spacing of the measurable signal.

Such a sampler has a bandwidth above 50GHz but also a large conversion loss (around 30-40dB) and therefore requires amplification before feeding to the ADC. Many intermodulation products are produced so an anti-aliasing filter is still used after the down-conversion as shown in Figure 2.12. The dynamic range of such a sampler is usually inferior to 65dB

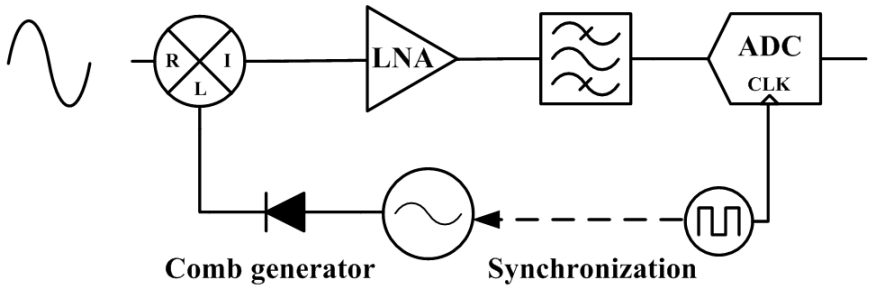

FIGURE 2.12: Harmonically pumped sampler use a local oscillator signal rich in harmonics to bring all the frequency components to intermediary frequency bandwidth

Track and hold circuit

A track hold circuit is designed to track and sample an analog signal and then hold the sampled value for the necessary time to be processed and finally start tracking again. Such a circuit transform an analog signal in a succession of steps.

However this step signal is not equivalent to the quantized signal that is outputted by an ADC as the step can take any value within the range of the circuit. A basic example of track and hold circuit is shown in Figure 2.13.

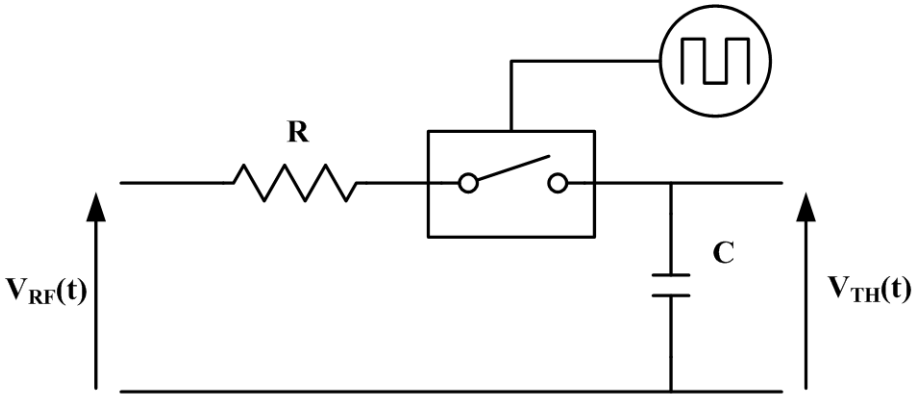

FIGURE 2.13: A basic track and hold circuit implementation

To alternate between the tracking and the holding phase a clock is used. As shown in Figure 2.14 during half a period of the clock the circuits tracks the signal and then hold it during the other half.

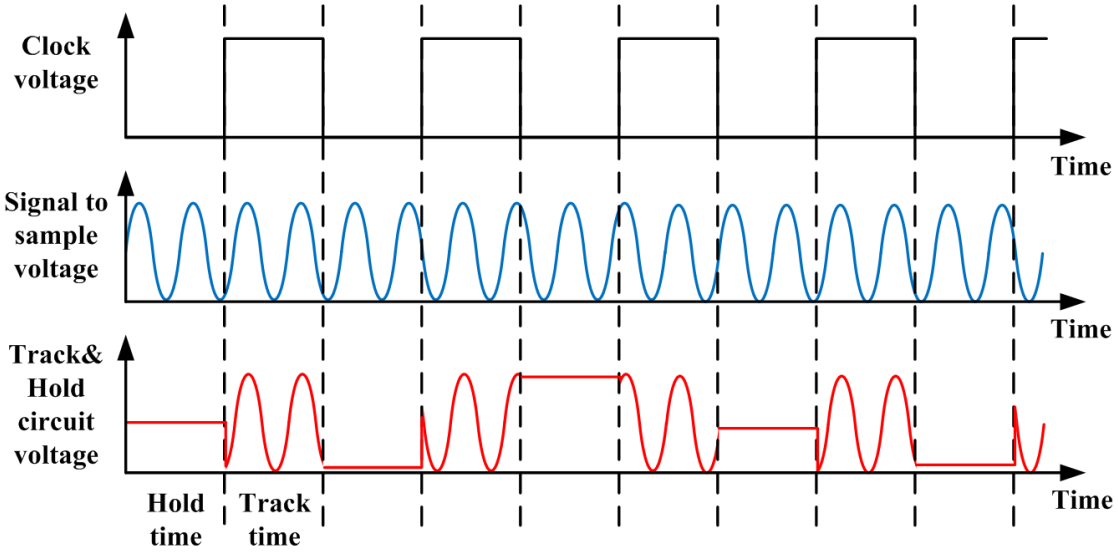

FIGURE 2.14: Alternance between tracking and holding state of a Track&Hold circuit triggered by a clock signal

A common implementation of track and hold circuit is the track and hold amplifier that is explained in [51].

With a maximum bandwidth inferior to 20GHz, this circuit is not adapted to high frequencies measurement however in its bandwidth a track and hold device

shows a better dynamic range than a sampler (around 70dB). As no frequency that would cause aliasing in the ADC is produced no anti-aliasing filter is required. In the case of a track and hold amplifier the conversion loss is small enough to not use an amplifier to feed the ADC. As shown in Figure 2.15 the circuit before the ADC is simplified also because the ADC and the track and hold circuit can use a common clock.

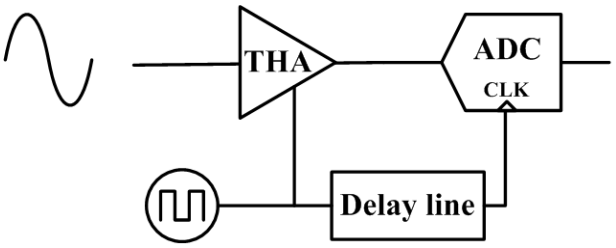

FIGURE 2.15: Circuit with track and hold amplifier instead of the harmonically pumped mixer

To produce a 100GHz sampler, the company Picosecond® proposed the circuit in Figure 2.16 combining down conversion by a mixer to a frequency suitable for a track and hold amplifier that down converts the signal to feed an ADC combining both the described approaches [52].

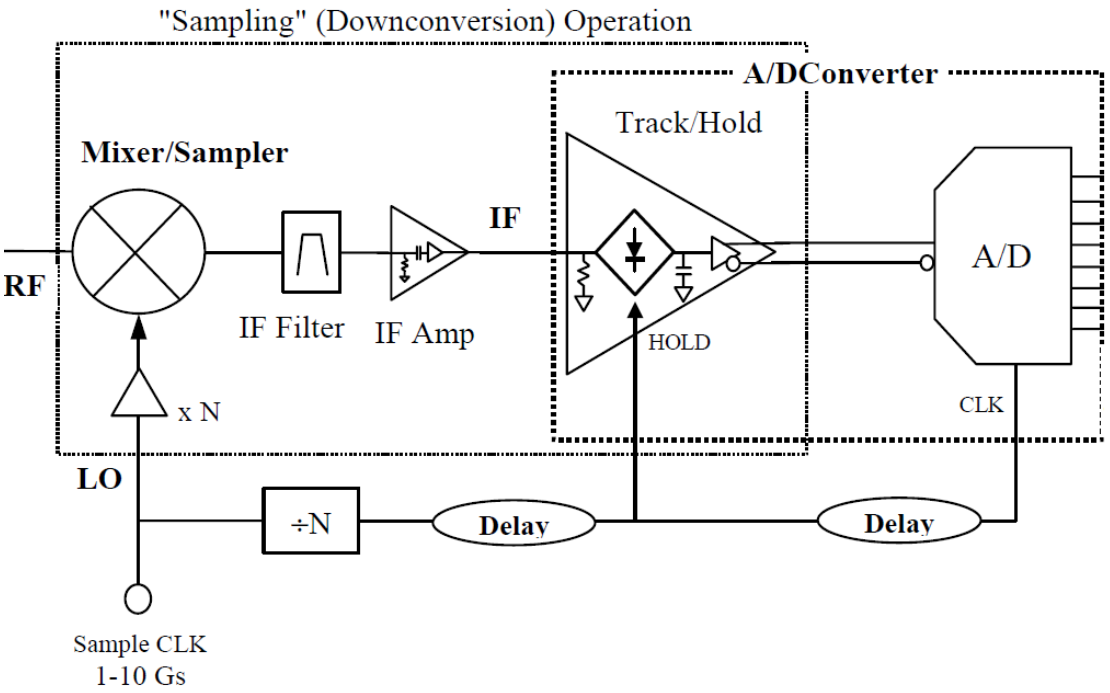

FIGURE 2.16: Hybrid circuit track hold amplifier mixer taking advantages of the gain of the amplifier while the mixer is used to increase the bandwidth [52]

Instruments based on sampler architecture

The LSNA is based on the harmonic sampling principle. The "sampling converter" MT44664 is using the subharmonically pumped mixer principle to downconvert the signal for the ADC. The pulsed signal characteristics are chosen so the sampling head can downconvert an analog signal into the Nyquist's bandwidth of the ADC. Historically the 50GHz instrument has a dynamic range of 60dB. The company VTD® proposed a version of the LSNA called SWAP and is now the property of Agilent Technologies®.

Track hold amplifier have been used by S. Ahmed at XLIM in [53] to replace the sampling head by the LSNA allowing improved dynamic range up with a bandwidth limited to 13GHz.

2.2.4 Mixer based architecture

Mixer based architecture of Figure 2.17 is more commonly referred as heterodyne receiver. The principle is to use a mixer to downconvert the signal to be treated by the ADC, but compared to the sampler described in 2.2.3 the local oscillator signal is composed of a single frequency CW signal that is swept along the bandwidth. Doing so the tones of the signal are treated sequentially and downconverted at a constant IF value. Having a constant IF value allows to relax the specification in bandwidth of the ADC allowing instead high quantization resolution providing a relatively better dynamic compared to the sampler architecture. Measuring each tone separately has for drawback to slow down the acquisition and the high quantization resolution prevents from using interleaving techniques but in exchange it is possible to measure any tone spacing.

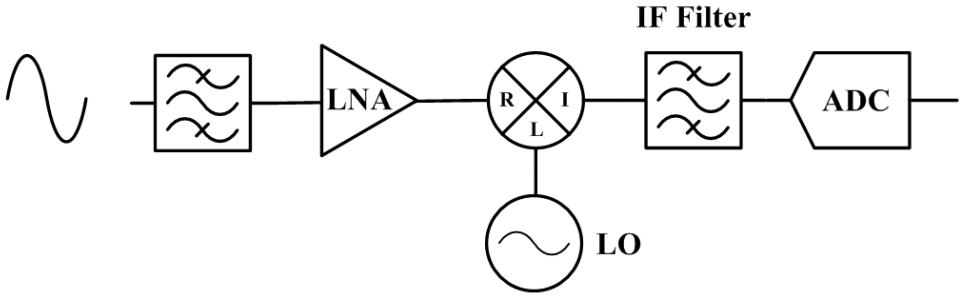

FIGURE 2.17: Common heterodyne receiver block diagram

Using such a receiver, every tone that has a frequency inferior to $f = f_s \pm RBW/2$ is also measured where Resolution BandWidth (RBW) is the bandwidth of the IF filter. The IF filter is therefore of prime importance to reduce the noise and therefore have a good dynamic range. However a steep filter will have a really long response time slowing down the measurement.

When designing a heterodyne receiver one must be careful to filter out the image frequency. The image frequency is a tone that does not have the same frequency as the signal we want to measure but as the same IF frequency once it is down-converted preventing the measurement of the wanted tone.

$$f_{img} = f \pm 2f_{IF} \tag{2.8}$$

In the practical case of radio receiver this phenomena causes the user to hear two stations at the same time or an increase of noise of the radio station. To reject the image frequency it is possible to add a bandpass filter before the downconverting mixer or use an image rejection mixer.

It is possible with this type of receiver to use both dithering and oversampling because the IF frequency is fixed and chosen. Often these receiver use high resolution ADC around 18 bits or even more closing the door to interleaving technique.

Instruments based on heterodyne principle

Many common instruments are using heterodyning, such as spectrum analyzers, signal analyzers and vector network analyzers.

Spectrum analyzers using heterodyne receiver have a way larger bandwidth compared to the FFT analyzer of part 2.2.2. As the spectrum analyzer is designed to measure signal by only presupposing of its range, a lot of effort is put into filtering the image frequency. Sadly spectrum analyzers are not yet designed to measure the phase of the tones and is therefore not a good candidate for nonlinear measurement.

Signal analyzers are often used for the measurement of modulated signal for telecommunication protocols. The frequency measured is usually fixed by the protocol used and a large IF filter is used to be able to measure all the frequency components caused by the modulation at the cost of a deterioration in dynamic

range. The image frequency filtering it easier to perform than on a spectrum analyzer because of the precisely predefined application and therefore the appearance of this spur is predictable. This category of instrument is not used for nonlinear measurement because of the limited number of measurement channels.

Vector network analyzers finally are probably the cornerstone of RF measurement. A measurement with a VNA is highly controlled as the instrument sends the excitation signal and prepare itself to receive the same frequency as we have seen in part 1.4.2. When used to characterize a linear system, the highly specialized VNA has the best dynamic range compared to all the other instruments described with a figure often stated above 110dB up to 67GHz.

2.2.5 Comparison of the receiver concepts for non linear measurement

All receiver concepts that were described are potentially suited for nonlinear measurement as they all have the potential for amplitude and phase measurement of a RF signal. In Table 2.1 they are compared according to characteristics that are important for nonlinear characterization of components:

- The dynamic range that was defined in Section 2.2.1.
- The frequency bandwidth
- The minimum measurable frequency spacing between two tones in frequency domain within the bandwidth
- Designed for multi-tone measurement
- The signal acquisition speed

As all the receiver concepts rely on the same component namely the ADC, an improvement in the field of DSP or ADC should profit to every receiver, not modifying the comparison established. Nevertheless the choice between the receiver architecture highly depends on the DUT and on the type of characterizations that need to be undertaken. If one expects from the DUT many tones of different powers the dynamic is important but if one wants to observe transient effects the measurement speed should probably be favored.

	Dynamic range	Frequency bandwidth	Minimum tone spacing within bandwidth	Designed for multitone measure-ment	Measurement speed
Digitizer	Inferior to 60dB	Limited by the absence of downcon-version around 20GHz	Not limited	Yes	Good
Sampler with harmonic mixer	Inferior to 70dB	At best limited by the LO comb signal used for the downconver-sion around 50GHz	Limited by the tone spacing of the comb. Often around tenth of MHz	Yes	Good
Sampler with track hold amplifier	Inferior to 80dB	Inferior to 18GHz	Not limited	Yes	Good
Heterodyne	Superior to 100dB	Superior to 100GHz	Limited by the LO generator frequency step. Often found around 1Hz	No	Poor

TABLE 2.1: Receiver technologies comparison in terms of dynamic, bandwidth, measurable tone spacing, and measurement speed for nonlinear measurement suitability evaluation

In this work a mixer based instrument will be used as it is the most mature solution proposed by Rohde&Schwarz®. The advantage of this class of instrument is that it allows potentially the best dynamic which is an important characteristic for radar high power amplifier characterization, as it allows power sweeps and the measurement of weak tones. Sadly the dynamic comes at the cost of measurement speed and therefore complicates the study of transient effects. Attention will be required on the effects of a multi-tone signals on an receiver designed mostly for single tone measurement. The good frequency bandwidth is a plus but is not critical as we will work at a maximum frequency of 12GHz. Within the mixer based instruments, a VNA modified for the needs of nonlinear measurement will be used as it is the most suited in terms of performance, number of measurement channel and versatility.

2.3 N-port vector network analyzer description

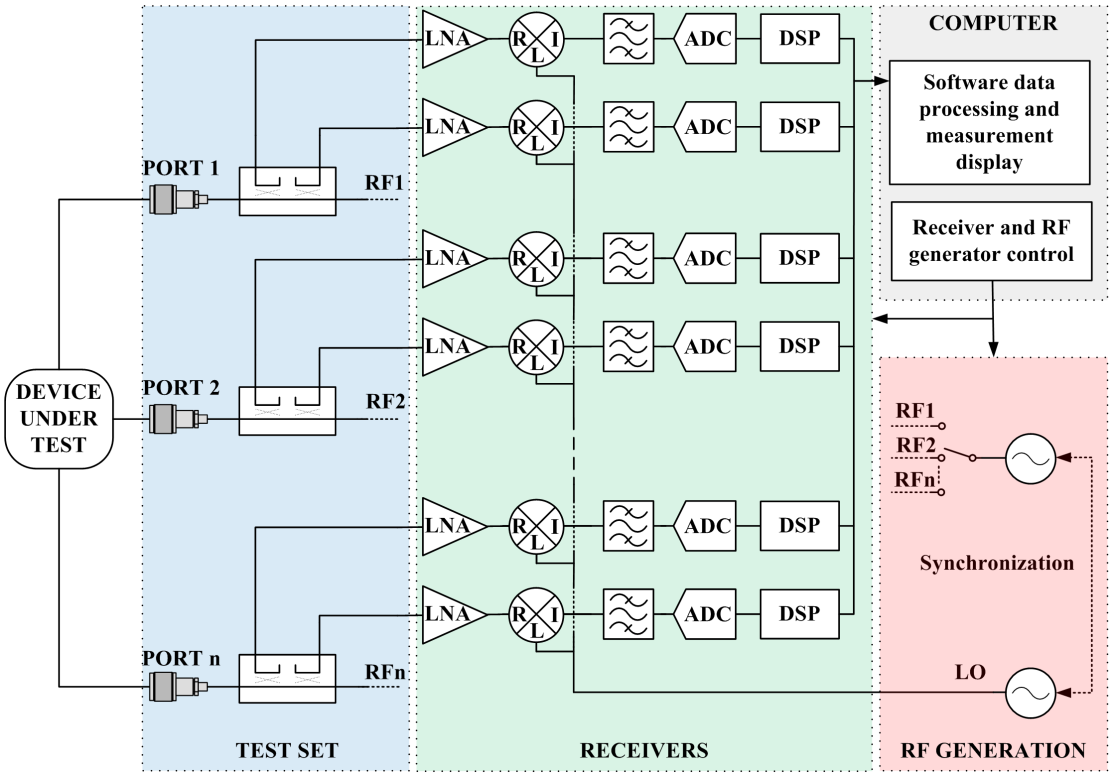

FIGURE 2.18: Exemple of an N port VNA block diagram with only one excitation source

A mixer based NVNA is relying on the architecture of a VNA. We will see in this section the architecture of a VNA and how it can acquire nonlinear measurement capabilities. The block diagram of Figure 2.18 shows that such an instrument is composed of four distinguishable parts: the test set, the generator, the receivers and the computer.

2.3.1 Test set

The description and influence of the test set of a VNA is extensively explained in [54] and [55]. A summary of theses sources is proposed in Appendix A for informational purpose as it is important to keep the influence of the test set in mind to perform measurements of good quality. However as it is not specific to nonlinear measurement, no more attention is given to this topic. Please note nevertheless that the problems introduced by the test set are not dependent on the receiver architecture, therefore the comparison between the available receivers and the conclusions drawn in the previous section are unchanged.

2.3.2 Radio frequency generator

The generator has for function to provide the RF excitation signal to the DUT as well as the LO signal to the receiver. In its simplest form the RF generator is only composed of a frequency synthesizer. Nevertheless the frequency synthesizer is often followed by an amplifier in order to output sufficient power for the characterization of the DUT.

A frequency synthesizer is defined as a system being able to generate a given range of frequencies from a single fixed frequency (usually coming from an oscillator or a digital clocking signal). The output frequency f_{out} and the reference frequency f_{ref} are linked by the general equation:

$$f_{out} = \frac{m}{d}.f_{ref} \; m, d \in \mathbb{N} \tag{2.9}$$

In such a system there is therefore a strong correlation between the quality of the synthesized signal and the quality of the reference, in fact a synthesized signal is at best as good as the oscillator signal used as reference. For test and measurement applications (X)crystal Oscillator (XO) are used and more specifically Temperature Compensated (X)crystal Oscillator (TCXO) and Oven Controlled Temperature (X)crystal Oscillators (OCXO) [56]. They can provide a reference signal up to some hundreds of MHz. The synthesizer and oscillator are evaluated for a given application according to a set of fundamental characteristics.

The first characteristic is the frequency range that corresponds to the lowest and highest frequency that can be synthesized. VNA application has a strong constraint on the range as it may require the synthesis of signals of up to hundreds of GHZ.

The frequency of the output signal of a synthesizer is not varying continuously within the frequency range. According to equation 2.9 the minimum spacing between two synthesizable frequencies is $\Delta f = f_{ref}/d$. The frequency step is highly dependent on the architecture used for the synthesizer but it is possible to find commercial synthesizer with steps within some μHz up to some MHz. A VNA synthesizer usually has a step of 1Hz.

Every synthesized frequency is only synthesized with a given tolerance. This characteristic is usually directly inherited from the frequency accuracy of the reference signal. Many synthesizer allow the use of an external oscillator that would

have the characteristics that the user requires. Extremely precise equipment such as GPS satellite use atomic clocking.

When the synthesizer is required to generate a new frequency different than the one it is currently generating, the new frequency is not obtained instantly. In fact there is a settling time that depends on the architecture and the technology used and is subjectively defined as the time required, when the frequency changes, to reach the determined performance at the new frequency. This characteristic is essential for a VNA as the synthesizer is destined to constantly sweep a given frequency range, having therefore a strong influence on the measurement time of the chosen frequency range.

A realistic frequency synthesizer will most likely generate other frequencies in addition to the one it was set for. The position of the spurious signals in the spectra depends once again on the architecture used, the most common spurious signals are:

- Harmonic frequencies of the wanted signal
- Harmonics of intermediary frequencies potentially used in the synthesizer
- Linear combinations of all the present tones

It is also possible with digital architecture to find spurious tones at determined frequencies that are not harmonically related to any present signal. Usually the maximal power of this tones is specified by the constructors in a similar manner than SFDR was defined for ADCs in Section 2.2.1. For VNA application, low or absent spurious is primordial to conserve the linear condition required by S-parameter measurements.

One of the most important characteristic of the generated signal is its spectral purity. It quantifies how close is the signal from the ideal sinusoid, or in frequency domain on what bandwidth around the wanted frequency f_{out} is the power spreading as shown in Figure 2.19. By extension it can quantify the noise and stability of the source. This characteristic should not be confused with the presence of spurious signal we just described that is a discrete phenomena. It is extremely important as it influences how dense can an emitted or measured spectra be before the tones become indistinguishable from each others or low power tones are

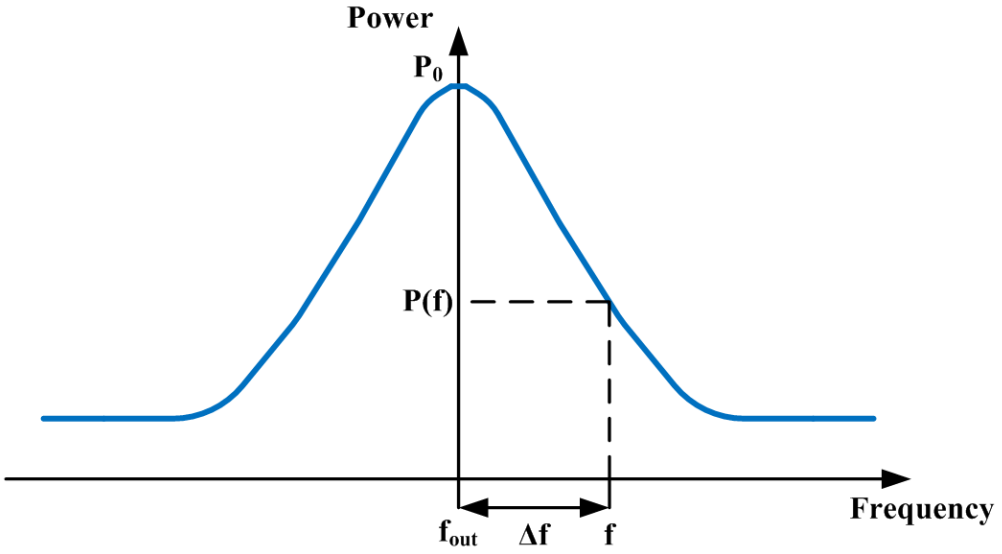

FIGURE 2.19: Power spreading of a frequency synthesizer caused by cyclostationary effects

drowned in unwanted signal. To understand the source of spectral impurity let us consider an ideal reference oscillator output:

$$V(t) = A\cos(2\pi f_{out}t + \phi_0) \tag{2.10}$$

Practically, noise sources in the oscillator will introduce amplitude and phase modulation changing equation 2.10 into:

$$V(t) = A.(1 + \alpha(t))\cos(2\pi f_{out}t + \phi_0 + \phi(t)) \tag{2.11}$$

where $\alpha(t)$ and $\phi(t)$ have random values induced by the noise. As the noise is frequency dependent, the related spectral power densities $S_\alpha(\Delta f)$ and $S_\phi(\Delta f)$ are often used to quantify the phenomena in frequency domain with $\Delta f = f - f_{out}$. The amplitude modulation is often overlooked as it is often limited by the phenomenon of saturation and considered negligible for synthesizers of good quality. On the opposite the phase modulation is often the major cause of the power spreading over adjacent frequencies and therefore the spectral purity and is considered with extreme attention [57]. This effect that is a form of cyclostationary noise [58] is related to the phenomenon of jitter. Constructors usually specify instead of the spectral power density $S_\phi(\Delta f)$ the phase noise defined as:

$$\mathcal{L}(\Delta f) = \frac{1}{2}.S_\phi(\Delta f) \tag{2.12}$$

It is expressed in rad^2/Hz but the logarithmic value expressed in dBc/Hz is often preferred. Using the quantities of Figure 2.19, phase noise can also be defined when expressed in dBc/Hz by:

$$\mathcal{L}(\Delta f) = 10 \log \frac{P(f)}{P_0} \tag{2.13}$$

Using equation 2.9, we can deduce the relationship between the phase noise of the output signal and the phase noise of the reference signal:

$$\mathcal{L}_{out}(f) = (\frac{m}{d})^2 . \mathcal{L}_{ref}(f) \ m, d \in \mathbb{N} \tag{2.14}$$

From equation 2.14, it can be seen that if the output frequency is superior to the reference frequency the phase noise increases until frequency collapse if the multiplication factor is too important. Frequency collapse is the fact that the power of the sidebands is so close to the power of the wanted frequency that it is not possible anymore to distinguish the wanted frequency limiting the maximum frequency achievable with a given reference. It is also possible to notice that the phase noise decreases when the output frequency is inferior to the reference frequency. This decrease is ultimately limited by the thermal noise.

When designing a VNA, some characteristics of the output of the synthesizer are also of interest such as the maximum output power, the output impedance and the resilience to power inserted in the output stage.

Aside from the amplitude, the phase of the output signal can be important. We have seen in Section 1.4.1 for example that the active loop load pull architecture uses synthesizers which output phase is controllable. Some synthesizer are also said to be phase coherent. Phase coherence between many different signals (different either by their frequencies or by the fact they come from different synthesizers) is defined as the fact that, by knowing exactly the phase of one of the signal at a given time, one can predict the phase of all the other signals at anytime. Generally the phase of the output signal of a VNA synthesizer is neither controllable nor coherent as it is not requested by linear characterization of a DUT.

There are many implementations of synthesizer depending on the application requirements but it is usually possible to classify them into two categories: direct and indirect synthesis.

Direct frequency synthesis

Analog direct synthesis method relies on a single stable source. This source is then used to generate many multiple or fraction frequencies that are then combined by addition or subtraction until achieving the wanted frequency. A common implementation of this technique is the mix-filter-divide architecture of Figure 2.20. Such a synthesizer uses a series of mixer and filters to achieve the wanted frequency. This method allows rapid frequency changes thanks to switching, which

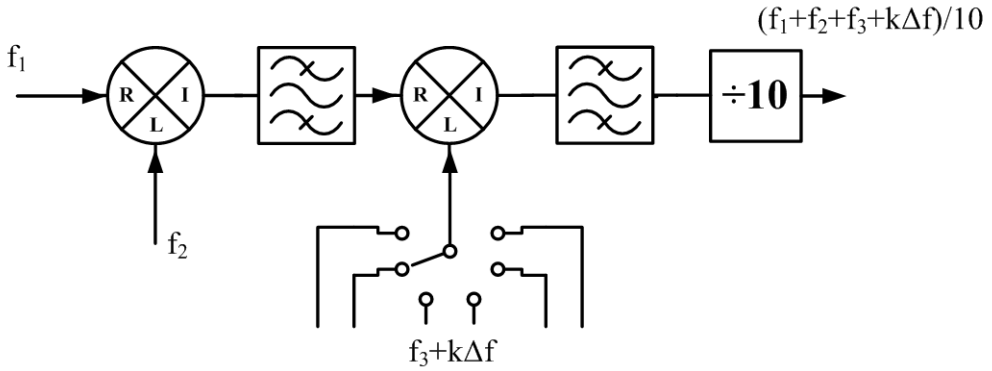

FIGURE 2.20: Mix filter divide architecture for analog direct frequency synthesis

is an advantage for VNAs. Sadly the losses caused by each mathematical operation makes this technique highly power consuming and the use of many switches, mixers and filters makes the synthesizer circuit extremely bulky and difficult to layout. The spectral purity can also suffer from insufficient filtering of the spurious tones created during mixing.

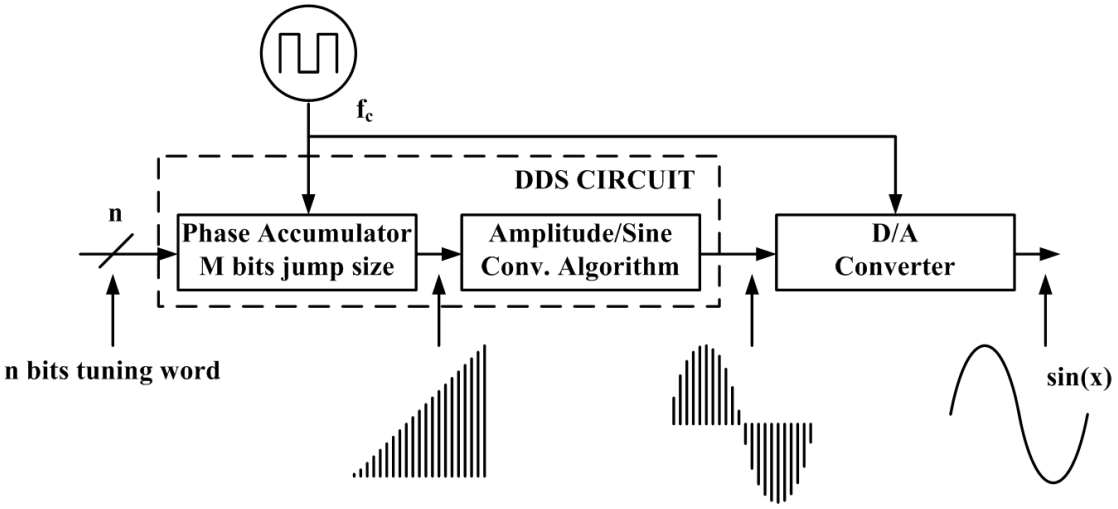

FIGURE 2.21: Direct digital synthesis block diagram

Direct Digital Synthesis (DDS) was developed in the early 1970s [59], the block scheme is shown in Figure 2.21. This method is based on a phase accumulator that changes state at a reference clock frequency, sending a digital word to a memory component that contains a look up table of a sine wave. The memory component converts the phase information from the phase accumulator into a numerical value representing the amplitude of the signal, and a DAC converts this numerical value into analog signal. The equation linking the output frequency f_{out} with the clock frequency f_c, the length in bits of the phase accumulator n and the jump size M between phases in bits is:

$$f_{out} = \frac{M.f_c}{2^n} \tag{2.15}$$

The strength points of this technique are a remarkably good frequency resolution, a quick frequency switching and low phase noise. Thanks to the use of a frequency counter, it is fairly easy to achieve phase coherence with this architecture. Nevertheless the maximum frequency that can be synthesized has to be inferior to half of the clock frequency even if the available components on the market have known a great improvement regarding this aspect (it is now possible to find components at 3.5GHz clock frequencies [60]). Many effects such has spectra folding or the bits limitation of the digital components are creating spurious signal that can be really close to the wanted frequency hence difficult to filter out. Thanks to the latest improvement in digital electronics, this type of synthesis is being used directly or in combination with indirect architectures in VNAs since a year as generator in commercially available models such as the ZVA67 while it was until then mostly used for low frequencies in Numerically Controlled Oscillator (NCO) for example.

Indirect frequency synthesis

Analog indirect frequency synthesis was proposed to solve the problem of spectral purity limitation in analog direct digital synthesis. The Phase-Locked Loop (PLL) architecture shown in Figure 2.22 is the dominant method for frequency synthesis in the industry. The name comes from the fact that this architecture relies on the phase comparison between a stable oscillator and the output frequency, being in fact a servo-loop. The phase detector outputs a voltage proportional to the phase difference between its two input signals. This voltage is sent to Voltage Control Oscillator (VCO) that transform the received voltage into a frequency. Between the phase detector and the VCO there is usually an element that ensures

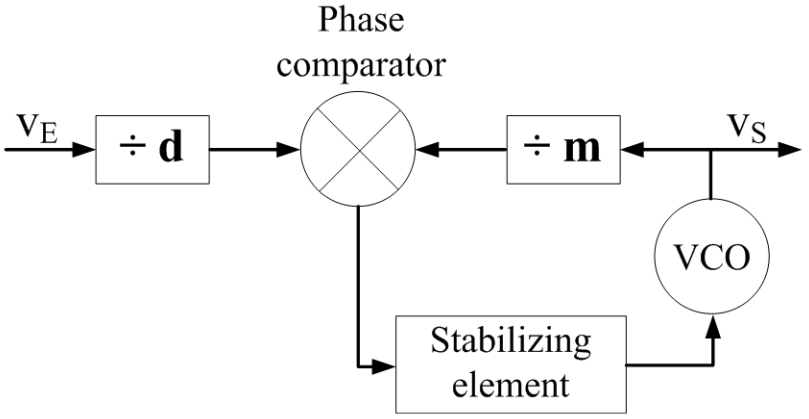

FIGURE 2.22: Phase locked loop block diagram

the stability of the loop like a low pass filter for example which is also used to filter out unwanted frequencies from the phase detector. The stabilizing element has to be tailored for every application, therefore its design in an important part of the effort to provide to design a PLL. In front of each phase comparator inputs, dividers are placed giving the factor m/d of equation 2.9. As long as the voltage at the output of the phase comparator varies, it means that the frequencies compared are different. When finally the voltage is constant, then there is a constant relationship between the phases of the compared signal and therefore both signal have the same frequencies, in that case the loop is said to be locked and outputs the required frequency. PLL circuit is one of the most important circuit of the RF engineering and complete description and design help can be found here [61]. The principle has also been transposed to the digital world [62] to create on chip PLL. Some DDS based PLL design were proposed [63] [64] to profit from both DDS and PLL qualities .

2.3.3 Receiver

As we have seen in Section 2.2.4, a VNA is based on heterodyne receiver. One possible implementation for a VNA's receiver is shown in Figure 2.23. The RF signal from the DUT is down-converted by a mixer to a fixed intermediary frequency that is then filtered to avoid aliasing and fed to a high resolution ADC of at least 14bits, 18 bits for recent instruments and around 80MHz sampling frequency.

The analog mixer is usually the limiting component for dynamic range as it receives the signal almost at maximum power. Nevertheless when the signal received

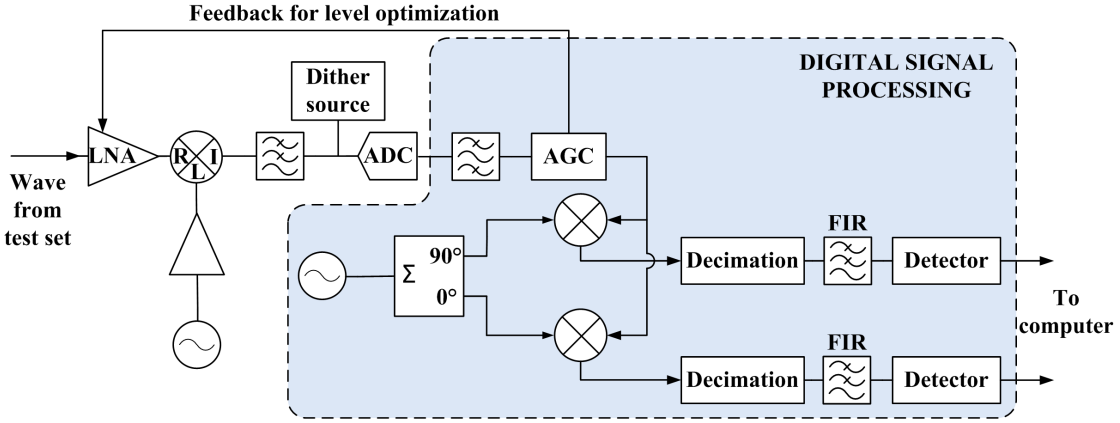

FIGURE 2.23: Example of VNA receiver implementation

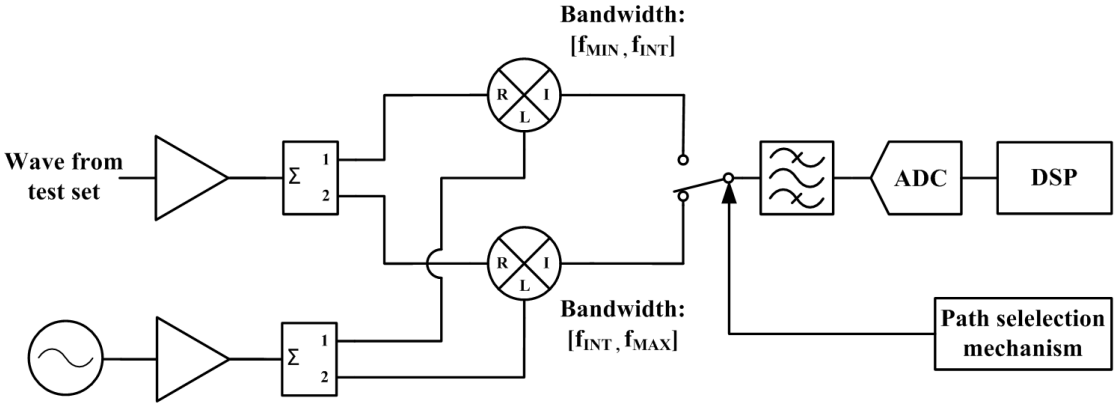

FIGURE 2.24: Front end with multiple mixing path to cover the entire instrument bandwidth

by the mixer is too low, the signal to noise ratio is degraded. The receiver are often equipped with switchable amplifiers to optimize the level received for best measurement. The optimization is performed after a fast first quick measurement that roughly evaluates the signal level. This technique is known as Auto Gain Control (AGC). This should not be confused with the Automatic Level Control (ALC) that is an option on some VNA that ensure a constant arbitrary power of the excitation signal. Because of the difficulty to design a mixer with the wanted performance over the entire instrument bandwidth, the actual front end often consists of several switchable path comprising different mixers as shown in Figure 2.24.

After analog to digital conversion, the signal may flow through a bandpass filter to remove part of the broadband noise generated by the ADC. Once filtered, the signal is demodulated using IQ demodulation to extract its real and imaginary part. This consist of separating the signal in two path and then down converting

each path to the frequency $f = 0$ thanks to a numerically controlled oscillator (NCO) operating at the IF frequency. One of the multipliers used for down-conversion has its NCO signal shifted in phase by 90^o in order to get the inphase (I) and the quadrature (Q) components respectively corresponding to the real part and the imaginary part of the signal once the high frequency part has been filtered out.

The filter that is meant to filter out the high frequency component from the demodulation as well as the rest of the noise generated by the ADC as well as the noise added on a portion of the ADC bandwidth to increase the resolution by dithering is the IF filter. The bandwidth of this filter defines the resolution bandwidth or IF bandwidth of the receiver. In the implementation of Figure 2.23, the IF filter is composed of a decimation filter that will as its name suggest decimate the oversampled and dithered signal to feed the Finite Impulse Response (FIR) filter with a signal with a lower sampler frequency. The role of the decimation filter is also to relax the constraint on the quality factor that will occur when the bandwidth of the filter is small compared to its center frequency. The narrower the filter bandwidth, the more noise is rejected increasing therefore the dynamic range of the measurement. Because the filter is digital, arbitrary bandwidth values can be implemented. The limits however are set by the settling time of the filter and the signal to noise ratio. In fact when divide by a factor N the resolution bandwidth, we multiply by N the measurement time due to an increase of number of sample and therefore time required by the decimation filter. However if the filter is too broadband the SNR will be degraded. Finally the maximum bandwidth of the filter is also limited by the distance between the IF frequency and the frequency at which noise is added for dithering.

Using heterodyne technique, a phase shift appears every time the signal is down converted. As long as there is phase a fixed phase relationship between the LO and the NCO of every receiver the phase shift introduced will be compensated during calibration. The best way to achieve such a relationship is to use the same LO and NCO for every receiver of the instrument, preventing synchronization problems between all the oscillators. Nevertheless the NCO and the LO must be synchronized to limit the phase noise or in other words to make them keep always the same IF frequency which is vital for the demodulation. For the similar reason, the excitation signal must be synchronized to the LO to prevent the frequency

of the IF signal from oscillating around the required value. There are different synchronization methods allowing synchronization between all the signals.

The synchronization method of Figure 2.25 uses LO and RF synthesizer that use both a PLL with a common crystal oscillator (or a common clock when used with DDS). With this technique it is possible to have an arbitrary offset between the LO and the RF as long as the frequencies are within the frequency range of the instrument. The generator and receiver frequency setting are completely independent from each other.

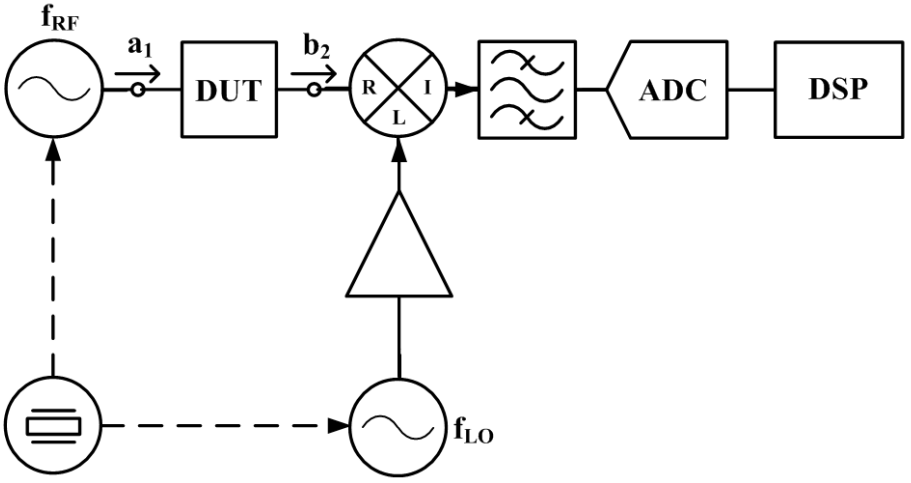

FIGURE 2.25: Source and local oscillator of the VNA sharing a common reference

It is also possible to lock the LO to the excitation signal with a PLL as shown in Figure 2.26. In this case the IF frequency is used as the control variable after down conversion of a fraction of the RF signal by a fraction of the LO. This method takes advantage of the compulsory presence of the excitation signal to simplify the implementation compared to the architecture of Figure 2.25. Sadly the signal used as oscillator for the LO is normally noisier than a crystal oscillator would be and therefore the quality of the measurement is decreased. As it is presented it is also not possible to set an offset between the receiver and the excitation signal frequency unless additional hardware would be used which would cancel the simplicity advantage.

A similar idea is to generate the excitation signal by mixing the LO and a low frequency generator synchronized to it as shown in Figure 2.27. A small frequency offset of maximum 100MHz is possible depending on the low frequency synthesizer

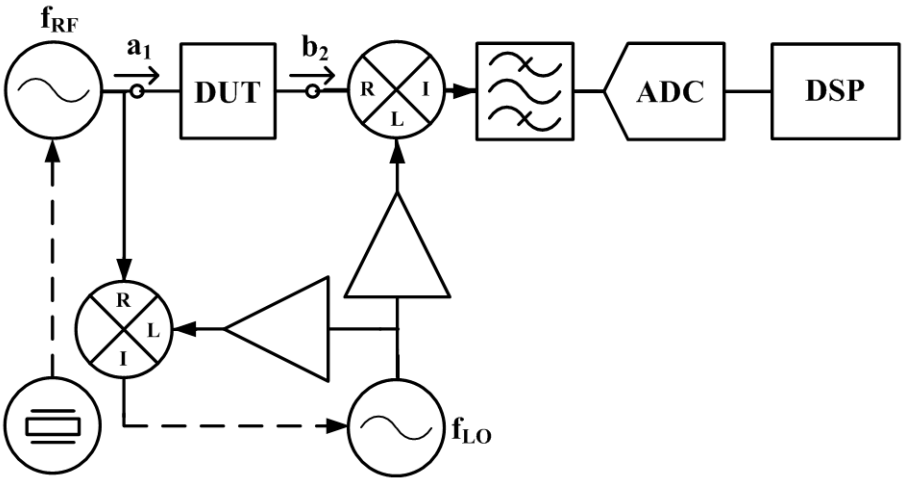

FIGURE 2.26: Local oscillator of the VNA locked on the RF signal

but the use of a mixer to synthesize the excitation signal is not so good in terms of spurious signal.

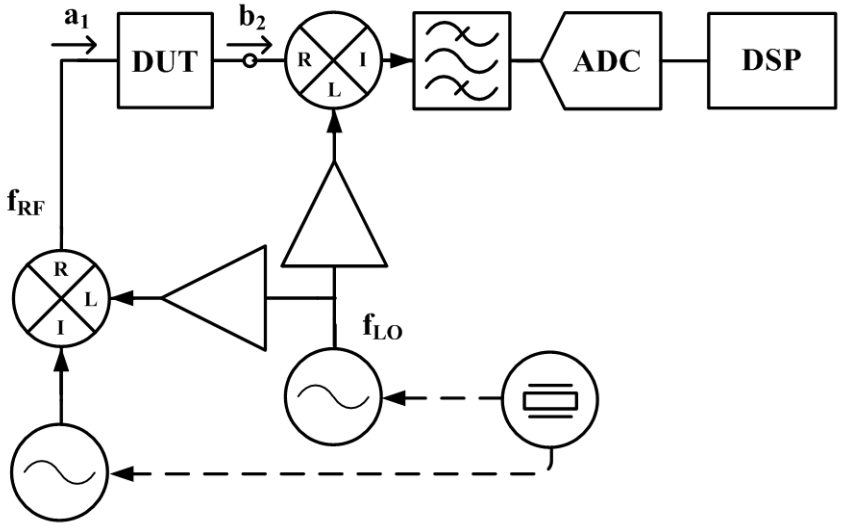

FIGURE 2.27: RF signal of the VNA locked on the local oscillator

For instruments functioning at high frequencies, harmonically pumped mixers that we have seen in 2.2.3 can be used for harmonic mixing. Contrary to harmonic sampling that we described, harmonic mixing is still using a single frequency as LO but instead of using the frequency $f_{LO} = f_{RF} + f_{IF}$ it uses of its subharmonics. Doing so the LO can cover only a fraction of the RF bandwidth but this is done at the cost of a a higher conversion loss and therefore a lower dynamic.

2.3.4 Computer

In modern network analyzers, the computer and the firmware installed on it are in charge of the coordination of all the elements and procedures of the instrument. The main tasks of the computer are the control of the physical measurement sequence, the processing of the recorded data and finally the conditioning of the data into user readable format.

The measurement procedure depends on the type of characterization realized. Network analyzers are optimized for S-parameters measurement. To fully characterize a N-port network at a single frequency, N partial measurements need to be performed. A simplified partial measurement procedure consists of:

- Turning on the excitation signal at the wanted frequency at port N and make sure that it is off at every other ports
- Measure the excitation signal
- Measure the reflected wave at port N
- Measure the transmitted waves at all the N-1 other ports
- Turn off the excitation signal and restart procedure with a different excitation port for new partial measurement.

There are two ways to perform a characterization over a chosen frequency range (also called frequency sweep), either we perform all the partial measurements for one frequency before changing frequency or we perform one partial measurement at all frequencies before changing port for next partial measurement. The last mentioned is also called alternating mode in some VNAs. Fundamentally both methods are equivalent but practically the fact that there is a steadying time of the frequency synthesizer used for the receiver and the excitation source as well as a level control may favor one method over the other depending on the DUT. However there is no absolute rule for favoring one over the other and this is mostly left to the experience of the user or the recommendations of the constructor.

As shown in Figure 2.28, this settling time of the synthesizers is a non negligible part of the measurement time of the VNA as the instrument will wait for this time to be over before allowing an acquisition. The settling time is not necessarily monitored during measurement, a simple solution being to determine an upper limit

of this time in many different configurations during the instrument factory tests and apply this time with a safeguard. At the end of a determined number sample acquisitions a raw complex value is obtained (oversampling) and transferred from the hardware to the computer. The instrument then prepares for the next frequency measurement and so on. There is relatively a longer pause between the last point of a sweep and the first of the next sweep compared to two consecutive measurement points in the same sweep. The reason for this difference comes from the fact that all the registers of the digital boards are being prepared after the last point of a sweep for the following sweep.

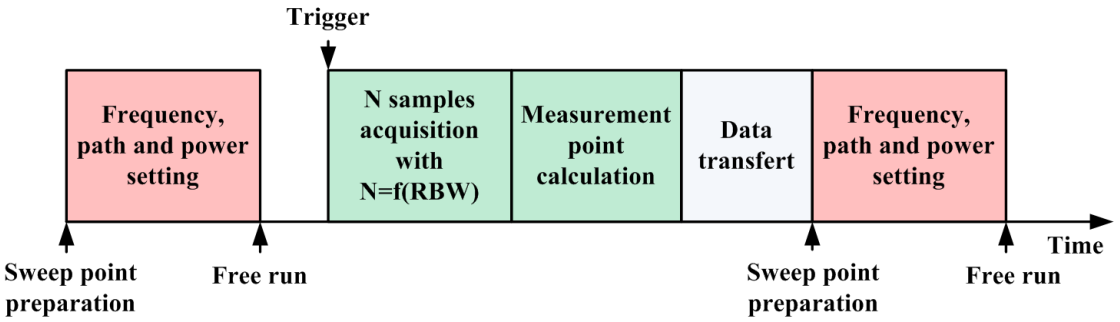

FIGURE 2.28: Acquisition time of a sweep for a single receiver

The data processing is in charge of converting the raw complex values measured by the receivers into corrected complex values that takes into account some errors introduced by the test set and receivers. The correction is performed thanks to the system error correction value that are determined during calibration. We will see the calibration procedure in detail in a later section. The user may also enter some phase and/or amplitude offset values and deembedding or embedding models that are processed by the computer at this step. The processing chain of a VNA is shown in Figure 2.29.

Finally the computer format the corrected data, applying the format required by the user and eventual mathematical operations on the data or between sets of data as shown in Figure 2.30.

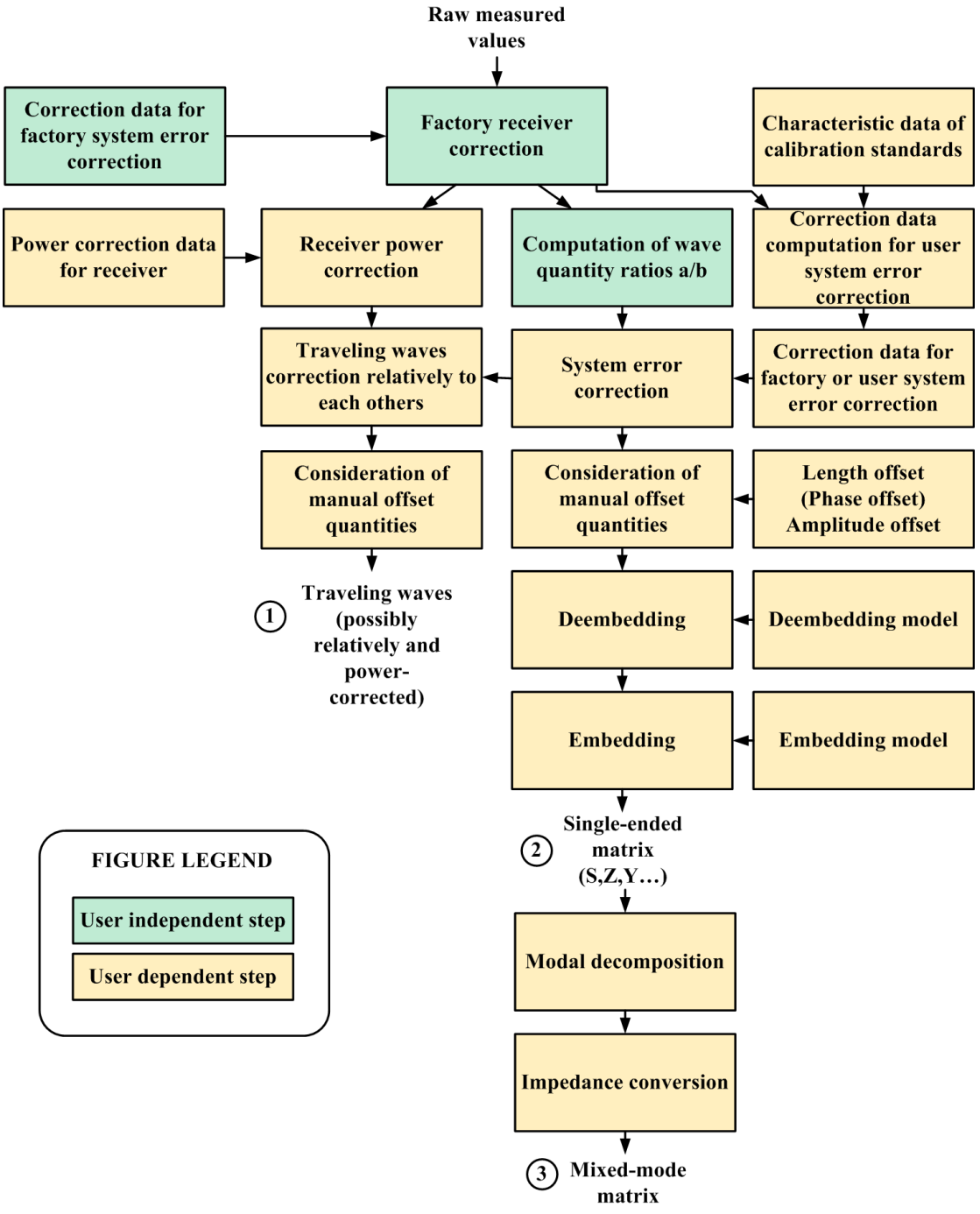

FIGURE 2.29: VNA data processing after raw complex value measurement

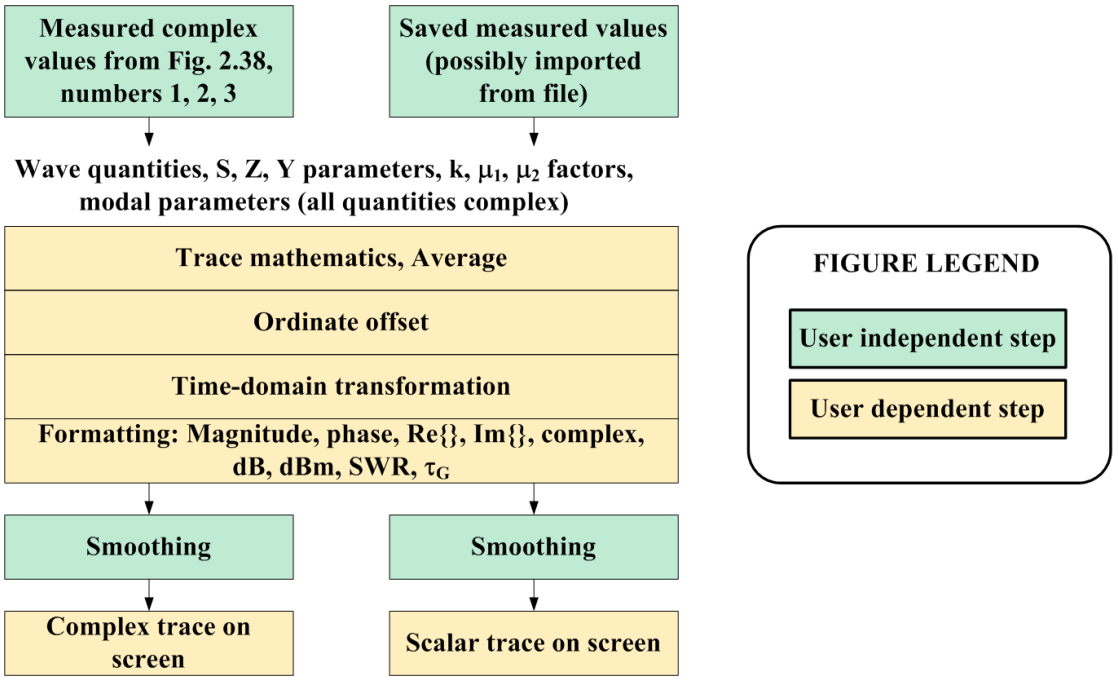

FIGURE 2.30: VNA data formatting after data processing for user readability

2.3.5 VNA accuracy and calibration

The raw data measured by the receiver are affected by two types of measurement uncertainties:

- Uncertainties caused by random or time varying errors such as thermal noise and thermal drift. It is possible to statistically describe such errors and to minimize them but it is impossible to correct them.
- Uncertainties caused by systematic errors such as the one brought by the test set or an imbalance between receivers. It is possible to correct them to some extent, the correction being limited by the overlying noise.

Minimization of random and time varying errors

The performance of each and every component of the VNA along with thermal noise are temperature dependent. Therefore fluctuations of the temperature (or thermal drift) of the instrument or in the environment will cause an evolution of the measurement. To minimize thermal drift it is important to let the instrument warm up after turning it on in order to ensure thermal equilibrium. It is also important to minimize all the unnecessary fluctuation of the laboratory temperature. For metrology applications, instruments are often left on for weeks before being considered thermally stable.

The correlation between successive measurement done in exact same conditions and a short period of time apart (to minimize the effect of thermal drift) is called repeatability. High repeatability is wished for measurement comparison between different DUT or to test the drift of a DUT at different times. It requires the use of high quality test cables and connectors as well as caution from the user. The torsion of test cables for example will change their electrical characteristics and therefore introduce a random drift in amplitude and phase. In a same way connectors that are not properly handled or cleaned will introduce changes. High repeatability is difficult to achieve at high frequencies and a increased amount of care is required from the user when frequency increases. To help tighten the nut of the connector in a constant manner, torque wrench are used when possible.

Correction of systematic errors

Theoretically it is possible to distinguish between linear and nonlinear systematic errors.

Nonlinear systematic errors are the errors caused by the nonlinear behavior of active parts in the VNA. When the receiver measures a power too high, compression effects will occur (often in the mixer). For S-parameter measurements, if all the receiver work at the same compression point the error would theoretically compensate. However, the power received by all the receivers is rarely the same therefore compression will affect the measurement. Such effects are almost impossible to calibrate as they are power dependent and the power the receiver will measure from the DUT is usually not known with precision. The best practice is to always avoid compressing the receivers and check for compression with a golden device in case of doubt.

We have seen in Section 2.3.1 the influence of the test set on the measurement uncertainty. There is also a possible mismatch between the result given by two different receivers used in their linear functioning and in the exact same conditions due to the tolerance of the components. All these effects are linear and can be accounted for. To correct the linear systematic errors, a network analyzer is separated into a linear error model (or error network) and an ideal network analyzer as shown in Figure 2.31. The parameters of the error network are known as error terms and have to be determined in order to provide corrected measurement. The characterization of the error network is realized thanks to elements that have known properties and are fully characterized also called calibration standards, they are described in detail in [54]. Every standard must be traceable to a common reference standard meaning that it exists an unbroken chain of comparisons between all the standards with a given uncertainty thus ensuring comparability between measurement with different instruments. This is also called measurement traceability.

Constructors talk about raw system data when dealing with the systematic error before system error correction and effective system data after correction. The effective system data are highly dependent on the accuracy of the determined error terms that depend on the measurement noise and the calibration standard quality and characterization, systematic error can therefore never be fully corrected.

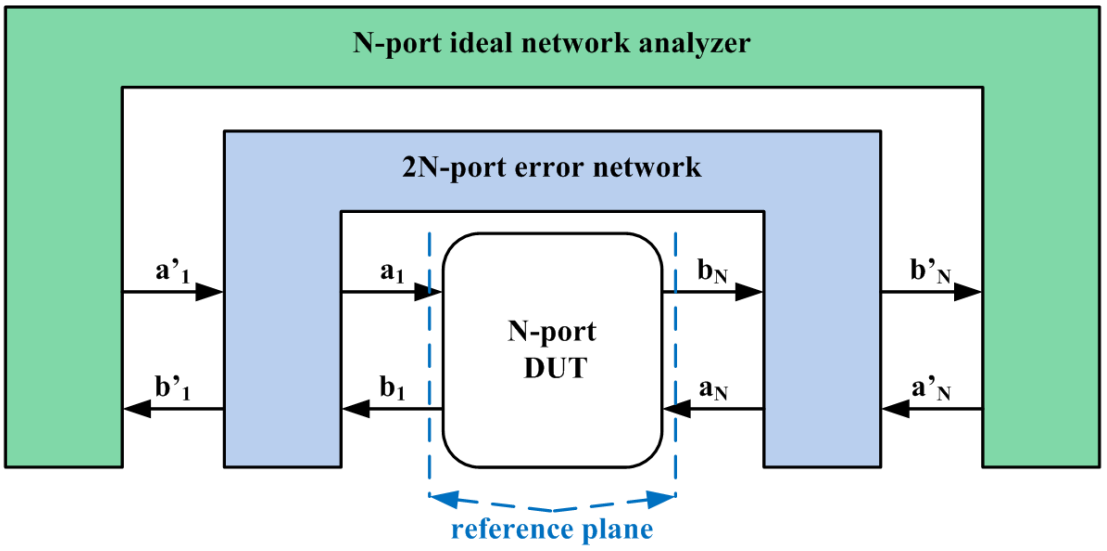

FIGURE 2.31: Ideal and error network separation for corrected measurement

There are many calibration procedures involving different standards, steps and number of terms. Different calibration procedures are explained and compared in [54] but it is important to have at least in mind the Open Short Match (OSM) and the TOSM techniques used respectively for one and two port VNA calibration to achieve good understanding of NVNAcalibration. A reminder of these two calibration methods is proposed in Appendix B.

2.4 Use of VNA as NVNA

As described in Section 1.4.3, the class of nonlinear system we will be characterizing is likely to output the frequency it was excited by plus a undetermined set of harmonics. The objective of the nonlinear characterization is to be able to measure the time domain waveforms at the ports of a DUT which is equivalent in frequency domain to measure the incident and reflected traveling waves for every tone at all the DUT's ports. As we have seen in Section 1.4.3, this ability to provide accurate time domain waveforms and frequency domain traveling wave is what characterizes a NVNA.

Therefore nonlinear characterization requires three main features from a VNA to be able to be used as a NVNA:

- The ability to set different frequencies for the receiver and the excitation signal.

- The ability to keep track of the phase relationship between signals that have different frequencies (equivalent to phase coherence as defined in 2.3.2 between every measured tone).
- A calibration procedure adapted to nonlinear measurement

To adapt a VNA to nonlinear characterization, there are four sorts of possible modifications that influence the measurement procedure of the available VNA:

- Use of user options of the firmware.
- Modification of the behavior of the instrument through functions that are not directly accessible by the user called service functions.
- Modification of the firmware and/or the FPGAs program present in some of the VNA modules
- Hardware modifications

In this work only the first two possibilities were unconditionally allowed by the department in charge of the network analyzer we will be using. These modifications induce the creation of a software that automatize the setting of the instrument for nonlinear measurement by remotely controlling the firmware as shown in Figure 2.32 . This solution limits the chances of optimization of the instrument for nonlinear characterization. This is nevertheless a limitation of many commercially available solutions of mixer based NVNA that are relying on a software that use the procedure implemented in the VNA for nonlinear measurement. The other two possibilities were tolerated at the condition that the modifications were easy to implement, cheap and/or needed for many different applications.

2.4.1 Measurement acquisition for nonlinear characterization

The major differences in the measurement acquisition for nonlinear measurement compared to the procedure for S-parameters extraction that we have seen in Section 2.3.4 are that the excitation signal frequency will be the same during the whole frequency sweep and that the excitation port will not change. The simplest procedure will be as follow:

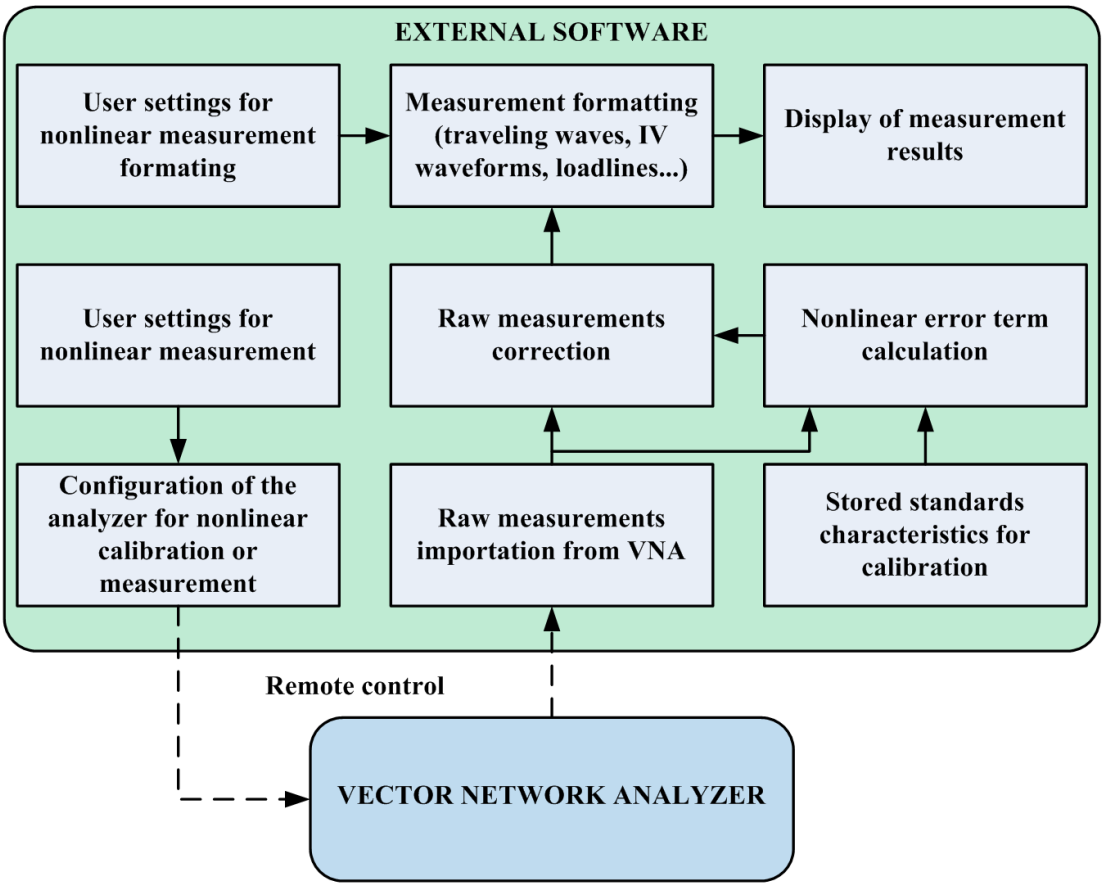

FIGURE 2.32: Block diagram of the chosen NVNA implementation using a VNA

- Turn on the excitation signal at required fundamental frequency at port N and make sure that it is off at all the other ports
- Select the local oscillator frequency for measurement of the traveling waves at the first frequency of the sweep
- Measure transmitted and reflected waves at all port of the DUT
- While excitation signal is still on, change the LO frequency for measurement of next point of the frequency sweep and proceed to measurement, repeat this until the end of the sweep
- Alter the excitation signal as needed by the user (keep it on or turn it off or change its frequency) and proceed or not to next sweep

A first constraint on the VNA that will be used for nonlinear characterization is that it has to allow the measurement of frequencies different than the excitation

signal. We have seen in Section 2.3.3 that there is an appropriate implementation of the receiver that allows it. Practically, because of the cost of this implementation, only top range instruments possess this capability that was implemented for scalar measurement of frequency converting devices such as frequency multipliers and mixers for example. It is possible from the instrument's interface to configure the excitation signal for each port while independently applying a setting for the receivers [65]. As the instrument has only one LO, the receiver setting will be shared by all the receivers of the instruments.

A second constraint is that, to be able to make sense of the measurements taken at different frequencies, the excitation signal must have an extremely steady power level during the duration of the sweep. In fact, especially in the case of a power amplifier driven at compression, the nonlinear behavior of a DUT depends on the excitation power therefore if the excitation signal fluctuates too much during the sweep we may have inaccurate reconstruction of the complex signal. On the Rohde&Schwarz® ZVA series of VNA used in this work, there is a possibility to set the excitation signal to constant generation meaning that the signal should be on, keep the same frequency and the same level during the entire duration of the sweep.

During the test of this capability, it was noticed however that the excitation signal was being turned off and on again before every sweep point despite the setting to constant generation as shown in Figure 2.33, potentially having an influence on the DUT behavior. This instrument's behavior is directly inherited from the linear characterization procedure. In fact as the frequency of the excitation signal is supposed to change at every frequency sweep point, the power amplifier used to bring the signal from the synthesizer at the required power level is turned off during the settling of the synthesizer. This is done to avoid to send to the DUT the varying frequency signal outputted by the synthesizer when the PLL is trying to lock again on the reference signal at a frequency change as shown in Figure 2.34. Once locking is achieved the power amplifier is turned on again resulting in a small overshoot due to impulse response of the amplifier but no frequency variation.

The constant generation option was implemented by sending all the time the same frequency to the synthesizer's Field-Programmable Gate Array (FPGA) during the sweep, tricking the instrument into always synthesizing the same frequency despite the frequency sweep. However the routine still expect the case where the

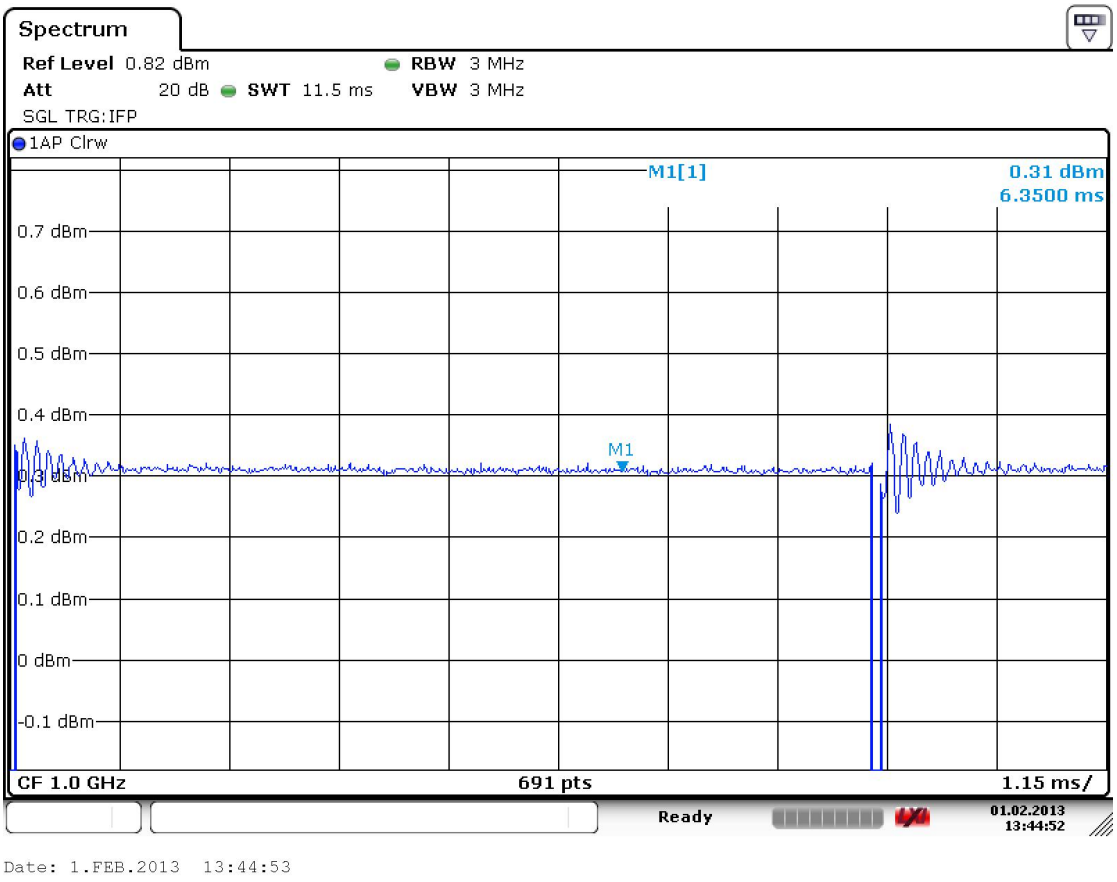

FIGURE 2.33: Power deep during signal synthesis caused by the restart of the synthesizer's amplifier by VNA prior every sweep point

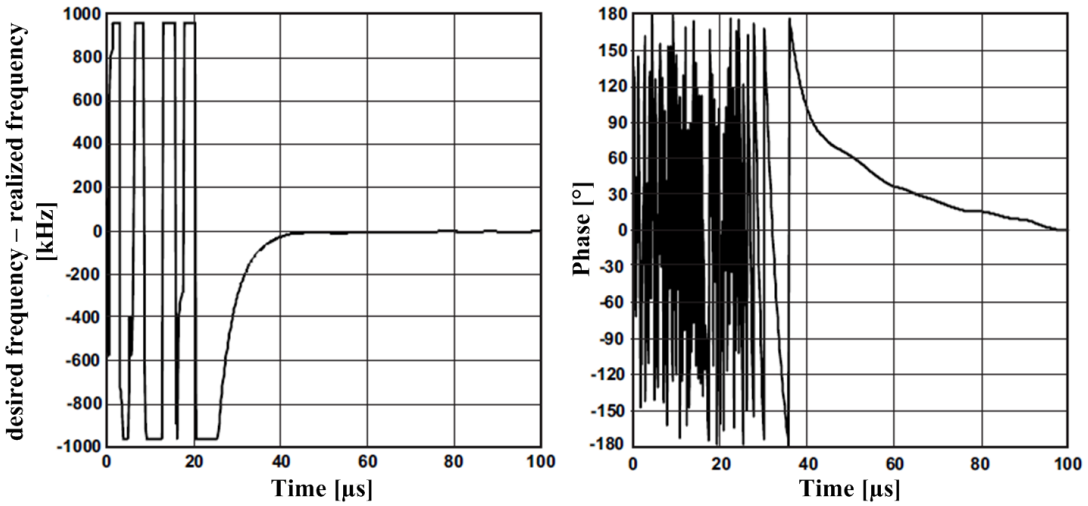

FIGURE 2.34: Phase and frequency of the PLL varying until locking when resetting the value to be locked on

excitation frequency is changing at each point so it still turns off and on again the amplifier at the output of the synthesizer resulting on the observed behavior

of Figure 2.33. Luckily, this behavior is the result of a firmware change based on a user request so the original behavior of the instrument that was not to turn the amplifier off is still available through a service function. Once the amplifier switching prevented, the steadier signal of Figure 2.35 could be obtained. The

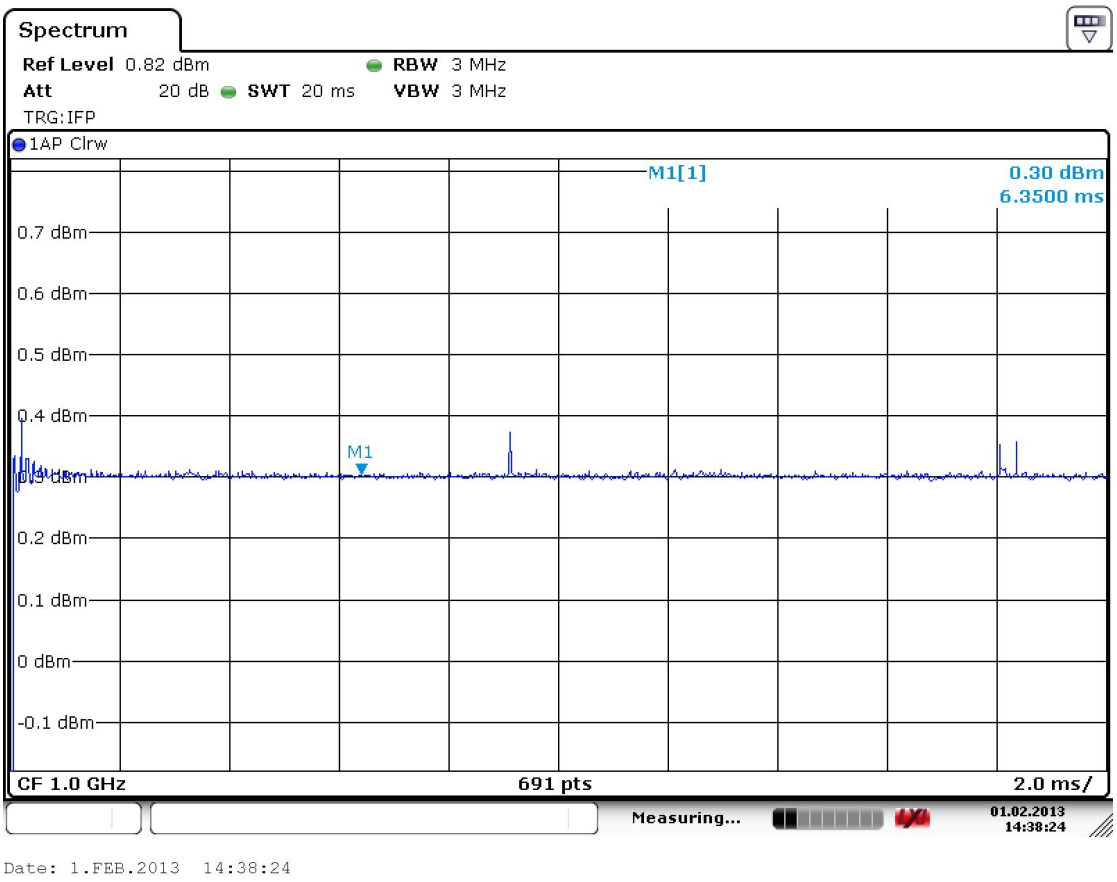

FIGURE 2.35: Source signal finally stabilized by the use of a function preventing the restart of the synthesizer amplifier

appearance of a little power spurious instead of the power deep can be noticed probably caused by the resetting of the synthesizer even if the same frequency is requested. We can also note that the power is still turned off before the first point of the sweep. This behavior is programmed directly in the FPGA to automatically come back to the first frequency of the sweep during a data transfer time when the FPGA can't be set by the firmware. It was therefore not possible to avoid this initial amplifier restart on the used VNA but its influence is slightly less problematic as the power will remain steady during a sweep.

Once the instrument behavior modified it is possible to acquire the traveling waves with a steady excitation signal and at frequencies different than the one of the excitation signal.

When acquiring data for nonlinear characterization, there is one consideration of which one must take great care namely the receiver compression. The influence on linear measurement of the nonlinear systematic error was already mentioned in Section 2.3.5. If in practice one can get away with a 0.1dB compression of the receiver during a linear measurement, such a compression is a disaster for nonlinear characterization as the tones produced by the receiver will often have the same frequencies as the tones to be measured and therefore create inaccuracies.

To evaluate the maximum power a receiver can handle without compressing, a sinusoidal signal of known power is sent directly to the receiver. While increasing the power of this driving signal and staying in the linear range of the synthesizer we monitor the apparition of harmonics on the measured signal that can be only attributed to the receiver compression. The maximum power for the receiver is then evaluated knowing the power it was driven with. Please note that for a given port, both receiver may not be identical by design and therefore both must be tested.

Once we know the maximum power before compression of each receiver, we can test for possible compression during the measurement. Of course the conditions during the measurement are different than the conditions we used to evaluate the possible compression. In fact during nonlinear characterization with have a multi-tone signal at the receiver instead of a single CW signal. The approach used is to consider that all the tones will add constructively and to compare the amplitude of the resulting signal to the evaluated limit. This method tends to overestimate the risk of compression as constructive addition of all the tones should be statistically rare. Of course false compression alert often occurs when a great number of frequencies are measured. For compression diagnostic to be applied, it is required to deactivate every constructor correction in order to evaluate the actual power measured by the instrument. This compression diagnostic method was to the author knowledge implemented for the first time by NMDG®.

The consequence of the multi-tone nature of the signal is also a virtual loss of dynamic of the instrument compared to the one expected by the user. In fact the user might expect from the instrument to have at each tone the same dynamic as the one stated in the datasheet of the instrument. Nevertheless the dynamic stated by the constructor only holds for a single tone CW signal. Depending on the complex signal imputed to the VNA, the upper limit of the range will be reached despite the fact each tone has a power bellow this maximum range. In

that particular case the dynamic must be considered according to the totality of the complex signal and not for each tones like it is done for linear measurement. As with a VNA we only see the frequencies that were selected, it may be a good idea to add a spectrum analyzer on the bench to monitor for big tones that appear in spots of the bandwidth where the VNA is blind.

Simplification of the compression diagnostic and better measurement of each tone may be reached thanks to the use of variable filters at the input of the receiver at the cost of more hardware and a possible increase of the measurement time of the sweep.

2.4.2 Preservation of phase coherence

The ability that characterize a NVNA is the ability to commute indifferently between time and frequency domain representation of nonlinear DUT behaviors. For example a sampler based NVNA such as an LSNA that is acquiring time domain measurements is able to reconstruct the frequency spectrum using Fourier transform. Similarly a mixer based NVNA that is, by its use of heterodyne principle, a frequency domain measurement can potentially rebuild the periodic time domain signal $s(t)$ from the measurement of the amplitude $a(f)$ and phase $\phi(f)$ at each frequency as follow:

$$s(t) = \sum_{n=1}^{\infty} a(nf_0) sin(n\omega.t + \phi(n.f_0)) \tag{2.16}$$

In practice of course we are limited in measurement bandwidth or sampling frequency so the result of the transformation is approximating the actual result. The quality of the approximation depends on the nature of the signal to approximate.

In equation 2.16 we can see that the reconstruction of the time domain signal requires the knowledge of absolute amplitude and phase of each tone used. More specifically for the phase, if one accepts a time shift of the time signal then only the measurement of the phase relationship between the frequencies is needed as the origin of the phases can be arbitrarily chosen once. Phase being normally defined only for signals of identical frequencies, we define the following phase difference between signals at different frequencies f_1 and f_2 respectively with phase ϕ_1 and

ϕ_2:

$$\Delta\phi_{f_1,f_2} = \phi_1 - \frac{f_1}{f_2}.\phi_2 \tag{2.17}$$

Sadly, if the measurement of the amplitude of the tones of a complex signal is possible with a VNA as it is, the measurement of the phase difference between the tones is not directly accessible. In fact, as it was explained in 2.3.3, the heterodyne principle a mixer based instrument is relying on induces an unknown phase shift at each down conversion depending on the phase of the local oscillator. As long as the VNA was used to measure ratios of signals at the same frequency measured at different receivers using the same LO then the influence of the LO on the phase would disappear. To perform nonlinear characterization a VNA is now measuring traveling waves, the influence of the LO during each measurement may negatively influence the measurements comparison in two ways:

- Prevent the comparison of signals at different frequencies within a same frequency sweep.
- Prevent the comparison of signals at the same frequency but measured during different frequency sweeps.

The first influence comes from the fact that the LO will not have the same phase value when set at different frequencies and will therefore influence differently the measurement of each tone. This issue is taken care of among other effects during the calibration as it is described in Section 2.4.3.

The second issue is due to the fact that a VNA is not designed to compare the traveling waves taken during different acquisitions even at a same frequency. In fact as the phase shift caused by the LO is supposed to compensate when measuring ratios during one measurement point, no care was put into having control of the LO phase. The consequence is that in most VNAs the LO has a random and changing phase between two measurement points of the same frequency but at different sweeps. Therefore when we measure a traveling wave during a frequency sweep and then the same wave at the next sweep we have no possibility to compare them as a random unknown frequency dependent phase shift was introduced. This is a loss of phase coherence.

There are two possible solutions to preserve phase coherence:

- Use an external reference generator that is constantly measured to keep track of the random phase shift (often referred to as synchronizer solution).
- Use a local oscillator that always assume the same phase during each measurement at a given frequency preventing then the random phase shift.

Use of a synchronizer

The use of an external reference or synchronizer was the solution chosen for the first generations of mixer based NVNA. It had for advantage to be implemented without any change in the VNA hardware and was therefore widely used, especially by companies that have no direct access to the VNA hardware. However this enforce the use of a four ports instrument even to perform a only two port measurement.

To preserve phase coherence, the synchronizer has for only task to provide at least a repeatable phase relationship between all the frequencies it outputs (that include all the frequencies required by the measurement). This phase repeatable signal is then measured by one of the receivers of the VNA as shown in Figure 2.36. The difference in phase between measurements at different sweeps of the synchronizer is directly attributed to the phase change of the local oscillator as the reference generator is supposed to have the same phase. To suppress the phase shift due to the LO during the measurement every traveling wave has its phase normalized by the measured phase of the synchronizer as follow for a a wave:

$$a'_i(f) = \frac{a_i(f)}{a_{SYNC}(f)}.|a_{SYNC}(f)| \tag{2.18}$$

This change of variable allows to have a phase of the traveling waves that is not influenced anymore by the local oscillator. Please note that no knowledge about the phase of the synchronizer's signal is required except from the fact that the phase is repeatable at the wanted frequencies.

At the time of this work, all the mixer based NVNA that are using external hardware to preserve phase coherence are using a comb generator (also called pulse generator) as synchronizer. A comb generator will output the same frequency of its input signal plus several harmonics with a fixed phase relationship between all these tones. Such generator is already widely used in electromagnetic compatibility measurements and is also a key component of the LSNA as described in Section 2.2.3.

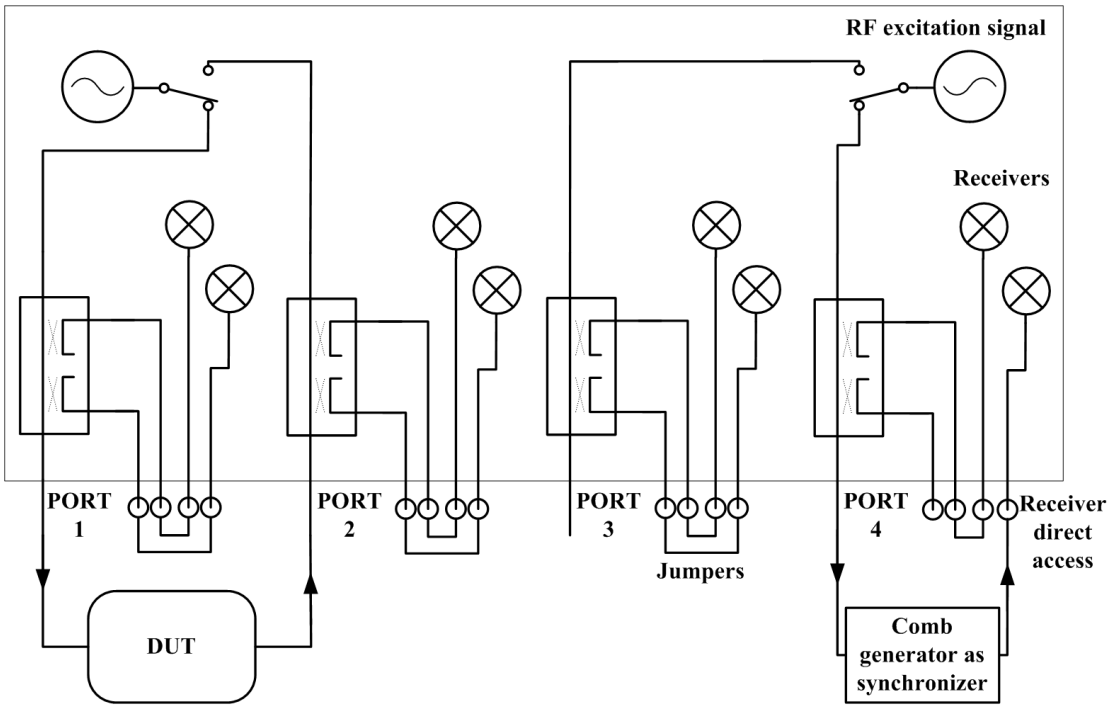

FIGURE 2.36: NVNA setup using a synchronizer for phase coherence preservation

One of the simplest comb generator is the one taking advantage of a strongly nonlinear component such as a diode or a transistor. For example one of the comb generators used in this work was provided by NMDG® and is simply based on a Step Recovery Diode (SRD) from Herotek® [66]. A SRD is used for pulse generation because when switched from forward to reverse bias, it has a fast recovery time allowing it to produce pulses with sharp and fast rise times. As we can see in Figure 2.37 the comb generator is only composed of an amplifier to drive the diode with a power sufficient to create the biasing inversion, the SRD and an attenuator to scale down the power to be measurable by the instrument and provide some padding to the diode avoiding some unexpected nonlinear effects caused by the matching of the diode. The driving signal that is meant to be provided by one of the instrument sources as in Figure 2.36 must be extremely constant as the output signal of the diode is highly dependent on its driving power which may interfere with repeatability. SRD tend to have in this operation mode a non negligible phase noise that is also a limiting factor for the nonlinear application. This synchronizer model performance is entirely inherited from the SRD meaning that it can output signals up to 20GHz with a limitation on the fundamental frequency comprised between 600MHz and 1.2GHz (giving a smallest tone spacing of 600MHz). Such a comb generator is sufficient for the characterization of the

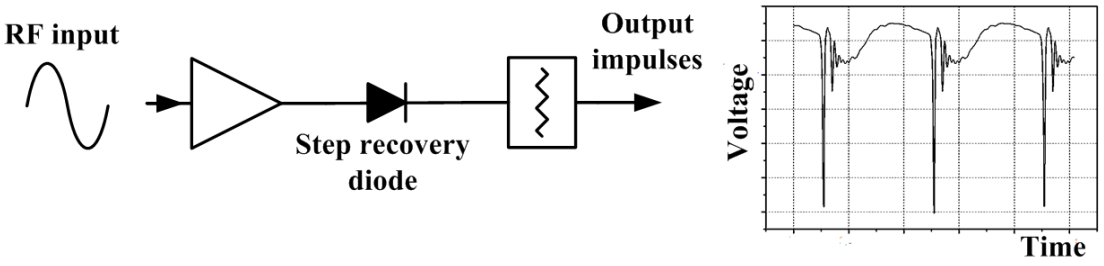

FIGURE 2.37: Step Recovery Diode (SRD) based comb generator

harmonics of an amplifier operating in the S-band that is the aim of this work.

Another approach using diodes allows a better bandwidth up to 30GHz with a fundamental range from 400MHz to 3 GHz [67] compared to the SRD one. NonLinear Transmission Line (NLTL) as shown in Figure 2.38 is a high impedance line loaded at defined fractions of its length by a reverse biased Schottky contact used as varactor. With increasing reverse bias of the varactor, the propagation delay is reduced in the NLTL therefore reducing the rise and fall time of a signal traveling in it. When a sinusoidal signal is inputted to the NLTL, the signal will be altered into forming a pulse. Sadly because of the losses in the line, a low pass effect will occur limiting the bandwidth of the line. As NLTL can be used as pulse

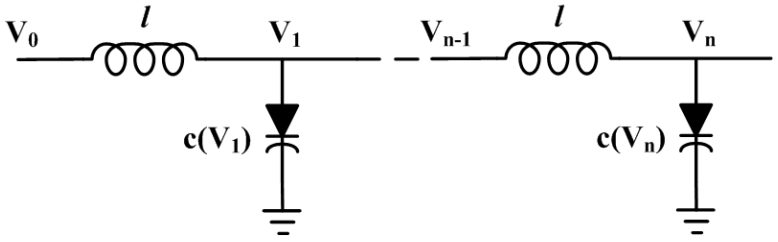

FIGURE 2.38: NonLinear Transmission Line NLTL based comb generator

sharpening device when inputted with a pulse, it is not uncommon to find a NLTL after a SRD diode in a comb generator as in [68].

Such synchronizers however are limiting the amount of nonlinear effects that one can investigate. For example one may want to observe signals that are not harmonics of the fundamental frequency as for mixer measurement. A smaller tone spacing may therefore be required to synchronize the measurement of all these frequencies.

An attempt to solve this issue by driving the SRD diode with a multi-tone signal was proposed in [69]. This solution will indeed slightly increase the tone density

but it is not providing the low fundamental frequency that may be required for frequency conversion components such as mixers. More recently a design aimed at providing a dense comb was proposed in [70]. As shown in Figure 2.39, it is based on a Non Return to Zero (NRZ) sequence provided by a Pseudo-Random Bits Sequence (PRBS) generator. This sequence is then split in two path and one

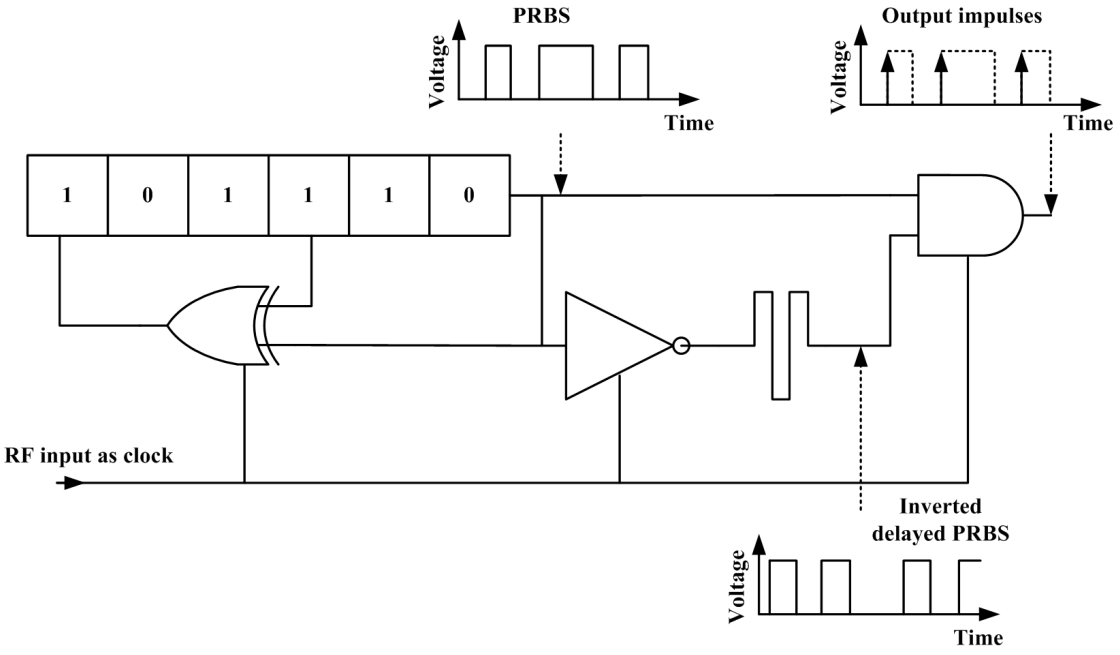

FIGURE 2.39: Pseudo-Random Bit Sequence (PRBS) based comb generator

of the sequences is inverted and delayed relatively to the other. The signals are then multiplied in a fast "AND" gate providing in result a short impulsion. The fundamental frequency of the comb generator will be equal to the clock frequency of the logic components and the shape of the comb will be related to the initial sequence of the PRBS generator. Many sequences are known and provided by the electromagnetic compatibility engineer community [71] that use such generator since longer than the nonlinear characterization community. During this work, such a comb generator was accessible and provided by Sympulse® and NMDG® [72] that had a maximum frequency of 40GHz and a guaranteed tone spacing of 20MHz (but up to 20GHz it was usable at 10MHz tone spacing) for a fundamental between 10MHz and 2.56GHz. As the clock signal is provided directly by a source of the VNA as previously, a programmable frequency divider is present to use the VNA's source around the GHZ and avoid the VNA's hardware performance degradation at frequencies inferior to 1GHz.

A closely related solution patented by Agilent Technologies® [73] and invented by D.B. Gunyan and J.B. Scott is using a Split Signal Pulse Generator (SSPG). Such a generator is composed as shown in Figure 2.40 of a splitter, a delay line and an inverter as for the PRBS based generator. The input impulse is provided by an unspecified pulse generator when it was provided by the PRBS previously and this time the recombination of the path is made through the use of a differential amplifier instead of an AND gate. The circuit is realized using the Indium Phosphide Monolithic Microwave Integrated Circuit (InP MMIC) technology. This comb generator is guaranteed to provide a tone spacing of 10MHz up to a maximum frequency of 67GHz and a fundamental frequency between 10MHz and 6GHz. This comb generator also has frequency divider for the same reason as for the PRBS based generator.

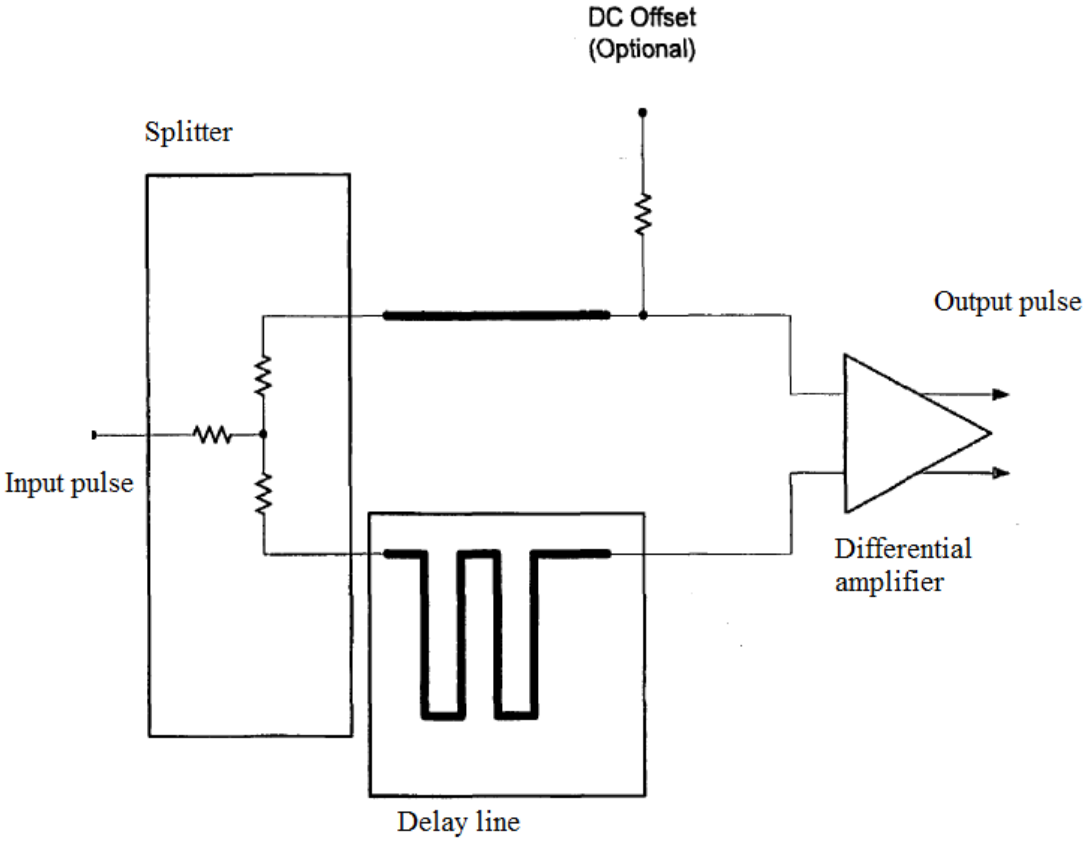

FIGURE 2.40: Split Signal Pulse Generator (SSPG) comb generator [73]

A general concern with nonlinear measurement is that it quickly requires a large frequency bandwidth to measure a significant number of harmonics for a high fundamental frequency. The maximum available frequency for a mixer based NVNA is 67GHz (which the maximum available frequency for a comb generator). To push

this maximum frequency limit, optoelectronic solutions have been investigated. An optical pulse is generated using a laser, a Mach-Zender modulator and a RF source as shown in Figure 2.41. This optical pulse is then converted into an electronic pulse thanks to a photodiode. Nevertheless, if the difficulty of generating a 100GHz bandwidth optical comb is moderate as many off the shelf components are available, the photodiode still limits the maximum bandwidth to frequencies around 75GHz [74]. There is no commercial solution to the author knowledge using this technology.

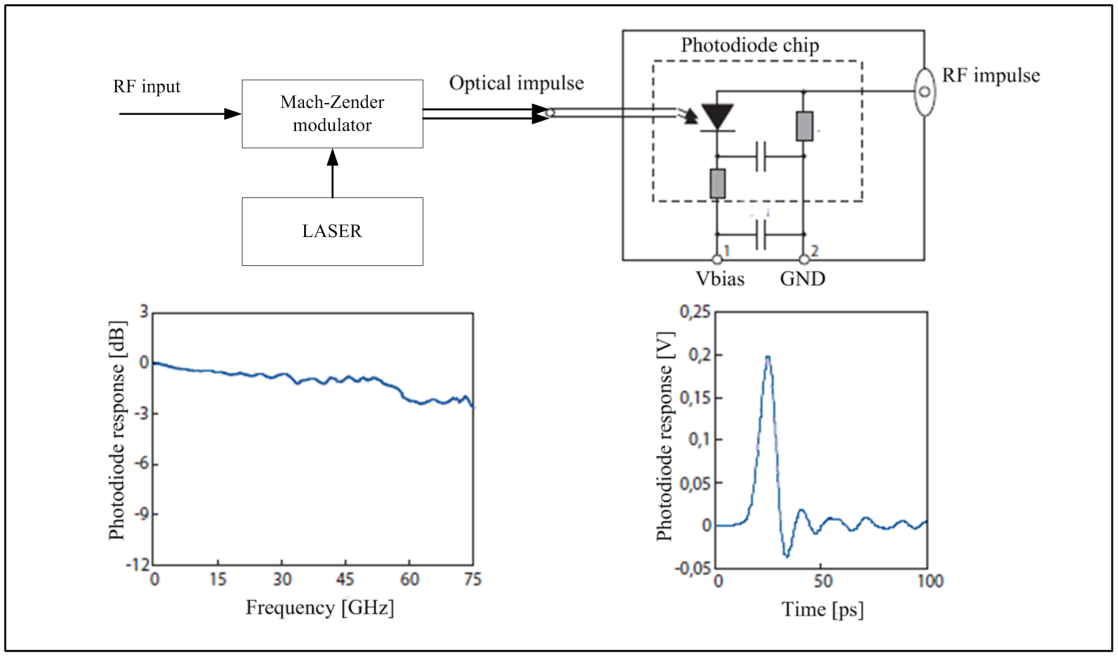

FIGURE 2.41: Optical comb generator [74]

A drawback of all the solutions using a comb generator is that the measurable bandwidth and the tone spacing are limited by the bandwidth and tone spacing of the comb which will never be as good as the tone spacing and bandwidth of a heterodyne based instrument such as a VNA. In fact the tone spacing and the maximum bandwidth of a VNA are not correlated which is not true for a comb generator with a finite available quantity of energy to spread over many tones. For this reason, solutions are proposed to provide only a selection of tones. A commercially available example is provided by Mesuro® that use a transistor providing the same harmonic content as the DUT up to 67GHz. A solution using digital electronics is also investigated at the University of Leuven [75] but is so far limited to some GHz.

From Figure 2.42 that shows the magnitude of the different tones composing the comb, it is possible to understand that the highest tones of the comb will be measured with decreased accuracy by the instrument as the SNR is degraded. This limits the accuracy of the NVNA at high frequencies.

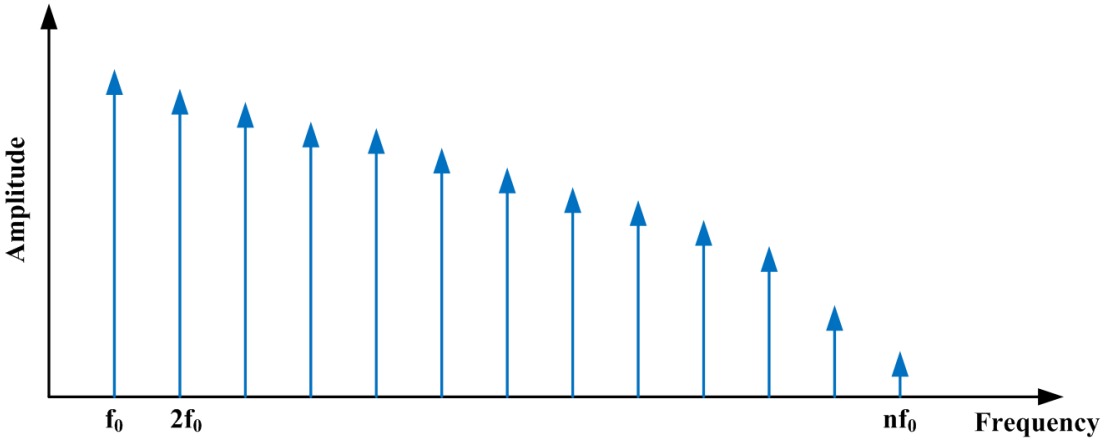

FIGURE 2.42: Comb magnitude decreasing with the frequency until fading

Phase repeatable local oscillator

Compared to the use of an external reference generator, having a local oscillator that can ensure the same phase relationship between the measured frequencies at each sweep allows to keep phase coherence while freeing one source and one receiver of the VNA and keeping the extremely small frequency step of the instrument.

A concrete realization of such a local oscillator makes use of the possibilities offered by the direct digital synthesis we encountered in Section 2.3.2. This type of synthesizer is based on a phase counter to generate a signal therefore the phase of the signal could, in an ideal case, be determined knowing the initial command word and the state of the phase counter (or the time elapsed since the starting of the DDS).

Knowing the exact value of the phase would be an overkill to keep phase coherence because the exact value of the phase is not required and correction of the phase relationship between the frequencies will be taken care of during calibration. Having a LO synthesizer that will output at each frequency a signal with the same phase provided that the initial word and the time between the beginning of the synthesis and the measurements are the same at each sweep is enough for phase coherence. Please note that phase coherence is preserved in case of a constant

delay being applied to every point of the sweep as the phase relationship between the frequencies will remain constant.

Luckily, as we have seen in 2.3.4, the acquisition time of every sweep point is constant as long as the VNA has all the settings that involve a non constant modification of the elapsed time between sweep points (such as some complex user triggering on point instead of the whole sweep for example) are unchanged between sweeps. We can use DDS to generate the LO signal and keep phase coherence with an arbitrary and extremely small frequency step. It also allows to release the stress on the number of port as a two port instrument can now perform a two ports nonlinear measurement.

A major issue of the direct digital synthesis use in the VNA environment is its bandwidth limitation. Because the clock signal as to be at least twice the DDS output frequency (four times is recommended) and that frequency multipliers increase the phase noise, it is difficult to synthesize a phase repeatable signal of good quality above 10GHz. It is possible to keep the advantage of the DDS while improving the bandwidth using a hybrid DDS/PLL approach. The DSS is used as reference signal of the PLL that locks on a phase controlled signal and outputs therefore a phase controlled signal. The PLL allows a higher bandwidth than the DSS and profits of its maturity being a widely studied component at the cost of an increase settling time at frequency change compare to the DDS.

Preserving phase coherence thanks to a instrument equipped with such an LO synthesizer was first shown by the company Mesuro® on a ZVA67 for frequencies above 1GHz.

2.4.3 Calibration

A NVNA is, as a VNA, prone to systematic errors. Many of them are identical to the ones we described for the VNA in Section 2.3.5. Some of them nevertheless are caused by the difference of measurement procedure between a VNA and a NVNA. In fact when calibrating a VNA, only the errors that were influencing the ratios of traveling wave at a same frequency were corrected. A mixer based NVNA is linking traveling waves at many frequencies so all the effects that were compensated when applying the ratio and the effects happening between the different frequencies are

also interfering with the measurement accuracy. The NVNA calibration consists of three different calibration procedures described by J. Verspecht [76]:

- A relative calibration
- A power calibration
- A phase calibration

We will be focusing on the procedure for connectorized measurement for a global understanding of the calibration method.

Relative calibration

The relative calibration is equivalent to the VNA calibration. It evaluates the errors applying on the traveling wave ratios at a same frequency due to the test set and differences in the receivers of the NVNA as we described for the VNA in Section 2.3.5. Historically this calibration procedure was implemented for what we nowadays generally call a NVNA on the LSNA, the model error was chosen based on the assumption that the instrument had four receivers (excluding the three receivers VNA implementation) allowing the choice of the following 7-terms model with:

$$\begin{pmatrix} a_1 \\ b_1 \\ a_2 \\ b_2 \end{pmatrix} = \begin{pmatrix} \alpha_1 & \beta_1 & 0 & 0 \\ \gamma_1 & \delta_1 & 0 & 0 \\ 0 & 0 & \alpha_2 & \beta_2 \\ 0 & 0 & \gamma_2 & \delta_2 \end{pmatrix} \begin{pmatrix} a_{1Measured} \\ b_{1Measured} \\ a_{2Measured} \\ b_{2Measured} \end{pmatrix} \tag{2.19}$$

The effects of crosstalk are, as we did in Section 2.3.5, neglected because the measurement is performed in connectorized conditions and the architecture of the instrument allows us to do so. For the good functioning of the instrument α_1 cannot be equal to 0 as no power would be sent to the DUT. Therefore we set $\alpha_1 = 1$ transferring its influence to all the other terms of the matrix. The error terms are identified in the LSNA using the same standards used for the TOSM calibration, it is equivalent to a VNA's 7-terms calibration as shown in Figure 2.43. Nevertheless it is important to note that the chosen error model is ordering the terms in a different order compared to the error model implemented in VNAs based on S-parameters.

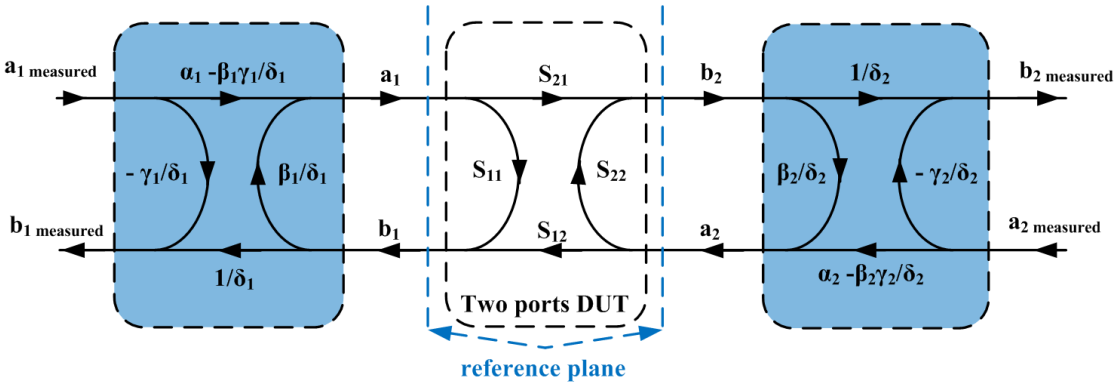

FIGURE 2.43: Equivalence between the relative calibration model and a 7-terms VNA model

It is therefore possible to convert the error terms calculated by the VNA firmware and stored as raw system data into the coefficient of the NVNA error model when a 7-terms calibration is performed. Having at disposal many calibration procedures implemented into the VNA, we will always convert the error model of the VNA into the NVNA model for nonlinear measurement instead of implementing a new procedure.

In practice, the three receivers VNA implementation historically preceding the four receivers one, the raw system data stored into many modern VNAs are the one corresponding to the 12-terms model (equivalent to the 10-terms we described plus two terms for the isolation) despite the fact they have four receivers. For example when performing a 7-terms calibration such as TRL (Through Reflect Line), the error terms are converted to the 12-terms model using a comparable method as the one exposed by R.B. Marks in [77]. The same method can be used to convert error terms stored in a VNA into the described NVNA 7-terms error model as follow:

Using the traveling waves of the model of equation 2.19 and identifying them to the waves of the 10-terms forward sub-model we obtain this system of equations:

$$a_1 = e_{11}.b_1 + e_{10}.a_{1Measured} \tag{2.20}$$

$$b_{1Measured} = e_{01}.b_1 + e_{00}.a_{1Measured} \tag{2.21}$$

It is then possible to link the corrected to the measured traveling waves:

$$a_1 = \frac{e_{11}}{e_{01}}.b_{1Measured} + (e_10 - \frac{e_{11}e_{00}}{e_{01}}).a_{1Measured} \tag{2.22}$$

$$b_1 = \frac{1}{e_{01}}.b_{1Measured} - \frac{-e_{00}}{e_{01}}.a_{1Measured} \tag{2.23}$$

And finally express the first four NVNA error terms using the forward 10-terms error terms:

$$\alpha_1 = e_{10} - \frac{e_{11}e_{00}}{e_{01}} \tag{2.24}$$

$$\beta_1 = \frac{e_{11}}{e_{01}} \tag{2.25}$$

$$\gamma_1 = \frac{-e_{00}}{e_{01}} \tag{2.26}$$

$$\delta_1 = \frac{1}{e_{01}} \tag{2.27}$$

Repeating the operation for the reverse sub-model we obtain the last four terms of the NVNA 7-terms model:

$$\alpha_2 = e'_{23} - \frac{e'_{22}e'_{33}}{e'_{32}} \tag{2.28}$$

$$\beta_2 = \frac{e'_{22}}{e'_{32}} \tag{2.29}$$

$$\gamma_2 = \frac{-e'_{33}}{e'_{32}} \tag{2.30}$$

$$\delta_2 = \frac{1}{e'_{32}} \tag{2.31}$$

Applying the normalization so $\alpha_1 = 1$ we finally get:

$$\alpha_1 = 1 \tag{2.32}$$

$$\beta_1 = \frac{e_{11}}{e_{10}e_{01} - e_{11}e_{00}} \tag{2.33}$$

$$\gamma_1 = \frac{-e_{00}}{e_{10}e_{01} - e_{11}e_{00}} \tag{2.34}$$

$$\delta_1 = \frac{1}{e_{10}e_{01} - e_{11}e_{00}} \tag{2.35}$$

$$\alpha_2 = \frac{e'_{23}e'_{32} - e'_{22}e'_{33}}{e_{10}e_{01} - e_{11}e_{00}} . \frac{e_{10}e_{01}}{e'_{32}} \tag{2.36}$$

$$\beta_2 = \frac{e'_{22}}{e_{10}e_{01} - e_{11}e_{00}} . \frac{e_{10}e_{01}}{e'_{32}} \tag{2.37}$$

$$\gamma_2 = \frac{-e'_{33}}{e_{10}e_{01} - e_{11}e_{00}} . \frac{e_{10}e_{01}}{e'_{32}} \tag{2.38}$$

$$\delta_2 = \frac{1}{e_{10}e_{01} - e_{11}e_{00}} . \frac{e_{10}e_{01}}{e'_{32}} \tag{2.39}$$

Sadly the term e'_{32} is not stored alone by the VNA but rather in form of the reverse reflection tracking $e'_{32}e'_{23}$ as explained in Section 2.3.5. Using the fact that both 8-terms and 12 terms model are describing the same setup, it is possible using the derivation described in Appendix A to extract the term e'_{32} using the other error terms as follow:

$$e'_{32} = \frac{e'_{32}e'_{23}}{e'_{01}e'_{23}} . (e_{01}e_{10} + e_{00} . (e_{22} - e_{11})) \tag{2.40}$$

It is now possible to measure corrected traveling wave ratios with the NVNA exactly as a VNA would.

Power calibration

As seen in Section 1.4.3 the performance of a nonlinear system is often power dependent contrary to a the linear system ones. Therefore the exact knowledge of the power of the excitation signal is of prime importance.

Both the test set and the receiver alter the measured power of the signal effectively present at the DUT input. The main causes of alteration are generally frequency dependent such as losses and mismatches in the test set and conversion loss or gain of the receiver's mixer during down-conversion. These losses were overlooked in the previously described relative error model when all the error terms

where normalized. All the terms calculated during relative calibration must therefore be offset by the error on the measured magnitude. This done by adding a frequency dependent term to the relative error model that accounts for the error in magnitude at each frequency:

$$\begin{pmatrix} a_1 \\ b_1 \\ a_2 \\ b_2 \end{pmatrix} = K. \begin{pmatrix} \alpha_1 & \beta_1 & 0 & 0 \\ \gamma_1 & \delta_1 & 0 & 0 \\ 0 & 0 & \alpha_2 & \beta_2 \\ 0 & 0 & \gamma_2 & \delta_2 \end{pmatrix} \begin{pmatrix} a_{1Measured} \\ b_{1Measured} \\ a_{2Measured} \\ b_{2Measured} \end{pmatrix} \tag{2.41}$$

The added term K only needs to be a real number to account for the magnitude error. This term is characterized by measuring the provided excitation signal with a power meter and compare it to the power measured by the VNA. Nevertheless power meter sensors also suffer from potential measurement mistake due to their reflection coefficient Γ_{PM} and transmission factor T_{PM} as modeled in Figure 2.44. These values are at least provided by the power sensor manufacturer and can be considered as known. The traceability of the calibration is ensured by the traceability of the power meter. At the power meter sensor we have:

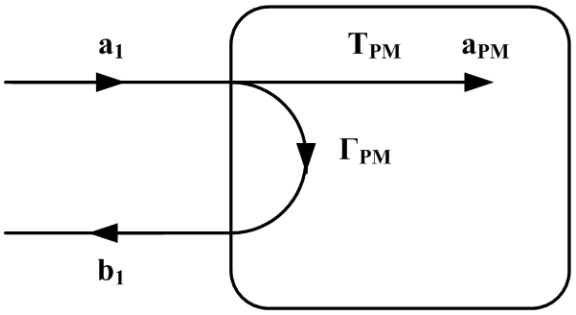

FIGURE 2.44: Power meter error model

$$|a_{PM}| = |T_{PM}.a_1| \tag{2.42}$$

Which can be written according to 2.41 as:

$$|a_{PM}| = |T_{PM}.K.(\alpha_1.a_{1Measured} + \beta_1.b_{1Measured})| \tag{2.43}$$

therefore using both power meter and VNA measurements we have:

$$|K| = \frac{|a_{PM}|}{|T_{PM}.(\alpha_1.a_{1Measured} + \beta_1.b_{1Measured})|} \tag{2.44}$$

Modern power meter often include the correction of the transmission factor in their outputted results. In that case we can assume that $T_{PM} = 1$ in equation 2.44.

It is now possible to measure traveling waves corrected in magnitude with the NVNA. Please note that the VNA used possesses the same capability using comparable methods [78] to perform scalar measurements of frequency conversion devices such as mixers.

Phase calibration

In Section 2.4.2 the importance of ensuring phase coherence of the instrument to be able to measure a fixed phase relationship between the traveling waves at different frequencies was explained. The accuracy of the measurement of this phase relationship is influenced by two main sources of error in a mixer based NVNA:

- The phase dispersion in the measurement frequency bandwidth induced by the test set and the receivers (common to every type of instrument).
- The sequential measurement of each tone and the influence of the local oscillator on the phase difference between signals at different frequencies (only influencing mixer based NVNA).

Both aspects are gathered and taken into account by a phasor $\exp^{-j\phi}$ to the error model. Often it is gathered with the magnitude correction term as follow:

$$\begin{pmatrix} a_1 \\ b_1 \\ a_2 \\ b_2 \end{pmatrix} = \bar{K}. \begin{pmatrix} \alpha_1 & \beta_1 & 0 & 0 \\ \gamma_1 & \delta_1 & 0 & 0 \\ 0 & 0 & \alpha_2 & \beta_2 \\ 0 & 0 & \gamma_2 & \delta_2 \end{pmatrix} \begin{pmatrix} a_{1Measured} \\ b_{1Measured} \\ a_{2Measured} \\ b_{2Measured} \end{pmatrix} \tag{2.45}$$

With:

$$\bar{K} = |K|. \exp^{-j\phi} \tag{2.46}$$

To evaluate the phase of $\bar{K}$ a reference generator is used. This reference generator that is also called Harmonic Phase Reference (HPR) is a generator that has the phase relationship (as defined in 2.4.2) between all the frequencies it outputs characterized and as for every standard is traceable. The model used for the reference

generator is shown in Figure 2.45 and mostly take into account its reflection coefficient Γ_{HPR}. When performing a measurement of the reference generator with

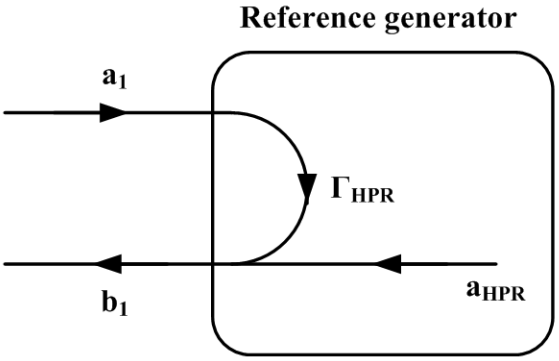

FIGURE 2.45: Phase reference error model

the VNA we have:

$$b_1 = a_{HPR} + \Gamma_{HPR}.a_1 \tag{2.47}$$

According to 2.45 it can be writen as:

$$\bar{K}(\gamma_1.a_{1Measured} + \delta_1.b_{1Measured}) = a_{HPR} + \Gamma_{HPR}\bar{K}(\alpha_1.a_{1Measured} + \beta_1.b_{1Measured}) \tag{2.48}$$

The phase of $\bar{K}$ is therefore:

$$\arg(\bar{K}) = \arg(\frac{a_{HPR}}{(\gamma_1 - \Gamma_{HPR}.\alpha_1)a_{1Measured} + (\delta_1 - \Gamma_{HPR}\beta_1)b_{1Measured}}) \tag{2.49}$$

It is now possible to measure traveling waves at different frequencies which relative phase is corrected with the NVNA. If the relative and power calibration were already used for other applications, the phase calibration is, with the phase coherence described in Section 2.4.2 for a mixer based instrument, the key feature allowing nonlinear measurement.

Phase calibration's practical realization

The first step to enable phase calibration is the realization of the reference generator. The requirement for such a generator is to be able to produce frequencies that have constant phase relationships between each other. Such devices were already described in the Section 2.4.2. In fact every concept of generator that phase phase coherence in mixer based instrument is a potential candidate for a reference generator. However, if comb generator are widely used, there is yet no commercial use

of DDS based designs as a phase reference. In this work only available commercial generators were used.

Next it is needed to characterize the phase differences between the tones as for a reference generator the insurance of repeatability is not sufficient. Also to be promoted to the rank of standard the generator must be characterized with a method allowing traceability. This is done with a sampling oscilloscope calibrated with the "nose to nose" method described by J. Verspecht in [79]. The reflection coefficient of the reference generator is characterized using a calibrated VNA. The characterization of the reference generator must be realized at least in the full bandwidth of usage with a frequency step small enough to allow interpolation between the characterized points that depends on the technology used. Every phase reference should come with at least these two characterizations stored in files. Because the correction of the raw traveling waves are performed in the frequency domain (even in a time domain instrument), these files are using frequency domain data.

When extracting error coefficients from any calibration method there are two desirable capabilities we want:

- The averaging of the raw measurements.
- The interpolation of the reference generator characterization data.

If averaging complex values is an easy mathematical task, averaging the complex raw data measured at different sweeps by the NVNA must be handled with some precaution. In fact the NVNA is designed to preserve the phase relationship between tones, but the absolute phase value of each tone may change over time. If we use the raw values as they are given we might get a wrong result due to this changes in the absolute phase value. A simple workaround is to use a common normalization of the phases of the different tones that is equivalent in time domain to finding a constant delay that make two time domain waveforms fit each others.

The most natural normalization would be to use the phase of the excitation signal measurement at the fundamental frequency to normalize the phases of the other tones of the sweep. Doing so at each sweep it is then possible to average all the tones. This simple method induces however a loss of accuracy. In fact, as every measurement comes with a given uncertainty, using the result at the fundamental

frequency to normalize the other phases will propagate the uncertainty of the measurement at the fundamental frequency Err_{f_0} and add it to the uncertainty of the n^{th} tone Err_{nf_0} as follow:

$$Err_{Normalized}(nf_0) = Err_{nf_0} + n.Err_{f_0} \tag{2.50}$$

With such a normalization method, the higher the order of the normalized tone the worst the error on the phase may potentially be. To avoid such a degradation of the performance due to post processing, a different method must be used.

Many synchronization techniques that addresses similar issues (especially in the field of sound processing) are available, most of them making use of either cross-correlation, least square estimators, total least square estimator or frequency domain identification of linear system (ELIS) [80]. All of them rely on the minimization of an error function or equivalently on the maximization of a likelihood function in different conditions. For example in the least square method, noise is attributed only to one of the signals to synchronize while total least square applies noise on both signals complicating the likelihood function to maximize. In the scope of phase comparison, care must be taken to choose a method that preserves the phase accuracy.

Of course, as every optimization method, the choice of the initial value has a great influence on the outcome of the optimization. A detrending procedure based on this concept was proposed by K.A. Remley [81] in 2003 addressing the particular case of NVNA measurement. The procedure relies on two main steps, first find an approximate delay between the time domain waveforms computed at each sweep and then minimize an error function to refine the found delay to a user defined precision. This method implies that the spectrum measured at one of the sweeps (often the first measured) is taken as reference for the spectra of all the other sweeps.

If making an educated guess of the delay before minimizing an error function is optional, it is recommended to fasten the convergence of the error function minimization and avoid local extrema. A first estimate can be taken for example using the delay found at fundamental frequency. Such an estimation is equivalent to the normalization by the phase of the fundamental frequency. Another method would be to estimate the delays between many consecutive tones and extract an

average value of a fraction of the delay (considering that the measurement delay to be found is a constant).

For the particular problem of synchronization, many error function are available. One could try to minimize the phase difference at each tone between each signal or minimize the difference between two complex vectors at each tone. Because it is better to identify the delay using the measurements taken at best SNR, methods taking into account the magnitude of the tones to weight the estimation of the delay can be useful.

For many optimization techniques such as the cross correlation, it may be better to compare vectors of the same magnitude to get a better estimate of the delay. The improvement brought by a simple non optimized cross correlation method is shown in Figure 2.46 and Figure 2.47. It is done by comparing the phase of given by the available phase reference characterization file and a same measurement treated with normalization by the phase of the fundamental and a cross correlation method optimized for frequencies lower than 12GHz.

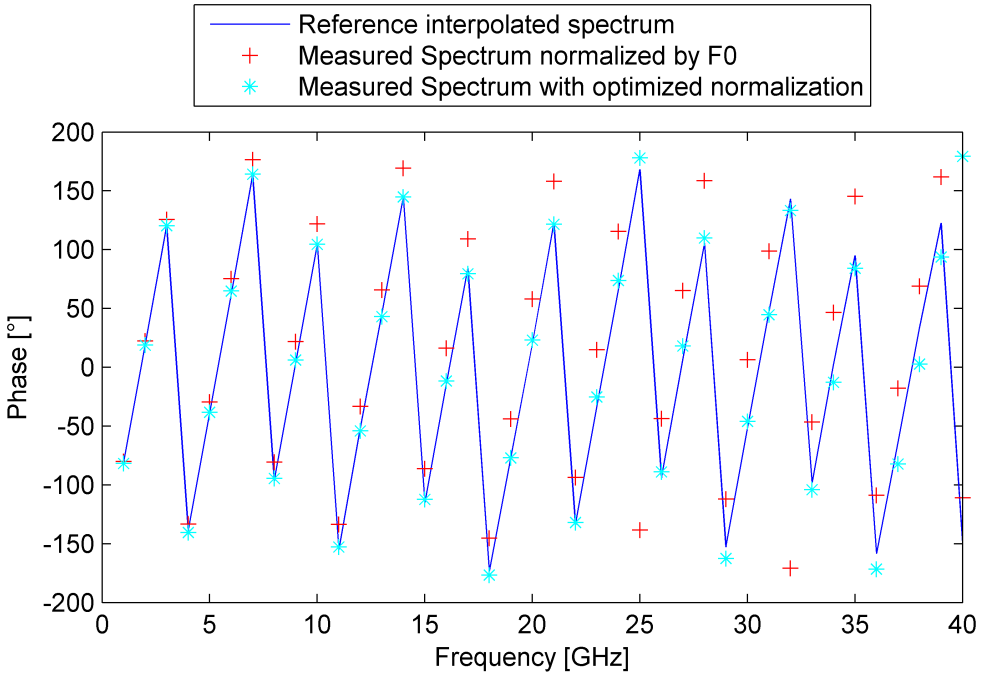

FIGURE 2.46: Phase of spectrum with different normalization methods

The interpolation method to be used generally depends on the data available or the law followed by the data. There is no absolute interpolation method. For

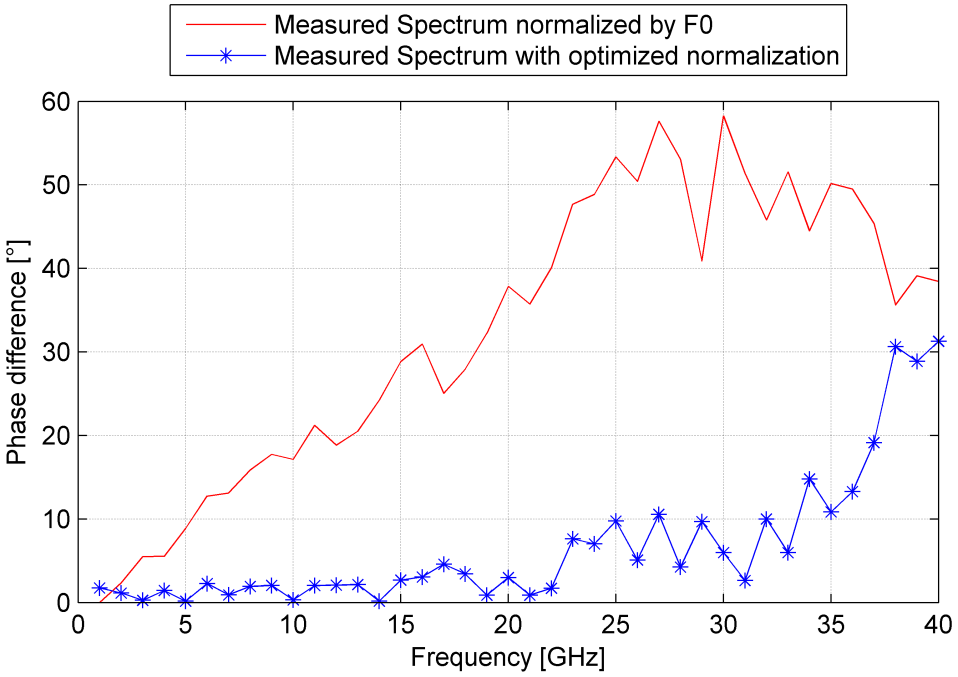

FIGURE 2.47: Phase difference of the normalization methods compared to the reference file phase

example a SRD based comb generator from the company NMDG® would come with a characterization file containing the spectra of the generator excited at different fundamental frequencies spaced only by some MHz. This results in a dense data grid where linear interpolation would probably work fine.

The characterization data provided with the phase reference NM300 from the company NMDG® used in this work consists of frequency samples taken every 250MHz up to 50GHz. Contrary to the characterization of the SRD based comb generator, the spectrum at only one fundamental frequency of 250MHz is available.

In time domain, this is equivalent to having a time waveform sampled at the sampling interval T. Building a new frequency grid from this band limited time domain waveform is equivalent to resample the time domain signal at a different interval T'. Resampling the waveform means that the new sample must be interpolated from the existing samples. This problem of digital signal processing as been addressed through a method called bandlimited interpolation.

The N samples $x(nT)$ of the waveform $x(t)$ outputted by the phase reference are available from the characterization file where n is integer and T is the sampling period inferior or equal to the Nyquist interval. Assuming that $X(\omega) = 0$ for

$|\omega| \geq \pi/T$ with $X(\omega)$ is the Fourier transform of $x(t)$, Shannon's sampling theorem states that that $x(t)$ can be uniquely reconstructed from the samples $x(nT)$ via

$$x(t) = \sum_{n=-\infty}^{\infty} x(nT) \sin_c(\frac{\pi}{T}(t - nT)) \tag{2.51}$$

It is therefore possible to extract the new sample $x(mT')$ by calculating using equation 2.51 at the new sampling interval T' so $MT' = NT$ where M is the new sample number as follow:

$$x(mT') = \sum_{n=-\infty}^{\infty} x(nT) \sin_c(\frac{\pi}{T}(mT' - nT)) \tag{2.52}$$

The interpolation process can be seen as the result of convolving the interpolation function $\sin_c(\frac{\pi}{T}t)$ with the samples $x(nT)$ and then resampling with interval T'.

Convolution can be done easily using a discrete Discrete Fourier Transform (DFT) and ressampling with DFT is possible by adding nul samples but it is limited to the solutions where $M = NT/T'$ is an integer.

In the particular case of interpolating the data of the available reference generator, M might not be an integer as the fundamental frequency required for the NVNA measurement may not be a multiple of 250MHz. This problem can be overcome by using the Chirp-Z Transform (CZT) algorithm [82] that allows resampling with better flexibility than the DFT. Tests were run to validate the interpolation used with the available phase reference.

As a new NVNA software was written for this work, the available phase reference is not used with its original firmware. Using the Agilent®'s PNA-X available at IEMN, the proper functioning of the phase reference was verified before verifying the interpolation procedure. In Figure 2.48 we can see the phase of the spectrum measured by the PNA-X compared after detrending to the phase given by the characterization file. Figure 2.49 shows a good agreement of the phase up to 40GHz keeping into account the precision of the PNA-X in the measurement condition and the fact that the highest tones of the phase reference are measured with degraded SNR.

The dependency of the phase reference output to the power was tested as, contrary to a SRD based model, no precaution seemed to be taken to precisely control the power. Different driving power where applied and the phases of the obtained

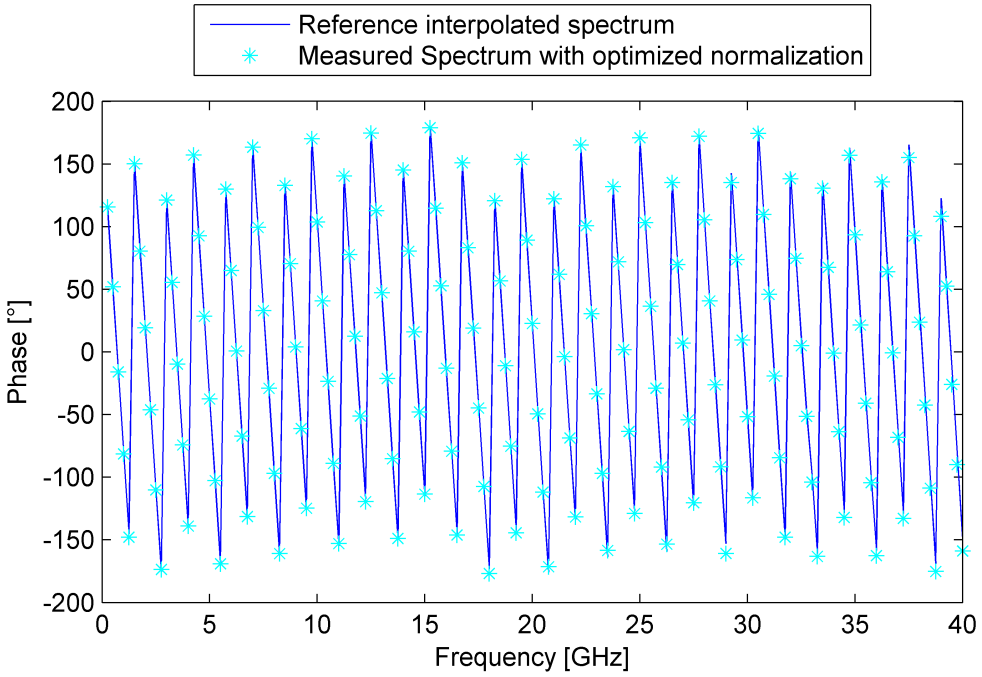

FIGURE 2.48: Spectrum phase measured and given by the characterization file of the phase reference

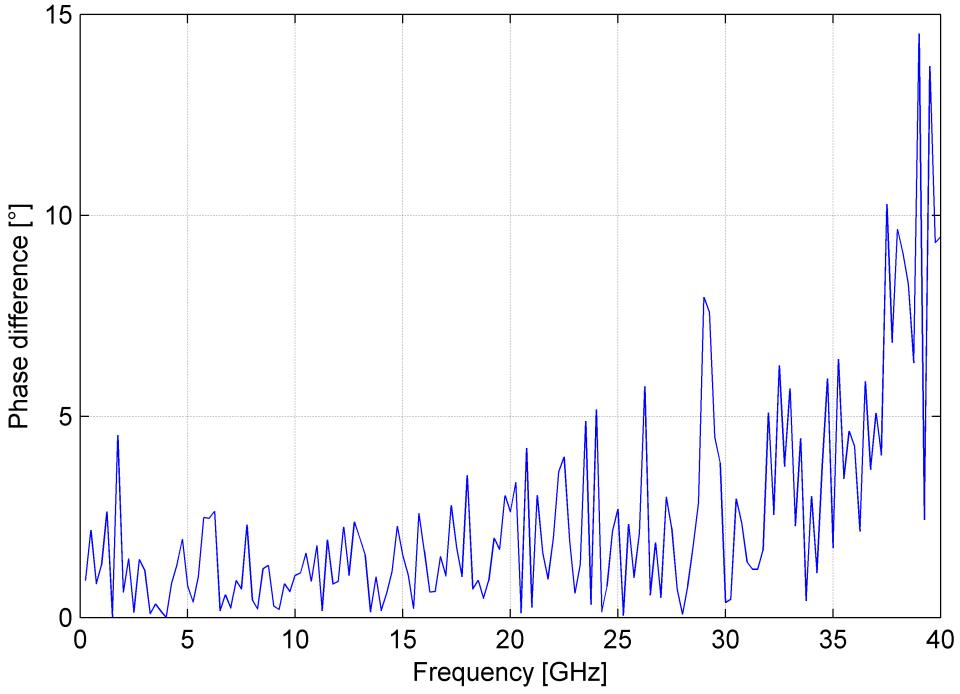

FIGURE 2.49: Phase difference between the phase measured and given by the characterization file of the phase reference

spectra were compared. In Figure 2.50, we can see on the comparison of the phases at different powers relatively to the phase at 2.5dBm that the power has no influence on the phase relationship between the tones at frequencies under 20GHz and the influence observed at higher frequencies probably come from the degraded measurement due to the loss of power at the higher tones.

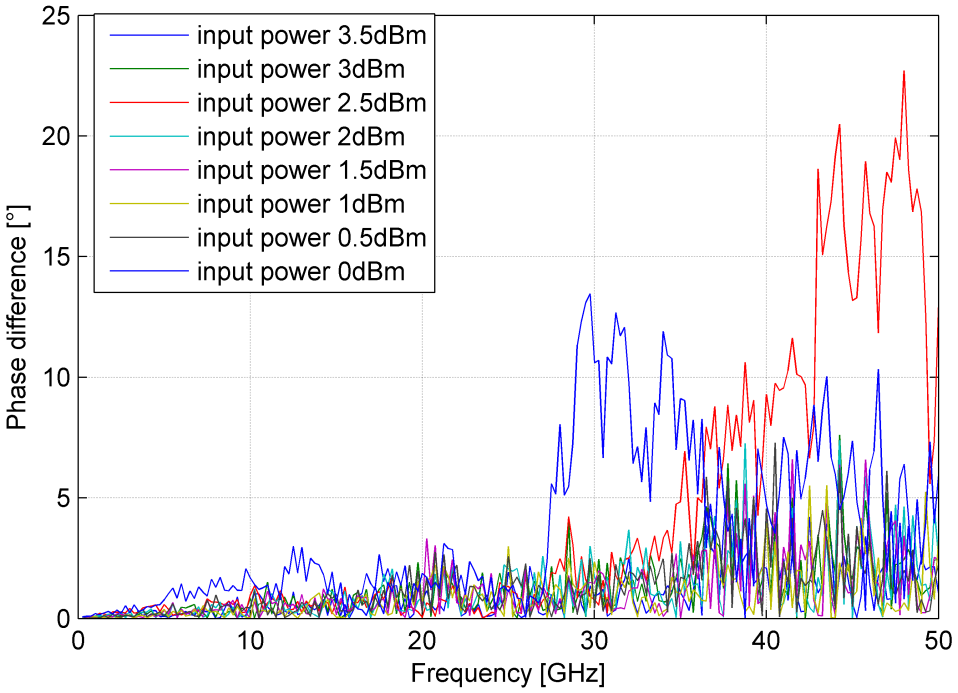

FIGURE 2.50: Normalized phase measurement at different phase reference input power

For the chosen interpolation method to work, the assumption that the phase relationship between the tones is independent of the frequency driving the reference generator was made. This assumption was enforced by the description of the concept of the phase reference [70] where independently of the frequency the signal goes through the same components used in their linear functioning applying the same delays. The fact that the provided characterization file only includes the measurement at a 250MHz fundamental was confirming our hypothesis. To verify the assumption, three different fundamentals with many common harmonics were used and the phase relationship between their common tones compared. Figure 2.51 shows the phase of the common tone using 250MHz, 500MHz and 1GHz as fundamental and synchronized to the values of the characterization file. The phase difference of each case compared to the characterization file is shown in Figure

2.52. The measured difference falls into the PNA-X precision in the measurement conditions.

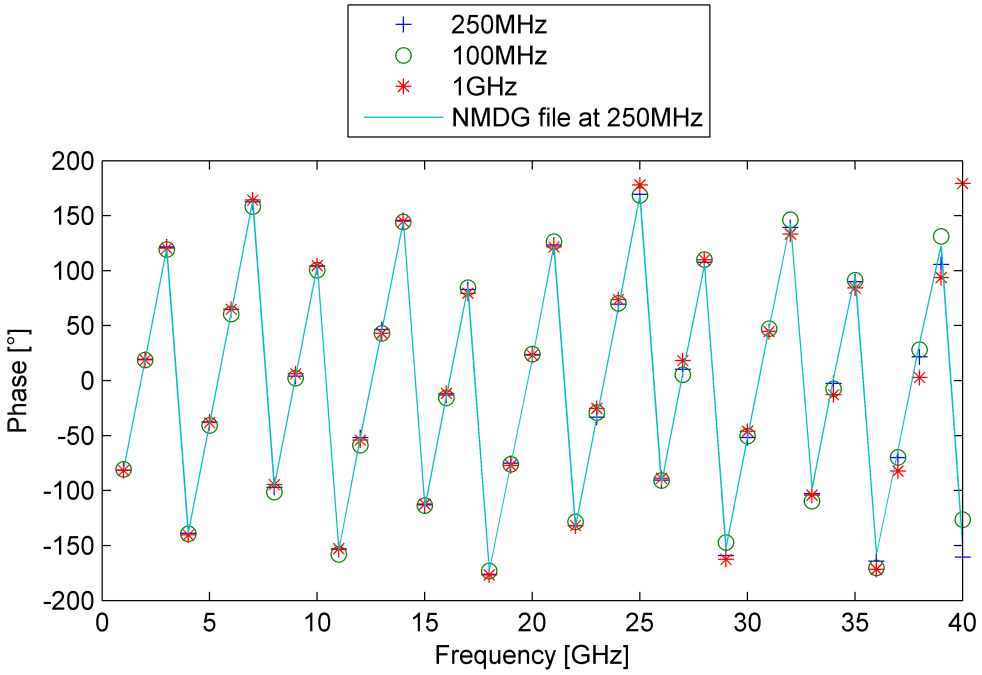

FIGURE 2.51: Spectrum phase at the common tones of phase reference at input fundamental of 250MHz, 500MHz and 1GHz and on characterization file

Finally the interpolation method was tested using a 2.9GHz fundamental frequency to drive the phase reference. Figure 2.53 shows the phases of the spectrum measured with the PNA-X along with the phases computed using interpolation. We can see in Figure 2.54 a good agreement between the measured phases and the calculated ones up to 20GHz which is sufficient for the purpose of this work.

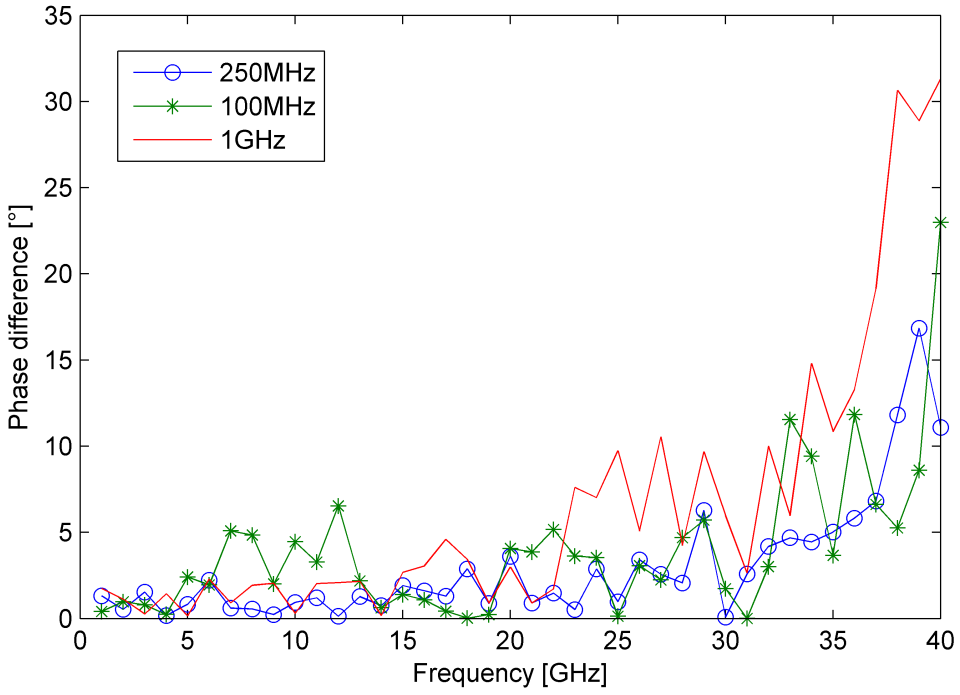

FIGURE 2.52: Phase difference between the phase measured at the common tones of a 250MHz, 500MHz and 1GHz fundamental and given by the characterization file of the phase reference

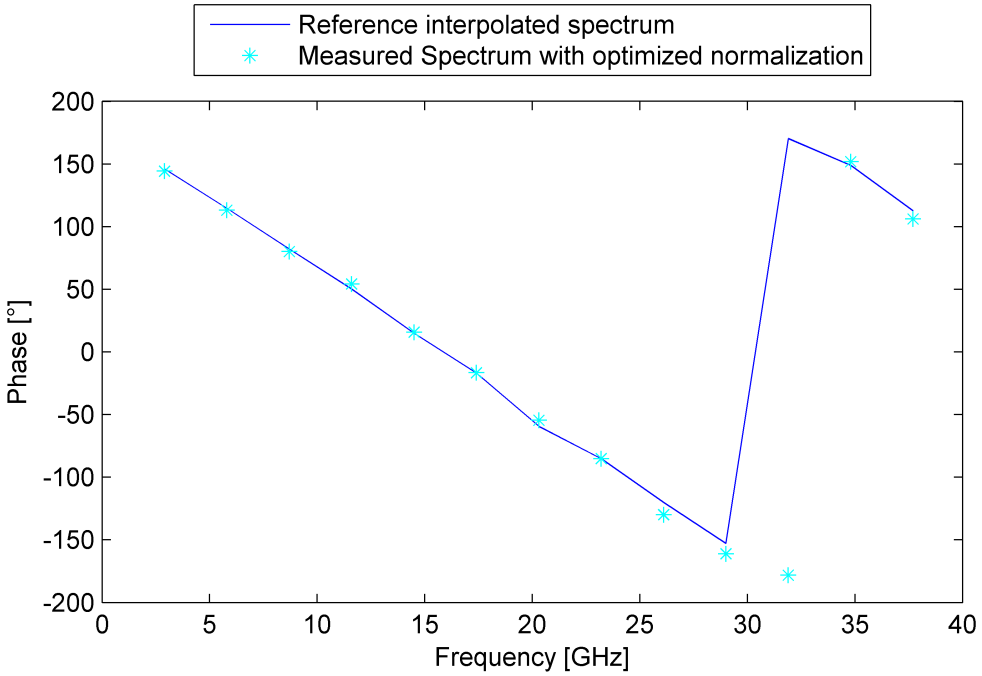

FIGURE 2.53: Phase of spectrum interpolated from the characterization file and measured

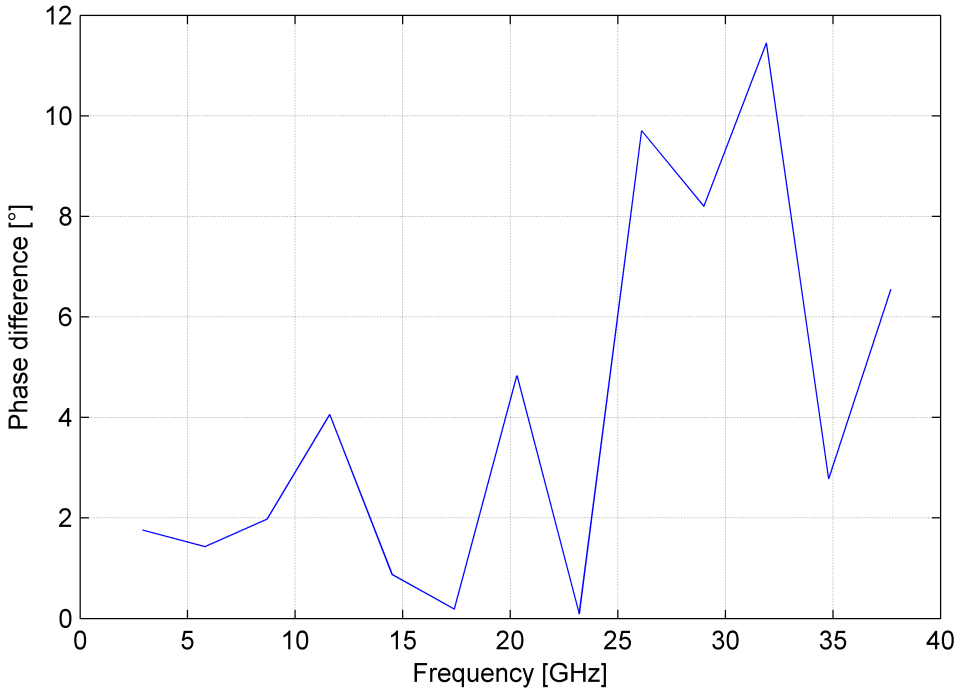

FIGURE 2.54: Phase difference between the spectrum interpolated from characterization file and the one measured

2.4.4 NVNA validation

Once the NVNA software written and the phase reference checked, a validation of the NVNA must be performed. To validate our instrument, we will compare measurements of a "golden device" performed with it, to the measurements performed with two systems available at the IEMN, Agilent®'s PNA-X (mixer based NVNA) and a LSNA (sampler based NVNA).

This methodology is inspired from the round robin organized within the European excellence network TARGET by Prof. D. Schreurs from the Katholic University of Leuven in Belgium. The objective of this round robin was to compare nonlinear measurement performed on the same device by different system. At this occasion the IEMN's LSNA was confronted to other systems and validated by D. Ducatteau [38]. It had later been used to validate the PNA-X present at IEMN allowing us today to use them to validate our own system.

As most of the effects that could influence the NVNA are frequency related, the measurement data will be exploited in frequency domain. The choice of representation between time and frequency depends on the measurement objective. For example for the maximization of the efficiency of an amplifier, time domain

may be preferred as it can easily show the overlap between current and voltage waveforms. Same thing for extraction of dynamic load lines. However comparison of measurements is often easier in frequency domain.

One of the figures of merit used to evaluate a NVNA is the Error Vector Magnitude (EVM). EVM is inherited from the digital signal transmission world and is a measure of the quality of the transmission by comparing the received complex voltage value to the ideally expected value. EVM is useful to NVNA measurement comparison because it contains the information about both amplitude and phase as well as their associated noise. It allows therefore to evaluate the measurement system including at once all the sources of error.

Sadly, EVM can be source of confusion as it has many different definitions depending on the field of engineering to which it is applied or the preferences of a given industry. None of the definitions have been yet accepted as a standard by the nonlinear measurement user community but the following two seems to get the favor of the majority so far and will be used in this work:

$$EVM_{rms} = \sqrt{\frac{1}{N}\sum_{n=1}^{N}|S_{received}(n) - S_{ideal}(n)|^2} \tag{2.53}$$

$$EVM_{rms} = \sqrt{\frac{\frac{1}{N}\sum_{n=1}^{N}|S_{received}(n) - S_{ideal}(n)|^2}{\frac{1}{N}\sum_{1=n}^{N}|S_{ideal}(n)|^2}} \tag{2.54}$$

Where $S_{received}$ is the received signal, S_{ideal} is the ideal signal and N the number of point for the averaging. It is mostly presented as a percentage percentage or in its logarithmic form.

The EVM of equation 2.53 will tend to make the error decrease for weak signals, as the error vector magnitude becomes naturally small. The EVM of equation 2.54 is said to be normalized, practically it tends to increase the error given by the figure of merit on low signals as they are usually measured with bad SNR so the error vector is often of similar magnitude than the magnitude of the reference vector. In fact the value of the EVM is directly linked to the the value of the SNR [83] so a degradation of the EVM is to be seen when the SNR of the measurement is low.

The normalization by the average power of the ideal signal is used to give to the EVM consistency whatever the magnitude of the vector is. In fact for a given phase error, the error stated by the EVM will increase with the magnitude of the vector to be compared. To validate a NVNA, result independent of the magnitude of the signals may give a better ground for comparison. However when trying to evaluate the quality of a given measurement, the normalization may hide the effect of the signal magnitude on the effective accuracy of the measurement. Whether to use a normalized form of the EVM or not is one of the debates taking place at the time of this work in the nonlinear measurement world.

The choice of the "golden device" is of prime importance. In fact the behavior of the reference device must depend as little as possible on the matching presented by the test sets of the different system in the measurement bandwidth. To identify this effect, measurements were performed on an amplifier at 3dB compression with a same NVNA but using different directional elements as test set. The reflection coefficient in the bandwidth of interest of the both couplers 1 and 2 are both acceptable for linear measurement as they are both couplers destined to VNAs. The NVNA was obviously recalibrated after each test set change. The measurement results obtained with both test sets on the same amplifier show that the behavior in power , shown in Figure 2.55, and phase, shown in Figure 2.56, of the amplifier used is extremely sensible to the impedance of the measurement port. This is confirmed by the poor EVM calculated in Figure 2.57 Measurement were repeated with renewed calibration several times to disqualify an effect from the instrument.

No verification measurement could be performed with such a device. More generally the measurement of such a device shows one of the major difficulty of nonlinear measurement which is the comparison of characterization performed on different NVNA models. Not only the problem arise when characterizing a DUT but also during phase calibration as the reference will react up to a given order to the different matching. One solution for the phase reference would be to use the DDS based generator that allows to output coherent signal one frequency at a time under the given timing conditions for the measurement seen in Section 2.4.2, thus being less sensible to the matching at the harmonics. This would not however solve the issue of differences in the characterization of DUT, where only a control of the impedance at the different frequencies would allow a common ground for

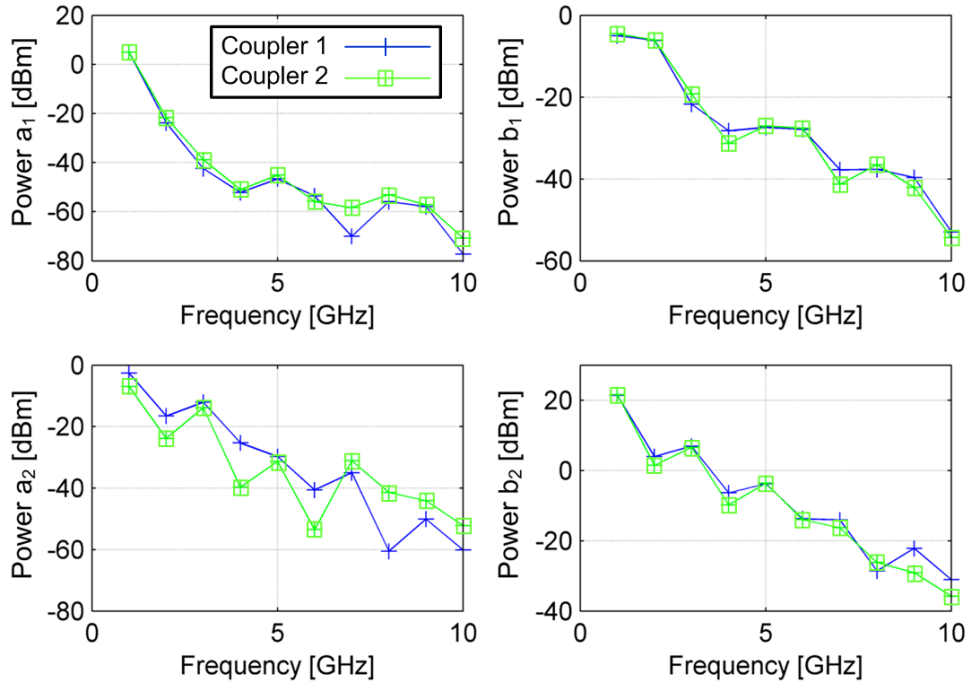

FIGURE 2.55: Power of the amplifier's traveling waves measured with coupler 1 (in blue) and 2 (in green) that have different input impedance

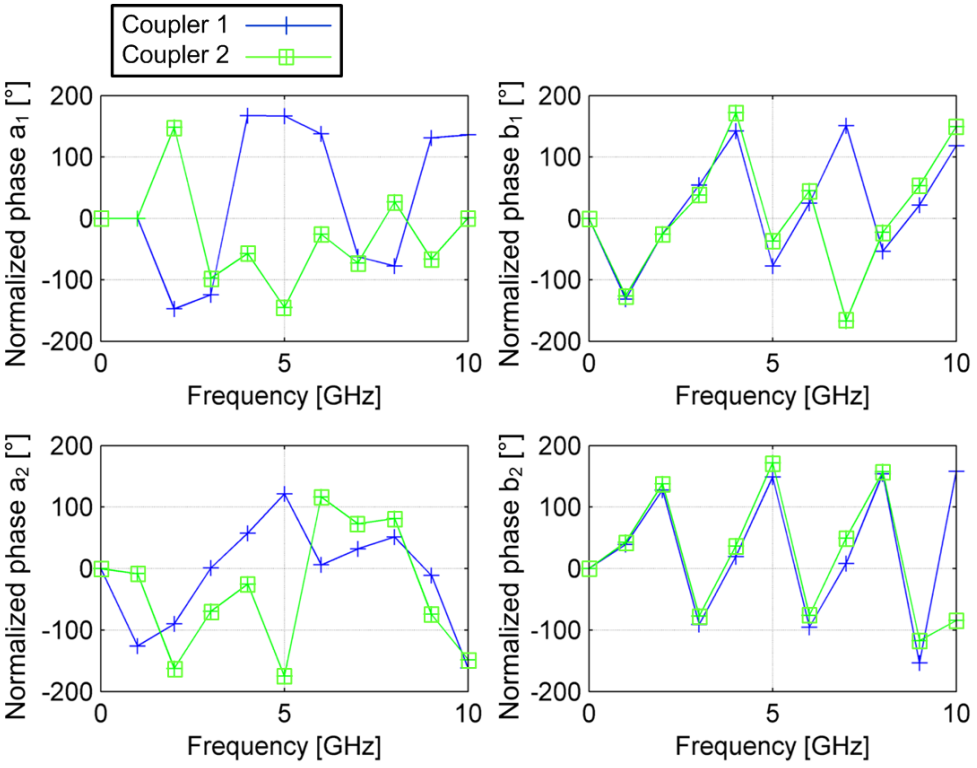

FIGURE 2.56: Phase of the amplifier's traveling waves measured with coupler 1 (in blue) and 2 (in green) that have different input impedance

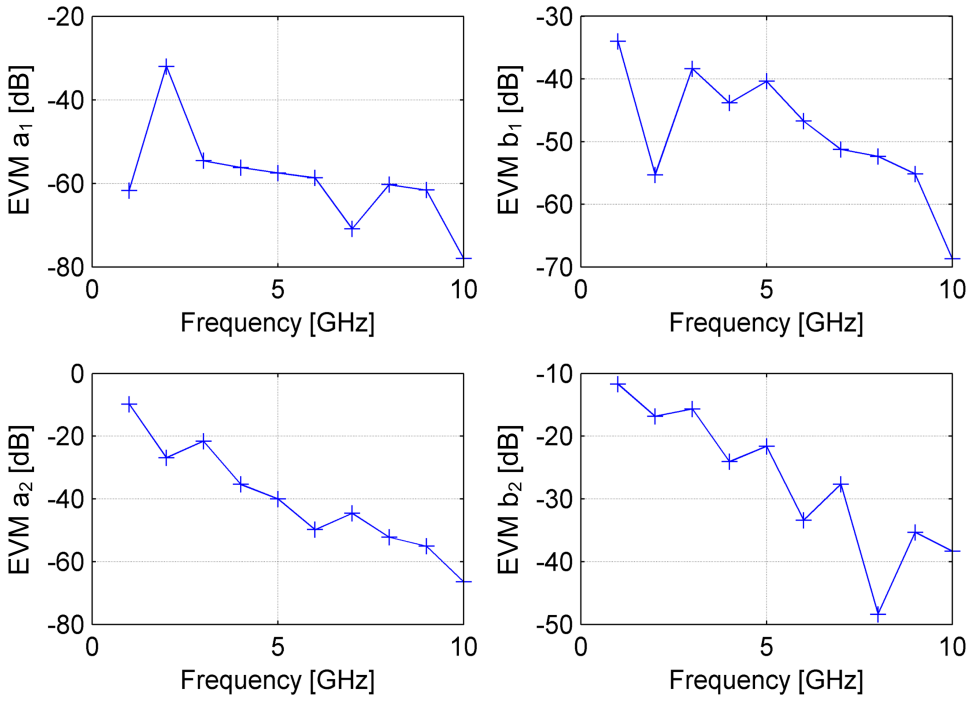

FIGURE 2.57: EVM of the amplifier's traveling waves measured with coupler 1 compared to the ones measured with coupler 2 that has different input impedance

comparison. Control of the matching could be achieved for example by the use of load pull techniques presented in Section 1.4.1.

To overcome the matching difference problem for NVNA validation, efforts were put to design generators outputting simultaneously many harmonics that would be immune to the matching of the test set of the instrument. An example of such an artifact designed by K. Wang [84], presented in Figure 2.58, consist of a 10GHz bandwidth C class amplifier with controlled DC bias.

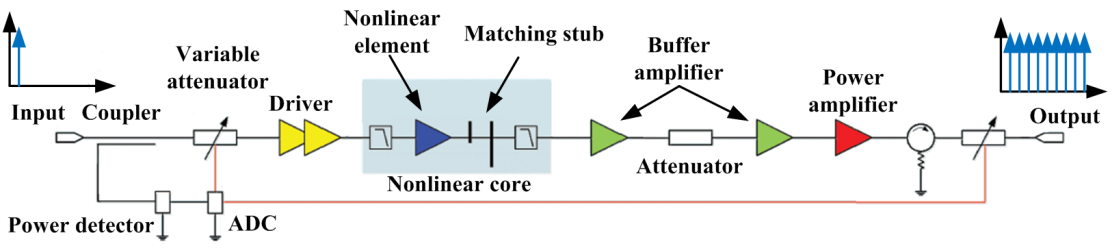

FIGURE 2.58: NVNA verification artifact example from K. Wang [84]

The "golden device" used at the IEMN is comparable to the one of K. Wang as it is also a transistor biased in C class, matched over the full bandwidth at which it will be measured and padded by attenuators, making it less sensible to the effects of matching brought by the test set. It is however more sensible than Wang's artifact as it does not include an isolator due to the fact it was designed to validate nonlinear instruments that have a 40GHz bandwidth. It has also a DC biasing control mechanism to limit the influence of the DC on its RF behavior as well as a low pass filter at its input to reduce the influence of the harmonics from the excitation source.

Measurement were performed with a LSNA, a PNA-X and our mixer based NVNA. To get a rich harmonic content from the reference device, it was driven at 5dB compression at 4GHz and six harmonics were measured. All the mixer based instruments were set to a 100Hz IF bandwidth.

Before comparing the different traveling waves measurement, one must think about their signification to give the importance each wave deserves during comparison of measurements taken with different instruments:

- The importance of the measurement of the excitation signal a_1 relies in the fact that the nonlinear behavior of the DUT is extremely dependent in terms of incident power. The harmonic content of the excitation signal is also important as it may also directly influence the behavior of the DUT.
- The signals reflected b_1 and transmitted b_2 by the DUT are the most important to compare. One must be careful however of the influence of the source and load match on the device used for the comparison. If the "golden device" is resilient enough to the matching at the different frequencies, these waves measurement should be comparable with every instrument.
- The signal a_2 reflected by the instrument is extremely dependent of the test set used. Ideally it should be the same for every measurement setup to have a good comparison ground between the results. In practice each test set will give different result for this wave.

in Figure 2.59 and Figure 2.60 we can see respectively the measurement of the magnitude and the phase of the outputted tones. Figures 2.61 and 2.62 are showing the difference between the measurements with the PNA-X and the custom NVNA

and the measurement of the LSNA taken as reference in magnitude and phase respectively. The LSNA is taken as reference as it was design for the nonlinear characterization purpose and it was validated during the TARGET's round robin.

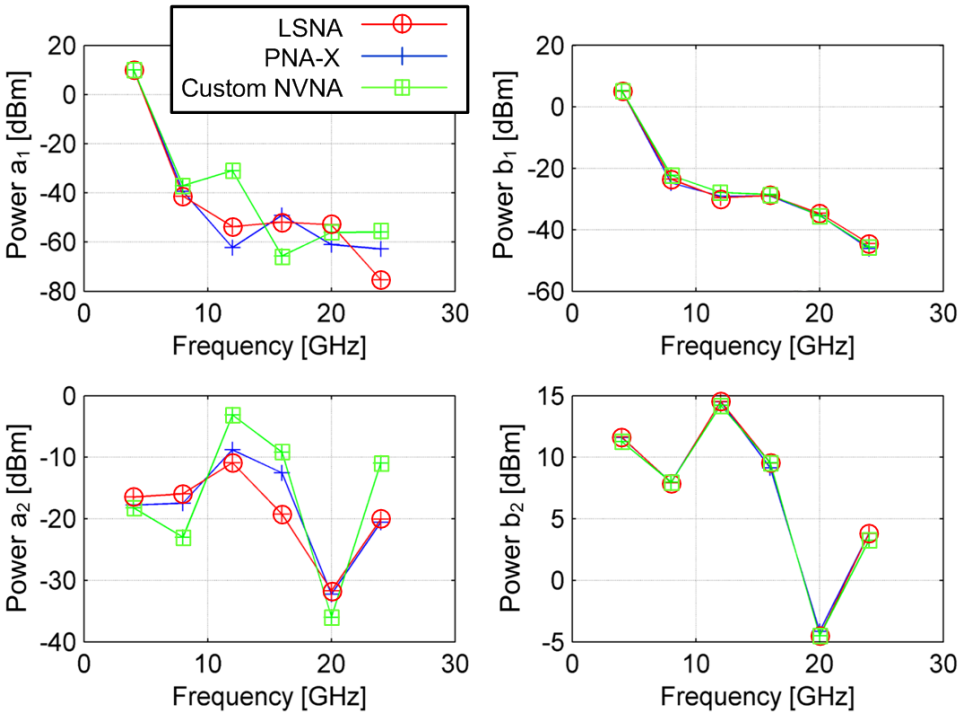

FIGURE 2.59: Traveling wave magnitude measurement with custom NVNA in green, PNA-X in blue and LSNA in red

What can be noticed is that the the DUT is excited at the same level by all the instrument. However the source of the VNA used in this work produces higher second and third harmonics than its counterparts. This may explain the fact that the wave b_1 reflected by the DUT has also a higher second and third harmonic, probably reflected by the filter present before the transistor in our golden device. As there is 20dB more of third harmonic outputted by the source compared to the source of the other instruments, it is also a likely explanation for the difference seen at the third harmonics of b_2 as some of the signal at 12GHz could have not been rejected by the filter and went through the transistor.

The difference between the PNA-X measurement and the two other at 20GHz is probably explainable by the bad SNR at this frequency. In fact, if the power measured in the DUT's plane at this frequency is around -5dBm, a 50dB attenuation is inserted before the receiver to not only protect the receiver but also avoid

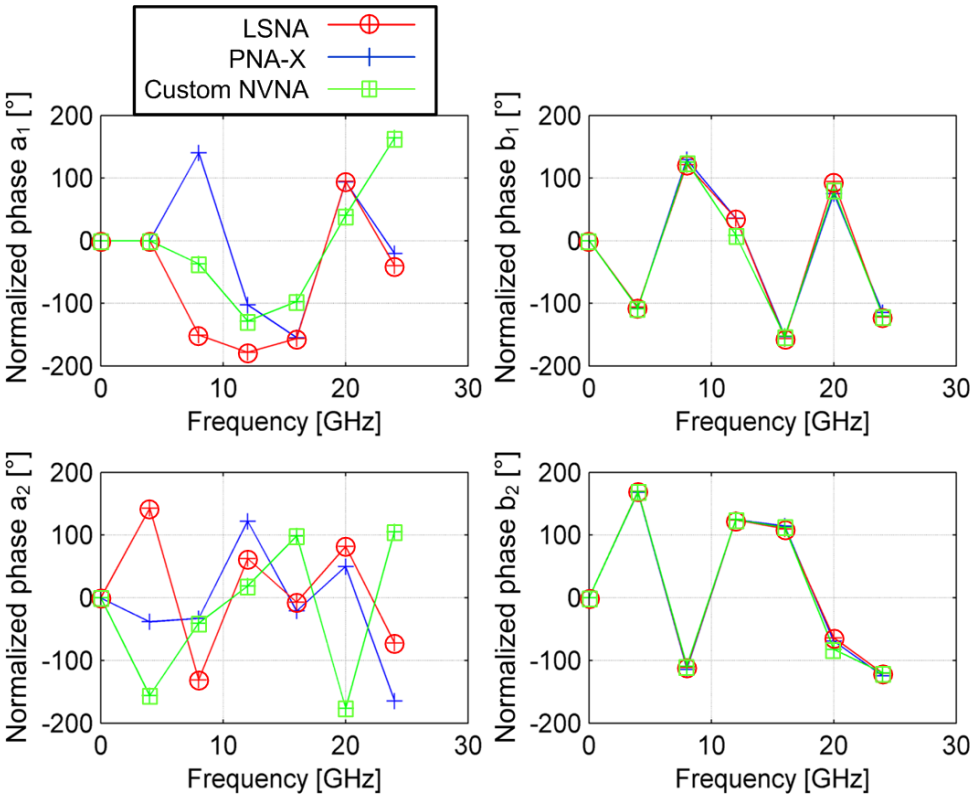

FIGURE 2.60: Traveling wave phase measurement with custom NVNA in green, PNA-X in blue and LSNA in red

compression. Counting the coupling, the measured signal must be more around -65dBm.

Finally the custom NVNA seemed to have underestimated the power at the fundamental of the $b2$ wave by 0.4dB while all the other measurement at the fundamental, including phase of $b2$, are close to the expected values. This might have been caused by the excess of third harmonic that went through the transistor compared to the other cases.

For the custom NVNA to be validated, the threshold value of 1% EVM for each tone was chosen with the LSNA measurement as reference on the b_1 and b_2 waves. As shown in Figure 2.63, the custom NVNA showed values under this threshold and is therefore validated even if it is penalized by its source compared to the PNA-X.

The time domain waveforms are calculated and shown in Figure 2.64 to visually demonstrate the time/frequency capabilities of both mixer and sampler based NVNA.

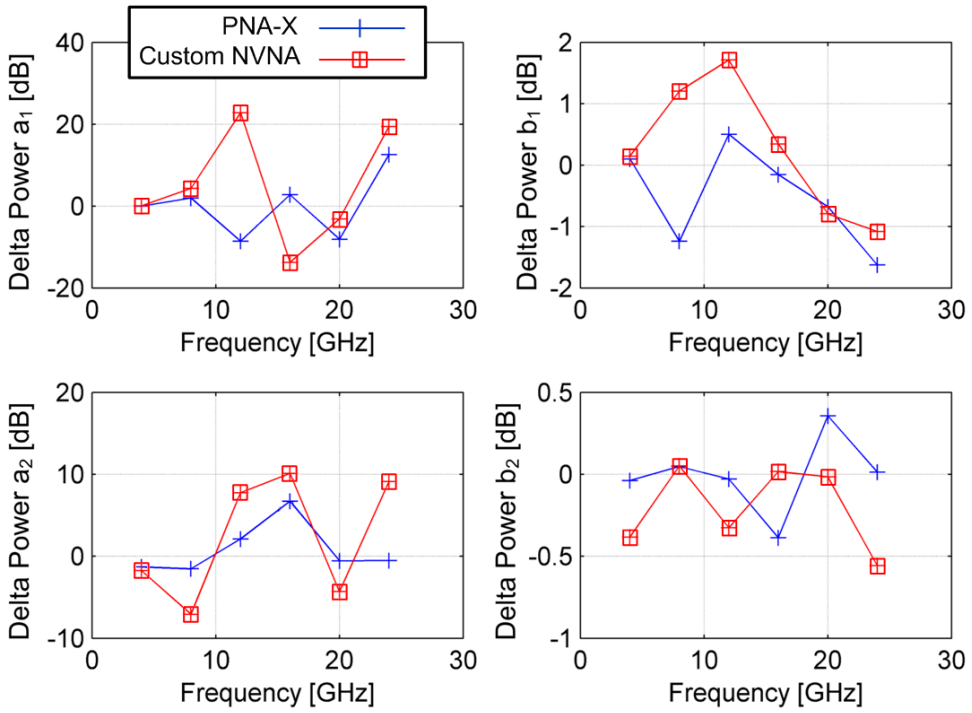

FIGURE 2.61: Magnitude comparison of the wave with LSNA measurement as reference with custom NVNA in red, PNA-X in blue

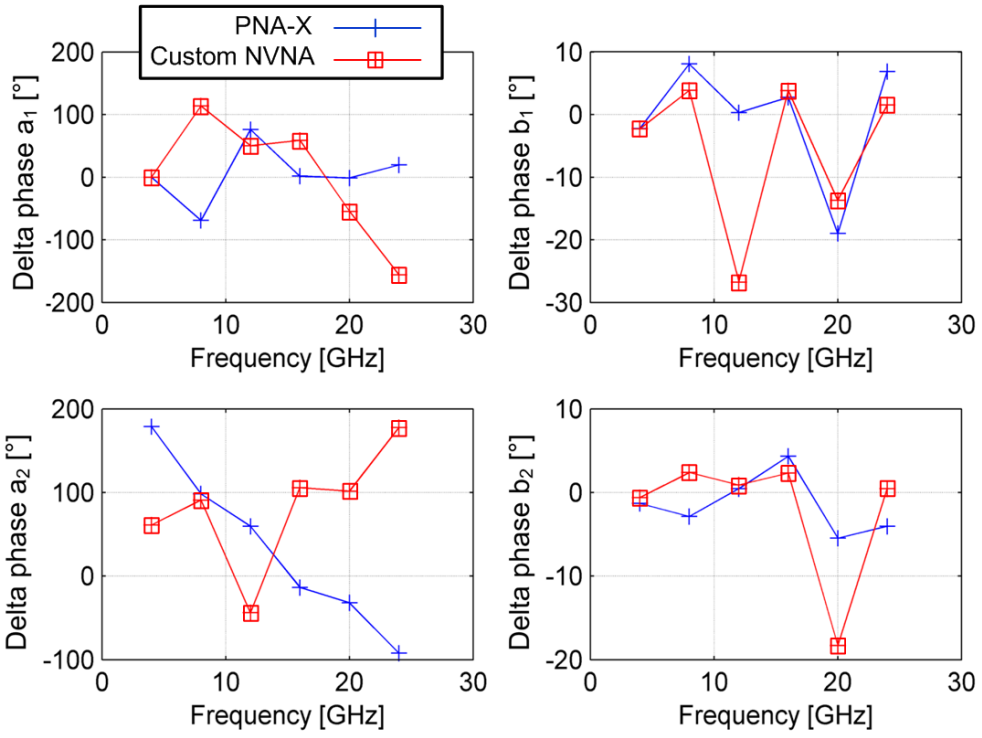

FIGURE 2.62: Phase comparison of the wave with LSNA measurement as reference with custom NVNA in red, PNA-X in blue

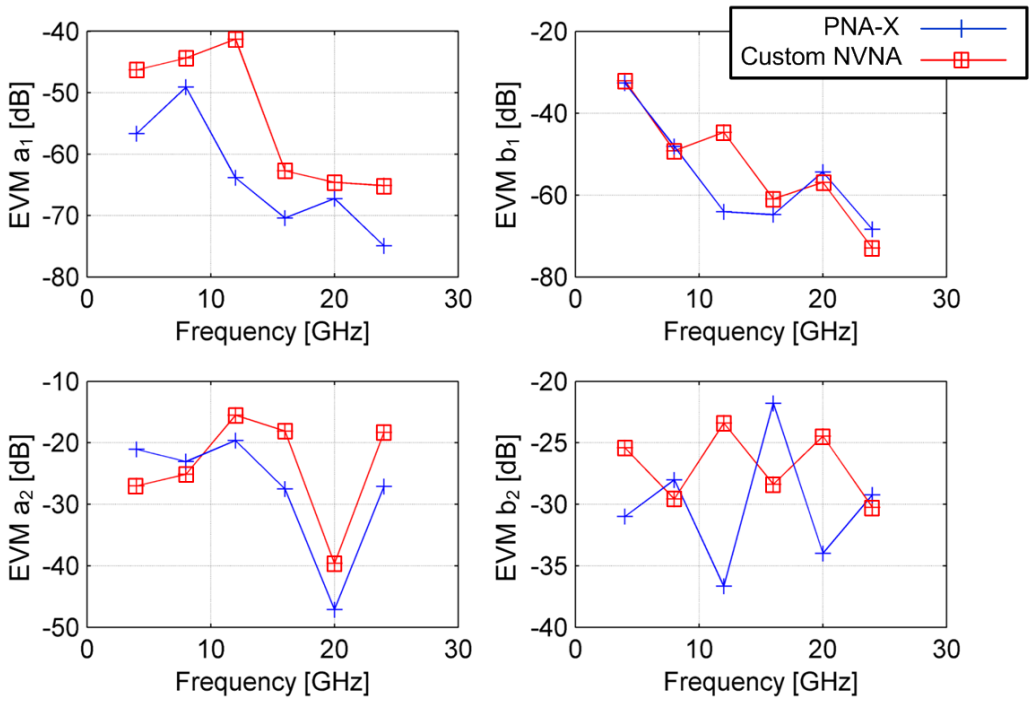

FIGURE 2.63: EVM with LSNA's measurement as reference with custom NVNA in red, PNA-X in blue

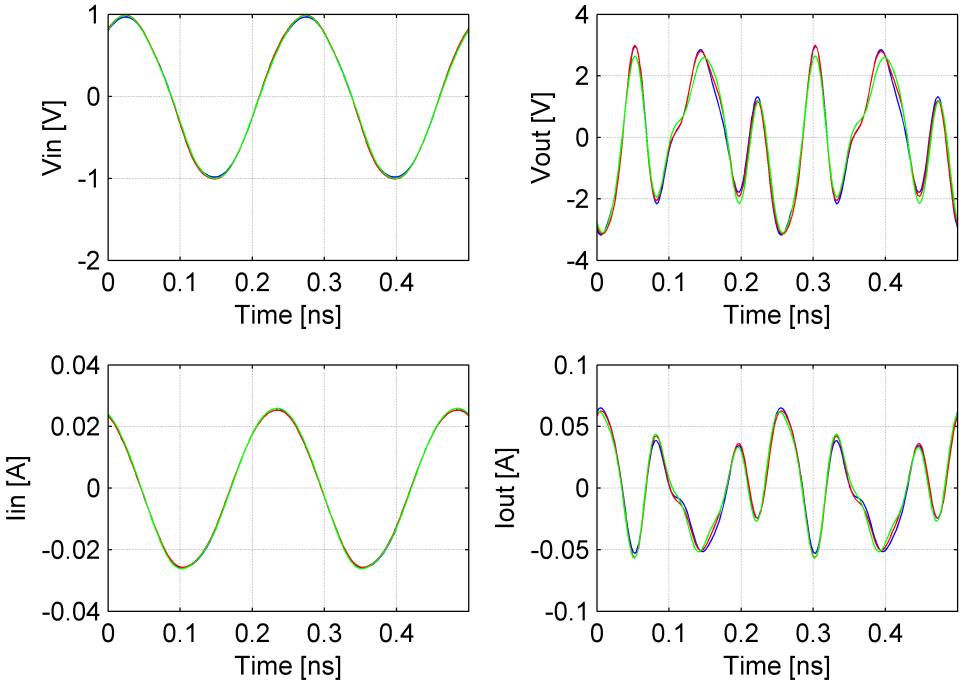

FIGURE 2.64: Time domain measurement with custom NVNA in pink, PNA-X in blue and LSNA in red

A final validation is realized by testing the repeatability of the measurement. This is done less to evaluate the repeatability of the NVNA that should be equivalent to the one of the VNA at a given SNR than to verify that no sweep dependent events are introduced by the phase coherence preservation. Therefore only the phase of the measurement is investigated after controlling that the excitation source was steady. One hundred consecutive measurements are performed on a 20dBm amplifier at a fundamental frequency of 1GHz and measuring every harmonic up to 10GHz with a VNA resolution bandwidth of 100Hz. In Figure 2.65 it is possible to see that at low frequencies the measurement of the phase seems repeatable. By watching the repeatability of the power measurement in Figure 2.66 one can explain the degradation of repeatability at high frequency from the bad SNR resulting from the low signal to be measured at higher tones. This conclusions are verified and comforted by the calculation of twice the standard deviation of the phase (Figure 2.67) and power (Figure 2.68) measurement at each frequency, for tones where the SNR is good, the repeatability correspond to the one of the VNA, while low power tones are perturbed by the noise.

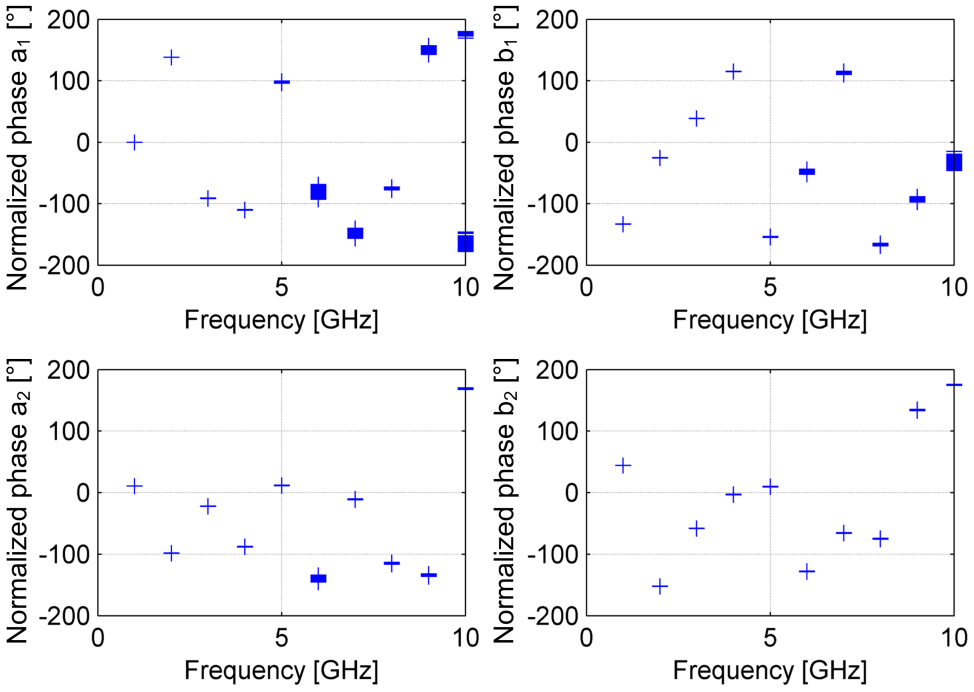

FIGURE 2.65: Repeatability of the phase measurement at 1GHz fundamental and 10 harmonics

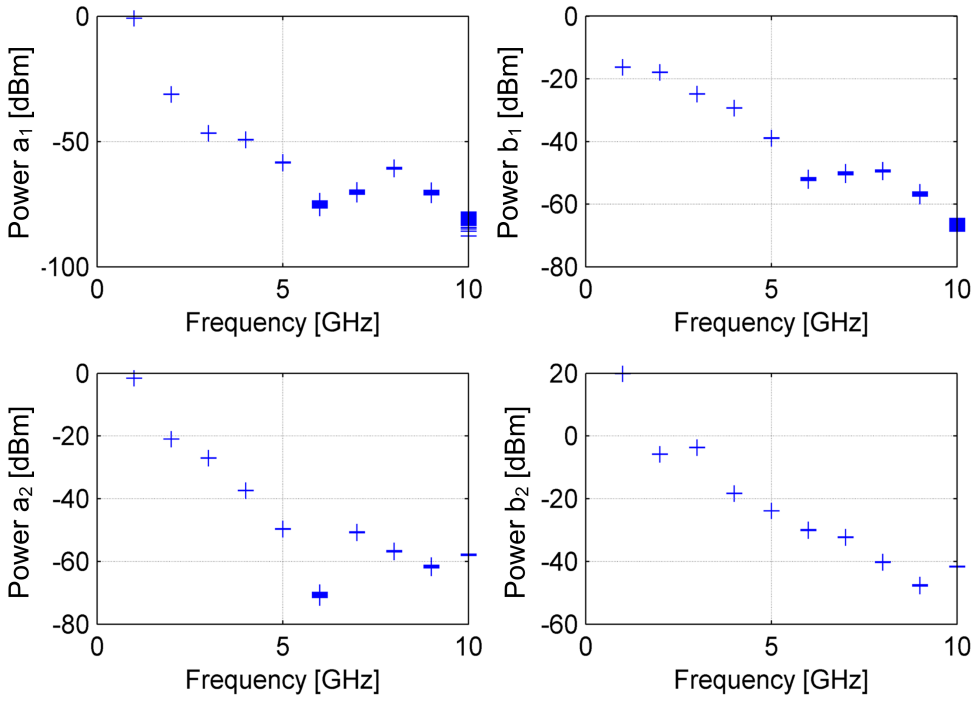

FIGURE 2.66: Repeatability of the power measurement at 1GHz fundamental and 10 harmonics

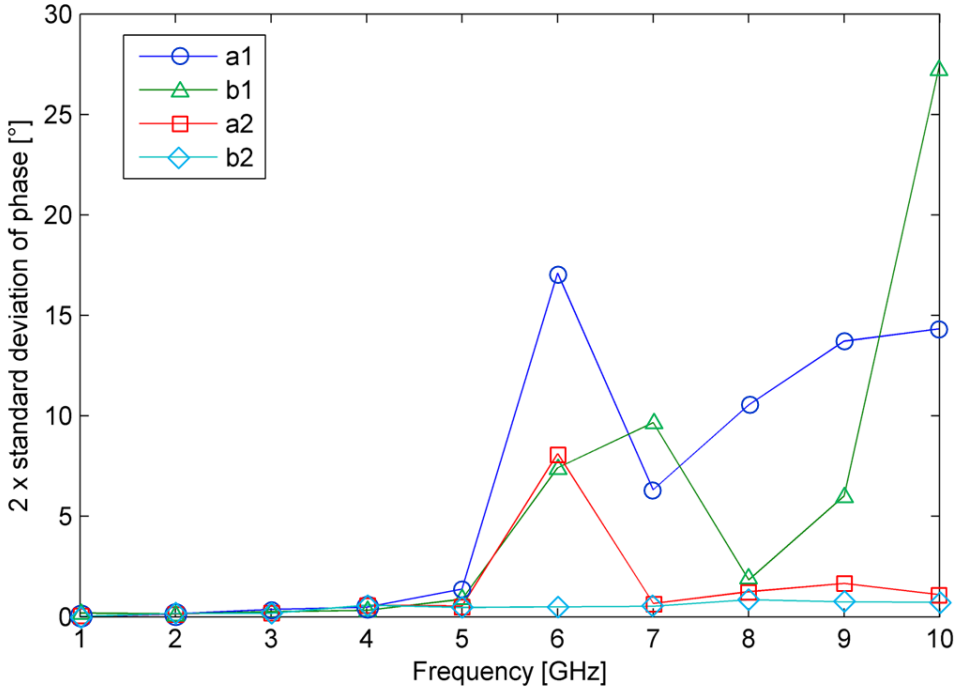

FIGURE 2.67: Two standard deviation of the phase measurement at 1GHz fundamental and 10 harmonics

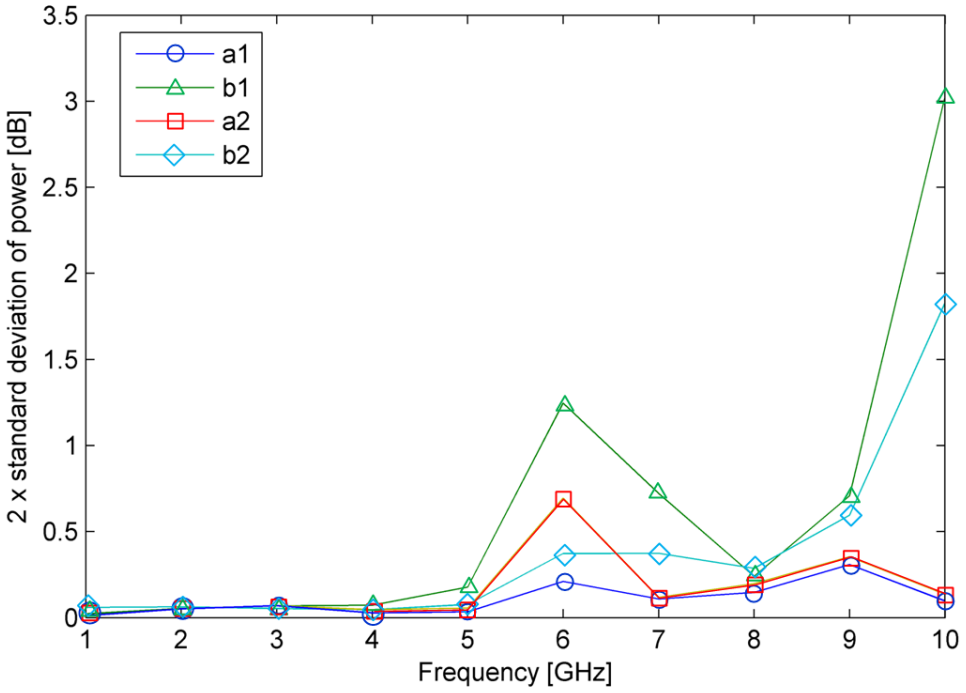

FIGURE 2.68: Two standard deviation of the power measurement up at 1GHz fundamental and 10 harmonics

2.5 Conclusion

In this chapter different instruments were sorted according to one of the three sampling and digitization concept they use namely digitizers, sampler or mixer based. Each group was then evaluated in the scope of nonlinear characterization to understand the strength and weaknesses of each technique. The tradeoff that appeared was between measurement speed (or bandwidth) and resolution of the measurement (or dynamic). As Rohde&Schwarz®, one of the partners of this project, is specialized in heterodyne instruments and especially in VNAs, the mixer based solution was chosen favoring the measurement dynamic in CW. Mixer based NVNA are already one of the possibilities available on the market but as Rohde&Schwarz® did not possess directly competences in nonlinear measurement, a NVNA had to be built from scratch.

After a description of the key components of the VNA in the light of nonlinear measurement, a nonlinear measurement software was written including calibration procedure, raw data acquisition and non linear correction in continuous wave. The instrument was finally validated by comparing it to existing solutions available at the IEMN such as the LSNA and the PNA-X from Agilent Technologies®.

In the next chapter we will extend the capabilities of this instrument to the measurement in periodic and non periodic pulse conditions in the S-band, to fulfill the need of the third partner and final user of the developed instrument, Thales Air System®.

Chapter 3

Nonlinear measurement in non periodic radar pulse train

3.1 Introduction

In the field of radar, as described in Chapter 1, systems are often operated under pulsed conditions. There are therefore two main reason that makes pulsed characterization of power amplifier required.

The first reason is that the amplifiers are generally specifically designed for pulsed conditions, so they would simply break if operated in CW, often because of power handling issues.

The second reason is that there is always better insight to gain for a developer to characterize his component under realistic conditions. This is this reason that triggered the research for approaching realistic radar conditions in terms of non periodicity of the pulse train and nonlinearity of the power amplifier presented in this chapter

Before accessing to the measurement in non periodic pulse, the NVNA that was designed and validated in continuous wave in the previous chapter must be able to support periodic pulses. Therefore the focus of the first part of this chapter is on studying the pulse measurement capabilities of mixer based instrument and comparing them when possible to sampler based instruments capabilities.

Then one of the investigated methods allowing further steps towards the objective of measurement in non periodic radar pulse train will be studied. In particular, the calibration of the instrument in periodic pulse conditions will be discussed and then the instrument will be validated in a periodic pulse measurement.

The last part of the chapter is entirely dedicated to the measurement in non periodic pulse train. First a straight forward extension of the periodic pulse is proposed for non periodic pulse, with the subsequent imperfections. Then a non conventional VNA prototype is converted into a NVNA thanks to the experience previously gathered, allowing the simultaneous measurement of up to three distinct frequencies up to 12GHz accordingly to the S-band requirement from Thales Air Systems. A series of measurements is finally performed to demonstrate the new possibilities enabled by the newly developed NVNA.

3.2 Periodic pulse measurement for nonlinear characterization

Pulse measurement of an active device such as an amplifier can be equivalent to two distinct measurements, pulsed RF and pulsed bias. Pulsed-RF measurement has for characteristic that the excitation signal is pulsed, the DC bias being on at least during the entire duration of the input pulse. Pulsed bias measurement is the measurement of the signals with pulsed DC-bias independently of the input RF CW signal. Both functioning conditions result in a pulsed output signal from the amplifier. Typically the pulsed-RF behavior makes use of a pulse modulator on the excitation signal and the input and output pulsed signal are measured either by a VNA at the carrier frequency or using envelope tracking techniques. The pulsed-bias measurement is usually performed with an oscilloscope associated with an Hall effect probe for the current measurement. In the domain of radar power amplifier, both techniques could be combined to try to minimize the power consumption of the amplifier.

The quality of the pulse modulator is of prime importance as it defines the quality of the pulsed-RF excitation signal. Ideally the rising and falling time of the modulator should be faster than the one of the DUT and its settling time should be as short as possible.

In this work, pulse measurement will always be pulsed-RF measurement.

From the instrument point of view, the main difference between the CW measurement and the pulsed measurement resides in the frequency spreading of the signal to be measured. Theoretically, the frequency bandwidth of a pulse signal with infinitely steep edges is infinite however the majority of the energy is included in a small portion of bandwidth centered on the carrier frequency. This is even truer in practice where the rising time of the pulse and the presence of noise limit the bandwidth to a given smaller portion of the frequency domain.

The VNA and therefore the mixer based NVNA pulse measurement capabilities are entirely dependent on the reaction of its receiver to this spread frequencies signal. However before evaluating the limitations of the receiver, let us define the possible comparison cases between the receiver and the signal bandwidth for a given pulse:

- The IF bandwidth of the receiver is larger or equal to the practical bandwidth of the frequency domain representation of the pulse as in Figure 3.1. All the tones are included in the measurement, this is wideband detection
- The IF bandwidth of the receiver is smaller or equal to the spacing of the tones representing the pulse in frequency domain as in Figure 3.2. Only one tone can be measured at a time, this is called narrow band detection

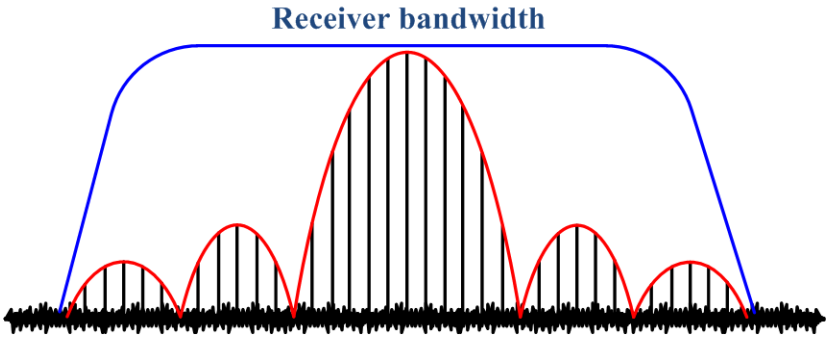

FIGURE 3.1: Pulse width and receiver bandwidth with wideband detection in frequency domain

It is possible that the IF bandwidth of the receiver is between the two cases. In that case more or less degenerated versions of one or the other detection mode appears. Whether the measurement is usable or not depends on how degenerated it is and should be at user discretion. In doubt the measurement should not be used at all.

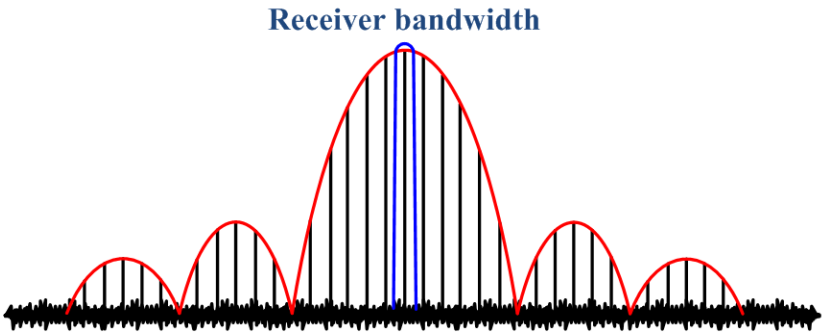

FIGURE 3.2: Pulse width and receiver bandwidth with narrowband detection in frequency domain

3.2.1 Wideband detection

Wideband detection as it was defined can be used only if the maximum IF bandwidth of the receiver is equal or larger than the pulse spectrum practical bandwidth. In that case most of the signal (and therefore the energy contained in it) will be measured when converted to baseband signal by the IQ demodulator of the receiver.

In time domain, this means that the data is acquired only during the ON state of the pulsed signal implying that the measurement triggering is synchronized to the measured pulse as shown in Figure 3.3. As every sample must be taken during the pulse, the settling time of the filter is of prime importance as it will define a period a time when no data should be recorded. Accordingly the measurement performance depend on the pulse width but not on the period of the pulsed signal.

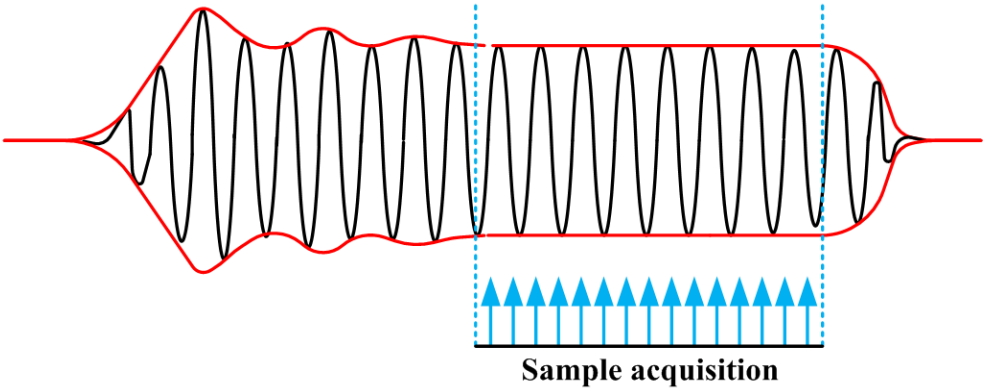

FIGURE 3.3: Pulse width and receiver bandwidth with wideband detection in time domain

The pulse width is important as it defines the bandwidth of the spectrum to be measured and therefore the receiver IF bandwidth. However, as explained in Section 2.3.3, the increase of IF bandwidth will result in a loss of dynamic range of the receiver due to the noise in the measurement band. Consequently there is a lower limit to the measurable pulse width corresponding either to the maximum bandwidth of the receiver or to the IF bandwidth before full degradation of the dynamic.

To compensate for the loss of dynamic range, averaging over many measurements can be used at the cost of measurement time.

For the best commercially available instruments the minimum measurable pulse width is in the order of the microsecond.

3.2.2 Narrowband detection

If the pulse width is too small to be measured by the previous method, narrowband detection can be a viable alternative. This technique consists in the sole measurement of the carrier frequency filtering out the rest of the spectrum. Therefore only the energy present in the carrier is measured.

In time domain, because of the use of a narrow IF bandwidth, the data acquisition time will be longer than the period of the pulsed signal as shown in Figure 3.4. There is therefore no use for measurement synchronization to the pulse as the total duration of the acquisition will at least include one pulse. However, some synchronization on the pulse is required when using a sample selection method such as software or hardware gating.

As most of the pulse spectrum is filtered, there is strictly speaking no limit on the pulse width. However the duty cycle of the signal, or in other words for a given pulse width the pulse period, will influence the dynamic range.

In fact, in frequency domain, for a given spectrum bandwidth, the increase of the pulse period will result into the spreading of the energy into as many more tones as the increase of the period. As a consequence the present energy at the carrier is invert proportional to the duty cycle degrading the dynamic of:

$$DynamicDegradation = 20\log(DutyCycle) \tag{3.1}$$

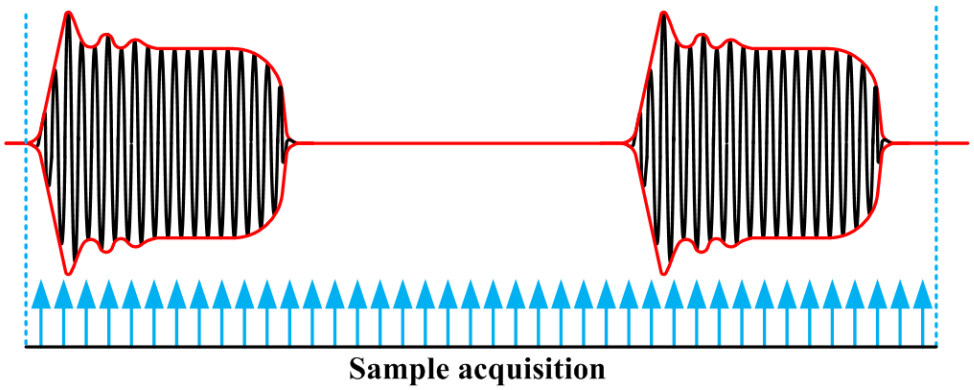

FIGURE 3.4: Pulse width and receiver bandwidth with narrowband detection in time domain

This dynamic degradation is called desensitization. In time domain, the same conclusion can be found considering that for an acquisition time comparable to the pulse period, a decrease of duty cycle by a factor two implies that twice less data are acquired during the ON state of the signal, implying that the resulting measurement point after averaging of the sample will have a magnitude twice smaller.

For a given pulse period, it is possible to use a narrower receiver bandwidth than necessary to at least lower the noise floor despite the dynamic degradation caused by desensitization at the cost of measurement time.

Agilent Technologies® also proposed a technique of spectral nulling [85] that allows to use a wider filter than normally necessary by making the zeros of the filter coincide with the side tones of the pulse spectrum, increasing the measurement speed at the cost of the dynamic.

Narrowband detection mode entirely relies on the periodicity of the pulse.

3.2.3 Comparison with detection techniques using sampler based NVNA

The narrow and wideband detection method that are frequency based are also available on the sampler based instruments. However because of a dynamic of 60dB for the LSNA, both methods are extremely limited, especially when measuring the harmonic frequencies.

To overcome this limitation in the LSNA, De Groote from VTD® proposed an upgrade of the LSNA pulse measurement technique in 2007 [86]. Using appropriate triggering provided by a custom made board, the LSNA was able to acquire samples during different acquisitions. The time domain measurement is then reassembled from the different acquisitions. The technique was applied to burst of pulses by Faraj [87].

In this stroboscopic approach, the time domain samples are consecutive samples, the rebuilding correspond to the juxtaposition of the different time windows as shown in Figure 3.5. The time between two samples is limited in that case by the sampling period. Another reconstruction method using coherent time interleaving

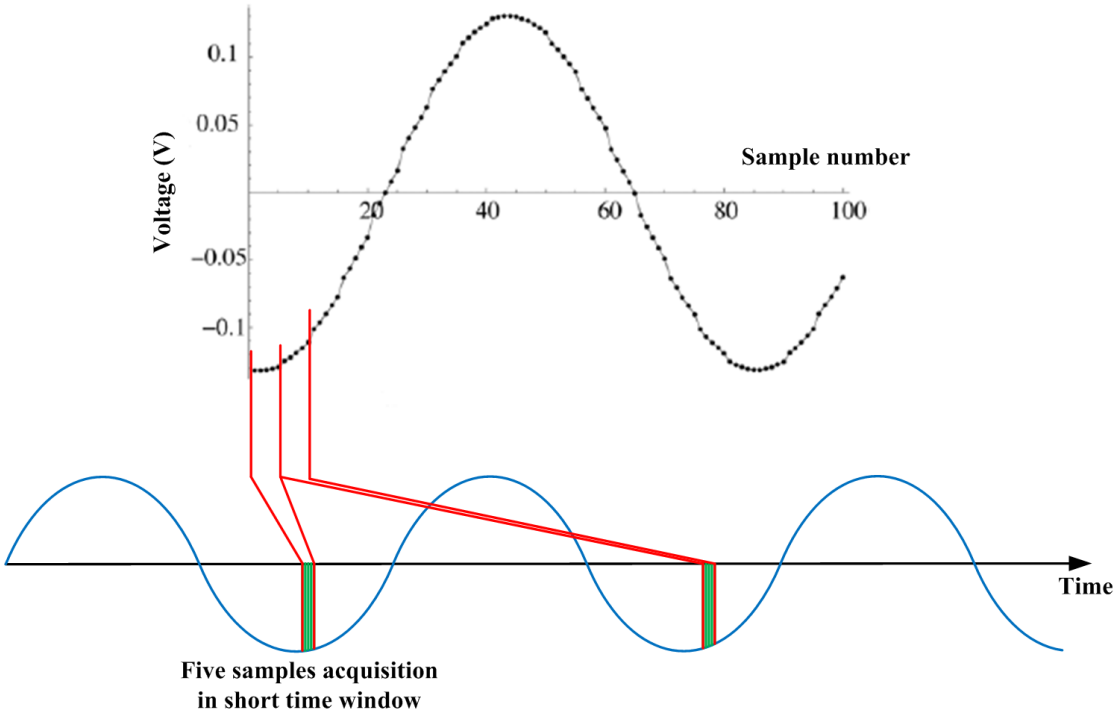

FIGURE 3.5: Time domain sampling on sampler based NVNA [86]

was proposed in 2012 by S. Ahmed [88]. The main advantage of this method is the possibility to have samples spaced by less than the sampling period by interleaving the samples and therefore increase the sample rate. As shown in Figure 3.6, it is possible from the knowledge of the position in time of a sample and the duration of the time window of the final result to rebuild the time domain signal from different acquisitions or frames.

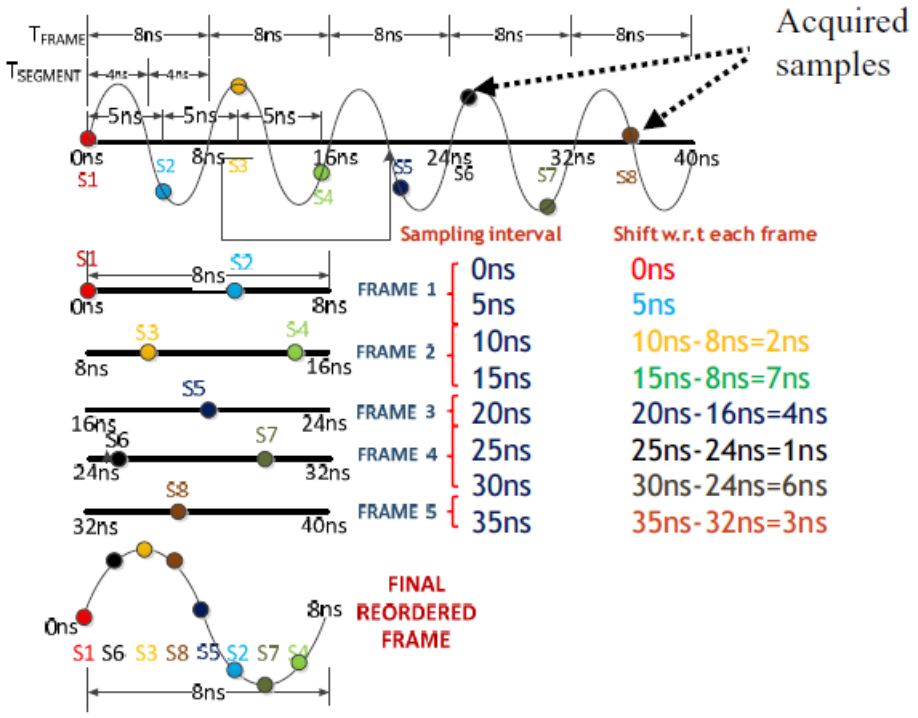

FIGURE 3.6: Sample interleaving for time domain sampling on sampler based NVNA [88]

With stroboscopic acquisition method in time domain, the dynamic is not degraded during pulse measurement, keeping the 60dB dynamic untouched in addition to the possibility to increase the sample rate at the cost of measurement time.

However these methods are based on the repetition of the signal over pulses and may therefore fail to reconstruct the waveforms in case of pulse to pulse effects if the pulses are too short.

3.2.4 Application of mixer based NVNA's detection techniques to different pulse measurement types

Using the data acquisition of pulses signal, there are three major types of pulse measurement that are required as shown in Figure 3.7:

- The measurement of an average value of magnitude and phase for the entire duration of the pulse as shown.

- The measurement of the average value during a given fraction of the pulse width, for example to avoid the overshoot region.
- Envelope tracking.

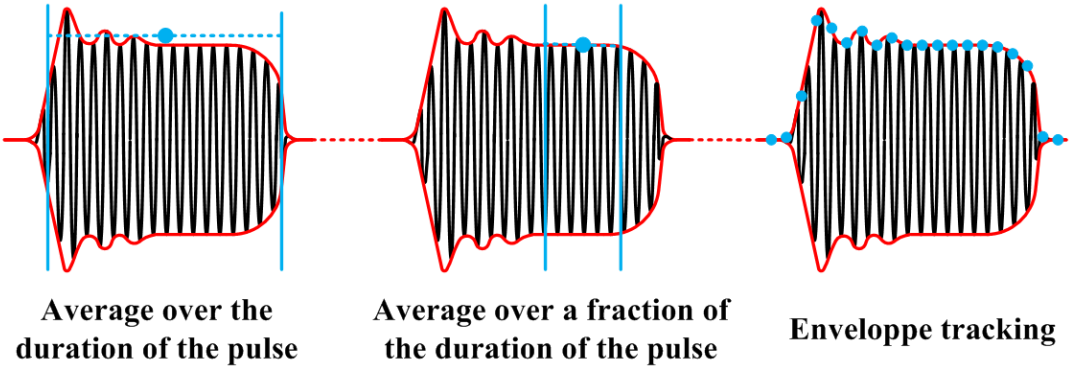

FIGURE 3.7: Pulse measurement types

Average over the duration of the pulse

Averaging all the samples taken during the pulse can be done with both detection methods. Obviously the correct magnitude information using the narrowband detection must be calculated accounting for the desensitization if the VNA is not power calibrated.

In practice, one would prefer that the samples are not acquired during the entire duration of the pulse but rather after the overshoot of the measured pulse and the settling time of the IF band pass filter. Hence the need for the next method where a fraction of the pulse is deliberately selected to perform the measurement.

Average over a fraction of the duration of the pulse

Averaging over a fraction of the pulse means that the sample must be acquired within this fraction time.

Using a wideband detection technique means choosing a filter bandwidth that allows acquisition during the chosen time window. Therefore the time window can not be smaller than the minimum measurement time set by the highest bandwidth or the SNR requirements. Then the triggering of the measurement must be delayed

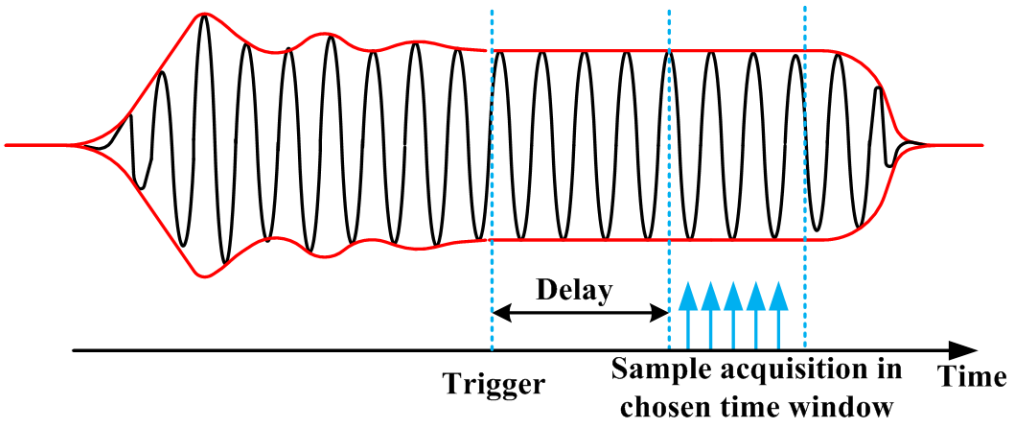

FIGURE 3.8: Measurement in fraction of a pulse with wideband detection

accordingly to the position of the time window in the pulse as shown in Figure 3.8.

This measurement is also available using narrowband detection but requires synchronization on the pulse to allow for triggering a sample selection mechanism. Agilent Technologies® proposed a solution [85] consisting of gating the acquisition thanks to switches either in RF or IF path. Therefore only the samples in the time window are acquired as shown in Figure 3.9. To improve the sensibility of the receiver, the sample outside of the time window that comprise sampling of the impulse response of the switch are replaced by null values. However the time window is limited by the rise time of the bandpass filter. A similar result can be achieved using software gating.

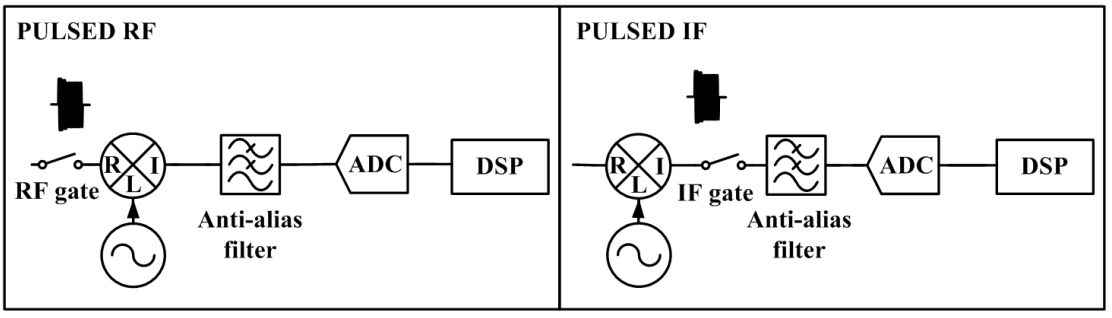

FIGURE 3.9: Measurement in fraction of a pulse with narrowband detection as Proposed by Agilent Technologies®

Envelope tracking

Envelope tracking is the measurement of the envelope of the pulse. This can be useful to quantify overshoot and ringing effects. It can be done using a the measurement within a time window by making the time window slide over many acquisition as shown in Figure 3.10. However depending on the required time spacing between the measurement points, the measurement time can quickly become an issue.

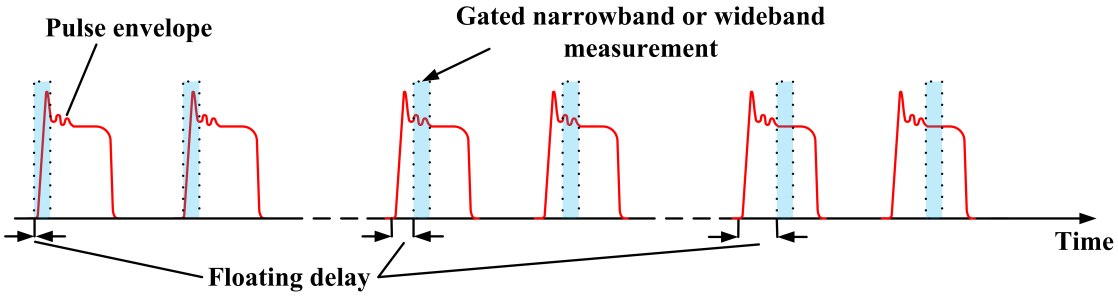

FIGURE 3.10: Envelope tracking with measurement taken in a sliding time window over several pulses

Another solution would be to give up oversampling and use only one sample per measurement point, reconstructing the envelope with a point every sampling period. In order to reconstruct the envelope with good fidelity, the IF filter must have a rise time equal to a fraction of the rise time of the measured pulse, otherwise the rise time of the IF filter is recorded instead. This usually implies a wide filter, on which usual effect on the dynamic are aggregating with the dynamic degradation due to the absence of oversampling/decimation.

Because of the poor quality of this measurement caused by the ADC resolution deterioration and the availability of optimized solutions for this purpose [89] [90], envelope tracking with a VNA will not be further considered.

3.2.5 Mixer based NVNA receiver limitations for pulse measurement

Depending on the detection technique used, the receiver must be able to either have a narrow or a wide IF bandwidth. Considering the receiver of Figure 3.11 seen in Section 2.3.3, it is understandable that every bandwidth limited element of the receiver may have an effect on the detection methods.

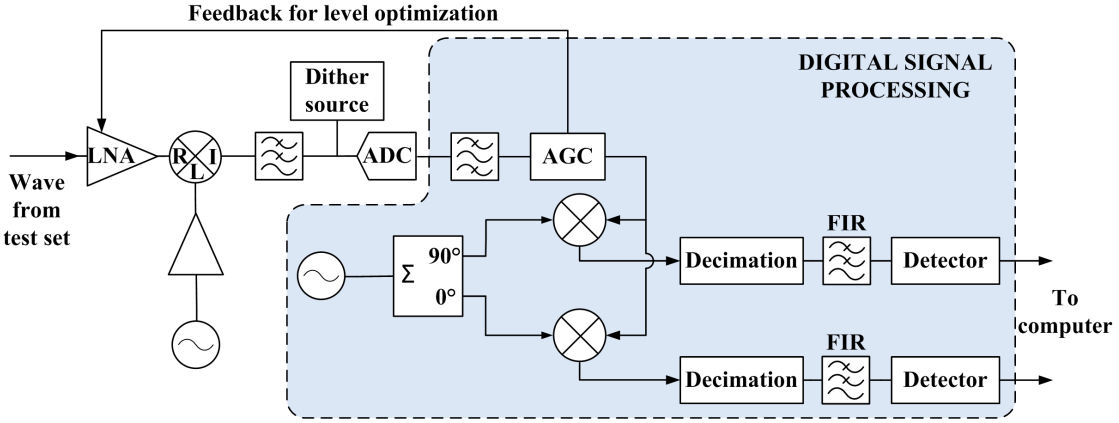

FIGURE 3.11: VNA receiver implementation

Receiver limitation in narrowband detection

For narrowband detection, the narrowest IF bandwidth of the receiver is equal to the narrowest IF bandwidth the digital IF filter can synthesize. Using digital filtering, this IF bandwidth can be smaller than the Hertz. If bandwidth in that case is not the problem, this is done at the cost of measurement time.

The main limitation of the receiver for this type of detection resides in the measurement dynamic that must be good enough to endure the dynamic degradation caused by the duty cycle.

The sampling period of the receiver ADC will in practice limit the minimum pulse width measurable using narrowband method as no holding circuit is present before the ADC. In fact, as narrowband method is asynchronous, it is possible that the ADC never acquires usable samples during the ON time of the pulse if the width is smaller than twice the ADC sampling period. With the instrument used in this work the sampling period is equal to 12.5ns limiting the minimum pulse width to 25ns using narrowband detection.

The time required by the receiver to acquire such a measurement is however the main limitation of the narrowband detection.

Receiver limitation in wideband detection

For wideband detection, one of the main limitation with the dynamic range is the maximum IF bandwidth width. The digital bandpass filter could synthesize a

filter IF bandwidth of several MHz, however other components have a fixed limited bandwidth.

The maximum IF bandwidth is in the first place limited by the ADC sampling frequency, as the maximum measurable IF bandwidth is equal to half the sampling frequency. In the case of a larger bandwidth, part of the signal would be filtered out by the anti aliasing filter.

The use of dithering to improve the measurement resolution may also limit the maximum bandwidth depending on the portion of the ADC bandwidth where noise is added. For example assuming a ADC of sampling frequency $f_c = 80MHz$ and the presence of a dither signal in the portion 0-10MHz, then the maximum bandwidth B of the receiver is equal to $B = \frac{80.10^6}{2} - 10^6 = 30MHz$ compared to the 40MHz without dithering. However increasing the sampling frequency would tend to reduce the dynamic as seen in Section 2.2.1.

In wideband detection, the phase delay of the receiver is supposed constant within the IF bandwidth, inducing no dispersion in the receiver. This assumption can be considered valid as long as the time delay $\Delta\tau$ is negligible compared to the inverse of the filter center pulsation $\omega_c = 2\pi f_c$. As the maximum dispersion is usually measured close to the cut off frequency, there is a compromise to make when choosing the IF filter that will best fit to the pulse spectrum. If it is too wide, a lot of unnecessary noise will be measured; if it is too close to the spectrum bandwidth, dispersion may occur.

Receiver limitation affecting both detection methods

Independently of the detection method, the finite linearity of the receiver may interfere with pulse nonlinear measurement. In fact, as seen in Section 2.3.5, compression of the receiver must be avoided at any cost to not generate harmonics. However the receiver is sensible to the peak power, therefore the peak power of the pulse, and especially its overshoot must be accounted for in the calculation of the receiver protection and in the best case monitored during the characterization. The power difference between the overshoot and the flat part of the pulse will be an additional dynamic loss compared to the CW case.

3.2.6 Detection techniques limitation for nonlinear measurement

For periodic pulse nonlinear characterization, all the pulse detection method are usable within the measurement procedure that was described in Section 2.4.1. However, as it was previously discussed, the dynamic range of a NVNA is not available for each tone, it is shared by all the tones present within the physical bandwidth of the instrument. As every pulse measurement method available on VNAs are inducing a degradation on the dynamic range, measurement of higher tones may be extremely noisy or simply impossible.

Taking the theoretical example of a DUT measured at a pulse width of $10\mu s$ for a duty cycle of 1% and that have output power in the DUT plane of:

- 37dBm at f_0
- 20dBm at $2f_0$
- 0dBm at $3f_0$
- -20dBm at $4f_0$

The first step for such a measurement is to protect the receivers to prevent compression (and in that case also destruction). If compression occurs above -10dBm in the receiver plane, the b_2 receiver would require roughly a 50dB attenuation implying the following powers in the plane of the receiver b_2:

- -13dBm at f_0
- -30dBm at $2f_0$
- -50dBm at $3f_0$
- -70dBm at $4f_0$

The narrowband method will imply a dynamic degradation of $40dB$ and with a pulse period of 1ms would require a filter bandwidth inferior to 1KHz. Assuming a VNA with 110dB dynamic at 100Hz IF bandwidth and a higher dynamic range threshold of -10dBm in the receiver plane, this makes in the best case a -70dBm noise floor.

The wideband method will require a 100KHz IF bandwidth. Assuming a VNA with 100dB dynamic at 100Hz IF bandwidth and a higher dynamic range threshold of -10dBm, this makes in the best case a -80dBm wideband measurement respectively.

In every case the tone at $4f_0$ is not measurable and with a 20dB to 30dB SNR, the measurement of the tone at $3f_0$ may not be usable. Please note that it was impossible to put any tone at best SNR because it is the total peak power that applies for the setup dimensioning.

For pulses wide enough to compare both solutions, what method prevails in terms of measurement dynamic compared to the other will depend on the duty cycle as shown on the example in Figure 3.12

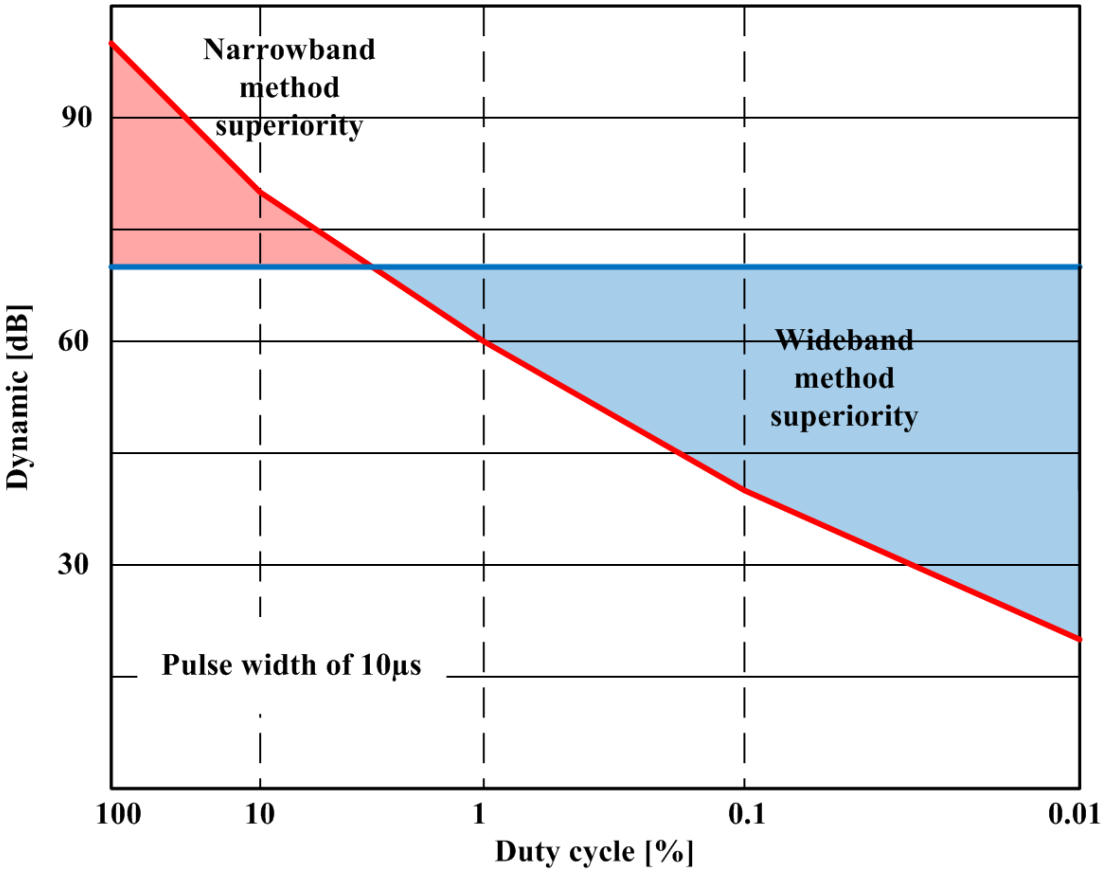

FIGURE 3.12: Comparison of measurement dynamic resulting from the use of narrowband and wideband techniques as a function of the duty cycle in the case of a $10\mu s$ pulse width

However in the particular case of this work, only the wideband measurement will be studied in detail for nonlinear measurement as the speed and the synchronous

nature of this method will allow an extension of nonlinear measurement to non periodic pulse train that the need of repetition of the narrowband method forbids as it will be explained further. This method also allows to minimize the effects occurring between pulses as one sweep point is measured in a single pulse, contrary to narrowband measurement that requires many pulses to extract a single sweep point.

3.2.7 NVNA calibration in pulsed conditions

NVNA calibration in pulsed conditions does not differ in principle with the calibration in CW conditions described in Section 2.4.3. However if narrowband detection is equivalent for the principle of functioning to CW measurement provided that the issues due to settling time of the receiver are avoided and that no thermal effect due to short pulses interfere.

For wideband detection, when applying directly the CW calibration procedure to wideband measurements with a mixer based NVNA, only the carrier frequency and its harmonics are calibrated, leaving the tones created by the pulsing uncalibrated despite the fact they take part in the measured value. The instrument not being aware that the measured signal is modulated, it does not correct the measurement on all the IF bandwidth but only at the IF frequency, and in fact it assumes that the rest of the signal in the IF bandwidth is noise hence the lack of correction.

Using the measurement result despite the incomplete correction relies on the following assumptions:

- The attenuation of the filter is constant over the filter bandwidth, correction in magnitude therefore applies to all the IF bandwidth.
- The phase delay of the IF filter is constant, no distortion of the complex signal appears.

Simulated gain and phase delay of filters eligible to be used as 20KHz, 200KHz and 1MHz IF-bandwidth filters are shown respectively in Figure 3.13, 3.14 and 3.15. From the observation of simulated digital filters, the assumptions seem reasonable for filters with the same profile as the one at 20KHz and 200KHz. Furthermore because the influence of a tone on the measurement outcome globally

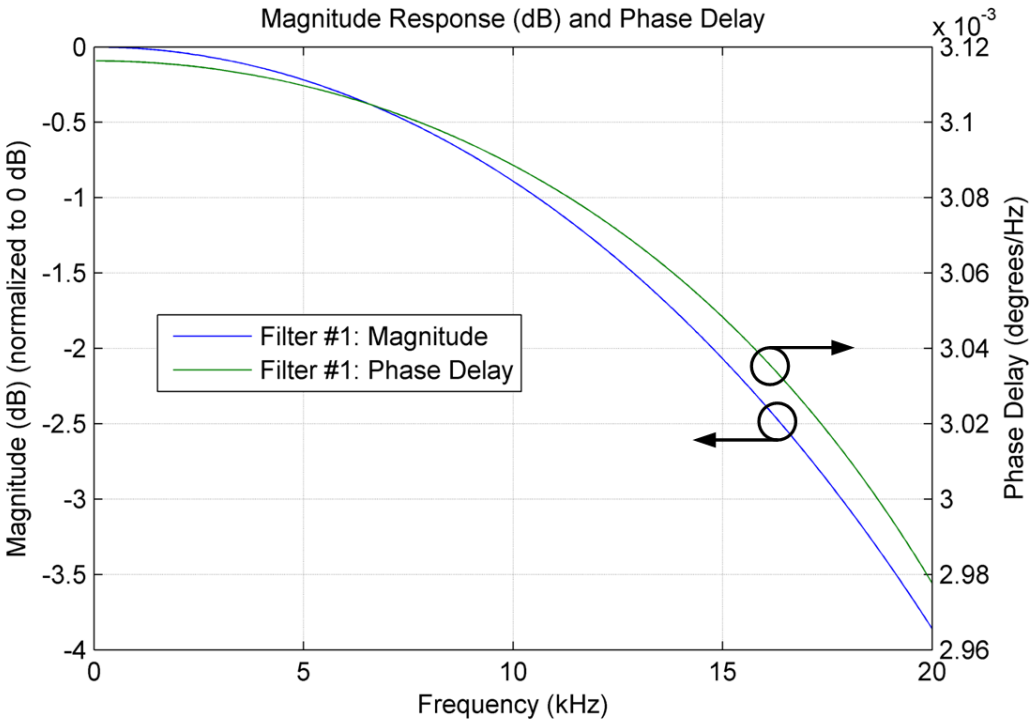

FIGURE 3.13: Phase delay and gain simulated for a filter equivalent to the receiver 20KHz IF filter

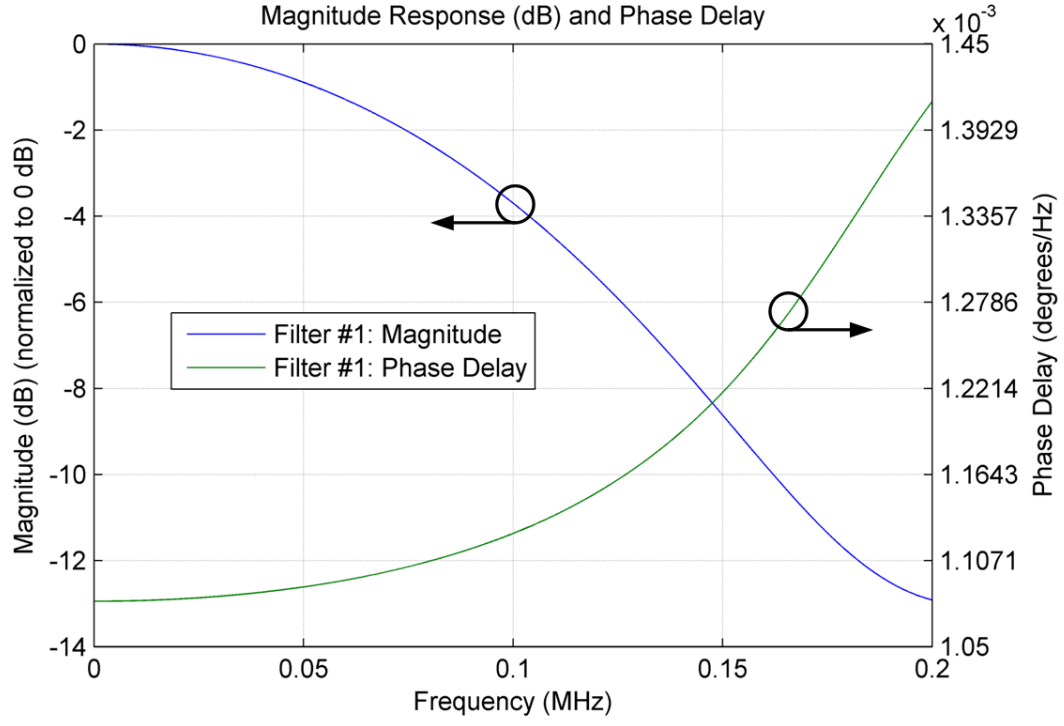

FIGURE 3.14: Phase delay and gain simulated for a filter equivalent to the receiver 200KHz IF filter

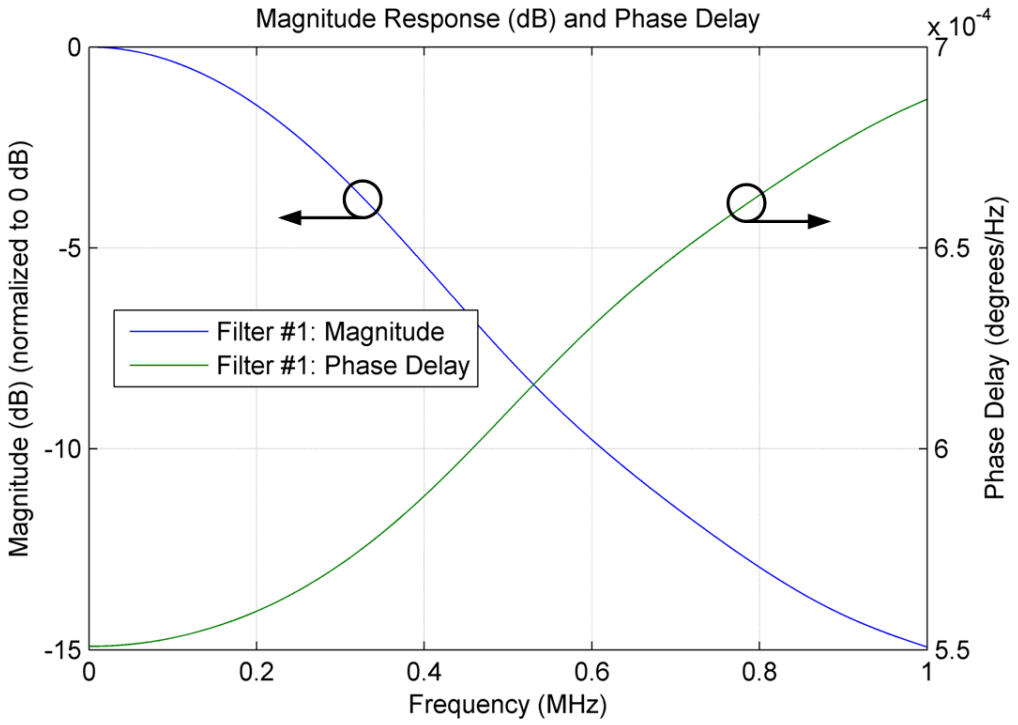

FIGURE 3.15: Phase delay and gain simulated for a filter equivalent to the receiver 1MHz IF filter

decreases with its relative frequency spacing to the carrier due to the sin_c envelope of the spectrum, the regions of the IF-bandwidth where these assumptions are possibly invalid should provide negligible influence on the measurement. Such an effect is supposed to be compensated when comparing traveling waves measured at the same frequency as the receivers are supposed to be identical. The simulated filter supposed to be equivalent to the 1MHz bandwidth fall short in terms of gain, so a measurement with such a filter would probably be error prone.

The wideband detection also implies synchronized measurement therefore effect of jitter and imbalance on the triggering may have an influence on the measurement. In fact the samples may be taken at different time of the pulse, potentially changing the value from one measurement to the other even if the DUT had the same behavior. This is especially true in the proximity of the overshoot region.

The effects of the wideband detection should be accounted for as much as possible at every step of the NVNA calibration.

Relative calibration

The instrument constructors are not exactly agreeing on their recommendations in terms of S-parameter calibration in pulsed conditions using wideband detection. In the application notes from Agilent Technologies® [91] and Rohde&Schwarz® [92], it is stated that the calibration performed in CW should apply equally in pulsed conditions at the condition that the test set is unchanged. This implies that the pulse modulator is included into the source path during the CW calibration to keep the same source port match when switching to pulsed condition. It also implies that every effect affecting the receiver induced by the pulse conditions is the same at every receiver and therefore compensate during relative calibration.

In the application note from Anritsu®'s VNA [93], it is recommended to perform the calibration directly in pulsed condition to avoid effects such as triggering imbalance between the receivers or thermal effects. Triggering imbalance or design differences between the receivers should be corrected when calibrating in the same conditions as the measurement.

As the power and phase correction factors of the NVNA depends on the relative calibration as seen in Section 2.4.3, the error made during the calibration will propagate to these terms. Choosing if the error measured can be overlooked can therefore be determinant for the quality of the characterization.

To evaluate the influence of the calibration conditions on the calibration outcome, the error coefficients of the following calibrations are extracted with the same IF bandwidth of 200KHz:

- A series of four OSM calibrations including the pulse modulator in the path, set to constant transmission.
- A series of four OSM calibrations in pulsed condition with a pulse width of $10\mu s$ and a 10% duty cycle (harshest conditions used in this work) using wideband detection.

The calibrations are performed from 10MHz to 24.01GHz with a measurement point every 200MHz. The EVM is then calculated taking as reference the measurement performed in CW and shown in Figure 3.16. It can be seen that except at 10MHz, which is a frequency where the performance of the NVNA is mediocre

especially because of its directional element that is not adapted to low frequencies, the error is stated to be inferior to -43dB for every correction coefficient. Therefore no strong effect caused by the measurement conditions in the studied case are observed.

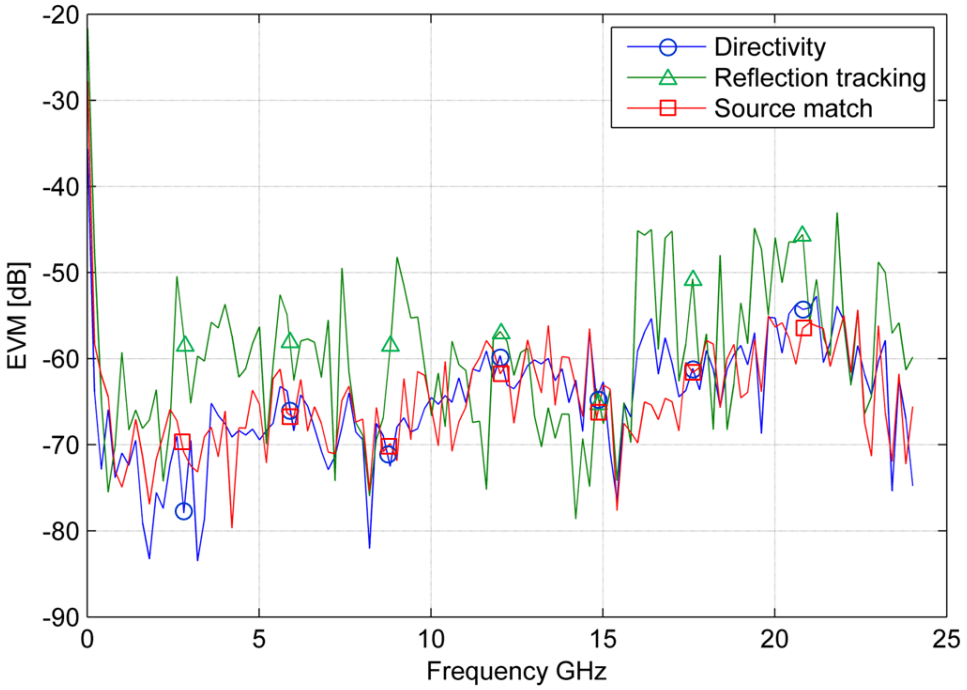

FIGURE 3.16: EVM of the error coefficients extracted in pulsed conditions using the CW error coefficients as reference

The choice of OSM calibration came from hardware limitations during the tests as no pulse modulator could be used on a second port source. To extend the conclusion in a transmission measurement, a series of two hundred pulses with $10\mu s$ pulse width and 10% duty cycle was sent in a thru standard at the frequency of 2GHz. The source was turned off (more specifically the amplifier after the source) for an hour before the measurement occurred so the first pulse measured is the first RF seen by the NVNA receiver since that time. The evolution of the measurement as a function of the pulse number is shown in Figure 3.17. There is a sensible evolution of the measurement from the first pulses to the end of the series. However this evolution seems to be negligible compared to the measurement accuracy. The test was repeated on all the instrument RF bandwidth with similar results.

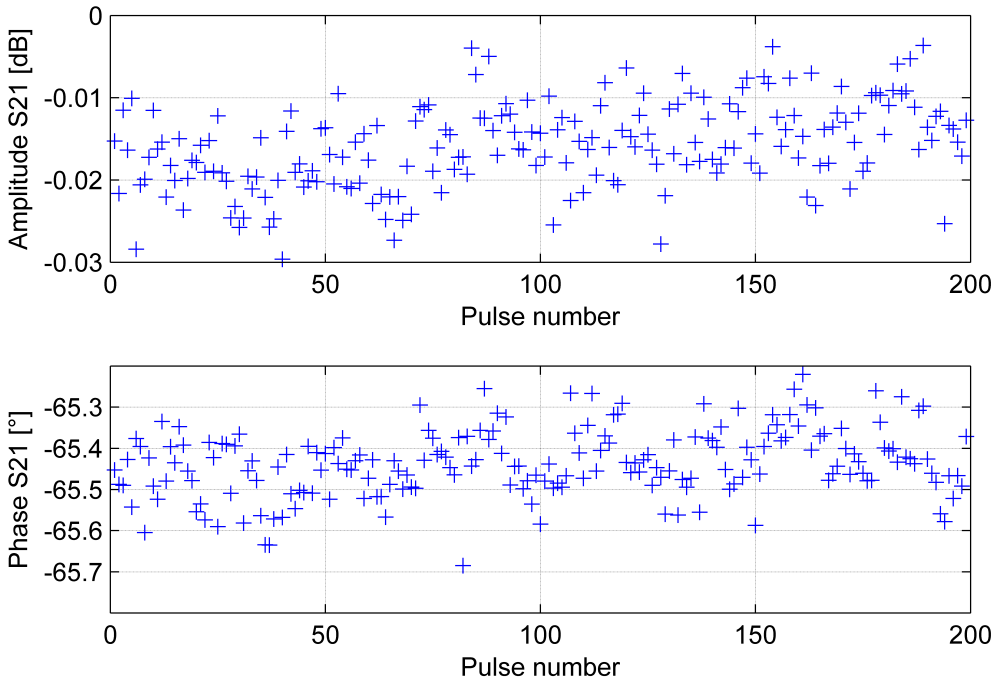

FIGURE 3.17: Evolution of transmission measurement of a thru at 2GHz as a function of the pulse position in the pulse train to account for effects due to the pulse measurement

The instructions from Rohde&Shwarz® and Agilent Technologies®, namely that the calibration can be performed in CW and used in pulsed measurement, will therefore be followed as no threatening effects appeared in the harshest pulse condition to be used in this work.

Power calibration

As the power calibration is not based on the comparison of two NVNA receivers measurement but on the comparison of one receiver and a power meter (and therefore no compensation of the potential effects will occur), it must be performed in the same conditions as the measurement.

The power calibration of periodic pulse signal can be performed using the same average power meter that was used for CW measurements and correcting the measurement using the duty cycle. The power meter acquisition can even be triggered by the "BUSY" signal of the instrument. The "BUSY" signal is a signal outputted by the NVNA that denote an acquisition event. There are many settings as explained in the manual of the Rohde&Scwharz® VNA used as NVNA [94] but

more importantly one of them allows us to detect the beginning and the end of the data acquisition of a sweep point as shown in Figure 3.18. This solution works particularly well using narrowband detection as both NVNA and power meter measure the exact same signal, making the comparison accurate.

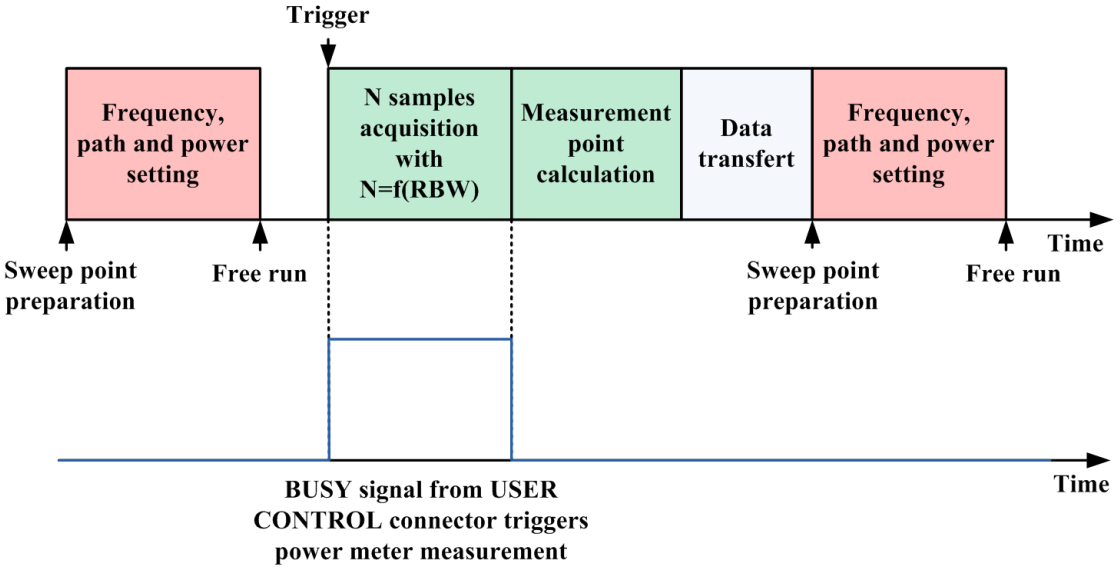

FIGURE 3.18: Synchronization signal for the power meter

Following the objective to compare signals that were acquired at the same time by the NVNA and by the power meter used for power calibration while duty cycle may not be defined, a fast (80MS/s) peak power meter is used when the NVNA use wideband detection. Thanks to the "BUSY" signal, the samples for the power measurement can once again be triggered to be acquired at the same time as the NVNA samples ensuring that the comparison of the measured power results is done on the same portion of signal. The use in this case of an average power meter is possible but the power meter measurement will not be taken in the same time window as the NVNA measurement, leaving room for potentially increased error.

Phase calibration

Following the same logic as for the power calibration, the phase calibration should be performed in the same pulsed conditions as the measurement. The problem arising in that case is the lack of commercially available reference generator characterized in the same pulse conditions as the measurement.

A solution would be to drive the phase reference with a pulsed RF signal. With a step recovery diode based HPR, this solution is practically impossible as the output spectrum is strongly dependent on the temperature of the diode. New characterization should be done for every pulse width and period that are required by the measurement. With a phase reference based on PRBS register, pulsing the RF signal is equivalent to pulsing the clock which will result in an unstable phase relationship between the tones in different pulses.

Another solution would be to modulate the RF signal from the HPR driven with a CW signal using a pulse modulator and then characterize the pulsed HPR. One assumption is that as long as the settling time of the modulator is small compared to the duration of the pulse, the pulsed HPR spectrum is independent of the pulse characteristics. Sadly no instrument was available at the time of this work to characterize the spectrum of such a phase reference.

Instead of characterizing the HPR, a possibility would be as proposed by P. Roblin [95], to characterize first the pulse modulator with a VNA and then to assume that the only difference between the spectrum of the HPR and the one from the pulsed HPR reside in the phase shift due to the transmission in the pulse modulator at each frequency. As seen in Section 2.4.4, comb generator based phase references as the one used in this work are sensible to mismatch. The 20 to 10dB return loss of the pulse modulator on the bandwidth of interest invalidates the last assumption so it would be impossible to determine with certainty the proportion of the change in phase calibration due to the instrument receiver and the one due to the mismatch of the pulse modulator. A characterization of the couple modulator HPR would be required which was not feasible during this work.

The phase calibration will be performed in CW conditions, accepting therefore the potential error from the measurement conditions change.

3.2.8 NVNA pulse measurement validation

Contrary to the NVNA validation performed in Section 2.4.4, it was not possible to compare the custom made pulsed NVNA with different systems. The validation consisted in the comparison of CW and pulsed measurement on an amplifier with the same fundamental frequency, compression, matching and IF bandwidth on the NVNA. The amplifier, a Minicircuit ZX60-43-S+, and the characteristics of the

pulse signal are chosen to avoid strong effects due to the pulsed signal compared to CW. The measurement conditions are the following:

- Fundamental frequency: 1GHz
- Number of harmonics: 8
- Compression: 3dB
- Pulse width 1ms and pulse period of 10ms
- IF Bandwidth: 2KHz

A power sweep is performed in CW and pulsed conditions to verify that the measurement conditions do not have a strong influence on the behavior of the amplifier. Figure 3.19 shows that the behavior of the amplifier seems indeed unchanged in both conditions, the difference between each power sweep being inferior to 0.01dB.

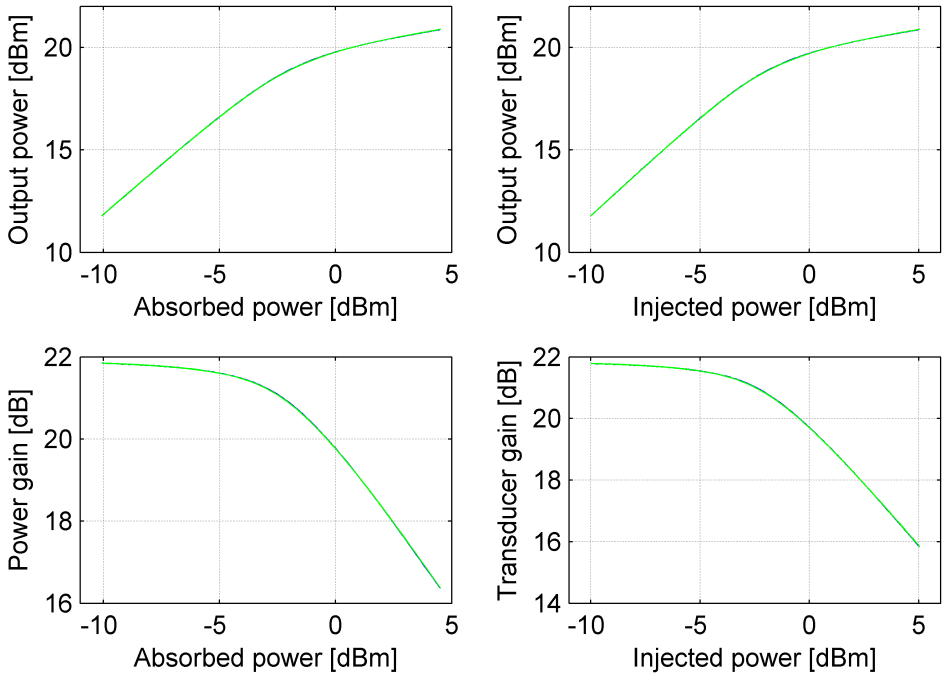

FIGURE 3.19: Power sweep on the test amplifier, the measurement in CW is in green and the pulsed measurement in blue

The measurement results in frequency domain in power and phase are shown respectively in Figure 3.20 and 3.21. The harmonic content of the a_1 wave seems

to be influenced by the pulse modulator operation, however the amplifier appears to have a similar behavior in both CW and pulsed conditions.

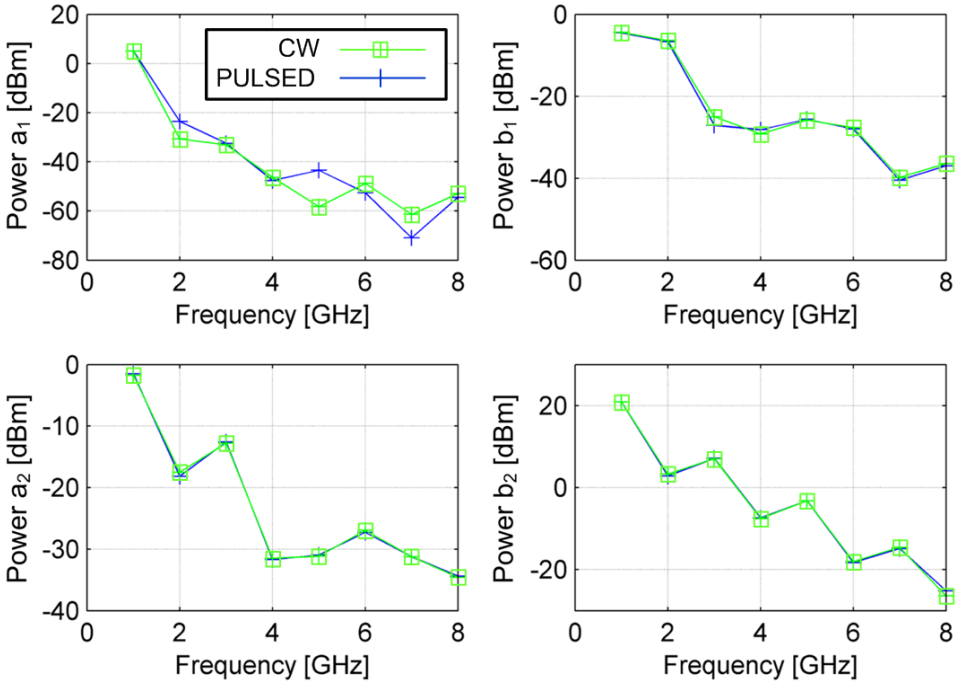

FIGURE 3.20: Power of each measured tone at 3dB compression, the measurement in CW is in green and the pulsed measurement in blue

The result of the EVM calculation in Figure 3.22 confirms that both measurements results are close enough to consider the NVNA in pulse measurement validated.

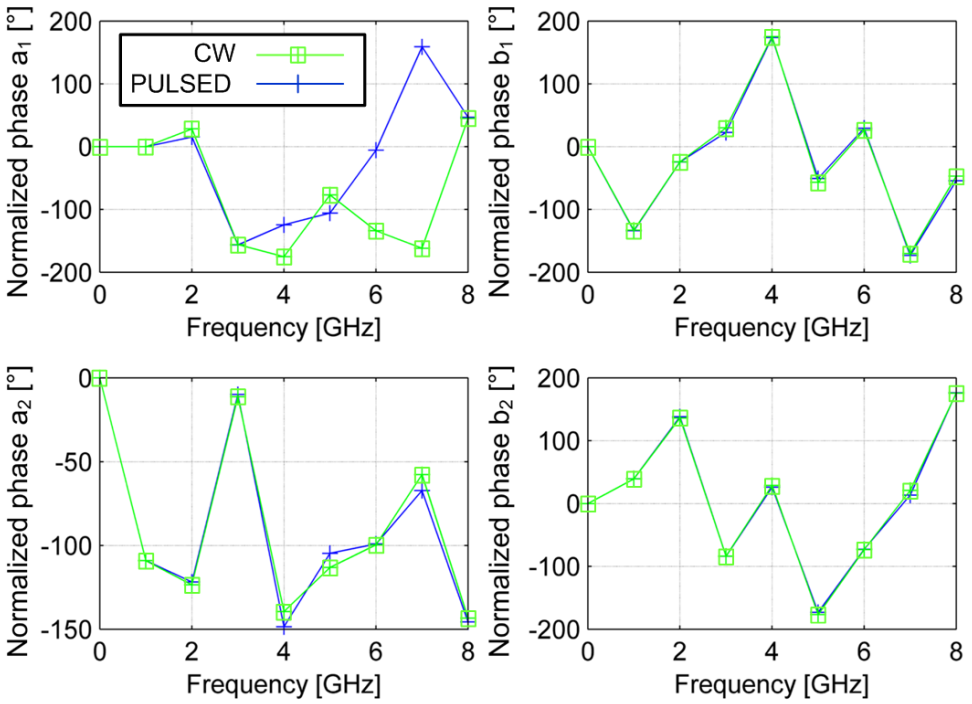

FIGURE 3.21: Phase of each measured tone at 3dB compression, the measurement in CW is in green and the pulsed measurement in blue

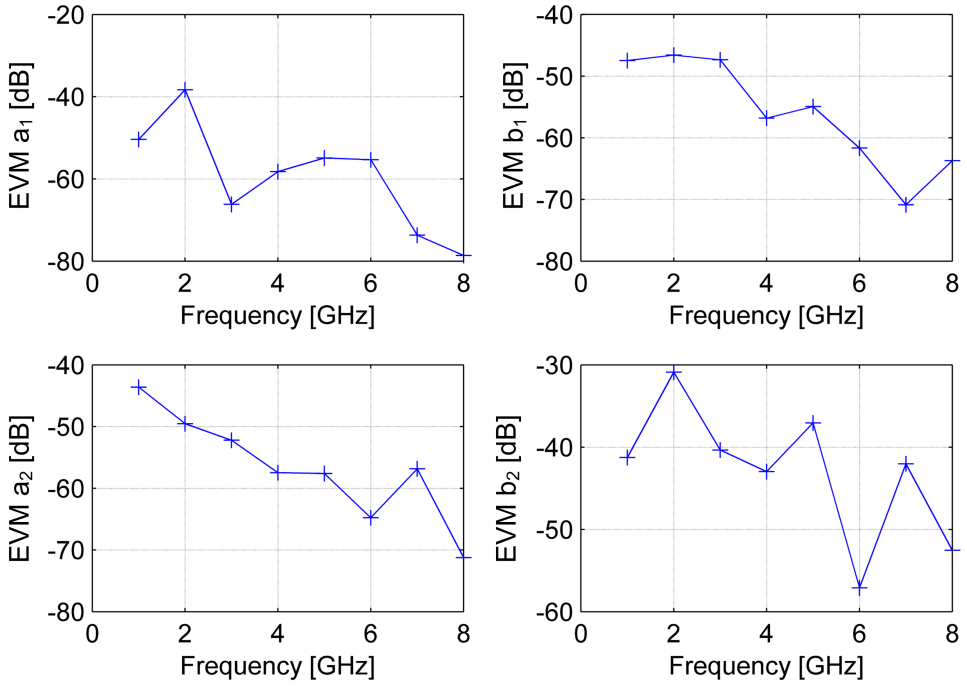

FIGURE 3.22: EVM of each measured tone using the CW measurement as reference at 3dB compression

3.3 Non periodic pulse measurement for nonlinear characterization

This work was undertaken to provide to radar designers a new tool to characterize power amplifiers in realistic conditions. As it was explained in Section 1.2.5, one of the characteristics of a radar pulse train is its non-periodicity that allows optimization of the speed and location detection performance . However a same non-periodic pattern is itself periodic as it is repeated over and over until a new pattern is used. Between each non-periodic burst, some long silence may be applied for detection of the echoes.

Such a non periodic pulse train to be modulated to the carrier signal can be generated by commercially available pulse generators [96]. The pulse generation is realized digitally and therefore every pulse generated must be a multiple of the pulse generator synthesis frequency. For example if the clock frequency of the pulse generator is 80MHz, the outputted pulse widths will always be multiple of 12.5ns. As this fraction is hundred to a thousand times inferior to the measurable time, this is not an issue. The memory limitation of the pulse generator will limit the number of synthesized pulses before restart of the train to 1024 pulses which should be enough to synthesize a burst.

It was seen in Section 1.3.2 that the radar power amplifier behavior could be modified by the temperature or other trapping effects. Considering only the thermal effects, the possible consequence of a non periodic pulse radar pulse train on the amplifier temperature is shown in Figure 3.23. In such a case the amplifier temperature and therefore behavior depends on all the pulses and the silence preceding the time of measurement, and no relationship can be found using periodicity. Unless the burst is long enough to achieve a thermally balanced state, every pulse of the burst must be considered as unique as the amplifier will be in a unique thermal state.

The partial loss of periodicity (partial because the burst will be periodically repeated) and the unique behavior at each pulse imply that every acquisition method that is dependent on the duty cycle will be disqualified for non periodic pulse measurement. It is therefore not possible to use narrowband detection technique for non periodic pulse measurement. Luckily the wideband technique is still available

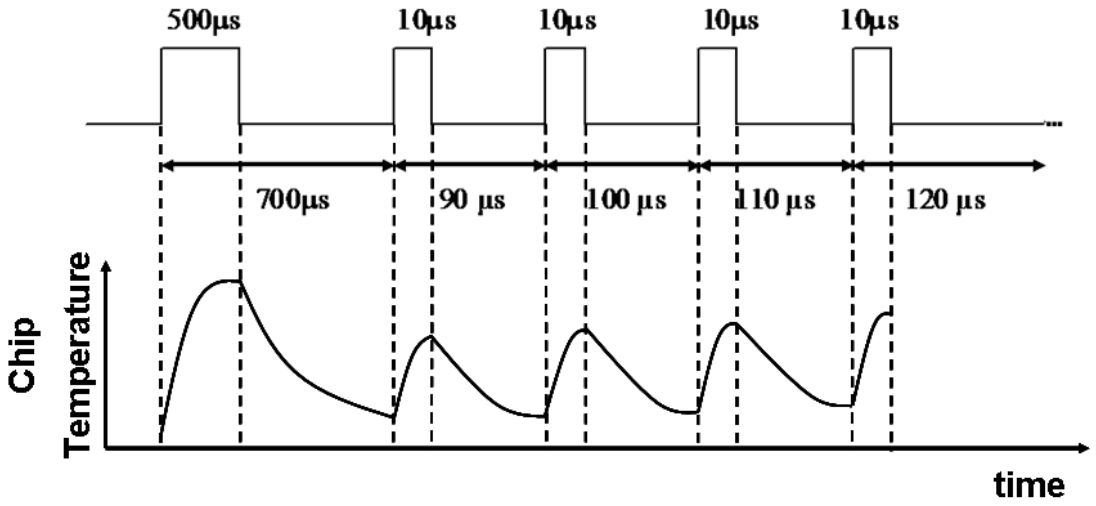

FIGURE 3.23: Amplifier temperature excited by a non periodic pulse train

as it only depends on the pulse width which is still defined for a non periodic pulse train.

The sequential measurement of each tone using heterodyne receiver was so far overlooked. The main reason is that with periodic signal, the assumption made is that every pulse is equivalent. The normal functioning of the wideband detection over a frequency sweep is has follow:

- The NVNA is preparing the acquisition by setting all the signal frequencies, during this time no trigger will be accepted.
- The NVNA is ready, next trigger and therefore for wideband detection next pulse will launch a measurement
- The NVNA set itself for the next sweep point, every trigger during that time will be ignored
- The NVNA is ready...

This implies that the NVNA may not measure every consecutive pulse but just a random selection which is not a problem as they are all considered equivalent, the NVNA rebuilds an approximation of the time domain signal from all the different frequencies measurements at different pulses. This assumption will probably be wrong during the measurement of a short periodic burst again due to thermal and trapping effects.

The assumption of pulse equivalence being invalid for non periodic pulse train and the measurement of every tone simultaneously being impossible with the present NVNA hardware configuration, a new assumption must be made to allow sequential measurement of the tones.

Considering that the effects influencing the transistor behavior have a time constant τ, if a relaxation time of a couple of τ is left between two pulse train measurements, it is possible to assume that the behavior of the amplifier is a function of the pulse position that is identical at every pulse train repetition. In that case the non linear characterization of the amplifier can be performed if every tone is measured at the same pulse position (and at the same time within the pulse).

The synchronization of the measurement on the pulse of interest can be realized using the pulse generator embedded in the VNA that possesses a second output that can synthesize a periodic signal of period equal to the total pulse train duration. This second signal is used as trigger to always perform measurements at a constant time within the non periodic pulse train for each sweep point as shown in Figure 3.24. Doing so every tone is measured at a given unique pulse over many pulse train repetitions making the nonlinear characterization possible.

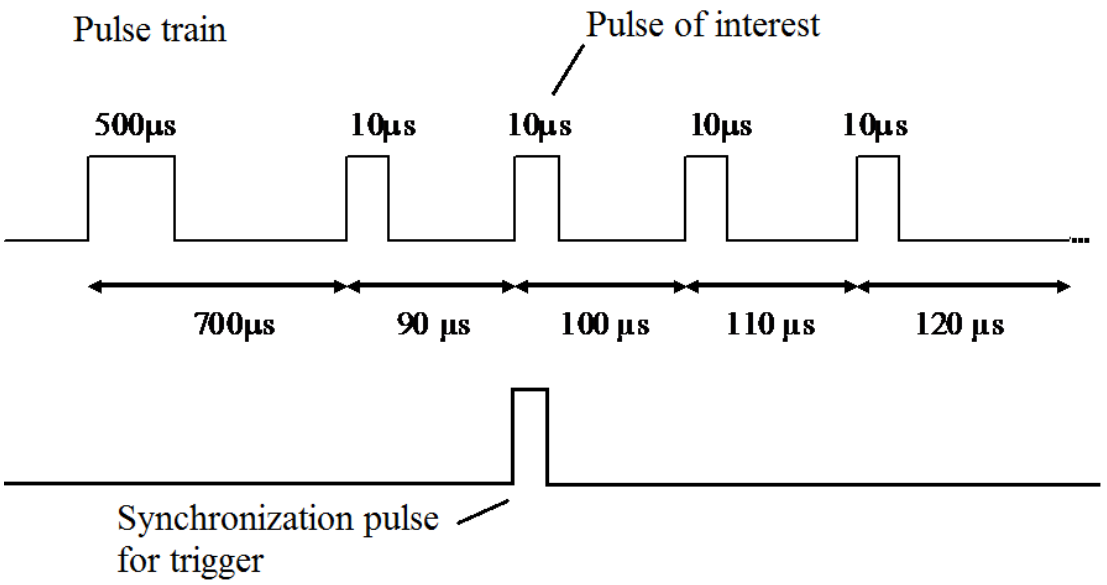

FIGURE 3.24: Measurement synchronization within the train

In the case of a realistic radar functioning, the time between two pulse train repetitions may be smaller than the time required for the DUT to go back to the

defined initial state. in such a situation, this technique will fail to capture the accurate nonlinear behavior of the DUT.

3.3.1 Parallel measurement

In the case where pulses are actually unique even between different bursts, usually meaning different initial conditions for the system common for radar, the previous assumption allowing a mixer based NVNA to characterize the nonlinear behavior at a given pulse is invalidated. A sampler based NVNA could potentially be able to capture the behavior, at the condition its dynamic is not too degraded by the measurement conditions as seen in Section 3.2.6 as the stroboscopic approach cannot be used in the case of pulse singularity. The dynamic is also the main problem of a solution based on a digitizer such as a real time oscilloscope that would normally be used to perform such a measurement.

A possibility to profit from the measurement quality of a heterodyne receiver to characterize the nonlinear behavior within a single pulse is to use as many receivers in parallel as the wanted number of tones. The LO of each receiver has a different frequency to be able to bring the measured tone to the IF frequency used. This solution is a practical realization of the analogy between samplers and mixers shown in Figure 3.25 stating that a sampler sampling N frequencies is equivalent to N mixers in parallel.

This solution is limited to a reduced finite number of tones as the commonly used mixer based NVNAs possess four port of which only three are actually usable for detection if a synchronizer is used as explained in Section 2.4.2. Most of the commercially available VNAs requiring a synchronizer and having only two excitation sources, this solution cannot be applied with such instruments.

Nevertheless this solution could be realized by modifying a Rohde&Schwarz® six port 20GHz VNA prototype with six independent generators and one local oscillator all hybrid DDS-PLL based. This instrument potentially allows the measurement of three harmonics simultaneously at each port of a two port DUT.

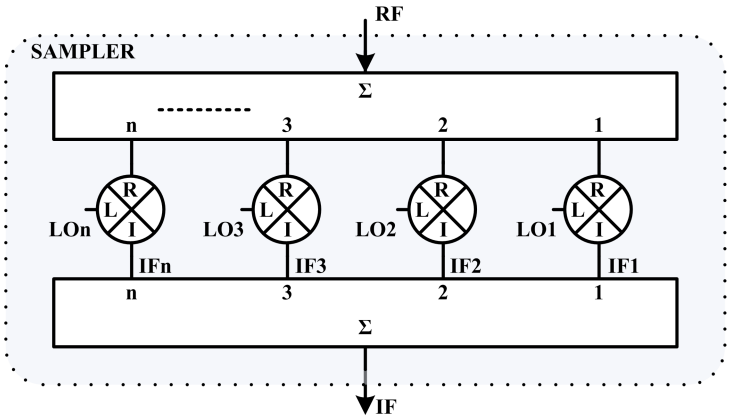

FIGURE 3.25: Sampler and mixer analogy

Receiver modification for parallel measurement

The DDS technology allows phase coherence without the use of a synchronizer as seen in Section 2.4.2. Moreover, as all the sources use the same oscillator as reference and that the reset of their registers is done at the same time (practically by using one source as master and all the others as slave), all the sources are phase coherent. They can therefore be used as LO signal for the receivers while keeping the phase coherence between the measurements at each frequencies. The VNA was rewired to direct the sources into the LO path of the receivers as shown in Figure 3.26 for two ports.

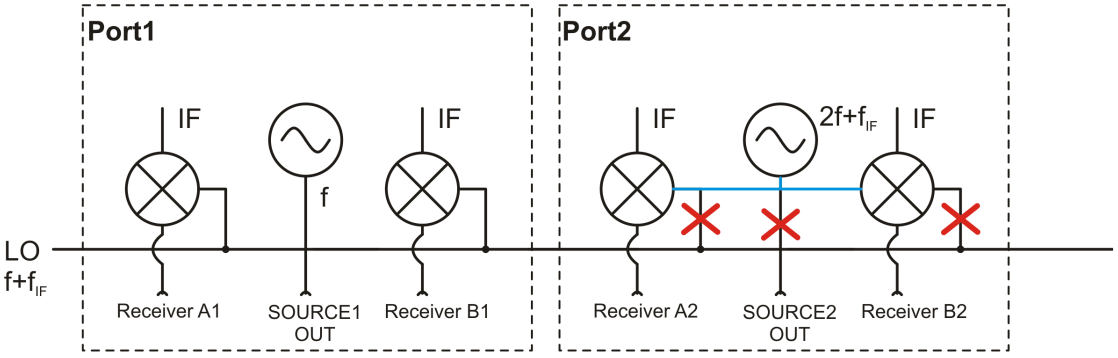

FIGURE 3.26: Rewiring of the VNA sources into the LO path of the receiver

All the measurement being performed simultaneously, the measurement does not consist anymore of a frequency sweep put of a single frequency measurement at firmware level. However as the firmware is not aware of the multiple LO signals, it consider that all the receivers are measuring the same frequency. This creates a problem when the tone measured are spanned over a bandwidth that require

the use of more than one path of the front end as explained in Section 3.2.5. In fact all the frequencies that are located on a portion of the bandwidth that use a different front end path than the frequency the instrument thinks it measure are cut out by the front end path in use and therefore not measurable.

As shown in Figure 3.27, to set the right front end path, the firmware compares the frequency measured with the available front end path ranges. Then the firmware sends a message to the switch that commutes to the adequate path. As no access was granted to the firmware, the workaround used was to interfere with the message sent to the switches. The bus used to carry the message being a multiple purpose access to the receiver FPGA, it was not possible to temper with it. The receiver card was therefore slightly modified to allow or not the command from the receiver FPGA to arrive to the switches, allowing the manual setting of the switch at a given receiver and leaving it unchanged during the entire measurement. Every receiver can now be set to measure a given frequency.

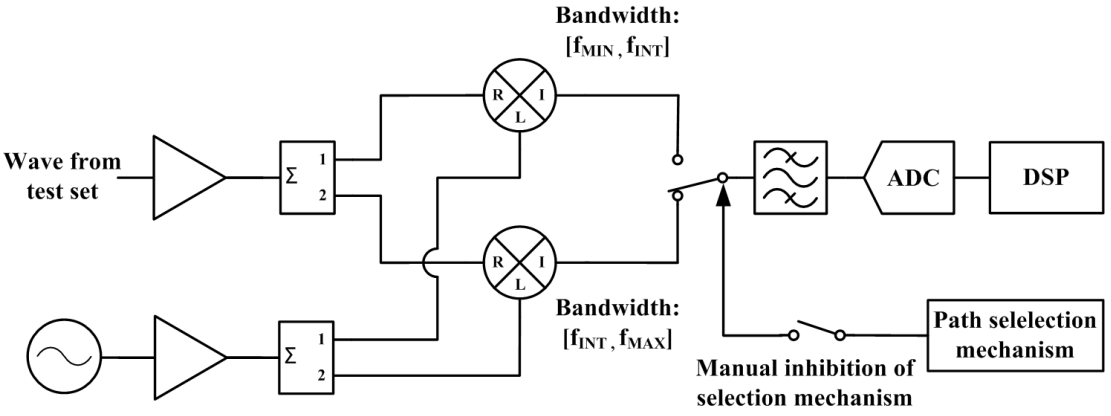

FIGURE 3.27: Modification of the path selection mechanism

Test set modification for parallel measurement of high power amplifier

Once the receivers are able to measure different frequencies simultaneously, the test set must be modified to feed every receiver with the signal they need to measure.

The test set is modified taking into account that the NVNA is to be used for high power amplifier measurement up to 100W, meaning that the available signal at the fundamental and at harmonic two and three should have a power higher than the power compressing the receiver. Accordingly an example of test set modification is shown in Figure 3.28.

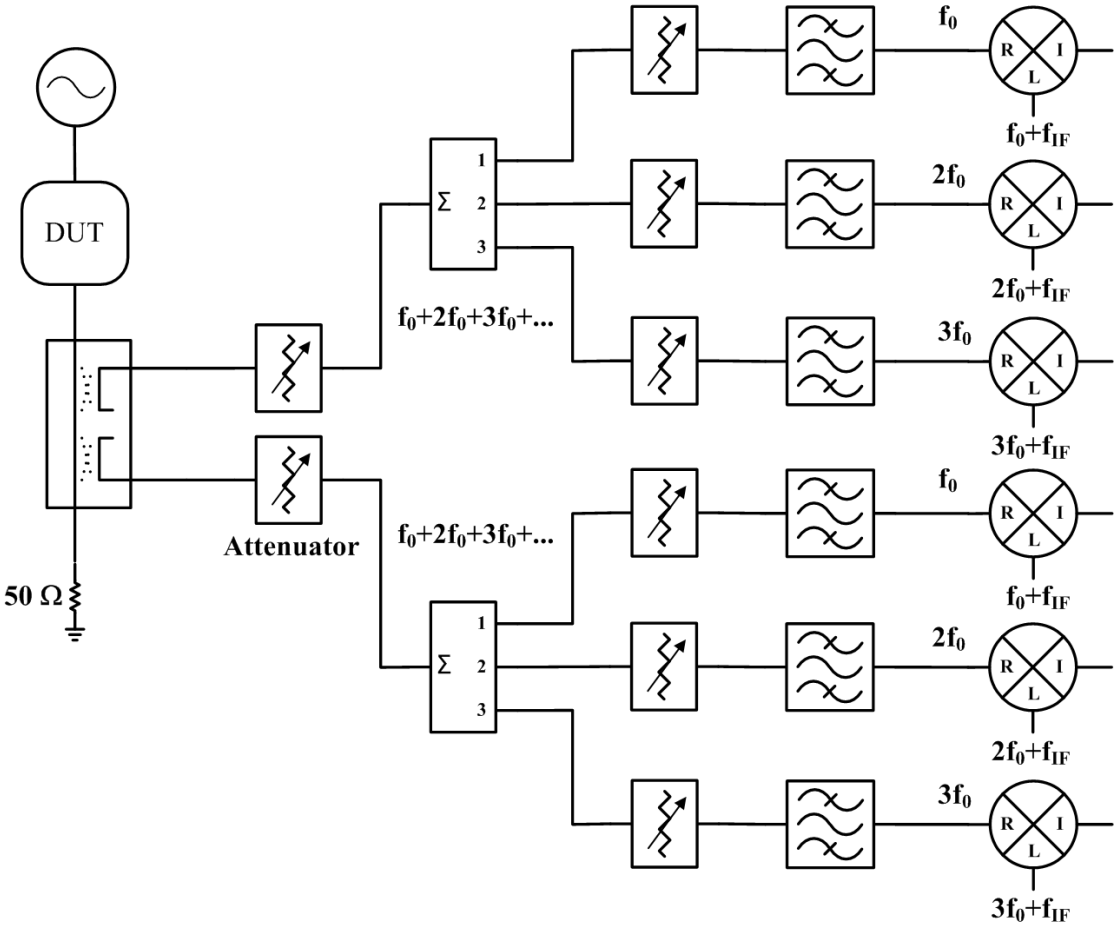

FIGURE 3.28: Modification of the NVNA test set at the output (identical to the input modification)

The power splitter is used in order to divide the complex signal in three parts and then each part is filtered and dynamically conditioned with the step attenuators to feed each receiver with a single tone signal providing the best signal to noise ratio possible without compressing the receivers.

Isolators could be used to prevent the signal rejected by the filters to access the other receivers. Practically they are replaced by fixed attenuator to circumvent their narrow bandwidth that makes the test set unpractical when changing the measured frequency. The fixed attenuators also improve the matching of the power splitter by padding.

The filters can be a bank of selectable bandpass filters or tunable filters. The bandwidth of the bandpass filter will limit the minimum fundamental that can be used. As in this work, the minimum required fundamental frequency is 2GHz, there was not strong constraint on the bandwidth. The presented synoptic purposely ignores the fact that there are more than one front end path to cover the instrument

bandwidth. It could be possible to relax the frequency range constraint on the bandpass filters by adding them on every front end path.

Thanks to the good matching and repeatability of the step attenuators it is possible to characterize every path combination using a VNA and then dynamically correct the measurements when a change in the path is needed compared to the path used during calibration. This is directly inspired from the dynamic attenuation feature present on the LSNA but absent on most commercially available mixer based NVNAs.

Calibration for parallel measurement

The exact same NVNA calibration procedure described in Section 2.4.3 for CW or Section 3.2.7 for pulsed measurement is applied. The only difference is that as every receiver now correspond to a frequency, the relative calibration can't be performed using the instrument firmware and has to be written again for the particular case of parallel measurement.

Parallel measurement compared to existing solutions

The measurement performance is equivalent to the performance of the VNA the system is relying on, it therefore compares to state of the art mixer based NVNA.

Aside from the measurement of single pulses, the parallel measurement compared to a classical mixer based NVNA allows an easier diagnostic of receiver compression compared to the one described in Section 2.4.1 as only one tone is measured per receiver.

For the same reason the stated available dynamic can be applied, as for linear measurement, to the measurement of each single frequency compared to the mixer and sampler based NVNA or oscilloscopes where the dynamic applies to the complex signal where the strong fundamental often blinds the instrument to the weaker harmonics.

The obvious drawback of this method is the number of simultaneously measurable frequencies limited to three. However in the case of power amplification, this drawback remains limited. In fact as explained in Section 2.4.4, the behavior of

a DUT often depends on the matching of all the present tones. Therefore only the measurements where the matching was at least known and in the best case controlled can be compared to other measurement. The matching is controlled by load pull techniques, that consist for the majority of the cases in the radar industry of passive load pull. With passive load pull, only tuners allowing to match three or four harmonics at the same time are commercially available [97], limiting the control over the matching.

Also, considering fundamental frequencies in the order of 15 to 20GHz, the number of harmonics is often limited to three by the availability of wide bandwidth instruments for non linear characterization. Therefore in that case, measuring only three frequencies is not a drawback compare to the other methods while keeping the advantages of the parallel measurement method. As the required components and techniques for parallel measurement are available, this concept could be extended up to 60GHz bandwidth, where the concept should show its full potential.

3.3.2 Parallel measurement validation

The parallel measurement is validated in CW condition comparing the measurement on the Minicircuit ZX60-43-S+ used for the pulsed validation, with the system validated in Section 2.4.4 in the same conditions of compression, matching and IF bandwidth. Then the validation in pulsed mode is performed using the same amplifier used to validate the NVNA in pulsed mode in Section 3.2.8.

The measurement conditions for the validation are as follow:

- Fundamental frequency: 2GHz
- Number of harmonics: 3
- Compression: 3dB
- Pulse width 1ms and pulse period of 10ms
- IF Bandwidth: 2KHz
- Identical test set

Validation in continuous wave condition

The CW measurement results in frequency domain in power and phase are shown respectively in Figure 3.29 and 3.30. The amplifier appears to have a similar behavior measured with both classical and modified NVNA despite slight difference in the instrument impedance as shown by the a_2 measurement. This difference can be explained by the different cabling of within both instruments. It can also be noticed on the a_1 measurement that the second harmonic is slightly stronger in the classic NVNA than on the modified NVNA. It can be explained by a loss mismatch between the source path of each instrument, making the classic NVNA generate higher power (and therefore higher second harmonic) to reach a power in the DUT's plane equivalent to the one provided by the modified NVNA.

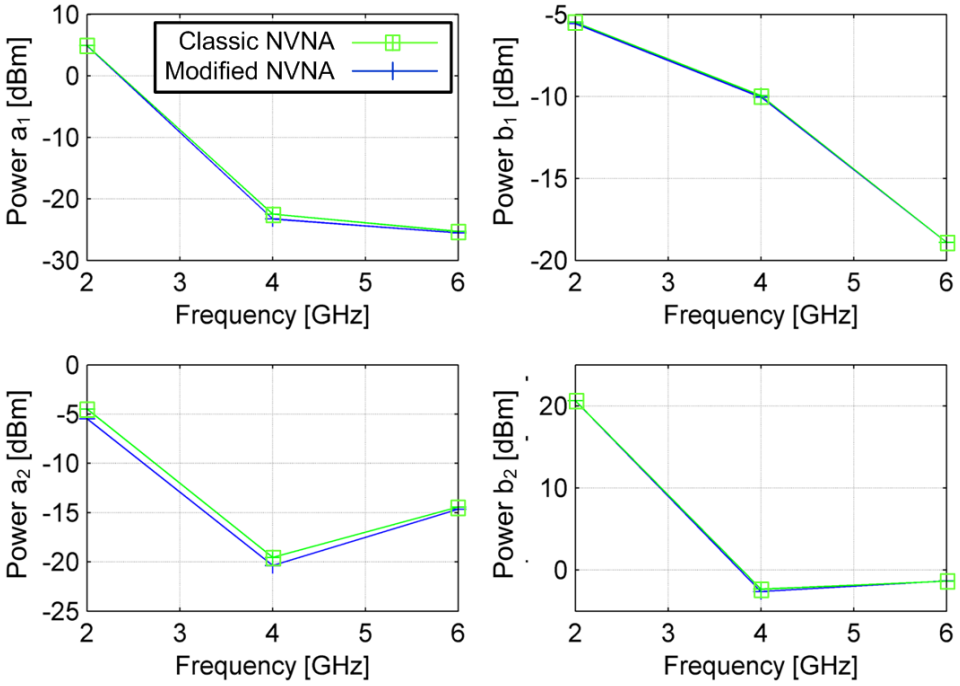

FIGURE 3.29: Power of each measured tone at 3dB compression, the CW measurement with the classic NVNA is in green and the CW measurement with the modified NVNA in blue

The result of the EVM calculation in Figure 3.31 shows however that the measurements in CW taken with the modified NVNA are close enough to the ones taken with the classical NVNA chosen as reference for the EVM calculation. The modified NVNA is therefore validated in CW.

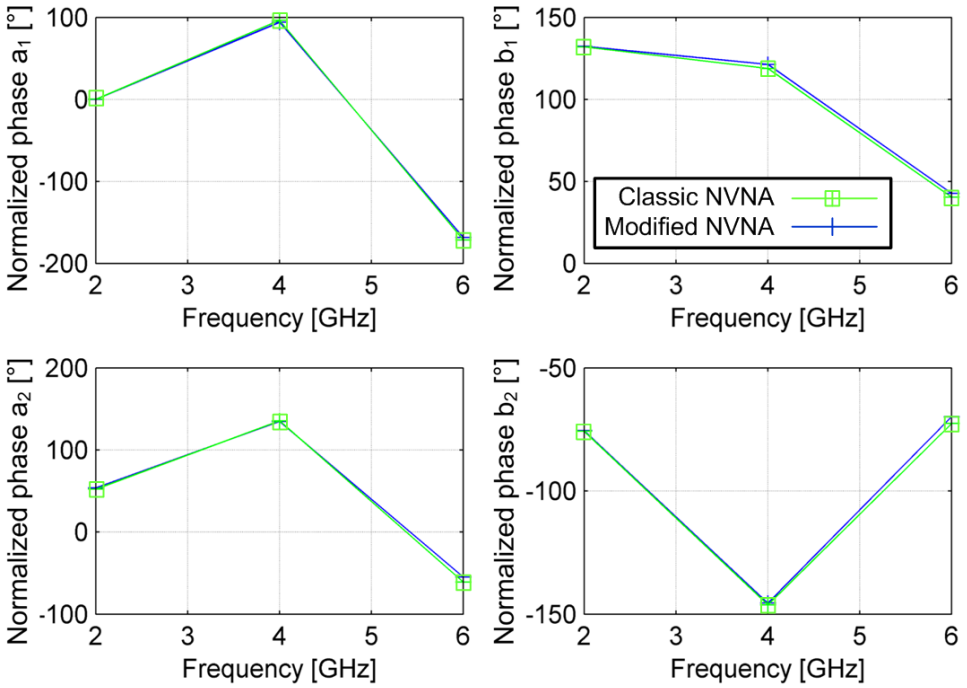

FIGURE 3.30: Phase of each measured tone at 3dB compression, the CW measurement with the classic NVNA is in green and the CW measurement with the modified NVNA in blue

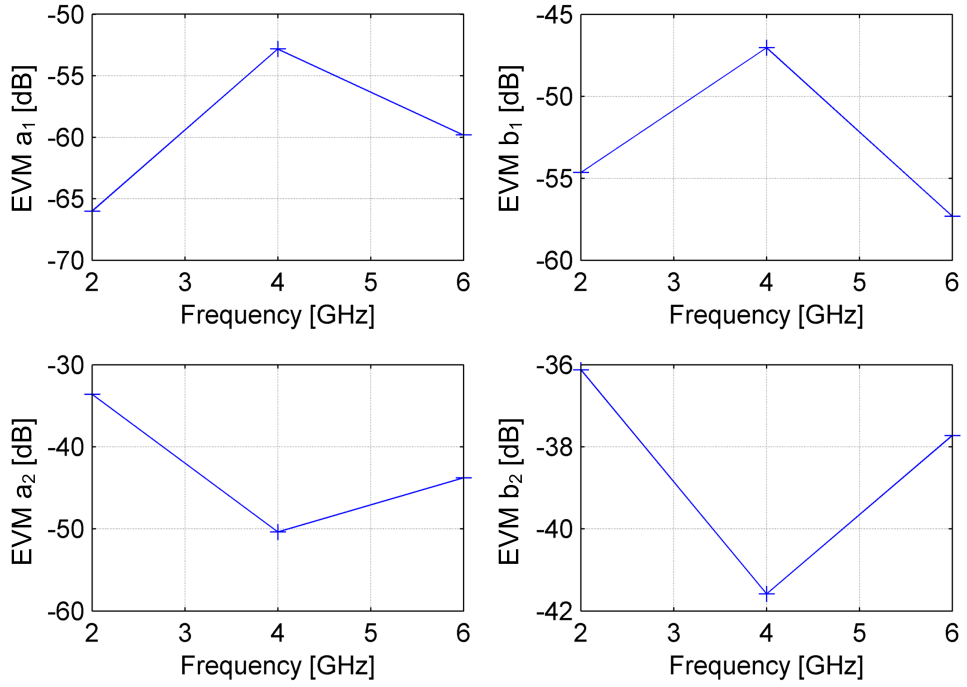

FIGURE 3.31: EVM of each measured tone of the modified NVNA CW measurement using the CW measurement with the classic NVNA as reference at 3dB compression

Validation in pulsed conditions

The pulsed measurement results in frequency domain in power and phase are shown respectively in Figure 3.32 and 3.33. The measurement of the amplifier's pulsed behavior seems, as it was during the CW validation, equivalent with both instruments. Identical mismatch between the instruments to the one observed in CW conditions are occurring. It can be seen on the a_1 measurement that the use of the pulse modulator worsen the differences of the loss mismatch already noticed in CW.

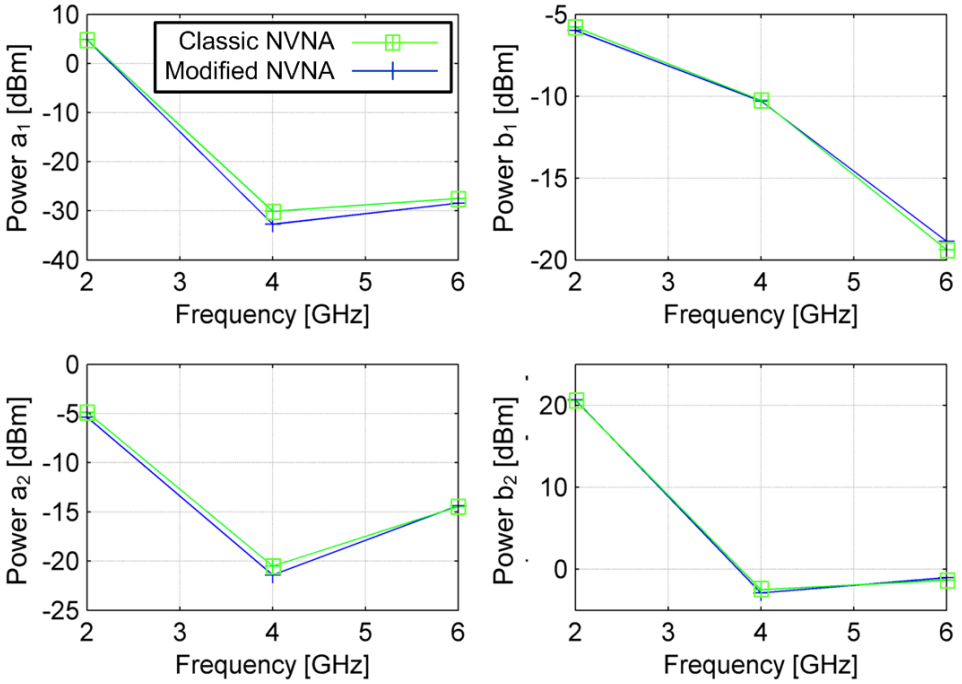

FIGURE 3.32: Power of each measured tone at 3dB compression, the pulsed measurement with the classic NVNA is in green and the pulsed measurement with the modified NVNA in blue

The result of the EVM calculation in Figure 3.34 shows that the measurements with both classic and modified NVNA are again close enough to validate the parallel measurement in pulsed mode.

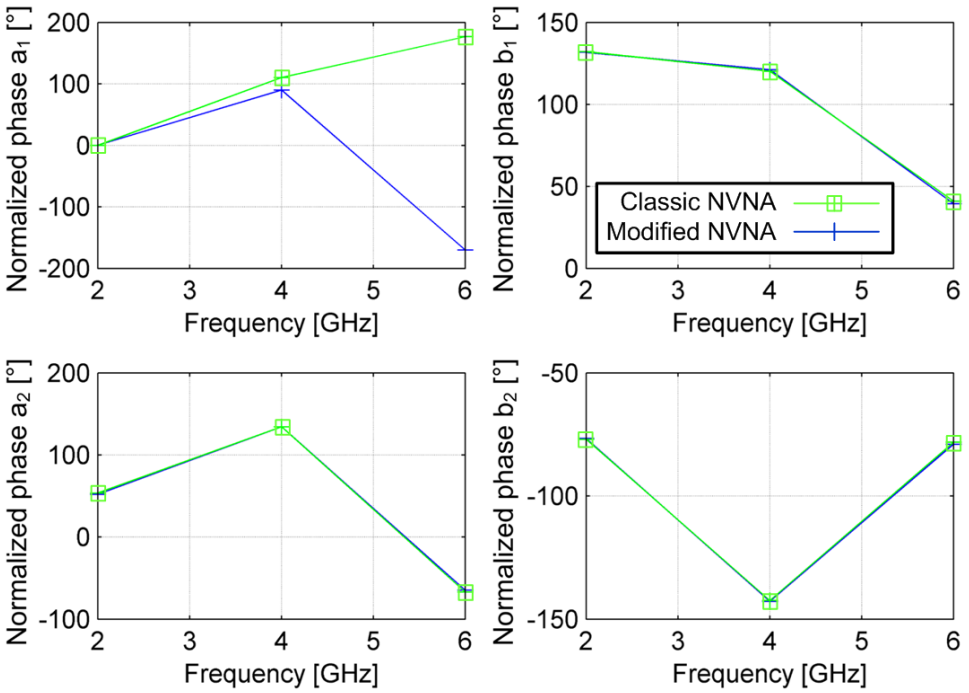

FIGURE 3.33: Phase of each measured tone at 3dB compression, the pulsed measurement with the classic NVNA is in green and the pulsed measurement with the modified NVNA in blue

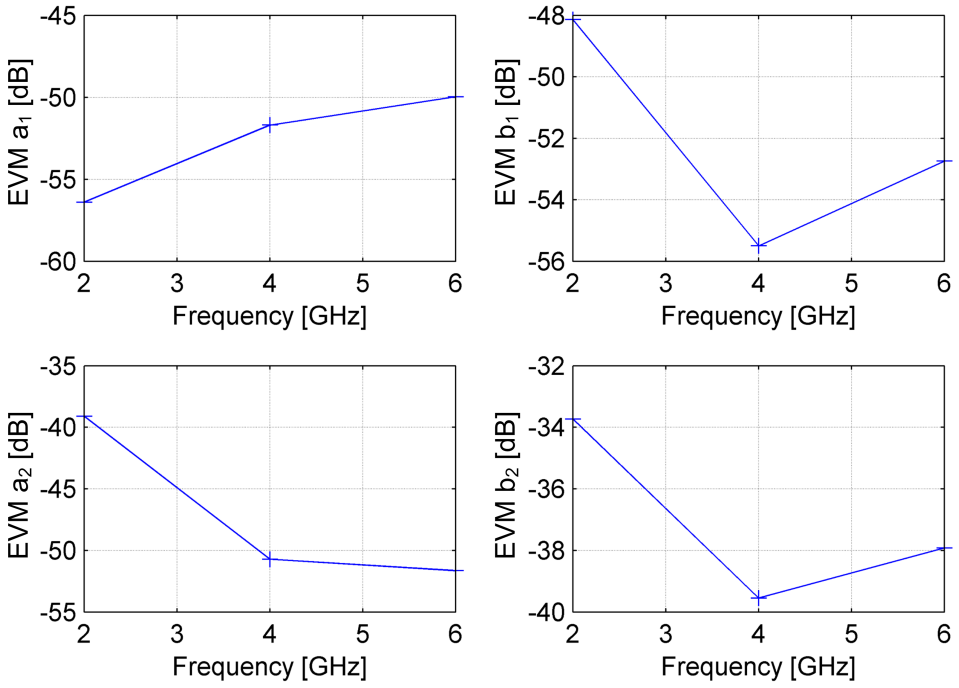

FIGURE 3.34: EVM of each measured tone of the modified NVNA pulsed measurement using the pulsed measurement with the classic NVNA as reference at 3dB compression

3.3.3 Measurement of the influence of different non periodic pulse train on the nonlinear behavior of a power amplifier

The measurements are performed on the S-band 5W GaN on silicon HEMT form Nitronex shown in Figure 3.35. For all measurements the fundamental frequency is 2GHz and harmonics two and three are measured. The gate voltage is -1.8V and the drain voltage is 28V corresponding to an idle drain current of 5mA, none of the biasing tensions are pulsed. The load and source impedance are not controlled but are the same for every measurement. All measurements are performed at 1dB compression.

FIGURE 3.35: S-band 5W amplifier used for the study

To avoid including an overshoot in the results, measurements are taken with a delay. Instruments IF bandwidth is chosen according to the wideband detection requirements i.e for measurement of a $10\mu s$ wide pulse, the delay before measurement is $3\mu s$ and the IF bandwidth of 200KHz.

Before every measurement the transistor was not used for at least 24 hours to minimize the long terms memory effect as much as possible.

To identify effects of the measurement conditions on the amplifier behavior, a power sweep is realized in CW, in periodic pulse $10\mu s$ width and 10% duty cycle conditions, and using the non periodic pulse train of Figure 3.36. The time

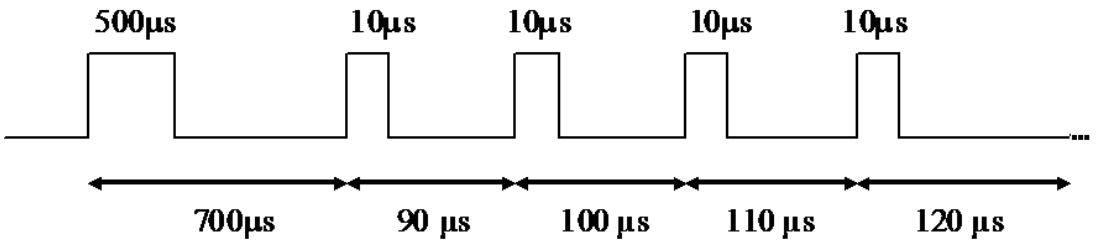

FIGURE 3.36: Radar pulse train used for the power sweep

characteristics of the non periodic pulse train are randomly chosen and do not correspond to any used train. Nevertheless it is mimicking a radar pulse train as a first long pulse is often used to warm up the amplifier before sending a staggered pulse train actually used for detection.

The measured power sweeps in CW, periodic pulse train with and at the first 10s pulse of the non periodic radar pulse train are compared in Figure 3.37. It shows that the radar pulse train has degraded gain compared to the periodic train that would be used to approximate it while CW presents the worst power gain. According to [21], the performance of GaN HEMT amplifiers is strongly related to thermal state of the transistor and tend to degrade when working temperature rises. An explanation of the described results would be that the long initial pulse used to reduce transient effects is also responsible for the performance degradation. This transistor self heating effect is overlooked when using a periodic pulse approximation of the radar pulse train.

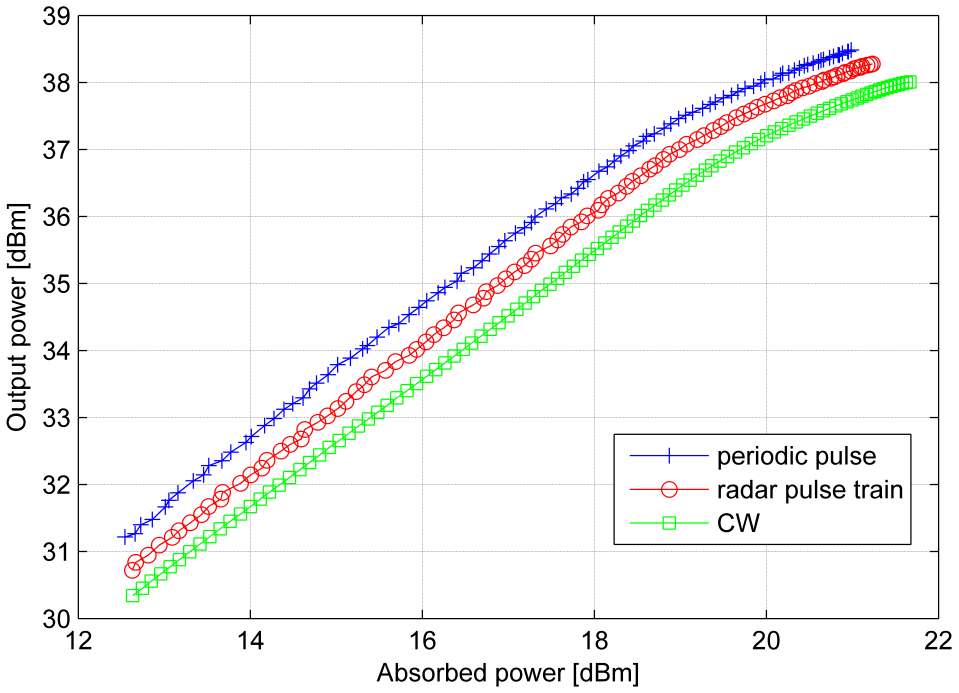

FIGURE 3.37: Output power versus input absorbed power in CW, 10s and 10% duty cycle pulse train and radar pulse train.

Measurement of the evolution of the nonlinear behavior of the amplifier excited with a burst of pulses

A 200 pulses long staggered burst of 10μs pulses with a 100 μs equivalent period is sent to the device under test. One measurement is taken at every pulse starting from pulse one in order to compare the behavior of the amplifier from one pulse to the other.

Measuring the evolution of the frequency domain output traveling wave normalized by the driving signal at fundamental at each pulse is represented in Figure 3.38 for the magnitude and Figure 3.39 for the phase, it can be noticed that the different tones evolve sensibly over the different pulses. The same degradation of performance that influences the fundamental frequency seems to also strongly influences the second harmonic. The third harmonics seems to be slightly favored instead. One explanation would be that, as it was observed during the power sweep, the degradation of the amplifier performance makes the 1dB compression point happen at higher input power. Therefore we are not compressing the transistor in the same manner from one pulse to another.

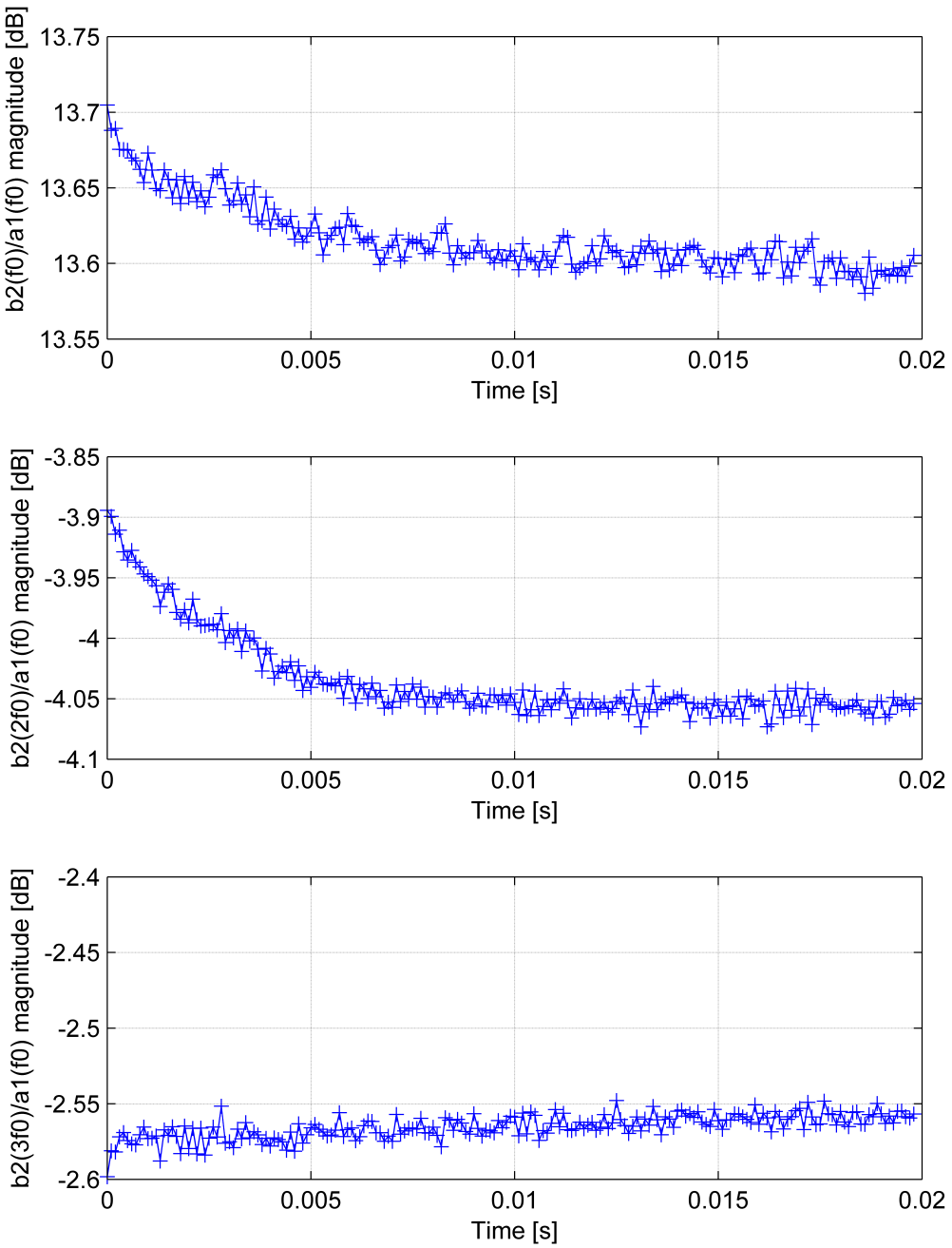

FIGURE 3.38: Magnitude at fundamental, harmonic 2 and 3 of output traveling wave normalized by the excitation traveling wave at fundamental for each $10\mu s$ pulse of the staggered pulse train. Measured at 1dB compression

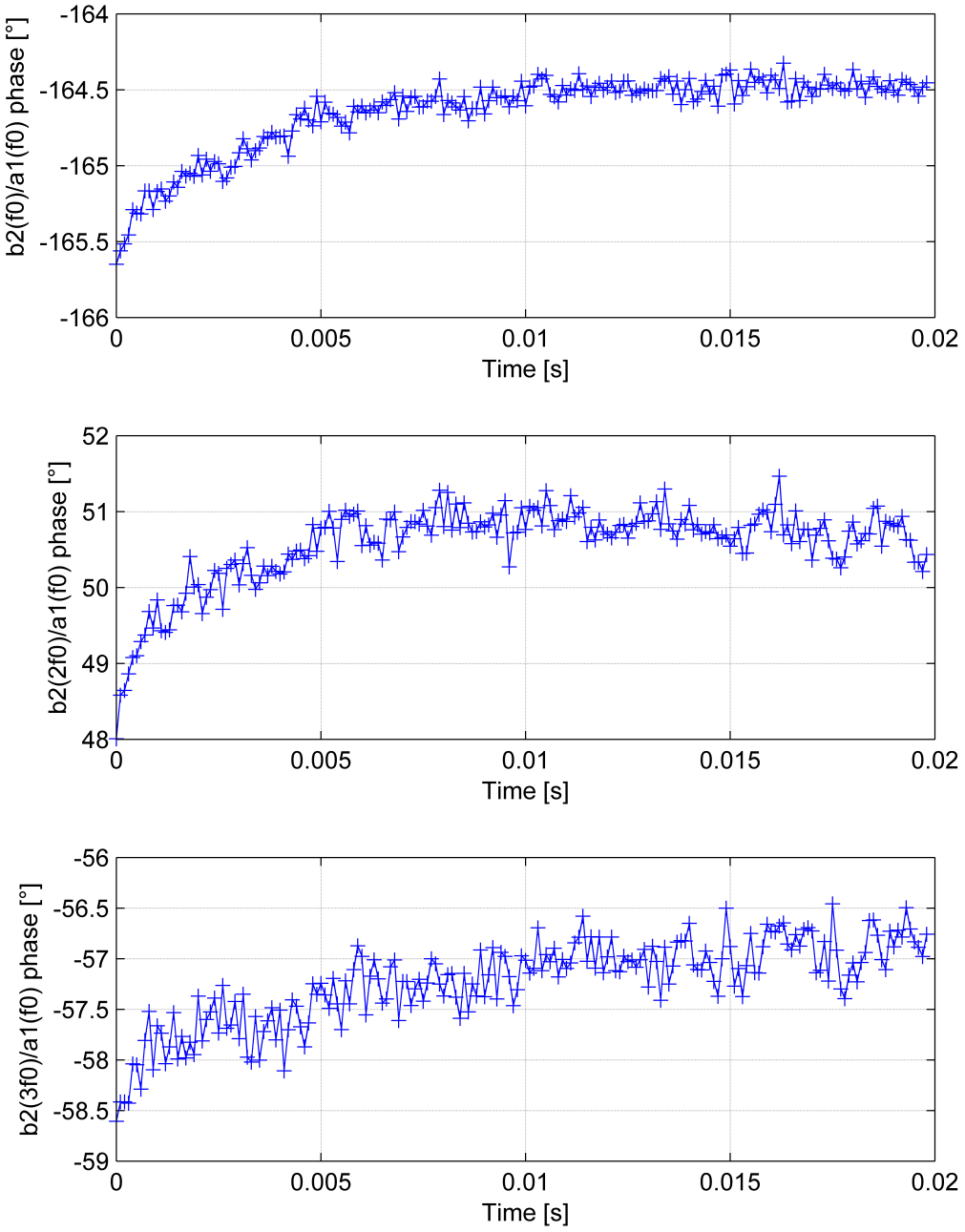

FIGURE 3.39: Phase at fundamental, harmonic 2 and 3 of output traveling wave normalized by the excitation traveling wave at fundamental for each $10\mu s$ pulse of the staggered pulse train. Measured at 1dB compression

Measurement of the evolution of the nonlinear behavior of the amplifier caused by different pulse width in a same pulse train

In order to evaluate the influence of different pulse width within same radar pulse train, we use a sequence of forty-nine times $10\mu s$ staggered pulses with equivalent period of $100\mu s$ followed by a pulse of $200\mu s$ as shown in Figure 3.40. We repeat this sequence until we have measured one hundred $10\mu s$ pulses, leaving $100\mu s$ between two sequences.

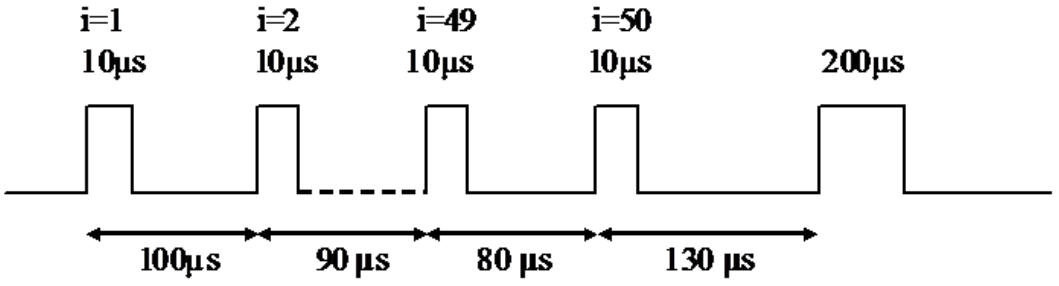

FIGURE 3.40: Non periodic pulse train used to evaluate the influence of pulses of different width on transistor performance

Looking in Figure 3.41 at the transmission magnitude over the pulses one can see an evolution of the performance of the amplifier.

The decrease of performance that was observed in the previous example can be seen again from pulse 1 to 50. This is expected as the trains used in both experiments are similar until pulse 50.

In Figure 3.40 we can see that after the 50th pulse a 200s pulse occurs before restarting the sequence. This long pulse according to Figure 3.41 alters the performance of the transistor changing its working temperature. However after thirty repetitions of $10\mu s$ pulses the amplifier comes back to an equilibrium state comparable to the one of the previous experiment. The harmonics are also affected by such a pulse train. In Figure 3.42 we can see that the phase is also evolving, especially at the second harmonic. This could be once again explainable by the varying compression point of the transistor as its performance evolves.

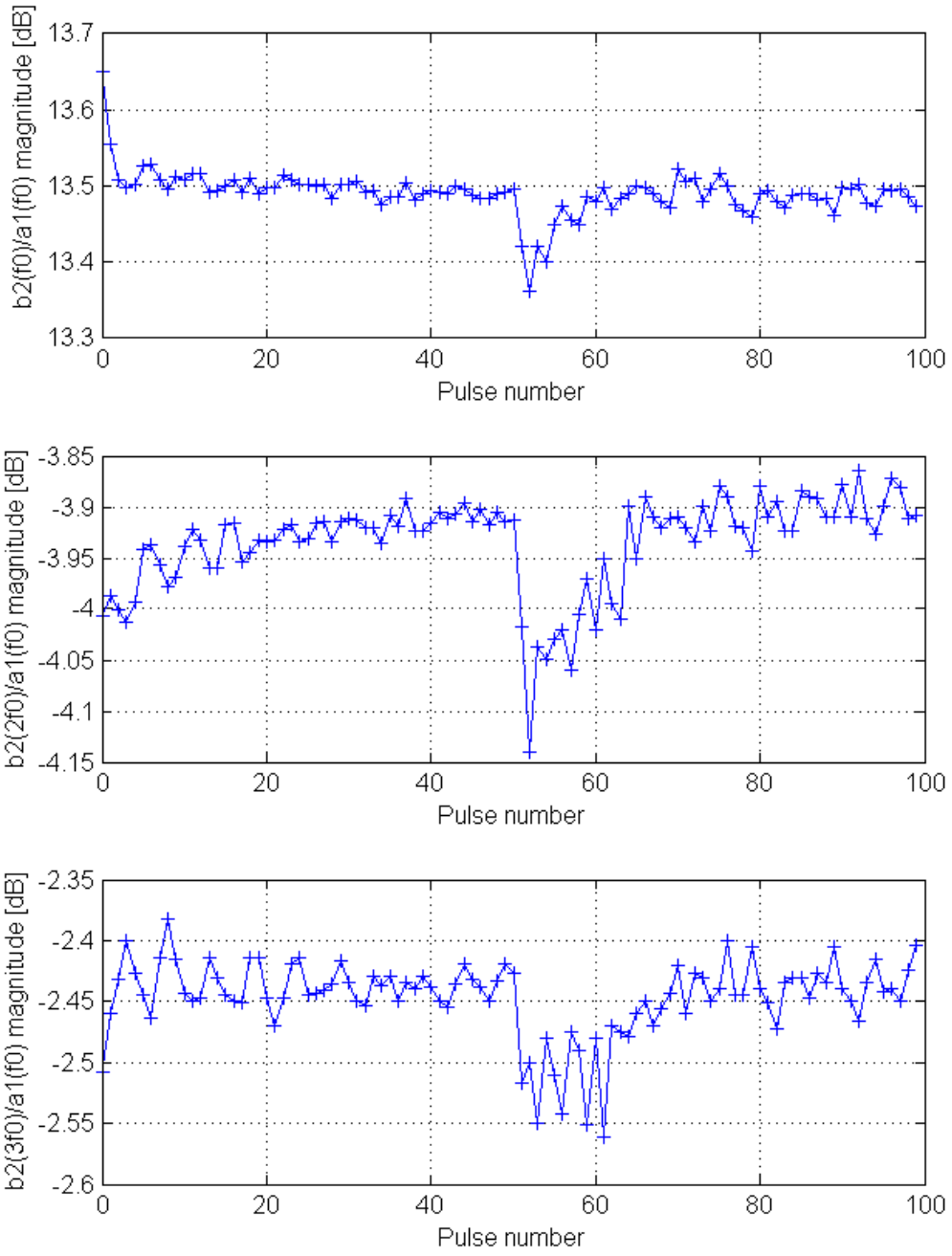

FIGURE 3.41: Magnitude at fundamental, harmonic 2 and 3 of output traveling wave normalized by the excitation traveling wave at fundamental at $10\mu s$ pulse versus the pulse number of the Figure 3.40 train (the $200\mu s$ pulse is ignored and not counted). Measured at 1dB compression

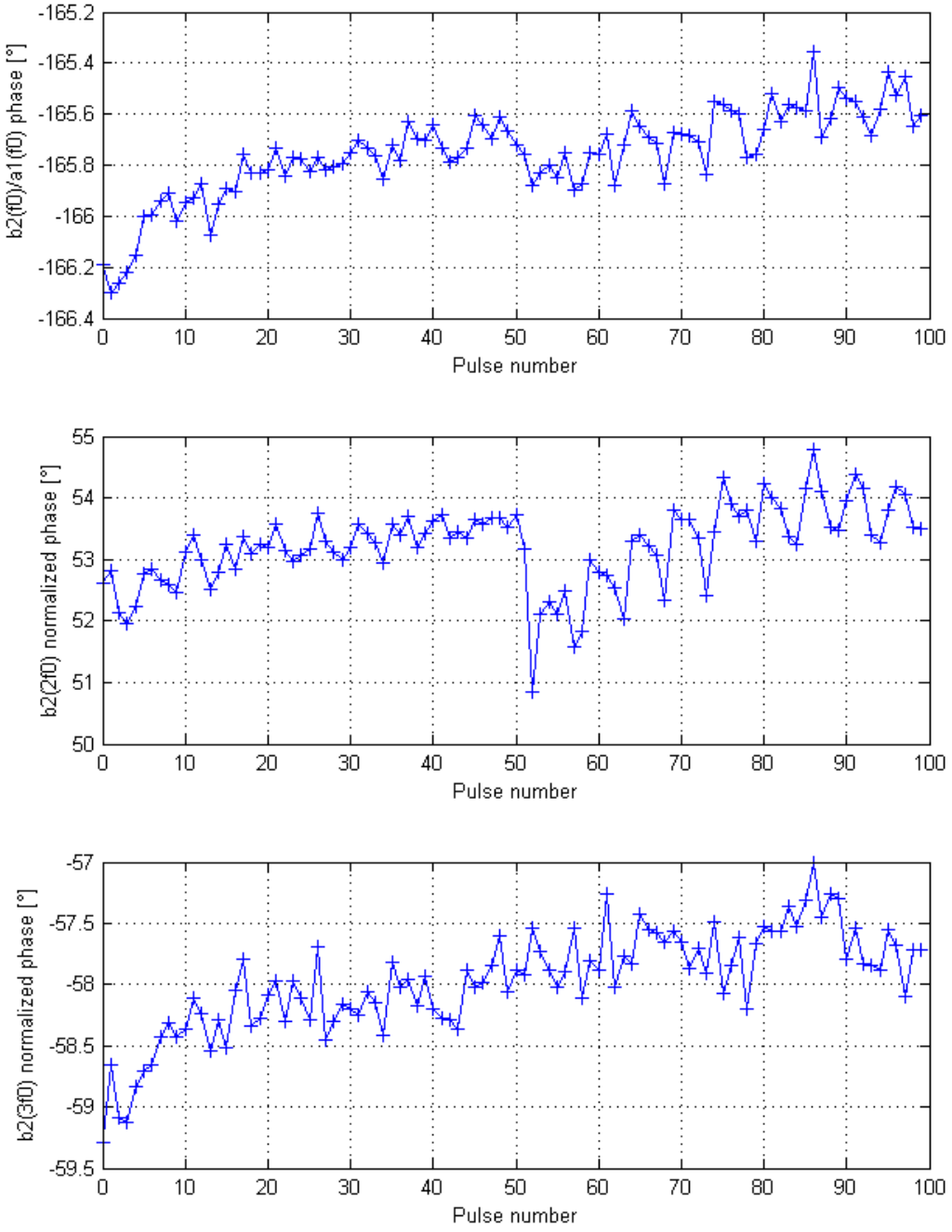

FIGURE 3.42: Phase at fundamental, harmonic 2 and 3 of output traveling wave normalized by the excitation traveling wave at fundamental at $10\mu s$ pulse versus the pulse number of the Figure 3.40 train (the $200\mu s$ pulse is ignored and not counted). Measured at 1dB compression

Sadly the ringing that can be observed on the measurements is caused by the driving amplifier used to drive the 5W amplifier in this experiment. It does not affect however the drawn conclusions as they are consistent with the rest of the experiments.

Measurement of the evolution of the nonlinear behavior of the amplifier caused by different duty cycle in a same pulse train

Change in duty cycle (or equivalent duty cycle in the case of staggered pulses) can be used in radar pulse trains to dynamically change the detection capabilities. The pulse train of Figure 3.43 is used in order to evaluate the influence of different duty cycles in a same pulse train. It consists of a series of one hundred $10\mu s$ staggered pulses with an equivalent duty cycle of 10% followed by a hundred $10\mu s$ staggered pulses with an equivalent duty cycle of 50%. The pulse train is run twice consecutively measuring each pulse.

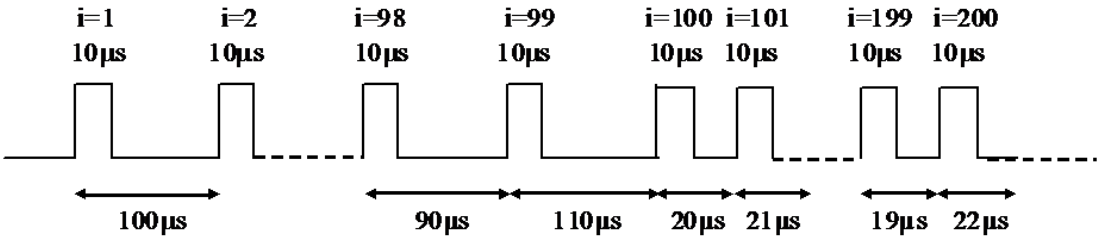

FIGURE 3.43: Non periodic pulse train used to evaluate the influence of pulses of different duty cycles on transistor performance

In Figure 3.44 we can see the evolution of the transmission magnitude over the pulses. Like for the previous experiment, the first hundred pulses of the pulse train are the same as the one used to get the result of Figures 3.38 and 3.39. Therefore we observe the same phenomenon in the first pulses. The harmonics are following a similar evolution.

At pulse number 100, the duty cycle is increased to 50% for the next hundred pulses. The performance of the transistor are changing to converge to a new steady state according to the new excitation. This effect is attributed to the increase of temperature of the transistor which degrades the performance in the case of our GaN HEMT amplifier.

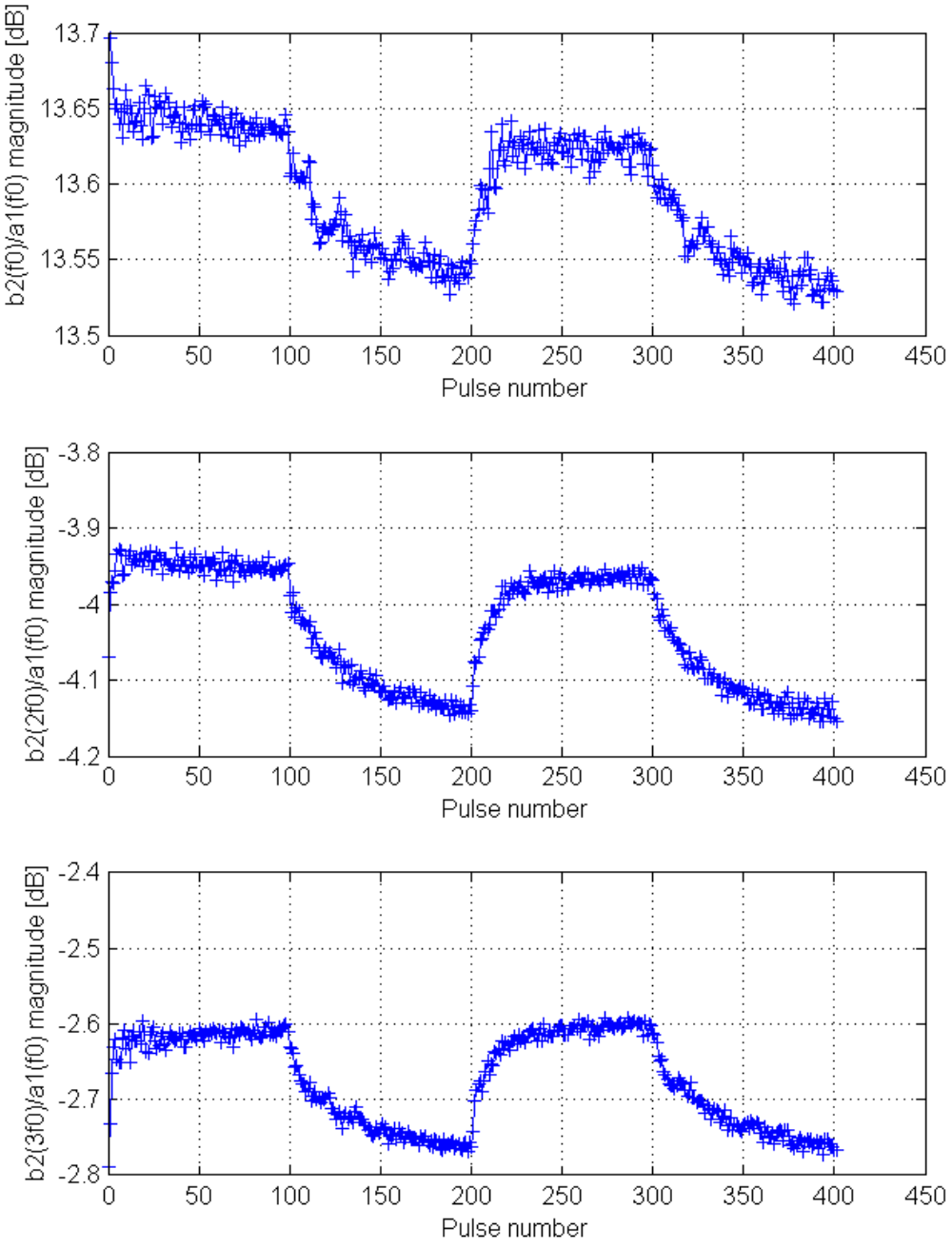

FIGURE 3.44: Magnitude at fundamental, harmonic 2 and 3 of output traveling wave normalized by the excitation traveling wave at fundamental at $10\mu s$ pulse versus the pulse number of the Figure 3.43 train. Measured at 1dB compression

Coming back at a 10% duty cycle after pulse 200, the transistors performance increase again to reach a new steady state similar to the one observed in the two previous experiments.

Looking at the phase of all the tones in Figure 3.45 it seems that the phase of the second harmonic is more affected than the other tones. As previously this is

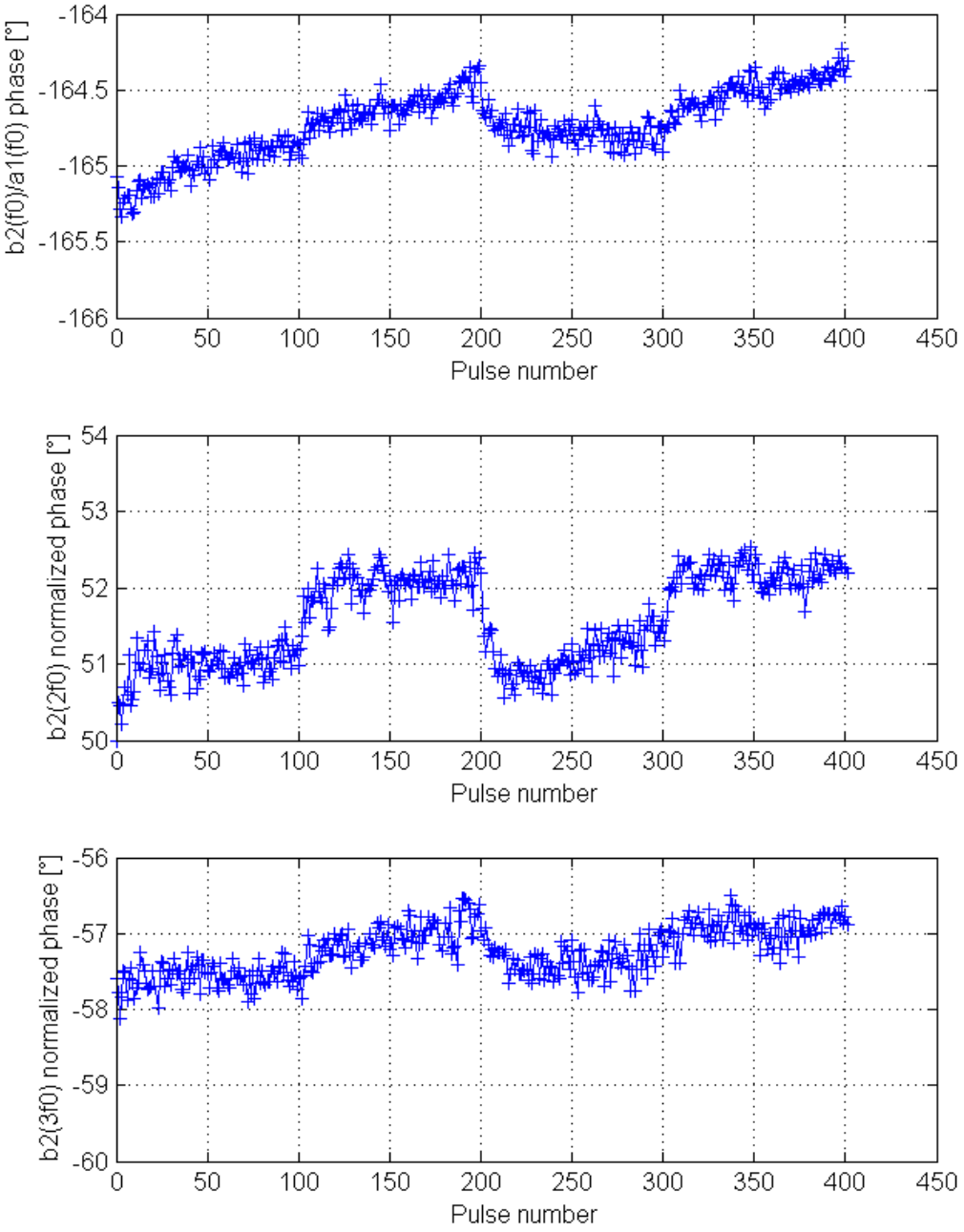

FIGURE 3.45: Phase at fundamental, harmonic 2 and 3 of output traveling wave normalized by the excitation traveling wave at fundamental at $10\mu s$ pulse versus the pulse number of the Figure 3.43 train. Measured at 1dB compression

again most probably due to the evolution of the compression point that for this amplifier influences more the second harmonic than the other tones.

Repeating the pulse train over and over makes the transistor alternate between two steady states, confirming the influence of different duty cycle in a same pulse train on radar power amplifier nonlinear behavior.

Conclusion of the different experiments

The presented experiments are aimed at showing the type of information brought by the parallel measurement method. It was showed that the non periodic pulse train integrating tricks used by the radar designers have a non negligible influence on the radar pulse train.

This feature adds up to the waveform engineering capability generally provided by every type of NVNA including the one presented.

3.4 Conclusion

In this chapter the extension of nonlinear measurement to various pulse measurements techniques was presented. Possible evolutions for pulse measurement using heterodyne receivers were discussed.

Extension of NVNA measurement to non periodic pulse train showing some periodicity in the train repetition was presented by extending the wideband pulse measurement technique, especially using its speed and synchronization.

Then, taking advantage of six port mixer based NVNA prototype, a measurement of three frequencies within a single pulse was proposed in order to allow measurements in non periodic pulse train allowing to approach realistic radar conditions. A series of experiments showed that information previously hardly accessible to designers on the behavior from pulse to pulse could be acquired with a simplicity equivalent to the one of a regular VNA measurement.

General conclusion

The main objective of this work was to provide to radar designers a nonlinear measurement technique that would allow them to take into account the influence on the power amplifier of the actual working conditions.

The importance of taking into account the actual conditions for characterization of the power amplifier was explained in the first chapter. There was also explained the organization of this work around a collaboration of radar designers through Thales Air Systems®, instrument designers through Rohde&Schwarz® and the academia through the IEMN was also presented along with the events that made us design our own nonlinear solution.

It was shown in the second chapter how the different receiver technologies compare when used for non linear measurement, finally choosing an heterodyne receiver due the context of this work to demonstrate the implementation of a mixer based NVNA that compare with the state of the art systems, as none of the existing NVNA was accessible to us for this work.

In the final chapter, a mixer based NVNA prototype able to measure three frequencies simultaneously keeping phase coherence between the frequencies demonstrated. It was used to measure the nonlinear behavior of a 5W S-band amplifier in non periodic pulsed condition. It was possible to evidence effects of the radar pulse train on the power amplifier from pulse to pulse that would be overlooked when using the periodic pulse approximation that is used today, increasing the insight of amplifier designers.

Moreover, thanks to the repartition of the tones of the complex signal between the different receivers, it was possible to measure all the tone at best signal to noise ratio available at the receivers contrary to what happen in state of the art

instruments where a main tone often blinds the instrument receivers to weaker tones.

In a near future, the bandwidth of this NVNA prototype could be extended up to 60GHz, providing this measurement to satellite communication designers as they are also in need of this type of nonlinear characterization.

The direct digital frequency synthesis technology that enabled the prototype to keep phase coherence would probably be a good candidate as a reference generator for NVNA phase calibration, potentially narrowing the frequency step that can be measured by a classical NVNA, while being less sensible to mismatches compared to comb based phase references.

Appendix A

VNA test set definition

The test set is in charge of separating the incident and reflected traveling waves at the instrument port. It also possibly includes attenuation of the waves before entering into the receiver stage to avoid receiver compression and attenuation of the source to decrease the lower power deliverable by the generator.

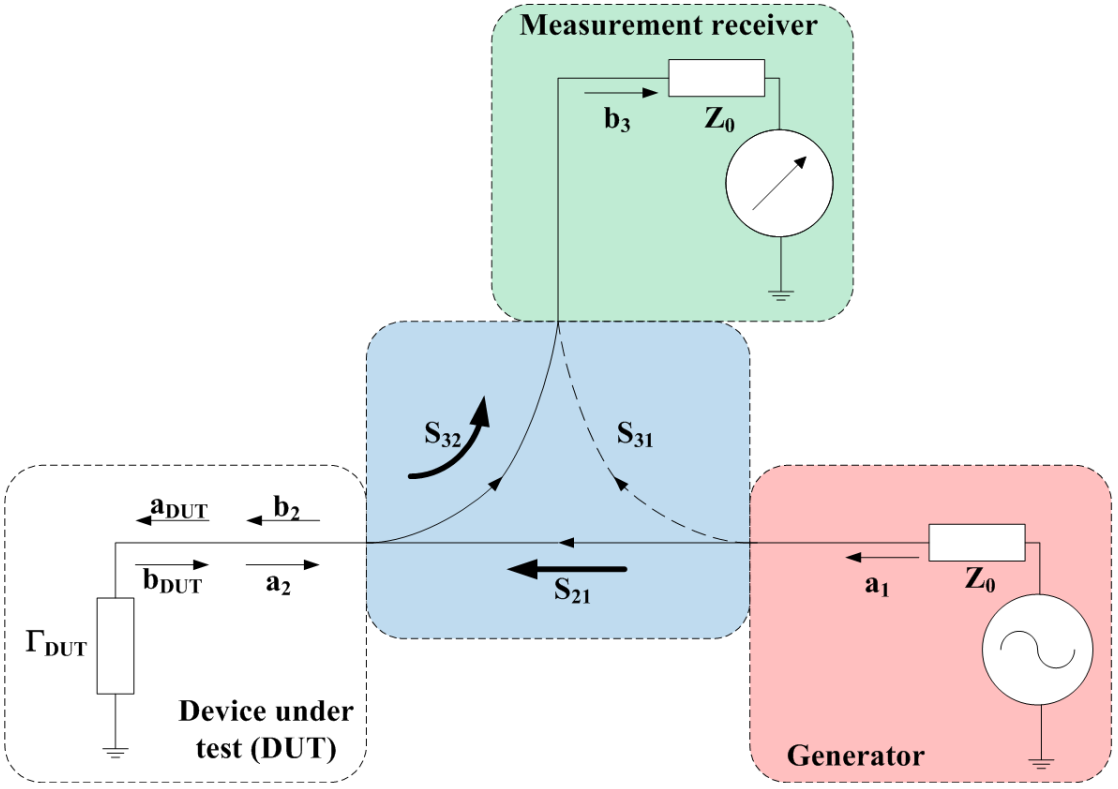

FIGURE A.1: Directional element model

The core of the test set is the directional element that enables the discrimination of the waves. Ideally, the unidirectional element included in the reflection measurement circuit of Figure A.1 allows the excitation signal a_1 to be forwarded without any loss ($S_{21} = 1$) to the DUT and then only collect all ($S_{32} = 1$) the signal b_1 reflected solely by the DUT to calculate the reflection coefficient of the DUT using the equation:

$$\Gamma_{DUT} = \frac{b_1}{a_1} \tag{A.1}$$

Because the level of the excitation signal a_1 is not perfectly constant over time it is necessary to constantly determine it. A power splitter can be used to split the signal into two parts, one a_1 going to the DUT and the other a'_1 to a reference receiver. The measured reflexion coefficient becomes:

$$\Gamma_{Measured} = \frac{b_1}{a'_1} \tag{A.2}$$

The difference between a_1 and a'_1 depends only on the measurement system and can be later corrected.

This equation has to be once more modified to take into account the realistic case of losses translating in a transmission coefficient $S_{21} > 1$ and a coupling factor $S_{32} > 1$ meaning that only part of the reflected wave is measured. We define the Reflection Tracking (RT) as the multiplication of the transmission loss and the coupling factor giving us a new relationship between the measured and the actual reflection coefficient:

$$\Gamma_{Measured} = RT.\Gamma_{DUT} = S_{21}.S_{31}.\Gamma_{DUT} \tag{A.3}$$

Reflection tracking creates a measurement inaccuracy that is independent of the DUT and can therefore be accounted for as long as we have sufficient dynamic range to detect the attenuated reflected signal.

The other assumptions we made *id.est* that we collect only the reflected signal and that the DUT is the only cause of reflected signal are also practically not met. Noise aside, the error caused by non ideal directivity and the test port matching is the main source of inaccuracy of the VNA independently of the technology used for the directional element.

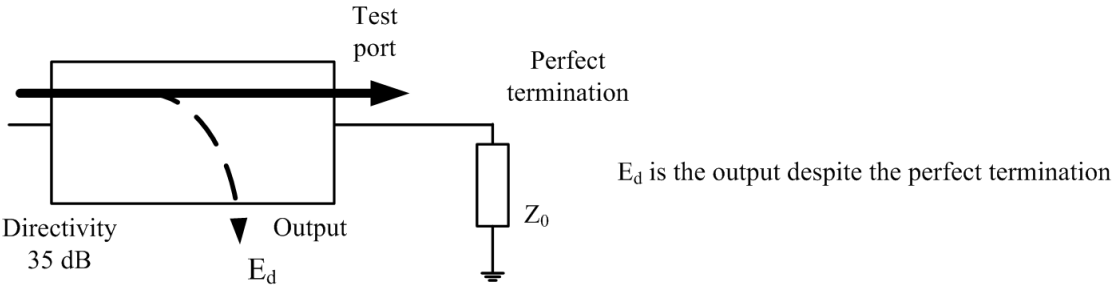

FIGURE A.2: Perfectly terminated directional element evidence the limited directivity flaw

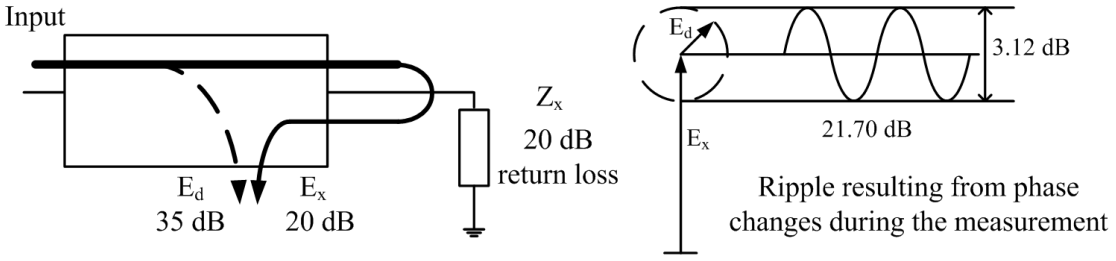

FIGURE A.3: Not perfectly terminated directional element reflects signal to the test port

Considering the ideally terminated directional element of Figure A.2, all the energy of the incident wave is absorbed by the termination and therefore there is no reflected wave heading to the receiver. Despite the absence of reflected signal there is a certain amount of energy detected by the receiver that is discernible from noise. The causes of this effect are multiple and depend on the technology used but the crosstalk between port 1 and 3 is completely characterized by S_{31}. The directivity Directivity (D) quantifies the deterioration of the directional element's behavior compared to the desired behavior and is defined by the complex ratio:

$$D = \frac{S_{31}}{RT} \tag{A.4}$$

In an actual measurement where the termination is not ideal, the wave resulting from crosstalk is combined to the measured reflected wave as shown in Figure A.3 resulting in the directivity being vectorially added to the actual reflection coefficient of the DUT:

$$\Gamma_{Measured} = RT.(\Gamma_{DUT} + D) \tag{A.5}$$

$\lvert D/\Gamma_{DUT}\rvert$	$1+\lvert D/\Gamma_{DUT}\rvert$	$1-\lvert D/\Gamma_{DUT}\rvert$	$\Delta\phi$
0 dB	6.02 dB	-∞	undefined
-3 dB	4.65 dB	-10.69 dB	45.07^o
-10dB	2.39 dB	-3.30 dB	18.43^o
-20 dB	0.83 dB	-0.92 dB	5.74^o
-30 dB	0.27 dB	-0.28 dB	1.81^o
-40 dB	0.09 dB	-0.09 dB	0.57^o
-50 dB	0.03 dB	- 0.03 dB	0.18^o

TABLE A.1: Estimate of magnitude and phase uncertainty for different D/Γ_{DUT}

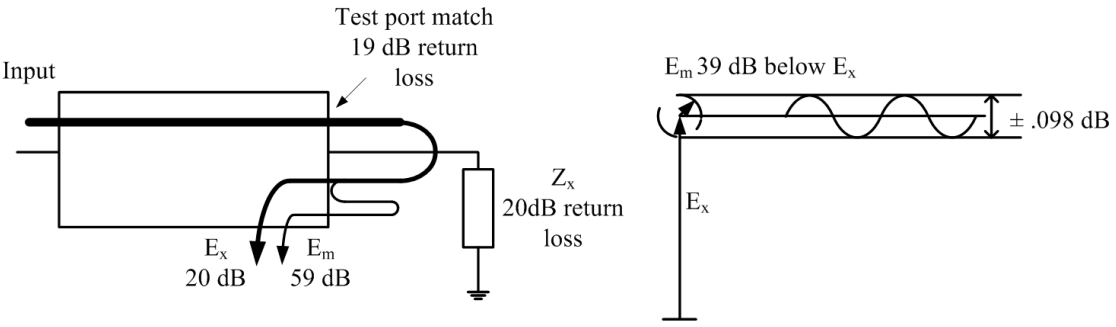

FIGURE A.4: Effect of test port match on a reflection measurement

To quantify the effect of directivity we can write A.5 under the form:

$$\Gamma_{Measured} = RT.\Gamma_{DUT}(1 + \frac{D}{\Gamma_{DUT}}) \tag{A.6}$$

The presence of an unknown deviation which value depends on the DUT in equation A.3 compared to equation A.6 implies a measurement uncertainty. This uncertainty can be estimated in magnitude and phase for different values of the complex ratio D/Γ_{DUT} and the extreme values are presented in Table A.1. If it is impossible to measure a reflection coefficient that is less than the directivity, the uncertainty due to directivity decreases drastically when measuring high reflection coefficients.

Until now we have been considering that the test port had a reflection coefficient equal to 0. In practice the test port match (often called Source Match (SM) in VNA correction terms) is different than 0 therefore the test set sends back part of the wave reflected by the DUT to it as shown in Figure A.4. The signal reflected by the test set will be reflected again by the DUT and so on. This phenomenon is called multiple reflections and results for N reflections in the sum of N terms of

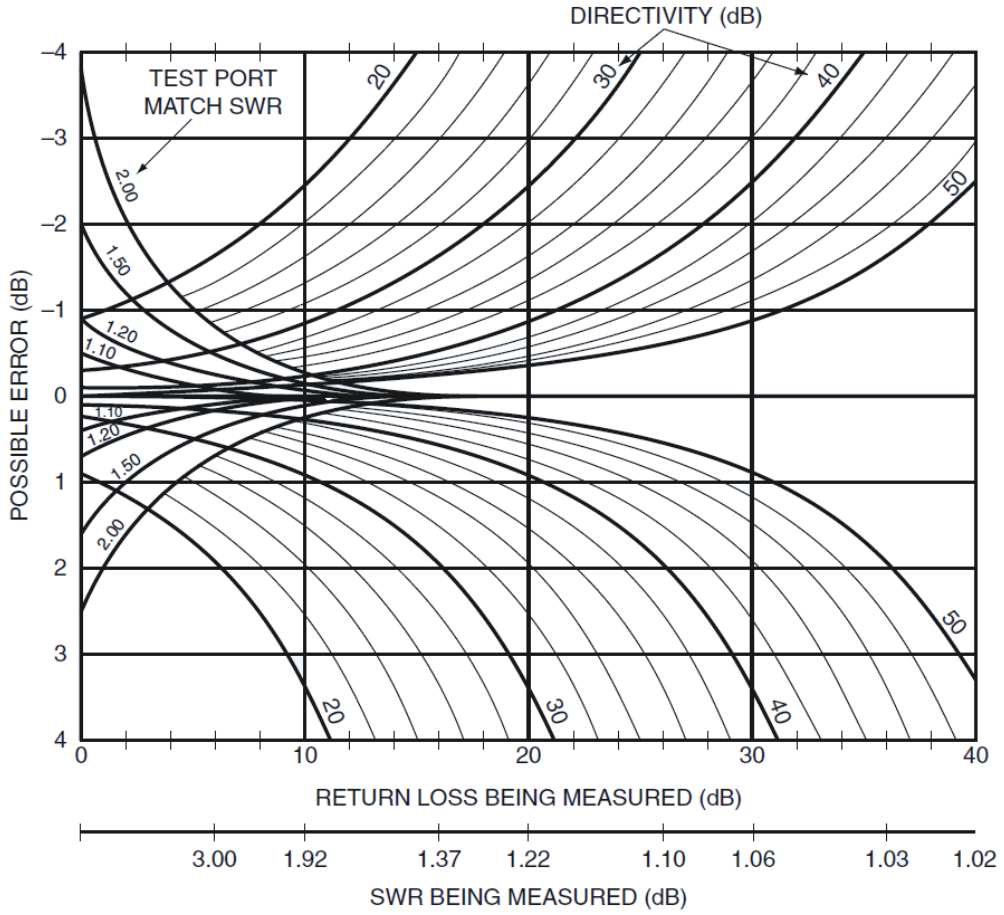

FIGURE A.5: Measurement uncertainty test set

a geometrical series of common ratio $SM.\Gamma_{DUT} < 1$ giving the result:

$$\Gamma_{Measured} = \frac{\Gamma_{DUT}}{\Gamma_{DUT} - SM.\Gamma_{DUT}} \tag{A.7}$$

The problematic case where $SM.\Gamma_{DUT} = 1$ does not happen in practice as the reflection coefficient of the test set is by design as close as 0 as possible. As for the directivity an unknown deviation depending on the DUT appears. This time it is prevalent for high reflection coefficient of the DUT while negligible for small reflection coefficient magnitude. The general uncertainty caused by the test set as a function of its directivity, test port match and measured return loss is shown in Figure A.5.

The case of a transmission measurement that therefore involves two directional

elements is a lot more complicated because of the numerous combinations of measurement errors. As for the reflection measurement, problems arise for transmission coefficient close to 0 and 1. Measurement of coefficients close to 0 are limited by the dynamic range and the directivity of the instrument while effects due to the directivity and mismatches in both directional elements interfere with the measurement of coefficients close to 1.

The most common directional elements for VNA test sets are VSWR bridges and directional couplers. VSWR bridges are usually used for frequencies between 100KHz and 8GHz but their important losses make them problematic to use at high frequencies if an excitation signal with high power is required. If power is not an issue then this technology can be found up to 40GHz [98].

On the opposite directional coupler can work up to 100GHz but even if they are used at 10MHz in the Rohde&Schwarz® ZVA for the models 24 GHz and above as well as in Agilent Technologies® PNA series it usually preferred not to use them under 1GHz as their performance drop. The use of dual-directional coupler is often preferred at high frequencies compared to the directional coupler as it allows to remove the power splitter allowing less losses on the excitation signal which is essential at high frequencies where high power synthesis can be problematic.

The lower losses of the directional couplers also gives it an advantage compared to bridges when using a passive load pull technique as the maximum coefficient reflexion synthesizable by the tuner is limited by the directional element losses if it is placed between the DUT and the tuner.

The compensation for the systematic errors introduced by the test set is exposed in Section 2.3.5 and in Appendix B.

Appendix B

Example of VNA calibration methods

The OSM technique is 3-terms error model as shown in Figure B.1. The error model is characterized by the following equation:

$$\begin{pmatrix} a_{DUT} \\ b_{measured} \end{pmatrix} = \begin{pmatrix} e_{11} & e_{10} \\ e_{01} & e_{00} \end{pmatrix} \begin{pmatrix} b_{DUT} \\ a_{measured} \end{pmatrix} \tag{B.1}$$

This technique uses three standards: an Open (O), a Short (S) and a Match (M) that have been previously characterized and have known reflection coefficients respectively Γ_O, Γ_S, Γ_M. To simplify the calculations we will assume an ideal

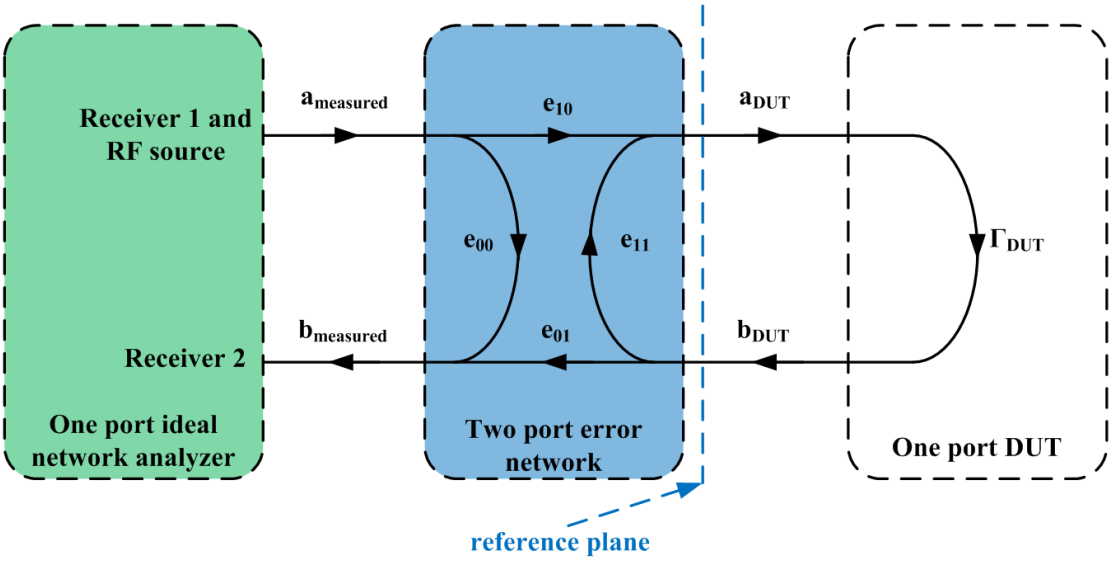

FIGURE B.1: 3 term error model

Raw system data	Error term
Directivity	e_{00}
Source Match	e_{11}
Reflection tracking	$e_{10}e_{01}$

TABLE B.1: Interpretation of system raw data in terms of error terms for 3 terms model

match or $\Gamma_M = 1$ even if the actual algorithm can take care of unideal match. Measuring each standard with the network analyzer we obtain the following results according to the conventions of Figure B.1:

$$\Gamma_{Omeasured} = e_{00} + \frac{e_{10}.e_{01}.\Gamma_O}{1 - e_{11}.\Gamma_O} \tag{B.2}$$

$$\Gamma_{Smeasured} = e_{00} + \frac{e_{10}.e_{01}.\Gamma_S}{1 - e_{11}.\Gamma_S} \tag{B.3}$$

$$\Gamma_{Mmeasured} = e_{00} \tag{B.4}$$

We have three equations for four unknowns error terms. Thankfully we can assume that either the term e_{10} or e_{01} are never equal to 0 which would mean that no power could ever be measured and therefore we can regroup them assuming that one of them is equal to 1 transferring its influence in the other term. This normalization could work because we are working with wave ratios. We have now three terms and we can solve the system of equations assuming $e_{01} = 1$:

$$e_{00} = \Gamma_{Mmeasured} \tag{B.5}$$

$$e_{10} = \frac{(\Gamma_O - \Gamma_S)(\Gamma_{Omeasured} - \Gamma_{Mmeasured})(\Gamma_{Smeasured} - \Gamma_{Mmeasured})}{\Gamma_O\Gamma_S(\Gamma_{Omeasured} - \Gamma_{Smeasured})} \tag{B.6}$$

$$e_{11} = \frac{\Gamma_S(\Gamma_{Omeasured} - \Gamma_{Mmeasured}) - \Gamma_O(\Gamma_{Smeasured} - \Gamma_{Mmeasured})}{\Gamma_O\Gamma_S(\Gamma_{Omeasured} - \Gamma_{Smeasured})} \tag{B.7}$$

In the Table B.1 we can see the interpretation of the system data in terms of error terms. It is important to note that the evaluation of the directivity depends only on the measurement of the match standard. Finally when we measure the reflection coefficient of a one port DUT Γ_{DUT} we can obtain the corrected value:

$$\Gamma_{DUT} = \frac{\Gamma_{DUTmeasured} - e_{00}}{e_{10} + e_{11}(\Gamma_{DUTmeasured} - e_{00})} \tag{B.8}$$

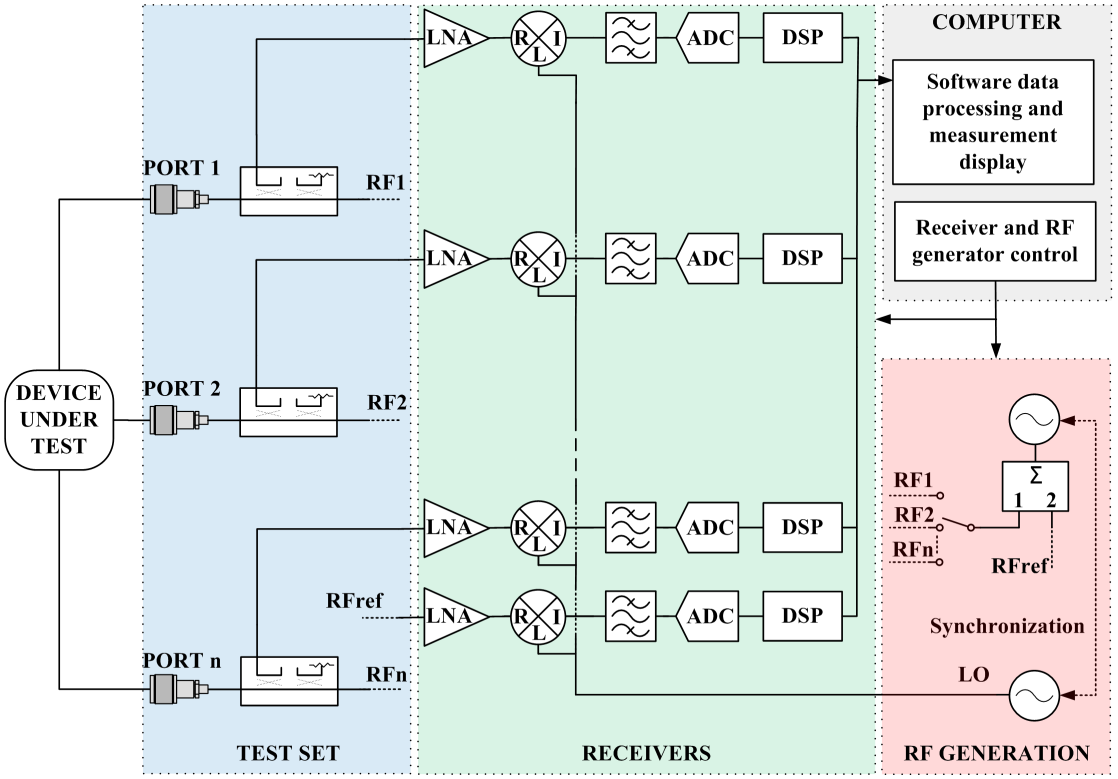

FIGURE B.2: 3 receiver VNA implementation

For two port network analyzers, even if the TRL technique has the favor of metrologist for the quality of the effective system data it allows, we will describe the most commonly used technique, the TOSM. This technique allows the calibration of two port analyzers having only three receivers as for example the implementation of Figure B.3 but is also used for four receivers implementations explaining is wide spread use. It consist of separating the error model into two sub-models, one for the forward and one for the reverse measurement as presented in Figure B.3. Using two sub-models allows to take into account the changes in the test set (especially the impedance of the VNA port) between forward and reverse measurements. This leads, using the convention of Figure B.3, to the following set of equations for the forward model:

$$\begin{pmatrix} a_{1DUT} \\ b_{1measured} \end{pmatrix} = \begin{pmatrix} e_{11} & e_{10} \\ e_{01} & e_{00} \end{pmatrix} \begin{pmatrix} b_{1DUT} \\ a_{1measured} \end{pmatrix} \tag{B.9}$$

$$b_{2measured} = e_{32} b_{2DUT} \tag{B.10}$$

$$a_{2DUT} = e_{22} b_{2DUT} \tag{B.11}$$

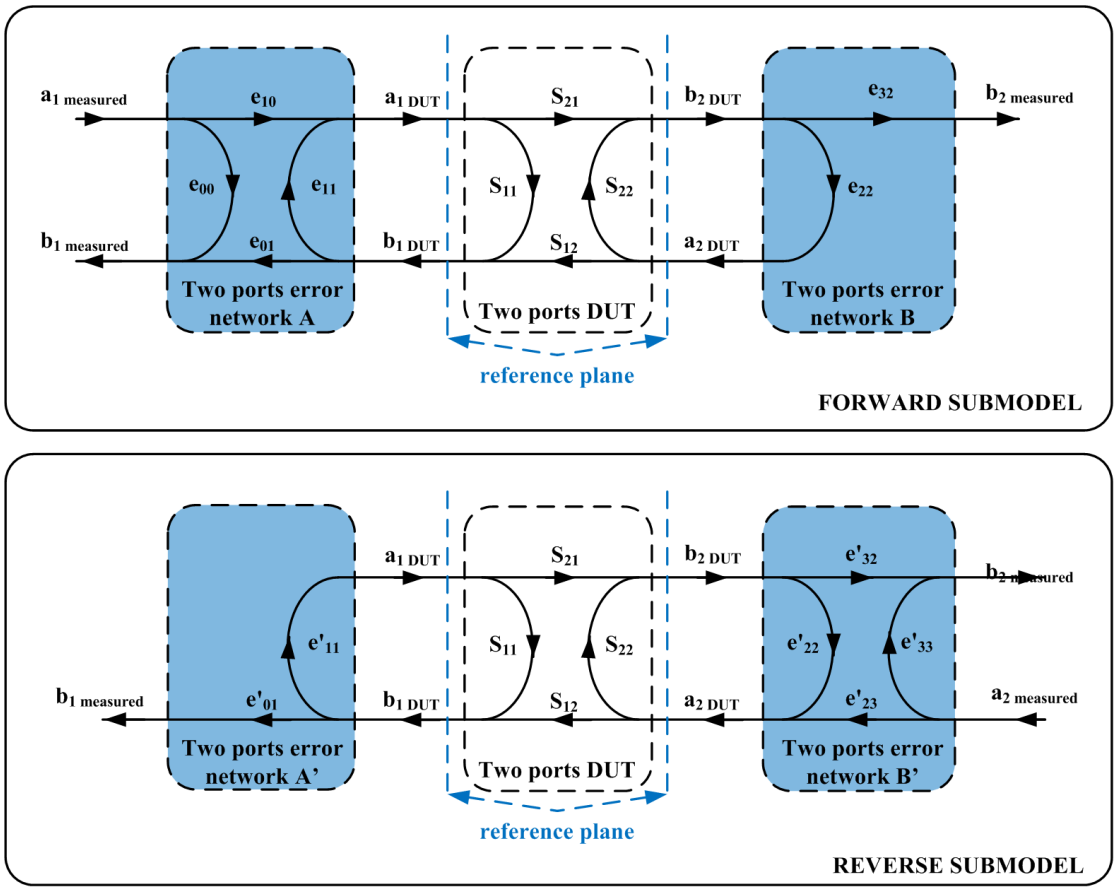

FIGURE B.3: 10 term error model

And for the reverse model:

$$\begin{pmatrix} a_{2DUT} \\ b_{2measured} \end{pmatrix} = \begin{pmatrix} e'_{22} & e'_{23} \\ e'_{32} & e'_{33} \end{pmatrix} \begin{pmatrix} b_{2DUT} \\ a_{2measured} \end{pmatrix} \tag{B.12}$$

$$b_{1measured} = e'_{01} b_{1DUT} \tag{B.13}$$

$$a_{1DUT} = e'_{11} b_{1DUT} \tag{B.14}$$

Please note that we have neglected the crosstalk between the ports for the sake of simplification. In practice it is indeed it is negligible in the majority of cases especially when working with connectorized elements. TOSM technique uses four standards, the same three as the OSM technique plus a Thru (T). The calibration actually consists for each sub-model of a one port OSM calibration (including the normalization $e_{10} = 1$ and $e'_{23} = 1$) of the excitation port and then a reflexion S_{iiT} and a transmission S_{ijT} measurement using the trough standard to take into account the second port. The trough standard is considered to have an impedance of 50 Ohm for the sake of simplification. For example for the forward sub-model

Raw system data	Forward measurement	Reverse measurement
Directivity	e_{00}	e'_{33}
Reflection tracking	$e_{01}e_{10}$	$e'_{32}e'_{23}$
Source Match	e_{11}	e'_{22}
Transmission tracking	$e_{32}e_{10}$	$e'_{01}e'_{23}$
Load Match	e_{22}	e'_{11}

TABLE B.2: Interpretation of system raw data in terms of error terms for 10 terms model

we obtain the equations for the error terms:

$$e_{00} = \Gamma_{Mmeasured} \tag{B.15}$$

$$e_{10} = \frac{(\Gamma_O - \Gamma_S)(\Gamma_{Omeasured} - \Gamma_{Mmeasured})(\Gamma_{Smeasured} - \Gamma_{Mmeasured})}{\Gamma_O\Gamma_S(\Gamma_{Omeasured} - \Gamma_{Smeasured})} \tag{B.16}$$

$$e_{11} = \frac{\Gamma_S(\Gamma_{Omeasured} - \Gamma_{Mmeasured}) - \Gamma_O(\Gamma_{Smeasured} - \Gamma_{Mmeasured})}{\Gamma_O\Gamma_S(\Gamma_{Omeasured} - \Gamma_{Smeasured})} \tag{B.17}$$

That are equivalent to the OSM calibration and for the transmission:

$$e_{22} = \frac{S_{11Tmeasured} - e_{00}}{S^2_{21T}((S_{11Tmeasured}e_{11}) - (e_{00}e11 - e10))} \tag{B.18}$$

$$e_{32} = \frac{S_{21Tmeasured}}{S_{21T}(1 - e_{00}e_{11})} \tag{B.19}$$

For the reverse sub-model the equations are of the exact same form. We can once again for each sub-model interpret the system data in terms of error term as shown in Table B.2. We finally get the corrected values of the S parameters using the equations:

$$S_{11} = \frac{1}{\Delta}((\frac{S_{11measured} - e_{00}}{e_{10}e_{01}})(1+(\frac{S_{22measured} - e'_{33}}{e'_{23}e'_{32}})e'_{22})-e_{22}(\frac{S_{21measured}}{e_{10}e_{32}})(\frac{S_{12measured}}{e'_{23}e'_{01}})) \tag{B.20}$$

$$S_{21} = \frac{1}{\Delta}(\frac{S_{21measured}}{e_{10}e_{32}})(1 + (\frac{S_{22measured} - e'_{33}}{e'_{23}e'_{32}})(e'_{22} - e_{22})) \tag{B.21}$$

$$S_{22} = \frac{1}{\Delta}((\frac{S_{22measured} - e'_{33}}{e'_{23}e'01})(1+(\frac{S_{11measured} - e_{00}}{e_{10}e_{01}})e_{11})-e'_{11}(\frac{S_{21measured}}{e_{10}e_{32}})(\frac{S_{12measured}}{e'_{23}e'_{01}})) \tag{B.22}$$

$$S_{12} = \frac{1}{\Delta}(\frac{S_{12measured}}{e'_{23}e'_{01}})(1 + (\frac{S_{11measured} - e_{00}}{e_{10}e_{01}})(e_{11} - e'_{11})) \tag{B.23}$$

With

$$\Delta = (1+(\frac{S_{11measured} - e_{00}}{e_{10}e_{01}})e_{11})(1+(\frac{S_{22measured} - e'_{33}}{e'_{23}e'_{32}})e'_{22})-(\frac{S_{21measured}}{e_{10}e_{32}})(\frac{S_{12measured}}{e'_{23}e'_{01}})e_{22}e'_{11} \quad \text{(B.24)}$$

Appendix C

Derivation of the e'_{32} result seen in Section 2.4.3

With the same notations as Section 2.4.3, using the port 2 as driving port, the VNA 7-terms model [54] gives at port 1:

$$b_{1Measured} = e_{01}.b_1 + e_{00}.a_{1Measured} \tag{C.1}$$

and the VNA 10 terms model of Figure B.3:

$$b_{1Measured} = e'_{01}.b_1 \tag{C.2}$$

Therefore:

$$e_{01} = e'_{01} - e_{00}e'_{01}.\frac{a_{1Measured}}{b_{1Measured}} \tag{C.3}$$

Which can be more conveniently written when multiplying Equation C.3 by e'_{23}, according to Table B.2, as:

$$e_{01}e'_{23} = TT_2(1 - D_1.\frac{a_{1Measured}}{b_{1Measured}}) \tag{C.4}$$

From the normalization common to both models $e_{10} = 1$ is is also possible to write:

$$e'_{23} = \frac{TT_2}{RT_1}(1 - D_1.\frac{a_{1Measured}}{b_{1Measured}}) \tag{C.5}$$

Which is also equal to:

$$RT_2 = \frac{TT_2}{RT_1}(1 - D_1.\frac{a_{1Measured}}{b_{1Measured}})e'_{32} \tag{C.6}$$

e'_{32} can then be expressed as follow:

$$e'_{32} = \frac{RT_2}{TT_2}.\frac{RT_1}{(1 - D_1.\frac{a_{1Measured}}{b_{1Measured}})} \tag{C.7}$$

To extract the value of e'_{32} the ratio $\frac{a_{1Measured}}{b_{1Measured}}$ needs to be calculated. Using the nonlinear relative model of Equation 2.19 one can write:

$$a_1 = \alpha_1.a_{1Measured} + \beta_1.b_{1Measured} b_1 = \gamma_1.a_{1Measured} + \delta_1.b_{1Measured} \tag{C.8}$$

So:

$$\frac{a_1}{b_1} = LM_1 = \frac{\alpha_1.\frac{a_{1Measured}}{b_{1Measured}} + \beta_1}{\gamma_1.\frac{a_{1Measured}}{b_{1Measured}} + \delta_1} \tag{C.9}$$

Therefore

$$\frac{a_{1Measured}}{b_{1Measured}} = \frac{\delta_1.LM_1 - \beta_1}{\alpha_1 - LM_1.\gamma_1} \tag{C.10}$$

From the array of Equation 2.27 we can deduce that:

$$\frac{a_{1Measured}}{b_{1Measured}} = \frac{LM_1 - SM_1}{RT1 + D_1.(LM_1 - SM_1)} \tag{C.11}$$

Finally merging Equation C.7 with Equation C.11:

$$e'_{32} = \frac{RT_2}{TT_2}.(RT_1 + D_1.(LM_1 - SM_1)) = \frac{e'_{32}e'_{23}}{e'_{01}e'_{23}}.(e_{01}e_{10} + e_{00}.(e_{22} - e_{11})) \tag{C.12}$$

Bibliography

[1] Y Blanchard. *Le radar, 1904-2004: histoire d'un siècle d'innovations techniques et opérationnelles*. 2004.

[2] M. I. Skolnik. *Introduction to Radar Systems, second edition*. 1981.

[3] J Darricau. *Physique et thorie du RADAR, Troisième édition*. 1993.

[4] Ieee standard radar definitions. *IEEE Std 686-1997*, pages i–, 1998.

[5] B.R. Mahafza and Elsherbeni A.Z. *Matlab simulations for radar systems design*. 2004.

[6] AW. Rihaczek. Radar resolution properties of pulse trains. *Proceedings of the IEEE*, 52(2):153–164, Feb 1964.

[7] C. Salmer, P. Eudeline, and P-A Rolland. Pulse to pulse stability of solid state transmitter module for radars application. In *Microwave Conference, 1998. 28th European*, volume 2, pages 79–84, Oct 1998.

[8] P. Pouvil. *Composants pour circuit intégré microondes*. Ecole nationale supérieure d'électronique et de ses applications, 2010.

[9] R.T. Kemerley, H.B. Wallace, and M.N. Yoder. Impact of wide bandgap microwave devices on dod systems. *Proceedings of the IEEE*, 90(6):1059–1064, Jun 2002.

[10] R.J. Trew. Wide bandgap semiconductor transistors for microwave power amplifiers. *Microwave Magazine, IEEE*, 1(1):46–54, Mar 2000.

[11] et a.l Burk Jr., A.A. *SiC and GaN wide bandgap semiconductor materials and devices", Solid-State Electronics, vol. 43, no. 8, pp. 1459-1464.* 1999.

[12] Umesh K. Mishra, Primit Parikh, and Yi-Feng Wu. Algan/gan hemts-an overview of device operation and applications. *Proceedings of the IEEE*, 90(6):1022–1031, Jun 2002.

[13] M. Gabrysch. *Electronic Properties Diamond*. 2008.

[14] V. Camarchia, F. Cappelluti, G. Ghione, E. Limiti, D.AJ. Moran, and M. Pirola. An overview on recent developments in rf and microwave power h-terminated diamond mesfet technology. In *Integrated Nonlinear Microwave and Millimetre-wave Circuits (INMMiC), 2014 International Workshop on*, pages 1–6, April 2014.

[15] N.O. Sokal. Rf power amplifiers, classes a through s-how they operate, and when to use each. In *Electronics Industries Forum of New England, 1997. Professional Program Proceedings*, pages 179–252, May 1997.

[16] M. Albulet. *RF Power Amplifiers*. 2001.

[17] N.O. Sokal. Class-e switching-mode high-efficiency tuned rf/microwave power amplifier: improved design equations. In *Microwave Symposium Digest. 2000 IEEE MTT-S International*, volume 2, pages 779–782 vol.2, June 2000.

[18] Junghwan Moon, Seunghoon Jee, Jungjoon Kim, Jangheon Kim, and Bumman Kim. Behaviors of class-f and class-f^{-1} amplifiers. *Microwave Theory and Techniques, IEEE Transactions on*, 60(6):1937–1951, June 2012.

[19] Y. F Wu, A Saxler, M. Moore, R.P. Smith, S.T. Sheppard, P.M. Chavarkar, T. Wisleder, U.K. Mishra, and P. Parikh. 30-w/mm gan hemts by field plate optimization. *Electron Device Letters, IEEE*, 25(3):117–119, March 2004.

[20] P. Draxler, I Langmore, T.P. Hung, and P.M. Asbeck. Time domain characterization of power amplifiers with memory effects. In *Microwave Symposium Digest, 2003 IEEE MTT-S International*, volume 2, pages 803–806 vol.2, June 2003.

[21] A. Prejs, S. Wood, R. Pengelly, and W. Pribble. Thermal analysis and its application to high power gan hemt amplifiers. In *Microwave Symposium Digest, 2009. MTT '09. IEEE MTT-S International*, pages 917–920, June 2009.

[22] Fadhel M Ghannouchi and Mohammad S Hashmi. *Load-pull techniques with applications to power amplifier design*, volume 32. Springer, 2012.

[23] Y. Takayama. A new load-pull characterization method for microwave power transistors. In *Microwave Symposium, 1976 IEEE-MTT-S International*, pages 218–220, June 1976.

[24] K. Kurokawa. Power waves and the scattering matrix. *Microwave Theory and Techniques, IEEE Transactions on*, 13(2):194–202, Mar 1965.

[25] D. Williams. Traveling waves and power waves: Building a solid foundation for microwave circuit theory. *Microwave Magazine, IEEE*, 14(7):38–45, Nov 2013.

[26] Doug Rytting. Network analyzers from small signal to large signal measurements. In *ARFTG Conference, 2006 67th*, pages 11–49, June 2006.

[27] J. Verspecht and D.E. Root. Polyharmonic distortion modeling. *Microwave Magazine, IEEE*, 7(3):44–57, June 2006.

[28] P.J. Tasker. Practical waveform engineering. *Microwave Magazine, IEEE*, 10(7):65–76, Dec 2009.

[29] M. Sipila, Kari Lehtinen, and Veikko Porra. High-frequency periodic time-domain waveform measurement system. *Microwave Theory and Techniques, IEEE Transactions on*, 36(10):1397–1405, Oct 1988.

[30] U. Lott. Measurement of magnitude and phase of harmonics generated in nonlinear microwave two-ports. *Microwave Theory and Techniques, IEEE Transactions on*, 37(10):1506–1511, Oct 1989.

[31] G. Kompa and F. van Raay. Error-corrected large-signal waveform measurement system combining network analyzer and sampling oscilloscope capabilities. *Microwave Theory and Techniques, IEEE Transactions on*, 38(4):358–365, Apr 1990.

[32] Hewlett Packard. *The microwave transition analyzer: a versatile measurement set for bench and test.*

[33] W.S. El-deeb, M.S. Hashmi, N. Boulejfen, and F.M. Ghannouchi. Small-signal, complex distortion and waveform measurement system for multiport microwave devices. *Instrumentation Measurement Magazine, IEEE*, 14(3):28–33, June 2011.

[34] M. Demmler, P.J. Tasker, and M. Schlechtweg. On-wafer large signal power, s-parameter and waveform measurement system. In *Integrated Nonlinear Microwave and Millimeterwave Circuits, 1994., Third International Workshop on*, pages 153–158, Oct 1994.

[35] J.G. Leckey, J.AC. Stewart, AD. Patterson, and M.J. Kelly. Nonlinear mesfet parameter estimation using harmonic amplitude and phase measurements. In *Microwave Symposium Digest, 1994., IEEE MTT-S International*, pages 1563–1566 vol.3, May 1994.

[36] J. Verspecht, P. Debie, A Barel, and L. Martens. Accurate on wafer measurement of phase and amplitude of the spectral components of incident and scattered voltage waves at the signal ports of a nonlinear microwave device. In *Microwave Symposium Digest, 1995., IEEE MTT-S International*, pages 1029–1032 vol.3, May 1995.

[37] J-P Teyssier, D. Barataud, C. Charbonniaud, F. De Groote, J. Verspecht, J.-M. Nebus, and R. Quere. A transistor measurement setup for microwave high power amplifiers design. In *Microwave Conference Proceedings, 2005. APMC 2005. Asia-Pacific Conference Proceedings*, volume 5, pages 4 pp.–, Dec 2005.

[38] D Ducatteau. *Caractérisation non linéaire et analyse de transistors à effet de champ pour applications hyperfréquences dans le domaine temporel*. Université de Lille 1, 2008.

[39] D. Barataud, Caroline Arnaud, B. Thibaud, M. Campovecchio, J.-M. Nebus, and J.P. Villotte. Measurements of time-domain voltage/current waveforms at rf and microwave frequencies based on the use of a vector network analyzer for the characterization of nonlinear devices-application to high-efficiency power amplifiers and frequency-multipliers optimization. *Instrumentation and Measurement, IEEE Transactions on*, 47(5):1259–1264, Oct 1998.

[40] http://cifre.anrt.asso.fr/.

[41] Hank Zumbahlen. *Basic Linear Design*. 2007.

[42] Ieee standard for terminology and test methods for analog-to-digital converters. *IEEE Std 1241-2010 (Revision of IEEE Std 1241-2000)*, pages 1–139, Jan 2011.

[43] S. Krone and G. Fettweis. Fundamental limits to communications with analog-to-digital conversion at the receiver. In *Signal Processing Advances in Wireless Communications, 2009. SPAWC '09. IEEE 10th Workshop on*, pages 464–468, June 2009.

[44] Luca Gammaitoni, Peter Hänggi, Peter Jung, and Fabio Marchesoni. Stochastic resonance. *Reviews of modern physics*, 70(1):223, 1998.

[45] Robert Alexander Wannamaker. *The theory of dithered quantization.*

[46] Bernard Widrow and Istvn Kollr. Dither. In *Quantization Noise*, pages 485–528. Cambridge University Press, 2008. Cambridge Books Online.

[47] Zwei-Mei Lee, Cheng-Yeh Wang, and Jieh-Tsorng Wu. A cmos 15-bit 125-ms/s time-interleaved adc with digital background calibration. *Solid-State Circuits, IEEE Journal of*, 42(10):2149–2160, 2007.

[48] C. Rauscher. *Fundamentals of spectrum analysis, Chapter 3: Configuration and Control Elements of a Spectrum Analyzer.* Rohde&Schwarz, 2008.

[49] Teledyne LeCroy. *Press release: Teledyne LeCroy Successfully Demonstrates Worlds First 100GHz Real-Time Oscilloscope.*

[50] M. Kahrs. 50 years of rf and microwave sampling. *Microwave Theory and Techniques, IEEE Transactions on*, 51(6):1787–1805, June 2003.

[51] Analoge Devices. *Tutorial: Sample-and-Hold Amplifier.*

[52] Picosecond Pulse Labs. *Real-time sampling downconverter front ends for digital radar and wide-band signaling.*

[53] S Ahmed. *Système de mesures temporelles 4-canaux à échantillonnage entrelacé ultra haute fréquence basé sur des amplificateurs "Track & Hold" pour la caractérisation impulsionnelle d'amplificateurs de puissance non linéaires.* Université de Limoges, 2012.

[54] M Hiebel. *Fundamentals of vector network analysis.* Rohde&Schwarz, 2008.

[55] Anritsu. *Application Note: Reflectometer Measurements Revisited.*

[56] John R Vig. Quartz crystal resonators and oscillators.

[57] A Hajimiri and T.H. Lee. A general theory of phase noise in electrical oscillators. *Solid-State Circuits, IEEE Journal of*, 33(2):179–194, Feb 1998.

[58] Joel Phillips and Ken Kundert. An introduction to cyclostationary noise.

[59] V. F. Kroupa. *Direct Digital Frequency Synthesizers*. Wiley-IEEE press, 1998.

[60] Analoge Devices. *Datasheet: AD9914. 3.5 GSPS Direct Digital Synthesizer with 12-Bit DAC*.

[61] Dean Banerjee. *PLL performance, simulation and design*. Texas INstrument, 2006.

[62] Anitha Babu, Bhavya Daya, Banu Nagasundaram, and Nivetha Veluchamy. All digital phase locked loop design and implementation.

[63] G. Avitabile, F. Cannone, and A Vania. Phase shifter based on dds-driven offset-pll. *Electronics Letters*, 42(25):1438–1439, December 2006.

[64] A Bonfanti, F. Amorosa, C. Samori, and AL. Lacaita. A dds-based pll for 2.4-ghz frequency synthesis. *Circuits and Systems II: Analog and Digital Signal Processing, IEEE Transactions on*, 50(12):1007–1010, Dec 2003.

[65] Rohde&Schwarz. *Manual ZVA: Port Configuration*.

[66] Herotek. *Datasheet: Step recovery diode comb (harmonic) generators*.

[67] Picosecond Pulse Labs. A new breed of comb generators featuring low phase noise and low input power. *Microwave Journal*, May 2006.

[68] M. El Yaagoubi, G. Neveux, D. Barataud, T. Reveyrand, J.-M. Nebus, Frans Verbeyst, F. Gizard, and J. Puech. Time-domain calibrated measurements of wideband multisines using a large-signal network analyzer. *Microwave Theory and Techniques, IEEE Transactions on*, 56(5):1180–1192, May 2008.

[69] Zhang Yichi and Lin Maoliu. An nvna poly-harmonic inter-modulation phase reference based on srd comb generator and multi-tone stimulus. In *Precision Electromagnetic Measurements (CPEM), 2012 Conference on*, pages 108–109, July 2012.

[70] Liesbeth Gomm and Yves Rolain. Design and characterization of an rf pulse train generator for large-signal analysis. *Measurement Science and Technology*, 20(2):025106, 2009.

[71] Maxim integrated. *Application Note : Spectral content of NRZ test patterns.*

[72] NMDG. *Product Note : NM300.*

[73] D.B. Gunyan and J.B. Scott. Pulse generator, September 9 2008. US Patent 7,423,470.

[74] Finisar. *Datasheet: 70GHz photodetecor XPDV3120R.*

[75] P. Barrnuta, F. Verbeyst, A Lewandowski, and D. Schreurs. Optimization of a next-generation comb generator for accurate large-signal measurements on a user-defined frequency grid. In *Integrated Nonlinear Microwave and Millimetre-wave Circuits (INMMiC), 2014 International Workshop on*, pages 1–3, April 2014.

[76] Jan Verspecht. Calibration of a measurement system for high frequency nonlinear devices. *Brussels, Belgium Vrije Univeriteit Brussels, Ph. D. Thesis*, 1995.

[77] Roger B. Marks. Formulations of the basic vector network analyzer error model including switch-terms. In *ARFTG Conference Digest-Fall, 50th*, volume 32, pages 115–126, Dec 1997.

[78] Rohde&Schwarz. *Manual ZVA: Enhanced Wave Correction.*

[79] J. Verspecht and K. Rush. Individual characterization of broadband sampling oscilloscopes with a 'nose-to-nose' calibration procedure. In *Instrumentation and Measurement Technology Conference, 1993. IMTC/93. Conference Record., IEEE*, pages 203–208, May 1993.

[80] R. Pintelon and J. Schoukens. Frequency domain identification of linear time invariant systems under non-standard conditions. In *Instrumentation and Measurement Technology Conference, 1996. IMTC-96. Conference Proceedings. Quality Measurements: The Indispensable Bridge between Theory and Reality., IEEE*, volume 1, pages 294–299 vol.1, 1996.

[81] K.A Remley, D.F. Williams, D. M M P Schreurs, G. Loglio, and A Cidronali. Phase detrending for measured multisine signals. In *ARFTG Conference Digest, Spring 2003. 61st*, pages 73–83, June 2003.

[82] Lawrence R. Rabiner, Ronald W. Schafer, and Charles M. Rader. The chirp z-transform algorithm and its application. *Bell System Technical Journal, The*, 48(5):1249–1292, May 1969.

[83] H.A Mahmoud and H. Arslan. Error vector magnitude to snr conversion for nondata-aided receivers. *Wireless Communications, IEEE Transactions on*, 8(5):2694–2704, May 2009.

[84] Kuangda Wang, S. Adhikari, A Ghiotto, and Ke Wu. Multiharmonic generator for large-signal-network-analyzer verification. *Microwave Magazine, IEEE*, 15(1):120–128, Jan 2014.

[85] R.E. Shoulders and L.C. Betts. Pulsed signal device characterization employing adaptive nulling and if gating, March 4 2008. US Patent 7,340,218.

[86] F. DeGroote, O. Jardel, T. Reveyrand, J-P Teyssier, and R. Quere. Very small duty cycles for pulsed time domain transistor characterization. In *Proceedings of the European Microwave Association*, volume 4, pages 112–117, June 2008.

[87] J. Faraj, G. Callet, F. De Groote, J. Verspecht, R. Quere, and J-P Teyssier. Bursts of pulses for time domain large signal measurements. In *Microwave Measurement Conference, 2009 73rd ARFTG*, pages 1–4, June 2009.

[88] S. Ahmed, G. Neveux, T. Reveyrand, D. Barataud, and J. M. Nebus. Time-domain interleaved high sampling rate system for large signal characterization of non-linear devices. In *Microwave Measurement Conference (ARFTG), 2012 79th ARFTG*, pages 1–4, June 2012.

[89] Rohde&Schwarz. *Application Note: Envelope Tracking and Digital Pre-Distortion Test Solution for RF Amplifiers.*

[90] F. Macraigne, T. Reveyrand, G. Neveux, D. Barataud, J.-M. Nebus, Arnaud Soury, and E. Ngoya. Time-domain envelope measurements for characterization and behavioral modeling of nonlinear devices with memory. *Microwave Theory and Techniques, IEEE Transactions on*, 54(8):3219–3226, Aug 2006.

[91] Agilent technologies. *Application Note: Active-Device Characterization in Pulsed Operation Using the PNA-X.*

[92] Rohde&Schwarz. *Application Note: Tackling the Challenges of Pulsed Signal Measurements.*

[93] Anritsu. *Application Note: Pulse measurement with Vectorstars*.

[94] Rohde&Schwarz. *Manual ZVA: Define busy signal*.

[95] P. Roblin, Youngseo Ko, Haedong Jang, and J.P. Teyssier. Pulsed rf calibration for nvna measurements. In *Microwave Measurement Symposium (ARFTG), 2012 80th ARFTG*, pages 1–6, Nov 2012.

[96] Rohde&Schwarz. *Manual ZVA: Define Pulse Train*.

[97] Focus Microwaves. *Datasheet: iMPT-Quattro-1018*.

[98] F. van Raay and G. Kompa. A new active balun reflectometer concept for dc to microwave vna applications. In *Microwave Conference, 1998. 28th European*, volume 1, pages 108–113, Oct 1998.

Publications related to this work

Bridier, V.; Ducatteau, D.; Olivier, M.; Simon, H.-J.; Graux, F.; Eudeline, P.; Dambrine, G.,
"Nonlinear measurement of non periodic pulse train with mixer based NVNA dedicated to radar power amplifier"'
Integrated Nonlinear Microwave and Millimetre-wave Circuits (INMMiC), 2014 International Workshop on , vol., no., pp.1,3, 2-4 April 2014
doi: 10.1109/INMMIC.2014.6815076

Bridier, V.; Ducatteau, D.; Olivier, M.; Simon, H.-J.; Graux, F.; Eudeline, P.; Dambrine, G.,
"Nonlinear measurement dedicated to non periodic pulse train for radar power amplifier characterization"
Microwave Symposium (IMS), 2014 IEEE MTT-S International , vol., no., pp.1,4, 1-6 June 2014
doi: 10.1109/MWSYM.2014.6848400

Bridier, V.; Ducatteau, D.; Olivier, M.; Simon, H.-J.; Graux, F.; Eudeline, P.; Dambrine, G.,
"Measurement of the influence of non periodic pulse train on the nonlinear behavior of radar power amplifier using mixer based NVNA"
Radar2014 , Not yet published by conference when releasing this document

Abstract

Contribution to the development of a new non linear characterization platform for radar power amplifier

Abstract: Radar high power amplifier, that is one of the performance defining elements of a radar system, is under constant investigation to improve its power and efficiency. Improvement can be provided through the combination of relatively new transistor technology such as HEMT GaN and the use of high efficiency functioning class such as commutation classes. Commutation classes making use of harmonic tones of the complex signal of the amplifier at compression, non-linear characterization is required. Such characterization already available for CW and periodic pulse signal. However periodic pulse only provide an approximation of the actual radar pulse train the amplifier will be submitted to, overlooking effects cause by the pulse train. This affect especially on HEMT GaN which is prone to thermal and memory effects.
This work propose a new measurement technique relying on a developed mixer based NVNA prototype able to measure three frequencies simultaneously, allowing the non linear characterization of a power amplifier in actual non periodic radar pulse train. The instrument was validated in CW and periodic pulse condition using commercially available NVNA and a LSNA. The measurement technique, optimized in this work to be performed up to 12GHz, allowed to see effects caused by the radar pulse train on a power amplifier performance while recording all three tones at best signal to noise ratio available thanks to the instrument architecture.

Key words: Radar applications, RF nonlinear characterization, Power amplifier, HEMT GaN, non periodic pulse train, radar pulse train.

Contribution au développement d'une nouvelle plateforme de caractérisation non linéaire pour amplificateurs de puissance hyperfréquences pour les applications radar

Résumé: L'amplificateur haute puissance d'un radar, qui est l'un des éléments définnissant les performances du système, est un sujet constant de rechecherche afin d'améliorer sa puissance et son rendement. Des améliorations des performances peuvent être apportées par la combinaison d'un technologie relativement nouvelle, le HEMT GaN et de classes de fonctionnement d'amplificateur á haut rendement telles les classes de commutation. Ces dernières faisant usage des harmoniques du signal complex émis par l'amplificateur en compression, une caracterisation non linéaire est requise. Ce type de caractérisation existe déjà en mode CW et pulsé périodique. Cependant, le mode pulsé périodique n'apporte qu'une approximation du train d'impulsions radar réel excitant l'amplificateur, négligeant les effets causés par le train de pulse. Cela concerne particulièrement la technologie HEMT GaN qui est susceptible à des effets thermique et de mémoire.
Ce travail propose une nouvelle technique de mesure reposant sur un prototype de NVNA basé sur des mélangeurs capable de mesuré trois fréquences simultanément, permettant la caractérisation non linéaire d'un amplificateur en condition radar réelle en terme de train d'impulsions. Cet instrument a été validé par des mesures CW et pulsée périodique en utilisant un appareil type LSNA et un VNA disponible sur le marché. La technique mesure, optimisée dans ce travail jusqu'à 12GHz, permet de visualiser des effets causés par le train d'impulsions sur l'amplificateur de puissance tout en mesurant les trois premiers tons du signal complexe au meilleur rapport signal à bruit disponible grâce à l'architecture de l'instrument.

Mots clés: application radar , caractérisation microonde non linéaire, amplificateur de puissance, HEMT GaN, train d'impulsions non périodique, train d'impulsions radar.